Supercritical Fluid Science and Technology

Volume 2

Series Editor
Erdogan Kiran

Previous volume in the series

Vol. 1 Supercritical Fluids and Organometallic Compounds: From Recovery of Trace Metals to Synthesis of Nanostructured Materials by Can Erkey

High-Pressure Fluid Phase Equilibria

Phenomenology and Computation

High-Pressure Fluid Phase Equilibria

Phenomenology and Computation

Ulrich K. Deiters and Thomas Kraska
Institute of Physical Chemistry
University of Cologne
Cologne, Germany

ELSEVIER
AMSTERDAM • BOSTON • HEIDELBERG • LONDON • NEW YORK • OXFORD
PARIS • SAN DIEGO • SAN FRANCISCO • SINGAPORE • SYDNEY • TOKYO

Elsevier
The Boulevard, Langford Lane, Kidlington, Oxford OX5 1GB, UK
Radarweg 29, PO Box 211, 1000 AE Amsterdam, The Netherlands

First edition 2012

Copyright © 2012 Elsevier BV. All rights reserved.

No part of this publication may be reproduced, stored in a retrieval system or transmitted in any form or by any means electronic, mechanical, photocopying, recording or otherwise without the prior written permission of the publisher Permissions may be sought directly from Elsevier's Science & Technology Rights Department in Oxford, UK: phone (+44) (0) 1865 843830; fax (+44) (0) 1865 853333; email: permissions@elsevier.com. Alternatively you can submit your request online by visiting the Elsevier web site at *http://www.elsevier.com/locate/permissions*, and selecting Obtaining permission to use Elsevier material.

Notice
No responsibility is assumed by the publisher for any injury and/or damage to persons or property as a matter of products liability, negligence or otherwise, or from any use or operation of any methods, products, instructions or ideas contained in the material herein. Because of rapid advances in the medical sciences, in particular, independent verification of diagnoses and drug dosages should be made.

British Library Cataloguing in Publication Data
A catalogue record for this book is available from the British Library

Library of Congress Cataloging-in-Publication Data
A catalog record for this book is available from the Library of Congress

ISBN: 978-0-444-56347-7
ISSN: 2212-0505

For information on all Elsevier publications
visit our website at *elsevierdirect.com*

Printed and bound in Great Britain
12 13 14 15 10 9 8 7 6 5 4 3 2 1

Working together to grow
libraries in developing countries

www.elsevier.com | www.bookaid.org | www.sabre.org

ELSEVIER BOOK AID International Sabre Foundation

Denn es ist ausgezeichneter Menschen unwürdig, gleich Sklaven Stunden zu verlieren mit Berechnungen.
(For it is not dignified for excellent men to lose hours, like slaves, over computations.)

Gottfried Wilhelm Leibniz (1646–1716)
German philosopher, mathematician,
and constructor of a mechanical calculator

Symbols

A	Helmholtz energy
a	attraction parameter of equations of state of the van der Waals type
B_i	ith virial coefficient
b	covolume parameter of equations of state of the van der Waals type
C	number of constraints (phase rule)
C_p	isobaric heat capacity
C_V	isochoric heat capacity
F	number of degrees of freedom (phase rule)
f	fugacity; in calorimetry: phase fraction
G	Gibbs energy
$g(r)$	radial distribution function
H	enthalpy
$\boldsymbol{I}$	unity matrix ($\boldsymbol{I}=[a_{i,j}], a_{i,i}=1, a_{i,j\neq i}=0$)
K_i	K factor (enhancement factor) of species i
$K_{\mathrm{H},ij}$	Henry's constant of species i dissolved in j
k_{B}	Boltzmann's constant
N	number of components of a mixture
N_{A}	Avogadro's constant
$\mathcal{N}$	number of molecules
n	amount of substance, "mole number"
P	number of phases (phase rule)
p	pressure
Q	system partition function
q	heat; in statistical thermodynamics: single-molecule partition function
q_V	volumetric quality
R	universal gas constant, $R=N_{\mathrm{A}}k_{\mathrm{B}}$
S	entropy
T	temperature
t	time
V	volume
U	internal energy
$u(r)$	intermolecular interaction potential
r	distance
w	work
x	mole fraction

Z	compression factor, $Z = pV/(nRT)$
α_p	isobaric expansion coefficient
γ	activity coefficient
ϵ	well depth of an intermolecular interaction potential
ζ	in global phase diagrams: relative difference of pure-fluid energy parameters
η	in global phase diagrams: relative difference of binary and pure-fluid size parameters
κ_T	isothermal compressibility
Λ	thermal de Broglie wavelength
λ	range of a pair potential ($u(r > \lambda\sigma) = 0$); in global phase diagrams: relative difference of binary and pure-fluid energy parameters
λ_k	kth eigenvalue of the $\boldsymbol{\Psi}$ matrix
μ	chemical potential; in phase stability calculations: eigenvalue of $\boldsymbol{\Psi}$
ξ	packing fraction; in global phase diagrams: relative difference of pure-fluid size parameters
π_T	internal pressure
ρ	molar density, $\rho = 1/V_\mathrm{m}$
$\hat{\rho}$	number density, $\hat{\rho} = \mathcal{N}/V$
σ	collision diameter
ϕ	fugacity coefficient
Ψ	Helmholtz energy density
$\boldsymbol{\Psi}$	Hessian of Ψ
Ω	orientation (set of Euler angles)
ω	acentric factor

Subscripts

assoc	association
att	attraction
b	boiling point
eff	effective
i	quantity or variable belonging to species i
m	molar quantity
p	derivative at constant pressure
r	reaction
rep	repulsion
T	derivative at constant temperature
(nT)	nth order derivative w.r.t. temperature, e.g., $A_{(T)} = (\partial A_\mathrm{m}/\partial T)$, $A_{(2T)} = (\partial^2 A_\mathrm{m}/\partial T^2)$ (cf. Eq. (1.1))
trp	triple point
V	derivative at constant molar volume
(nV)	nth order derivative w.r.t. molar volume, e.g., $A_{(V)} = (\partial A_\mathrm{m}/\partial V_\mathrm{m})$, $A_{(2V)} = (\partial^2 A_\mathrm{m}/\partial V_\mathrm{m}^2)$ (cf. Eq. (1.1))
(nx)	nth order derivative w.r.t. mole fraction, e.g., $A_{(2x)} = (\partial^2 A_\mathrm{m}/\partial x_1^2)$

Superscripts

az	azeotropic
c	critical
E	excess quantity
f	fluid phase
g	gas or vapor phase
id	ideal gas
idmix	ideal mixture
l	liquid phase
n	normal (noncritical) phase
r	residual quantity
s	solid phase
T	transposed (matrix or vector)
α	belonging to phase α
σ	saturation, vapor pressure
$\ominus$	reference state in the ideal-gas regime
$\circ$	thermochemical standard state
∞	infinite dilution
$*$	characteristic property of a substance

Acronyms

AEP	azeotropic endpoint
CEP	critical endpoint
CPEM	critical pressure end minimum/maximum
CPSP	critical pressure step point
CSRK	Carnahan–Starling–Redlich–Kwong equation of state
CSvdW	Carnahan–Starling–van der Waals equation of state
DCEP	double critical endpoint
DSC	differential scanning calorimetry
DTA	differential thermal analysis
dCPM	degenerated critical pressure maximum
GAS	gas antisolvent crystallisation
LCEP	lower critical endpoint
LCST	lower critical solution temperature (point)
MDP	mathematical double point
RESS	rapid expansion of supercritical solutions
RK	Redlich–Kwong equation of state
RKS	Redlich–Kwong–Soave equation of state
SAFT	statistical associating fluid theory
SPHCT	simplified perturbed-hard-chain theory
TCP	tricritical point
UCEP	upper critical endpoint
UCST	upper critical solution temperature (point)
vdW	van der Waals (equation of state or mixing rules)

Foreword

It is with great pleasure that I introduce Volume 2 "*High-Pressure Fluid Phase Equilibria: Phenomenology and Computation*" in the Elsevier book series on Supercritical Fluid Science and Technology.

Advances in supercritical fluid science and technology are so linked to our understanding of the fundamentals of high pressure phase equilibria that this book is extremely timely and provides a comprehensive look at the phenomenology and computational aspects of pure fluids as well as binary and ternary mixtures and also deals with experimental techniques. The book is written by Professors Ulrich Deiters and Thomas Kraska of the University of Cologne, two renowned world experts, who have the first-hand experience to write such an authoritative treatise. The book is not only technical but also highly pedagogical and philosophical with extremely valuable insights.

The book starts out by posing the question "why one should read this book?" and sets the stage in Chapter 1. As someone who has spent nearly three decades of his research effort in the area, I can unequivocally state that this book is an essential reading for anyone who is engaged in or planning to enter the field of high-pressure research or is already involved with supercritical fluid science and technology. It is a self-teaching book at the highest level but without giving you any feeling of being lost in the complexities of the topic. Concepts and tools are developed in an easy-to-follow pedagogical manner with questions included at the end of each chapter. The reviews of essential mathematical tools and the solutions to each question that are provided in the appendices are expected to be very helpful and bring further insight and improved understanding of the concepts that are discussed.

Chapter 2 is a thorough treatment of the phenomenological aspects of phase diagrams without the mathematical complications. Experimentally known binary phase diagrams are discussed under eight different classes. For each class, unique discussions are provided on the variants such as those displaying positive or negative azeotropy or those displaying Bancroft points that are rarely considered in detail in any other book of this nature. Ternary phase diagrams are also treated for systems showing one, two, or three partially or totally immiscible binary subsystems. Phase diagrams for polymer solutions that display lower or upper critical solution temperatures are discussed along with clear descriptions of the cloud point and shadow curves in ternary mixtures.

Chapter 3 is devoted to the experimental determination of phase equilibria using synthetic, analytical, and transient (that are based on mass or heat flow) methods. Due consideration is given to experimental uncertainties and their impact on the determination of phase boundaries.

The remaining chapters of the book deal with more quantitative aspects of phase equilibria. Chapter 4 provides a review of the thermodynamic variables and functions, setting the stage for the computational aspects that are covered in the chapters that follow. Chapter 5 is devoted to stability and equilibrium criteria with specific discussions addressing the phase equilibria of pure substances as well as binary mixtures and “special states” like critical points, azeotropic points, or critical endpoints. Algorithms are provided for calculations of phase equilibria and critical curves. The thermodynamic aspects of calculations related to solid-fluid equilibria are treated in Chapter 6.

Chapter 7 is a concise but thorough treatment of equations of states for pure fluids such as the ideal gas, virial equation, cubic equations (van der Waals, Redlich–Kwong, Redlich-Kwong-Soave, and Peng–Robinson) and equations of state based on molecular theory (hard sphere, perturbed hard chain, SAFT). Equations of state for mixtures are treated in Chapter 8 with a focus on mixing theories and combining rules that are developed from consideration of radial distribution functions. How these mixing theories and rules are used in transforming the known equations of state for pure fluids to mixtures is discussed. In Chapter 7, the authors raise the question “which equation of state is the best?” and discuss this in terms of warnings for pitfalls and how one obtains the parameters needed.

The final chapter of the book is on global phase diagrams. This chapter describes the tools for the discovery of phase diagrams in a systematic manner which may not have yet been experimentally observed. Global phase diagrams that can be parametrically generated for specific models such as van der Waals, Redlich–Kwong, Carnahan-Starling-Redlich-Kwong, and Carnahan-Starling-van der Waals equation of states are presented.

I do hope that you will find this monograph of great value and view it as an indispensable volume.

Erdogan Kiran
Series Editor
Blacksburg, Virginia
December 2011

Preface

Why yet another book on phase equilibrium thermodynamics?

Why a book on phase equilibrium thermodynamics now?

Of course, many textbooks on thermodynamics, especially on the subject of phase equilibria, have been published during the previous 100 years. Some textbooks, however, deal with high-pressure phase equilibria only superficially or not at all. This is regrettable, because high pressures can do more than merely shift boiling temperatures by a few degrees. Instead, high pressures can bring about qualitative changes of phase equilibria and give rise to unusual phase separation phenomena.

This has been known for a long time. But only the advent of electronic computers made the rapid development of this field of science possible that we have seen since the last third of the previous century, and that is still going on. One of the reasons for this is the fact that many authors of old were hampered by the lack of fast computers in their time, and therefore forced to leave many concepts unexplored. In this book we want to review the phenomenology and thermodynamics of fluid phase equilibria with a special focus on their computation, bringing together the old (better: timeless) concepts and up-to-date numerical mathematics.

The other reason is that the development of electronic computers, but also the progress in fluid phase thermodynamics, led to completely new insights and ideas — of which many have not been fully explored yet, and which are seldomly found in recent textbooks.

The number of high-pressure applications in chemical and petrochemical technology, especially those involving supercritical fluids, has been increasing over the previous decades: there are high-pressure polymerisation processes, drug and flavour extractions from biological material by supercritical fluid extraction, toxic waste treatment by supercritical water oxidation, or the wide field of natural oil and gas recovery and processing, etc. — a quantitative as well as qualitative understanding of these processes and their underlying principles is more important than ever.

Our personal motivation for writing this book, however, is that we find this field of high-pressure fluid phase equilibria fascinating. Even after so many years of research, there is still so much to do: new classes of chemical compounds have to be modelled, the phase behaviour of new equations of state analysed, new phase diagram topologies discovered, better algorithms designed, and connections to other fields of science explored (quantum mechanics, theory of transport properties, . . .).

With this book we hope to convey some of this fascination to our readers.

* * *

First of all, we wish to thank our mentor, Gerhard M. Schneider (Ruhr University, Bochum), who introduced both of us to the world of high pressures and the beauty of thermodynamics.

This book owes its existence to Erdogan Kiran (Virginia Tech, Blacksburg, VA), the editor of the series, who encouraged us to write it and helped us with valuable advice.

We furthermore wish to thank Attila R. Imre (KFKI Atomic Energy Research Institute, Budapest) for critically reading the manuscript.

We cordially thank many colleagues with whom we cooperated and who inspired us. They will find their tracks in this book.

Last but not least we wish to thank our families, without whose unfailing support we would not have been able to write this book.

Ulrich K. Deiters
Thomas Kraska

Chapter 1

Introduction

Before going to the main chapters of the book, it seems advisable to describe its objectives and scope. Furthermore, we will introduce some conventions and (hopefully) provide the reader with motivation to continue.

1.1 WHAT ARE FLUIDS?

It is a common knowledge that there are three different states of aggregation, namely solid, liquid, and gas.[1] Why is the term “fluid” needed?

In everyday life, it is easy and practical to distinguish between liquids and gases (or vapors). However, everyday life takes place at low pressures around 0.1 MPa only – for humans at least. But there are environments where high pressures naturally occur, for instance at the bottom of the oceans (up to 110 MPa), in deep geological strata, and especially in natural oil and gas reservoirs. Furthermore, there are many technical applications that involve elevated pressures, e.g., gas and oil pipelines, thermal power plants, refrigeration systems, and numerous chemical production processes. In the world of high pressures, however, it is no longer trivial to distinguish between liquids and gases. In fact, there are continuous transitions between the liquid and the gas state, i.e., gradual transitions that change one into the other without ever involving a phase transition, namely by passing through the supercritical region, where the distinction between liquid and gas is no longer meaningful.

We use the word “fluid” here as a generic term for all states of aggregation that are not solid, where “solid” indicates a state of matter with a long-distance order (periodicity of molecule locations)[2]: fluids have no long-distance order, and their constituent molecules can move about.[3]

---

[1] Sometimes, the plasma state is counted as the fourth state. A plasma, however, contains ionized species and is, therefore, chemically different from the normal gas.

[2] There are borderline cases, e.g., amorphous solids, glasses, or liquid crystals, but these will not be considered in this book.

[3] There is also mobility in solids, but the diffusion constants are usually smaller than those of liquid and gases by several orders of magnitude.

High-Pressure Fluid Phase Equilibria. DOI: 10.1016/B978-0-444-56347-7.00001-3

Because of this mobility, the equilibration of fluid phases is usually rapid, unless the viscosity is very high. If a phase separation occurs, the coexisting phases separate on a macroscopic scale. Phase equilibria involving fluid phases are, therefore, the foundation of many chemical separation techniques. Important examples are distillation or extraction.

1.2 WHY SHOULD YOU READ THIS BOOK?

What is so complicated about fluid-phase equilibria that one should write a book about this subject?

At a first glance, the subject seems simple: the most common type of equilibrium between two fluid phases is the liquid–vapor transition (boiling or condensation) of a pure compound. Of course, the boiling point of a pure compound depends on pressure. The relationship between boiling temperature and pressure is graphically represented in a phase diagram by the vapor pressure curve.

The phase diagram of a pure compound contains exactly one vapor pressure curve, which originates in a triple point and ends – if the physically accessible temperature range is not restricted by decomposition reactions – in the critical point. Here, liquid and vapor become identical. There is only one critical point, and there is only one kind of fluid-phase equilibrium, namely the vapor–liquid equilibrium.[4]

The situation is more complicated in mixtures: in a mixture of two compounds, each compound has its own vapor pressure curve, and the vapor–liquid phase behavior of the mixture depends on the locations of these vapor pressure curves relative to each other. Because a binary mixture, according to Gibbs' phase rule, has one thermodynamical degree of freedom more than a pure compound, there are now critical curves to consider instead of merely critical points. As a further complication, a new kind of phase equilibrium can occur, namely liquid–liquid demixing. Here, the mutual miscibility of the compounds depends on the external parameters pressure and temperature. Furthermore, there can be complicated interactions between liquid–liquid and vapor–liquid phase behavior. Like the latter, liquid–liquid phase equilibria have critical curves too. Therefore, it is possible to have two or three critical curves in the phase diagram of a binary mixture; theoretically, far higher numbers are conceivable.

Now the thermodynamic conditions of phase equilibrium and phase stability have been known since the end of 19th century. Since more than 100 years, there are thermodynamic models, especially thermal equations of state and lattice gas models, which yield expressions for the Gibbs or Helmholtz energy

---

[4] An apparent exception from this rule are liquids undergoing chemical reactions on heating, like phosphorous or sulphur, but these should rather be treated as mixtures from a thermodynamic viewpoint.

of fluid mixtures.[5] One might expect that, by application of the criteria for phase equilibria to these models, one should be able to derive all possible phase equilibrium phenomena in liquid or gaseous mixtures.

However, even for simple equations of state, the criteria of phase equilibrium lead to systems of nonlinear equations of such complexity that their solution has become practically feasible after the invention of electronic computers only. The earliest publications on the quantitative calculation of fluid-phase equilibria from equations of state using electronic computers date from about 1960.[6] Nowadays, with powerful computers being available worldwide, more than 1500 different equations of state and mixing theories are used for modeling various thermodynamic properties of mixtures. In connection with modern electronic data banks, phase diagrams can be – seemingly – generated at the press of a button.

Does this mean that the theory of phase equilibria has become obsolete? This would be a dangerous conclusion: Automated computation methods may work well for some not too complicated mixtures, but seriously fail otherwise; this book contains many phase diagrams that cannot be treated as routine cases. We feel that an understanding of the principles of fluid-phase equilibria is essential.[7] Moreover, the experimentalist constructing an apparatus for the determination of phase equilibria as well as the theoretician developing a computer program for their calculation always start with some preconception of what the outcome will be or might be. But there are pitfalls, e.g.:

- It is a common technique to determine two-phase equilibria by removing and analyzing samples from the top and bottom of an otherwise sealed vessel. But then an unexpected three-phase equilibrium may escape detection.
- A computer program for the calculation of heats of mixing will not warn its users if the input data specify a state within a two-phase region – unless the programmer had been aware of this possibility.

Evidently it is necessary that those working with thermodynamic apparatus or programs are aware of the phase-theoretical possibilities and pitfalls of their objects of study. Phase diagrams may sometimes be confusing, but they obey certain rules, and it is important to know these rules. This book aims at providing the necessary in-depth information about fluid-phase equilibria and their calculation, combining recent developments in thermodynamics and numerical mathematics.

---

[5] Readers interested in the history of the modeling of fluid-phase equilibria are advised to read the charming book *How fluids unmix* by J. M. H. Levelt Sengers [1].

[6] Van Laar investigated theoretical aspects of the phase behavior of mixtures based on the van der Waals equation of state already around 1900. At the end of his life, he remarked “My hair stands on end even today when I am reminded of that work.” (cited after [2], p. 163)

[7] “Perilous to us all are the devices of an art deeper than we possess ourselves.” (Gandalf, cited in [3])

1.3 WHAT IS THE SCOPE OF THIS BOOK?

This book will help the reader to understand and interpret phase diagrams of fluid mixtures, especially fluid mixtures under elevated pressures, where the vapor phase – if the term is meaningful – is no longer ideal. It will introduce the reader to the multitude of phase-diagram topologies that can occur even for two-component mixtures. In addition, it will also present some ternary phase-diagram topologies of special importance.

Furthermore, this book discusses the thermodynamic conditions of phase equilibria and their application to the calculation of phase equilibria and related properties from equations of state.

The calculation of phase equilibria is, in fact, a central theme of this book. Therefore, it considers all aspects of such calculations: thermodynamic principles, equations of state and mixing rules, algorithms, programming considerations – all that is needed to let the reader eventually write his or her own computer program.

Of course, an exhaustive treatment of all aspects of phase diagram computation would require not one book but many. Therefore, some aspects can only be touched superficially:

- In this book, we assume that the reader is familiar with the basic concepts of thermodynamics.
- In the end, thermodynamic calculations are usually compared with experiments. Therefore, we briefly discuss the main types of phase equilibrium apparatus and provide references to contemporary reviews. However, this book is not a handbook for experimentalists, nor is there enough space for reviewing the experimental designs of more than a century.
- The number of equations of state of the fluid state that were proposed in the past decades is huge. Herein, we can only list a few representative equations of state and mixing rules – enough to explain principles and to demonstrate their use, but certainly far from exhaustive. In particular, the statistical thermodynamics of equations of state and mixing rules is treated rather superficially only.
- In many places, algorithms for the computation of phase equilibria and related properties are outlined. But we do not present ready-to-compile computer code. Instead, it is assumed that the reader can formulate these algorithms in his preferred programming language.

This book focuses on phase equilibria and related thermodynamic properties, including some solid–fluid phase equilibria, mostly of binary fluid mixtures. Many of the computational methods discussed here can also be applied to multicomponent mixtures. However, a full discussion of multicomponent phase equilibria would have increased the size of this book too much; furthermore, the knowledge of the phase behavior of fluid multicomponent mixtures is still rather incomplete, even after more than 100 years of research.

1.4 DO YOU HAVE TO READ THE WHOLE BOOK?

No!

If only an overview over the possible phase diagram topologies is desired, it is sufficient to read Chapter 2 and eventually – for a systematic approach to the problem – Chapter 9.

Readers interested in thermodynamic calculations should be interested particularly in Chapter 4, which contains a short overview of the thermodynamic functions relevant for phase equilibrium calculations as well their mutual relations, and Chapter 5, which contains the thermodynamic conditions of phase equilibria, their applications, and many algorithms.

Chapter 6 deals with solid–fluid equilibria. It can be skipped by readers not interested in solid phases.

The chapters on equations of state and mixing rules are necessary for those interested in the development of computer programs. They offer some criteria for the selection of equations of state. Evidently, readers who already know which equation they need may skip these chapters.

But of course the various aspects of fluid-phase equilibria – phenomenology, thermodynamics, equations of state, etc. – are interconnected, and the attentive readers will find many cross-references between the chapters of this book. Therefore, reading the whole book is recommended.

1.5 SOME CONVENTIONS

Before entering into the discussions of phase behavior and its thermodynamic background, it is necessary to adopt a few conventions and definitions:

- Unless stated otherwise, the most volatile component of a mixture (more precisely: the component with the lower critical temperature) is referred to as species 1. In lattice gas models, index 0 refers to the vacancies ("hole species").

  At present, there is no universally accepted standard for the numbering of components. Care is advised when studying further literature.

  If – for improved clarity in lengthy equations – the component subscripts are omitted, symbols without subscripts refer to component 1.
- No distinction is made between "vapor" and "gas".[8] If phases must be indicated in equations or diagrams, the following abbreviations are used:
  - l – liquid phase
  - g – gas/vapor phase
  - f – fluid phase
  - s – solid phase

---

[8] In the literature, the term "vapor" is sometimes reserved for a gas phase in equilibrium with a liquid phase.

If more than one solid phase is present, the phases are referred to as s_α, s_β, …, with s_α denoting the phase that is stable at the highest temperature.

- Combinations of phase indicators denote phase equilibria, e.g.,
  - **lg** – vapor–liquid equilibrium, coexistence of a liquid phase **l** and a gas phase **g**
  - **llg** – (more explicitly: **l₁l₂g**) – Three-phase equilibrium between two liquid phases, **l₁** and **l₂**, and a gas phase **g**
  - **l=g** – liquid–vapor critical point, coalescence of a liquid and a gas phase
  - **sl=g** – coexistence of a solid phase **s** and a critical fluid phase **l=g**
- In many instances, a shorthand notation for partial derivatives is employed:

$$A_{(iVjx)} \equiv \left(\frac{\partial^{i+j} A_\mathrm{m}}{\partial V_\mathrm{m}^i \partial x_1{}^j} \right)_T \tag{1.1}$$

Unless stated otherwise, the variables that are kept constant on differentiation are the *natural* variables of the function (see Section 4), i.e., in case of the Helmholtz energy the (molar) volume and temperature,

$$A_{(x)} = \left(\frac{\partial A_\mathrm{m}}{\partial x_1} \right)_{V_\mathrm{m},T}, \tag{1.2}$$

but pressure and temperature in case of the Gibbs energy,

$$G_{(x)} = \left(\frac{\partial G_\mathrm{m}}{\partial x_1} \right)_{p,T}. \tag{1.3}$$

Chapter 2

Phenomenology of Phase Diagrams

In this chapter, phase diagrams of binary fluid mixtures are described and discussed qualitatively (with the barest minimum of equations). It provides a short introduction into the art of interpreting phase diagrams and gives an overview of the practically relevant phase diagram classes.

2.1 BASIC CONSIDERATIONS

2.1.1 Phase Diagrams — Cuts and Projections

The number of thermodynamic degrees of freedom, i.e., the number of variables[1] that can be *independently* varied to change the state of a system, is given by Gibbs famous *phase rule*, which can be stated as

$$F = N - P + 2 - C, \tag{2.1}$$

where N is the number of components of a mixture, P is the number of coexisting phases, C is the number of constraints, and F is the resulting number of thermodynamic degrees of freedom, which is the difference between the number of thermodynamic variables and the number of equations connecting them. C is often left out, which is a possible source of errors and misunderstandings. At least in the context of this book, the constraints are very important and should not be omitted.

An example is the number of degrees of freedom at the critical point of a pure fluid: there is only one phase present ($N = 1$ and $P = 1$), but the critical conditions Eqs (5.30) and (5.31) provide two constraints ($C = 2$); hence, a pure-fluid critical point has no degree of freedom, i.e., it is a point in graphical representations.

Similarly, one can conclude that critical states of binary mixtures must have $F = 1$, i.e., in this case, there are critical curves.

---

[1] More accurate: intensive variables; see Chapter 4.

High-Pressure Fluid Phase Equilibria. **DOI: 10.1016/B978-0-444-56347-7.00002-5**

According to the phase rule, a binary fluid mixture in the single-phase state has got three degrees of freedom, i.e., a thermodynamic state is specified by three variables, e.g., pressure, temperature, and the mole fraction of one of its components.[2] A two-phase state has got two degrees of freedom: the mole fractions are fixed if pressure and temperature are specified. Its graphical representation is consequently a two-dimensional object in three-dimensional space.

However, three-dimensional phase diagrams are awkward to draw and often hard to understand. In the case of multicomponent mixtures, the dimensionality of the domains is even higher. For practical purposes, it is, therefore, important to reduce the number of graphical dimensions. This can be achieved by two methods, namely by presenting

- cross sections, i.e., by keeping one or more relevant variables constant. This means that the number of constraints, C, is increased, and the number of degrees of freedom, F, is decreased. Cross sections commonly used for the discussion of phase equilibria are:
    - *Isothermal:* constant temperature
    - *Isobaric:* constant pressure
    - *Isoplethic:* constant composition

  Also, *isochoric* (constant volume) or *isopiestic* (constant density) cross sections can prove useful. For multicomponent mixtures, it is desirable or even necessary to keep more than one variable constant.
- projections, i.e., allowing one or more variables to assume all possible values, but omit their axes (dimensions) in the diagram. In this case, the number of graphical dimensions is reduced but not the number of degrees of freedom F.

Figure 2.1 is a schematic phase diagram for a pure fluid. Here, the number of degrees of freedom for an ordinary state is $F = 2$. Therefore, we can plot the phase diagram without reducing the number of graphical dimensions. For the vapor pressure curve lg, there is $F = 1$. The critical point has $F = 0$, as explained above, and is therefore represented by a point. For simplicity, the regions of solid phases have been omitted; hence, the vapor pressure curve extends to absolute zero.

Figures 2.2 and 2.3 are three-dimensional pTx diagrams of a simple binary fluid system, including some phase equilibrium isotherms and isopleths, respectively. A more detailed discussion of the curves and the phase diagram classification will be given later in this chapter. The "front plane" (pT plane at $x_1 = 1$) and the "back plane" (pT plane at $x_1 = 0$) contain the pure-fluid vapor pressure curves as shown in Fig. 2.1. Figure 2.4 shows the projection of Fig. 2.3 onto the

---

[2] The mole fraction of the other component is then given by $x_2 = 1 - x_1$ and hence not an independent variable.

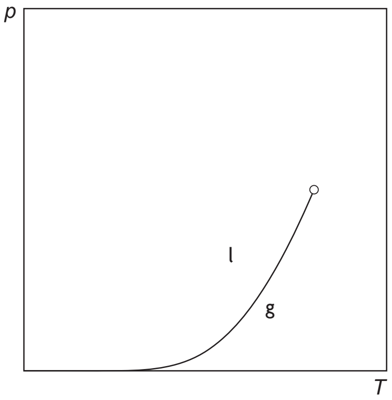

FIGURE 2.1 Schematic pT phase diagram of a pure fluid. ——: vapor pressure curve, ○: critical point. Solid-phase regions have been omitted.

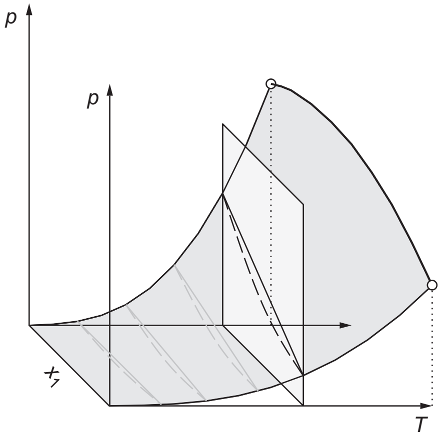

FIGURE 2.2 Schematic pTx phase diagram of a simple binary fluid mixture, with a px cross section indicated. ○: pure-fluid critical point; ——: vapor pressure curve; ━━: critical curve, gray area: two-phase region. Solid-phase regions have been omitted.

pT plane. Evidently the projection and the cross section can look quite different, even if they describe the same two-phase region.

It should be noted that the isoplethic cross section in Fig. 2.3 contains only one critical point $F = 0$, namely, where it touches the critical curve, whereas Fig. 2.4 contains a critical curve ($F = 1$).

Caution is advised when cross sections and projections appear in the same diagram.

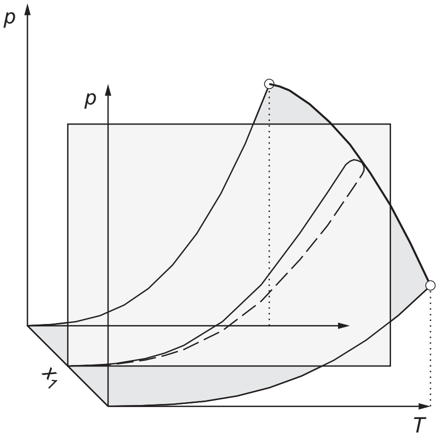

FIGURE 2.3 Schematic *pTx* phase diagram of a simple binary fluid mixture, with a *pT* cross section indicated. The symbols are the same as shown in Fig. 2.2.

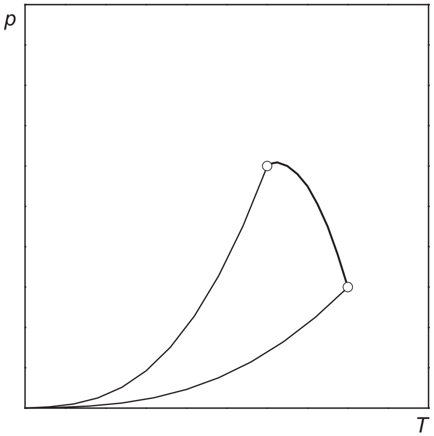

FIGURE 2.4 *pT* projection of the three-dimensional phase diagram as shown in Fig. 2.2 or 2.3.

2.1.2 Subcritical Vapor–Liquid Equilibria

The simplest kind of phase diagrams occurs when both components are nearly ideally miscible (a more precise definition will be given in Section 4.3), and the temperature is below the critical temperature of both components. In this case, the binary phase diagrams must contain the boiling points of both pure components.

An example of an isothermal phase diagram is shown in Fig. 2.5. If component 1 is the more volatile one, it has got the higher vapor pressure.

A pure fluid shows a sharp vapor–liquid transition: at a given temperature, there is a fixed boiling pressure. Mixtures generally have boiling pressure

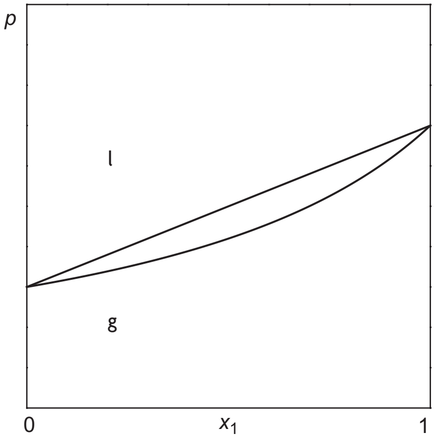

FIGURE 2.5 Isothermal phase diagram of the vapor–liquid equilibrium of an ideal mixture (schematic).

ranges. The pressure at which the liquid begins to boil is not the same as the pressure at which the last drop evaporates. Consequently, the phase diagram shows two phase boundary curves. The upper curve, called the *bubble point curve*, separates the liquid domain at high pressure from the two-phase region; the lower curve, called the *dew point curve*, separates the vapor region at low pressures from the two-phase region.

In the special case of an ideal mixture, the two curves can be calculated from Raoult's and Dalton's laws. According to the former, the partial pressure of a component is related to its vapor pressure, p_i^σ, and to the composition of the liquid:

$$p_i = x_i^{\mathrm{l}} p_i^\sigma . \tag{2.2}$$

The total pressure is then

$$p = x_1^{\mathrm{l}} p_1^\sigma + x_2^{\mathrm{l}} p_2^\sigma = p_2^\sigma + (p_1^\sigma - p_2^\sigma) x_1^{\mathrm{l}}, \tag{2.3}$$

and therefore, the bubble point curve $p(x_1^{\mathrm{l}})$ is linear. The dew point curve $p(x_1^{\mathrm{g}})$ can then be obtained from Dalton's law:

$$p_i = x_i^{\mathrm{g}} p. \tag{2.4}$$

Equating the partial pressure with that from Raoult's law, Eq. (2.2), and using Eq. (2.3) to eliminate x_1^{l} then gives

$$p = \frac{p_1^\sigma p_2^\sigma}{p_1^\sigma - (p_1^\sigma - p_2^\sigma) x_1^{\mathrm{g}}}, \tag{2.5}$$

which is clearly a hyperbolic function. Alternatively, we can use Eq. (2.3) to eliminate p, which leads to the relation between the liquid and the vapor composition,

$$\begin{aligned} x_1^{\mathrm{g}} &= \frac{x_1^{\mathrm{l}} p_1^{\sigma}}{p_2^{\sigma} + (p_1^{\sigma} - p_2^{\sigma}) x_1^{\mathrm{l}}} \\ &= \frac{\alpha x_1^{\mathrm{l}}}{1 + (\alpha - 1) x_1^{\mathrm{l}}} \quad \text{with } \alpha = \frac{p_1^{\sigma}}{p_2^{\sigma}}. \end{aligned} \tag{2.6}$$

A plot of x_1^{g} versus x_1^{l} is called a McCabe–Thiele diagram; it shows the concentration enhancement obtained by a single distillation step (Fig. 2.6). This kind of diagram is very important in chemical engineering, where it is used for the design of rectification columns.

The ratios of the vapor and liquid mole fractions are called K factors:

$$K_i = \frac{x_i^{\mathrm{g}}}{x_i^{\mathrm{l}}}. \tag{2.7}$$

For an ideal mixture, Raoult's and Dalton's laws imply

$$K_i = \frac{p_i^{\sigma}}{p}. \tag{2.8}$$

Consequently, a double logarithmic plot of K_i versus pressure must be linear with a slope of −1 (Fig. 2.7).

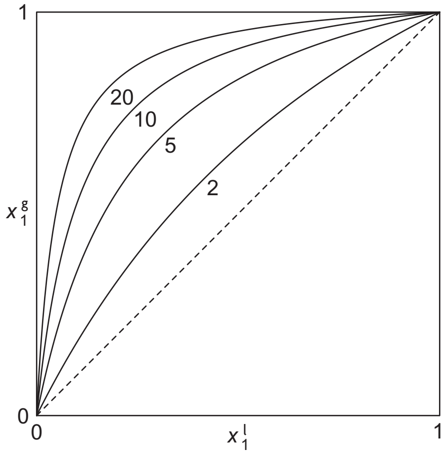

FIGURE 2.6 Isothermal McCabe–Thiele diagram of an ideal mixture. Parameter: ratio of the pure-fluid vapor pressures.

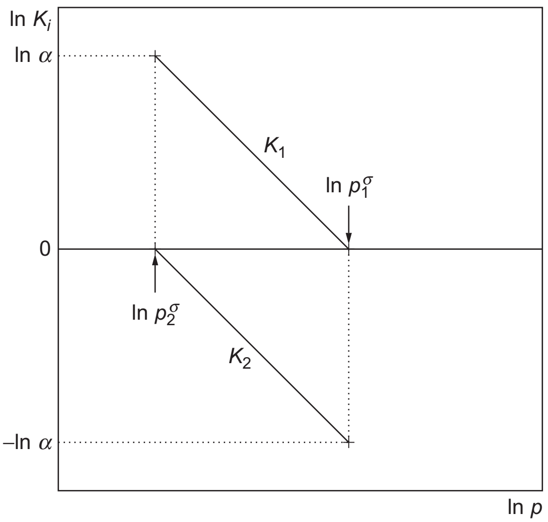

FIGURE 2.7 K factors of an ideal subcritical mixture, isothermal cross section.

The *isobaric Tx* diagram of an ideal mixture is more complicated to derive and will be dealt in Section 5.5.5.

2.1.3 The Lever Rule

A point within the two-phase domain of Fig. 2.5 describes an impossible situation. The mixture represented by such a point undergoes a phase separation and splits into two coexisting phases. Their amounts can be calculated with the *lever rule of phase equilibria*, which can be derived from the material balance equations. The amount of substance of component 1 in the system, n_1, can be obtained from the amounts of the coexisting phases, n' and n'', and the overall mole fraction x_1, i.e., the mole fraction that the mixture would have if there were no phase separation,

$$n_1 = x_1 n = x_1(n' + n''), \tag{2.9}$$

or from the amounts of component 1 in each phase,

$$n_1 = n_1' + n_1'' = x_1' n' + x_1'' n''. \tag{2.10}$$

Equating these two relations and rearranging yields

$$n'(x_1 - x_1') = n''(x_1'' - x_1), \tag{2.11}$$

which looks like the lever rule from mechanics, if the x_i differences are interpreted as lengths of the lever arms and the n_i as attached weights. The application of the lever rule is illustrated in Fig. 2.8.

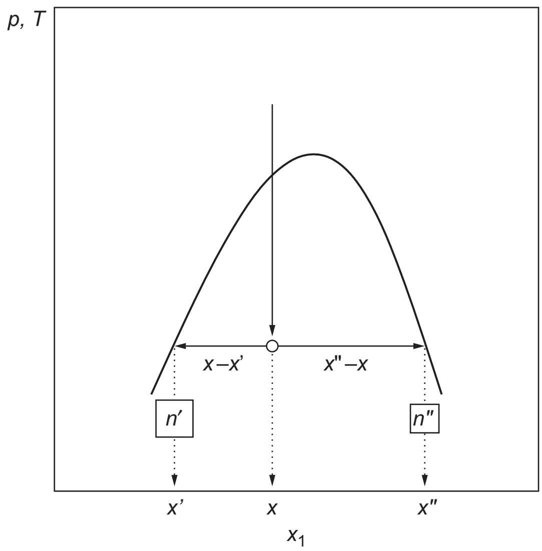

FIGURE 2.8 Schematic representation of the "lever rule" of phase equilibria: the amounts of the coexisting phases, weighted with their "lever lengths" $x_1 - x_1'$ and $x_1'' - x_1$, respectively, must be equal.

The lever rule can be used to explain the complete evaporation of a liquid mixture:

- The evaporation process begins with a liquid of composition x_1 (state A in Fig. 2.9).
- When the pressure is slowly reduced, nothing happens until state B is reached, the intersection with the bubble point curve. Here, the first infinitesimal bubble of the vapor phase forms. This bubble has a higher mole fraction of the more volatile component 1. As the "lever" of the liquid phase, $x_1 - x_1'$, is still zero, so is the amount of the vapor phase.
- When the pressure is lowered further, the amount of vapor increases and that of the liquid decreases; furthermore, the liquid predominantly loses component 1. Consequently, the composition of the liquid of the two-phase equilibrium state C is shifted toward lower mole fractions, and the composition of the equilibrium vapor phase decreases, too.
- At state D, the vapor phase has reached the original composition x_1. Now the "lever" $x_i'' - x_1$ becomes zero, and therefore, the liquid phase vanishes: the last drop of liquid evaporates at the dew point curve.
- Below this state only single-phase vapor is expanded (state E).

This consideration might seem trivial, but it will be shown in the next section that there are phase diagrams that lead to counter-intuitive results.

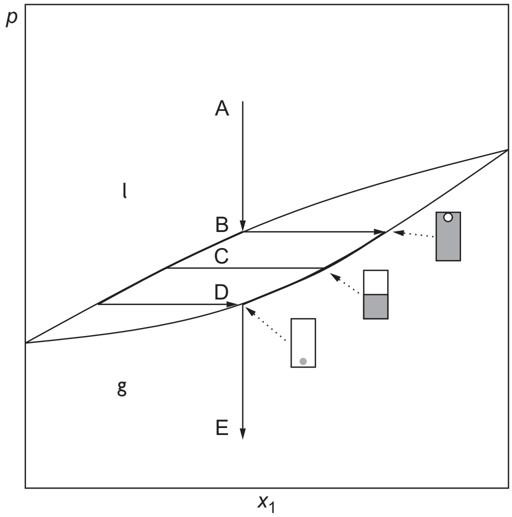

FIGURE 2.9 Schematic representation of an isothermal evaporation: the path through the phase diagram and the contents of a pressure vessel. See the text for a detailed explanation.

The horizontal lines connecting the liquid states with the coexisting vapor states are called *connodes*, binodes, or tie lines.

2.1.4 Supercritical Vapor–Liquid Equilibria

If one of the components of a mixture is above its critical temperature, the shape of the phase diagrams changes dramatically (Fig. 2.10): the two-phase region starts at the boiling point of the less volatile compound as shown in Fig. 2.9, but now there is no boiling point of the volatile component to which the phase boundary curves could run. Instead, the dew point curve bends around and meets the bubble point curve in a *binary critical point*, which in isothermal or isobaric vapor–liquid phase diagrams is an extremum of the phase envelope.

Figure 2.10 also demonstrates a peculiarity of supercritical phase diagrams: if the initial state of an expansion experiment is at high pressure and at an overall mole fraction to the right side of the critical point, a reduction of the pressure does not make the fluid boil, but rather causes the condensation of a liquid. Further, pressure reduction lets the amount of the liquid first grow, then shrink; because of the lever rule, the maximum amount of liquid phase occurs where the dew point curve has its mole fraction maximum. Finally, the last drop of the liquid evaporates, and the system is in a single-phase gas state.

Along this special path in the phase diagram, a pressure reduction can cause condensation and a pressure increase can cause evaporation. An analogous discussion of an isobaric phase diagram would have shown the possibility of condensation on heating or evaporation on cooling. This phenomenon is

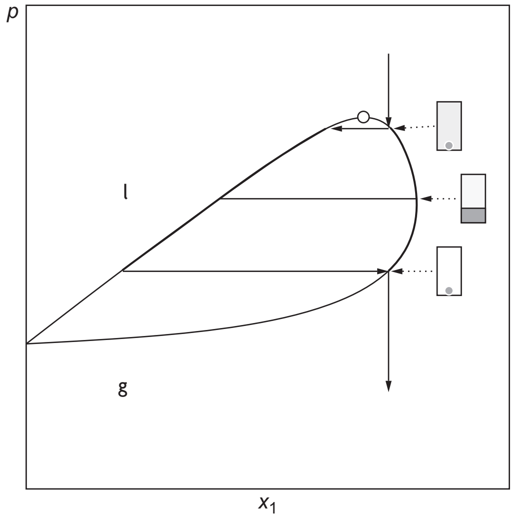

FIGURE 2.10 Schematic representation of an isothermal evaporation (supercritical case): the path through the phase diagram and the contents of a pressure vessel. A more detailed explanation is given in the text. ○: binary critical point.

called *retrograde condensation* or *evaporation*, and it is often observed in phase equilibria involving supercritical compounds.

The mole fraction maximum of an isothermal dew point curve is called *maxcondentherm* or *cricondentherm* (for isobaric dew point curves: *maxcondenbar* or *cricondenbar*). It represents the highest mole fraction up to which a phase separation can be achieved by pressure variation at constant temperature (maxcondenbar: temperature variation at constant pressure). Mixtures beyond the maxcondentherm composition can be expanded from high to low pressures without crossing phase boundaries. Along an isopleth, the maxcondentherm is a temperature maximum and the maxcondenbar a pressure maximum.

The McCabe–Thiele diagram for this case, Fig. 2.11, shows that the equilibrium curve ends on the diagonal in a binary critical point with a slope of −1 (see Section 5.5.2 for the proof).

The volumes of the coexisting phases can be calculated from their molar volumes and the amounts of substance, $V = nV_\mathrm{m}$. Inserting this into the lever rule gives

$$\frac{V'}{V'_\mathrm{m}}(x_i - x'_i) = \frac{V''}{V''_\mathrm{m}}(x''_i - x_i). \tag{2.12}$$

If the two phases occupy equal volumes in the phase equilibrium cell, $V' = V''$, this equation can be rearranged to give the “central” overall mole

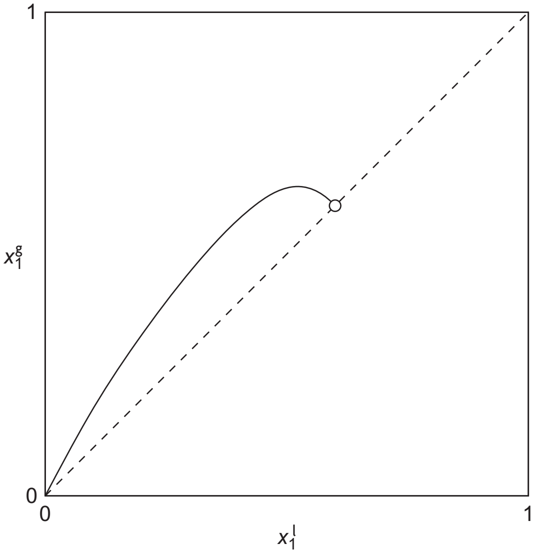

FIGURE 2.11 McCabe–Thiele diagram (schematic) for a mixture where component 1 is supercritical. ○: binary critical point.

fraction

$$x_{i,q_V=0.5} = \frac{V'_\mathrm{m}x''_i + V''_\mathrm{m}x'_i}{V'_\mathrm{m} + V''_\mathrm{m}} = \frac{x'_i\rho' + x''_i\rho''}{\rho' + \rho''}. \tag{2.13}$$

Conversely, if – at given pressure and temperature – a mixture of composition $x_{i,q_V=0.5}$ is introduced into the pressure vessel, it splits into two phases, each taking up half of the available space. At a first glance, it may seem surprising that neither the amount of the mixture nor the size of the vessel have to be specified, but of course only with the "right" amount of substance, the desired pressure can be reached.

The fraction of a system taken up by the vapor phase is called *quality*,[3]

$$q_V = \frac{V''}{V' + V''}. \tag{2.14}$$

Curves measured at constant gas-to-liquid ratio are called *quality lines*. A curve representing the "central" mole fraction $x_{i,q_V=0.5}$ in a phase diagram has got the quality $q_V = 0.5$; the quality lines 0.0 and 1.0 correspond to the bubble and dew point curves, respectively.

---

[3] This fraction can be defined in terms of volume or amount of substance; both definitions exist in the current literature. Herein, we use the volumetric quality, which is of greater practical importance, for it can be measured without knowing the chemical composition of the system.

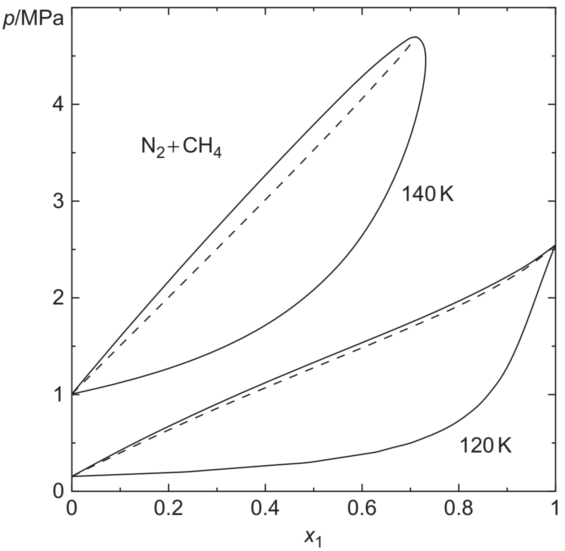

FIGURE 2.12 Isothermal phase diagram of the {nitrogen + methane} system, subcritical and supercritical case. ——: phase boundaries; – – : quality curves 0.5.

For vapor–liquid equilibria at low pressures, the molar volume of the vapor is much larger than that of the liquid, and consequently, the quality curve 0.5 is close to the bubble point curve, $x_{i,q_V=0.5} \approx x_i^{\mathrm{l}}$, as can be seen in Fig. 2.12. For liquid–liquid phase equilibria or high-pressure vapor–liquid equilibria, however, the densities of the coexisting phases are of comparable size and change slowly with temperature or pressure. This is illustrated in Fig. 2.13. In supercritical phase diagrams, the quality curves end on critical points of the mixture.

The transition from the subcritical phase diagram type, Fig. 2.9, to the supercritical type, Fig. 2.10, occurs through a phase diagram with a cusp at $x_1 = 1$, as shown in Fig. 2.14. The slopes of the dew point curve and the bubble point curve are usually not zero[4]; the proof is given in Section 5.5.4.

Phase diagrams in the vicinity of the critical point of the volatile component sometimes show a “bulging” of the dew point curve as illustrated in Fig. 2.15. A fluid mixture with a high concentration of the volatile component would, on decompression, first precipitate a liquid phase, then become homogenous, then precipitate a liquid again, and finally become homogeneous. This phenomenon is called *double retrograde behavior*. It has been experimentally observed for few mixtures only – probably not because it is rare, but because its observation is difficult: the “bulge” of the dew point curve is usually less than 10^{-3} mole

---

[4] The exception is critical border azeotropes.

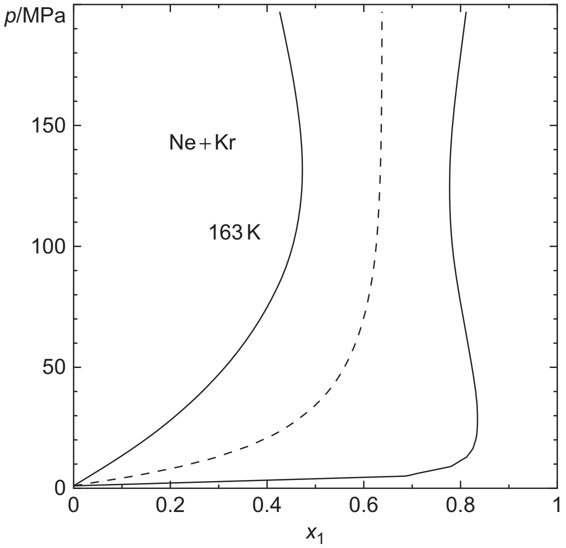

FIGURE 2.13 Isothermal phase diagram of the {neon + krypton} system. ——: phase boundaries; – – : quality curve 0.5.

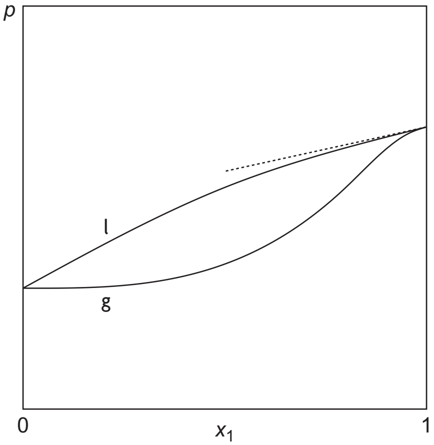

FIGURE 2.14 Isothermal phase diagram of a binary mixture at the critical temperature of the volatile component (schematic). The tangent to both equilibrium curves at the critical point is not horizontal.

fraction units. Double retrograde behavior has been found not only in simple systems like {nitrogen + ethane} or {methane + butane} but also in more complicated systems like {ethane + limonene} or {carbon dioxide + 1-nonanol }[4]. Retrograde behavior of a higher order than 2 is rather unlikely [5].

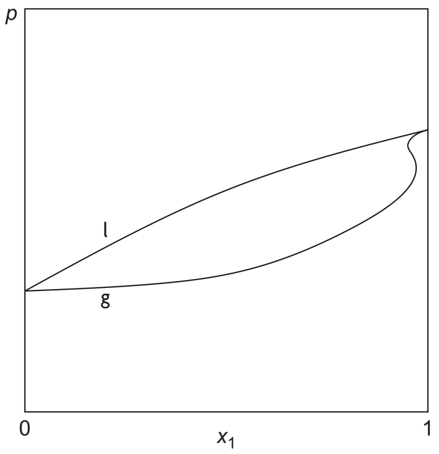

FIGURE 2.15 Isothermal phase diagram of a binary mixture showing double retrograde behavior (schematic; the "bulge" of the dew point curve is very much exaggerated for clarity).

2.1.5 Volumetric Behavior

Fig. 2.16 displays a volumetric phase diagram for a simple vapor–liquid equilibrium case like the one shown in Fig. 2.12:

- In the subcritical case, there are two distinct curves, one for the liquid phase and another for the vapor phase. As the pressure increases with increasing mole fraction of the volatile component, the molar volume of the vapor phase declines rapidly. The liquid phase is usually not very compressible; its density varies little with pressure.
- In the supercritical case, the liquid and the vapor branch meet at the binary critical point. Because of the retrograde behavior, the vapor branch passes over a mole fraction maximum (maxcondentherm or maxcondenbar). The liquid branch sometimes exhibits a shallow minimum. It is the result of two conflicting influences, namely, the pressure increase along the curve and the increased solubility of the volatile component. Usually the critical point does not coincide with this minimum.

Between these two cases, there is the critical case, where the binary critical point coincides with the critical point of the pure fluid 1 ($x_1 = 1$, $T = T_{c,1}$). In this case, the binary critical point is necessarily at a mole fraction maximum of the $V_m(x_1)$ curve.

In the case of high-pressure vapor–liquid equilibria, the vapor phase can of course attain relatively high densities. If the volatile component has a large molar mass, it can happen that the mass density (specific gravity) of the vapor phase becomes larger than that of the liquid phase. This phenomenon is known as *barotropy* or *barotropic inversion*. It has been experimentally observed for mixtures of hydrocarbons with CO_2, SF_6, or halocarbon refrigerants.

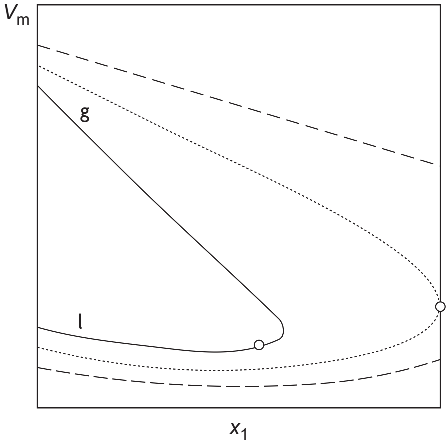

FIGURE 2.16 (Isothermal) volumetric phase diagram for a simple vapor–liquid equilibrium case (schematic). – – : subcritical case; ⋯⋯: critical case ($T = T_{c,1}$); ——: supercritical case.

What happens when a mixture is taken to the barotropic inversion conditions depends very much on the experimental circumstances. Sometimes the liquid and the vapor simply exchange places inside the pressure vessel, with the consequence that analytical instruments look at the “wrong” phase. Sometimes, however, the system forms a fog or foam that can persist for days, because liquid droplets or gas bubbles are no longer separated by gravity anymore; in this case, analytical instruments would eventually report the average composition and create the impression that the mixture is in a single-phase state. Therefore, overlooking barotropic phenomena can be a source of misinterpretations for some classes of phase equilibria.

A crossing of the *molar densities* of the coexisting fluid phases is possible, too, although not for simple systems. Mixtures of class III and higher (see the next sections), however, exhibit continuous transitions from liquid–vapor-like to liquid–liquid-like phase behavior, and here, a switch of the molar densities is possible.

An overview of barotropic phenomena was given by Quiñones-Cisneros [6].

2.2 EXPERIMENTALLY KNOWN BINARY PHASE DIAGRAM CLASSES

As discussed earlier in the previous section, the representation of a complete phase diagram of a binary mixture requires at least three variables, the pressure p, the temperature T, and the mole fraction of one of the substances, e.g., $x = x_1$; sometimes molar volumes or enthalpies have to be considered, too, which increases the number of dimensions that need to be handled. It is clear that, for practical purposes, two-dimensional px and Tx cross sections are the preferred means of visualization. Although these cross sections are relatively easy to read, they represent only a fraction of the total phase behavior of a binary mixture. This is evident if the three-dimensional representations shown in Figs 2.2 and 2.3 are compared with two-dimensional cross sections shown in Figs 2.9 and 2.10.

A *pT* projection, however, is a different matter, because it contains all the relevant topological information, i.e., the connections and relative locations of the points and curves representing special thermodynamic states. For the example shown in Fig. 2.2, the *pT* projection Fig. 2.4 contains the vapor pressure curves and the critical points of the pure components as well as a continuous binary critical curve. For a classification, the information contained in the *pT* projection is already sufficient, as it shows that, in this case, the binary critical curve forms a continuous connection between the pure-component critical points. Furthermore, the *pT* projection can reveal the existence of temperature or pressure extrema of critical curves.

In this chapter, we discuss the *pT* projections of the most important classes of binary phase behavior, including some subclasses involving azeotropy, and provide the corresponding *px* and *Tx* cross sections. For convenience, common line types and symbols are listed in Fig. 2.17. We employ the commonly used nomenclature of van Konynenburg and Scott for binary phase diagrams. The more systematic nomenclature of Bolz *et al*. will be introduced later.

“Most important classes” means that for these classes, experimental evidence has been found. From topological considerations and mathematical models, it is clear that there exist many more phase diagram classes, some of which will be discussed later in this book. But with the phase diagrams presented in this section, the reader should be able to construct cross sections also for unusual phase diagram classes.

○	Critical point of a pure substance
☆	Binary critical point
▽	Lower critical end point
△	Upper critical end point
◇	Critical azeotrope
x	Maxcondentherm and maxcondenbar
———	Vapor pressure curve
———	Binary critical curve in *pT* diagrams or coexistence curve in *px* and *Tx* diagrams
—·—·–	Three-phase curve
············	Curve of azeotrope
············	Isopleth

FIGURE 2.17 Legend for the symbols and lines in the phase diagrams.

Note: The phase diagrams in this section are schematic diagrams only, not real (computed or experimentally determined) examples. They are sometimes distorted to show topological details which might be difficult to make out in real diagrams.

2.2.1 Class I

The simplest binary phase diagram class, class I, contains only one binary vapor–liquid (l=g) critical curve, which connects the critical points of the pure components. Examples for class I phase behavior are the mixtures {Ar + Kr} [7], {N_2 + O_2}, or {C_2H_6 + n-alkane} for carbon numbers up to 18 [8]. Quite often class I critical curves exhibit a pressure maximum as shown in Fig. 2.18.

Fig. 2.18 also contains an isopleth. In a binary system, this is not a coexistence curve,[5] but just a cross section through the three-dimensional vapor–liquid space for a constant mole fraction (see also Fig. 2.3). The critical point of an isopleth is not at one of its extrema – it is merely the point at which the isopleth touches the critical curve and can be located anywhere. In the example shown here, it is between the temperature and the pressure maxima of the isopleth, the maxcondentherm and maxcondenbar states (cf. previous section).

How can the isobaric or isothermal cross sections be constructed from the *pT* diagram? If *Tx* cross sections are desired, one draws a horizontal line in the *pT* projection at the given pressure. For each intersection of this line with a curve of the *pT* projection, a point is plotted into the *Tx* diagram.

- For a pressure below the critical pressures of the two pure components (line 1 in Fig. 2.18), the horizontal line crosses the two vapor pressure curves only. Therefore, one marks the two intersections at $x=0$ and $x=1$ in the *Tx* diagram (cross section 1 in Fig. 2.19). Because there are no other special states at this pressure, there is no other way to connect them but by a subcritical vapor–liquid coexistence region.
- At a pressure between the critical pressures of the two components, the horizontal line crosses the vapor pressure curve of the less volatile substance and the binary critical curve (line 2 in Fig. 2.18). The vapor pressure curve of the less volatile substance is, therefore, marked at $x=0$ in the *Tx* projection. The binary critical point is located at a lower temperature and at a mole fraction somewhere between 0 and 1 (cross section 2 in Fig. 2.19). The two points are connected by a supercritical vapor–liquid coexistence curve with the minimum at the binary critical point.
- When the critical pressure of the less volatile substance is reached, the vapor–liquid coexistence region detaches from the ordinate at $x=0$ and forms a closed loop with a critical point at its maximum and another one at its minimum.
- Finally, when the maximum pressure of the binary critical curve is reached, this closed loop contracts to a single point and vanishes. This point, which corresponds to the pressure maximum of the critical curve in Fig. 2.18, is called an *elliptic pressure maximum critical point* [9].

---

[5] Except for azeotropes, the phase coexisting with a given phase on one isopleth is located on *another* isopleth.

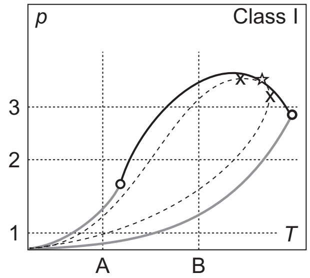

FIGURE 2.18 Phase diagram class I. Note that the pure-fluid critical point with the lower temperature belongs to component 1.

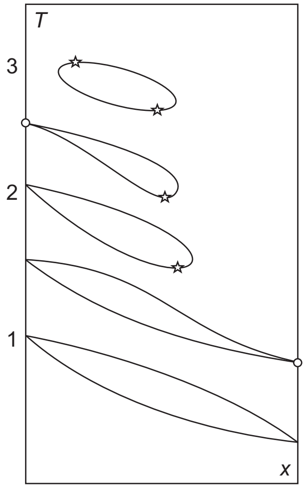

FIGURE 2.19 Class I *Tx* cross sections.

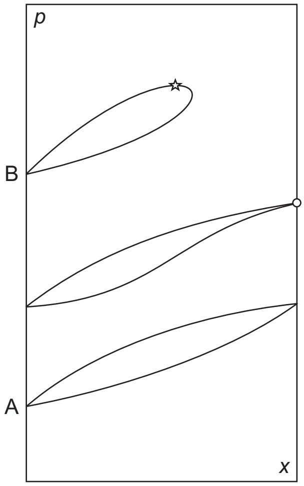

FIGURE 2.20 Class I *px* cross sections.

An isothermal *px* cross section can be constructed in an analogous way by plotting a vertical line in the *pT* projection. The intersections of the curves with this line are plotted into a *px* diagram in Fig. 2.20.

- At low temperatures, the vapor pressure curves of both substances are intersected, yielding a regular vapor–liquid coexistence region in the *px* diagram such as cross section A in Fig. 2.20.
- At the critical temperature of the more volatile substance, this vapor–liquid region detaches from the pressure axis at $x=1$ (cross section between A and B). Then a coexistence region connected to the ordinate at $x=0$ forms, as shown in cross section B. Its pressure maximum is a binary critical point.
- This coexistence region finally contracts and vanishes at $x=0$, when the critical temperature of the less volatile substance is reached.

2.2.1.1 Variants of Class I: Critical Curve with a Pressure Minimum or an S-shape

For some class I mixtures, the binary critical curve passes through a pressure minimum; in such cases, the critical curve often exhibits an S-shape. There may even be a pressure maximum, as depicted in Fig. 2.21. The *px* cross sections belonging to this phase diagram look similar as before, but the S-shape gives rise to some new kinds of *Tx* cross sections. This behavior has been found for mixtures of trifluoromethane with some nonpolar compounds.

- Cross section 1 is below the minimum of the binary critical curve and hence intersects the vapor pressure curves of the pure components only. The resulting *Tx* cross section shows a regular vapor–liquid coexistence region (Fig. 2.22).
- For cross section 2, located between the minimum of the binary critical curve and the critical point of component 1, the horizontal line crosses the two vapor pressure curves and, in between, twice the critical curve. The first point in the *Tx* diagram is, therefore, the boiling point at $x = 1$. Then, with increasing temperature, a critical point is passed, then another, and finally the boiling point at $x = 0$ is reached.
- When the pressure is increased, one of the two coexistence regions shrinks; it vanishes at the critical pressure of the more volatile component 1, while the second 2-phase region remains. This eventually vanishes in the same way as described above for the regular class I phase behavior.

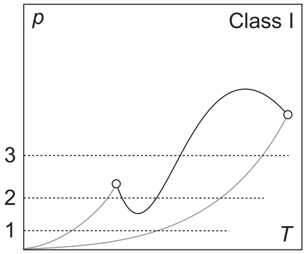

FIGURE 2.21 Class I phase diagram with an S-shaped critical curve.

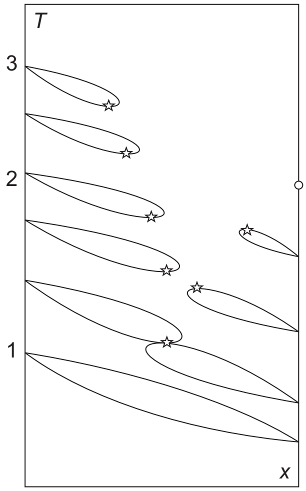

FIGURE 2.22 Corresponding *Tx* cross sections.

2.2.1.2 Variants of Class I: (Positive) Azeotropy

A class I phase diagram can exhibit azeotropic behavior, in which case it is called class I-A. At an azeotropic point, the mole fractions of the coexisting liquid and vapor phase are identical. Therefore, the identification and modeling of azeotropic phase behavior is very important in phase separation technology.

According to Gibbs phase rule, an azeotropic state has $F = 1$ degree of freedom. Therefore, azeotropes correspond to points in px and Tx cross sections, but to a curve in the pT projection. For the termination points of azeotropic curves, there are several possibilities: they can start or end at

- a border azeotrope $x^{\mathrm{az}} = 0$ or $x^{\mathrm{az}} = 1$, i.e., on a vapor pressure curve,
- a critical azeotropic point (here, azeotropic curve and critical curve meet in the pT projection with the same slope; this behavior is also called *absolute azeotropy*),
- an azeotropic endpoint (not for class I systems),
- an azeotropic cusp in case of double azeotropy,
- absolute zero (0 K, 0 MPa)[6]; this termination is hypothetical only, because real mixtures would solidify.[7]

If the vapor pressure of an azeotropic mixture is larger than the vapor pressures of the pure components, this corresponds to a positive deviation from Raoult's law. Therefore this case is called *positive azeotropy*; if the azeotropic vapor pressure is smaller than the vapor pressures of the pure components, the term *negative azeotropy* is used. An azeoptropic pressure between the pure-component vapor pressures can occur only in the case of double azeotropy (see below), which is an extremely rare phenomenon.

At an azeotropic point, the bubble point curve and the dew point curve meet with zero slope. This is also true for the termination points of azeotropic curves. The proof is given in Section 5.5.6.

In the pT projection, the azeotropic curve is above the vapor pressure curves of the pure substances in case of positive azeotropy and below for negative azeotropy. For nonpolar or weakly polar substances, positive azeotropy is more likely, while negative azeotropy is usually found in mixtures where there are strong interactions between the unlike molecules.

Class I-A with positive azeotropy can be further divided into two subclasses, one having a temperature minimum along the critical curve and the other one not. A pT projection for the latter kind of class I-A is shown in Fig. 2.23; the corresponding Tx and px cross sections are sketched in Figs 2.24 and 2.25, respectively. In both representations, the lowermost phase envelopes

---

[6] Mixtures with positive deviations from Raoult's law large enough to cause positive azeotropy would probably show liquid–liquid immiscibility at sufficiently low temperatures. It seems that systems classified as I-A based on experiments are in fact class II-A systems, which solidify before reaching the liquid–liquid immiscibility region.

[7] {^{3}He + ^{4}He} is an exception.

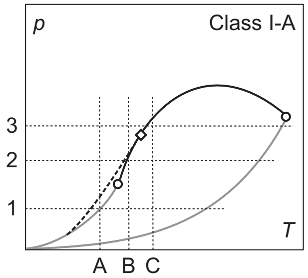

FIGURE 2.23 Class I-A phase diagram.

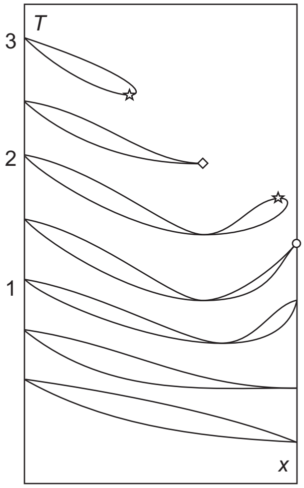

FIGURE 2.24 Corresponding *Tx* cross sections.

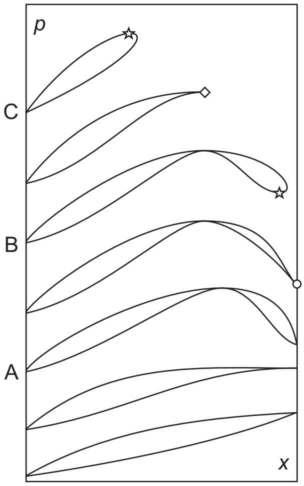

FIGURE 2.25 Corresponding *Tx* cross sections.

are nonazeotropic. Then border azeotropy develops: the bubble point curve and the dew point curve come together in a cusp at $x = 1$ with a horizontal tangent. A further increase of temperature or pressure lets the (still subcritical) azeotrope move away from $x = 1$. Then the two-phase region detaches from the $x = 1$ ordinate and contracts, until it vanishes in a critical azeotropic point.

Examples for this subclass are the systems {ethane + hydrogen sulfide} [10], {carbon dioxide + ethane} [11], and – most important – {ethanol + water}.

It is very easy to confuse the phase envelopes of border azeotropes and critical azeotropes: in both, the bubble point curve and the dew point curve meet in a horizontal cusp; both look like half a regular azeotropic curve. The border azeotrope, however, is a subcritical two-phase state, whereas the critical azeotrope is a one-phase state.

A schematic phase diagram of class I-A with a temperature minimum along the critical curve is shown in Fig. 2.26. The *Tx* cross sections are topologically

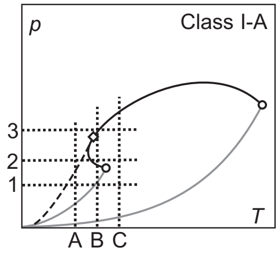

FIGURE 2.26 Class I-A phase diagram with a temperature minimum in the critical curve.

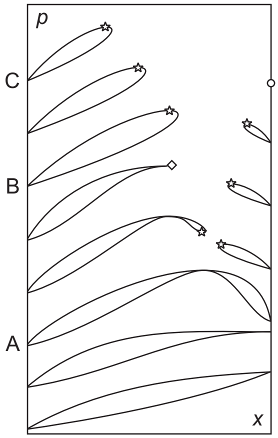

FIGURE 2.27 Corresponding *px* cross sections.

the same as those without the temperature minimum, but the *px* cross sections differ, as shown in Fig. 2.27. In cross section B, the critical curve is intersected two times; hence, there are two critical points in the *px* cross section. These two critical points merge at the temperature minimum of the critical curve. Above that temperature, the two-phase region splits into two parts; below that temperature, it is a regular azeotropic diagram.

Examples for this kind of phase diagram topology are {ethane + dinitrogen oxide} [12] and {ethane + hydrogen chloride} [13].

2.2.1.3 Variants of Class I: Negative Azeotropy

Negative azeotropy is seldomly observed for mixtures of nonpolar compounds. The phenomenon is usually caused by attractive interactions between unlike molecules which are stronger than those between like molecules, and this is often the result of chemical interactions. Examples are {hydrogen chloride + methanol}, where there is strong hydrogen bonding or even proton transfer between the acid and the alcohol,[8] and {hydrogen bromide + water}. In the case of {carbon disulfide + acetone}, the negative azeotropy is explained with the existence of a charge transfer complex.

A schematic binary phase diagram with negative azeotropy is shown in Fig. 2.28. The azeotropic curve originates at the vapor pressure curve of the less volatile substance and terminates in a critical azeotropic point at high temperature. The *Tx* cross sections (Fig. 2.29) and the *px* cross sections (Fig. 2.30) may differ, depending on the pressure at which the azeotropy sets in at $x = 0$. The

---

[8] This is probably not the best example, for here chemical reactions producing methyl chloride, dimethyl ether, and water may take place, so that this is not really a binary mixture.

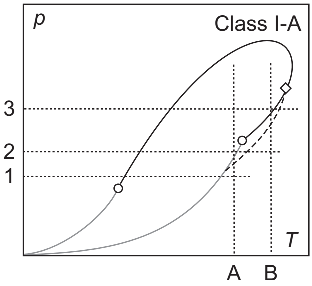

FIGURE 2.28 Class I-A phase diagram with negative azeotropy.

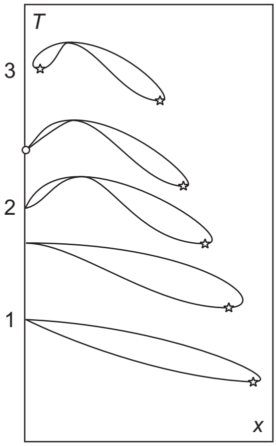

FIGURE 2.29 Corresponding *Tx* cross sections.

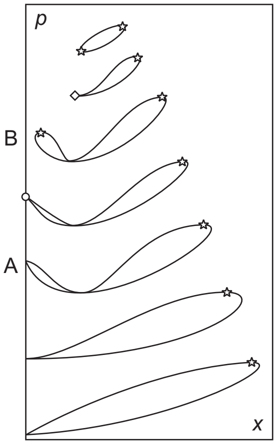

FIGURE 2.30 Corresponding *px* cross sections.

sequence begins with a regular vapor–liquid phase equilibrium with a binary critical point, followed by the formation of an azeotropic point at $x = 0$, and the detachment from the ordinate at the critical point of the less volatile substance. The *Tx* and *px* cross sections are topologically similar; merely minima and maxima appear to be switched. At high pressures or temperatures beyond the critical azeotropic point, closed-loop phase envelopes appear. Closed-loop two-phase regions in *Tx* diagrams are nothing special; they occur also in the regular class I. But closed-loop two-phase regions in *px* diagrams are a rare phenomenon.

If the azeotropic curve ends on the critical curve, it is unavoidable that the critical curve runs through regions above the critical temperature of the less volatile component. Negative azeotropy is, therefore, one of the rather few phenomena that causes phase separation above the critical temperatures of the mixture components.

2.2.1.4 Variants of Class I: Phase Diagrams with Bancroft Points

There are two more azeotropic subclasses of class I-A, both with a so-called *Bancroft point*. This is a point where the vapor pressure curves of the two pure components intersect in the *pT* projection (so it is not really an intersection point!). A Bancroft point is usually associated with azeotropic behavior, because the vapor pressures of the two pure components are very similar in its vicinity, so that even a very small nonideality can cause a maximum or a minimum of the phase boundaries.

In Fig. 2.31, a *pT* projection of such a system is shown. Here, the azeotropic curve originates on the vapor pressure curve of one component and ends on the vapor pressure curve of the other one. Therefore, in the *Tx* and the *px* cross sections depicted in Figs 2.32 and 2.33, respectively, the azeotropic point appears (for low p, T) at $x=0$, moves through the mole fraction range, and disappears at $x=1$.

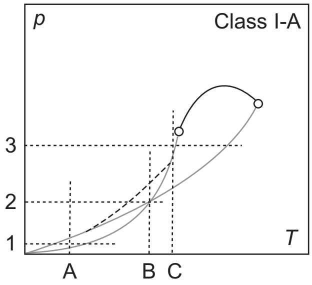

FIGURE 2.31 Class I phase diagram with a Bancroft point.

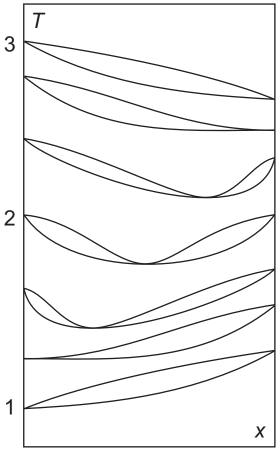

FIGURE 2.32 Corresponding *Tx* cross sections.

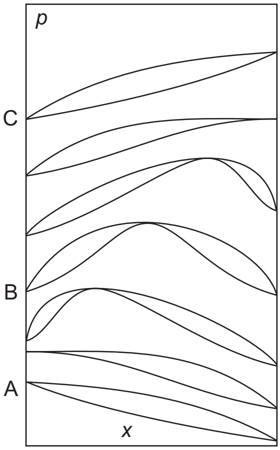

FIGURE 2.33 Corresponding *px* cross sections.

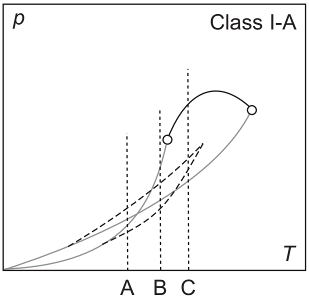

FIGURE 2.34 Class I phase diagram with double azeotropy.

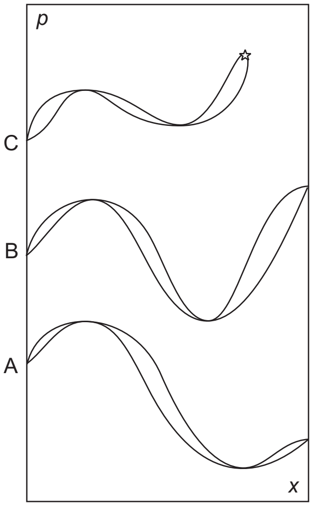

FIGURE 2.35 Corresponding *px* cross sections.

It can happen that a system with a Bancroft point exhibits two azeotropic curves. Such a case, known experimentally for the system $\{C_6H_6 + C_6F_6\}$ [14], is depicted in Fig. 2.34. The two azeotropic curves start from border azeotropes on the two vapor pressure curves and terminate together in an azeotropic cusp. In the *px* sections, a negative and a positive azeotrope are present. When moving from cross section A in Fig. 2.35 to cross section B, the order of the vapor pressures of the pure components is reversed. In cross section C, the two-phase region is detached from the ordinate at $x = 1$, but still has got two azeotropic points. These two azeotropic points approach each other with increasing temperature and coincide when the cusp in the *pT* diagram is reached. Above that temperature, a regular supercritical vapor–liquid equilibrium exists.

2.2.2 Class II

Phase diagram class II is characterized by a continuous vapor–liquid critical curve (l=g) like class I and, in addition, a liquid–liquid critical curve (l=l). The latter originates from a critical endpoint at low pressure on a three-phase curve llg, i.e., a curve along which two liquid phases and one gas phase are in equilibrium. At high pressure, it theoretically ends at the so-called jamming point, a hypothetical ultradense liquid state with vanishing compressibility. In real systems, the l=l critical curve is usually terminated by the solidification of the system, i.e., it ends in an sl=l critical endpoint.

For the regular class II, the three-phase curve is located between the two vapor pressure curves and hence ends (theoretically) at absolute zero. Depending

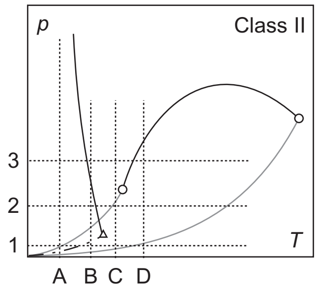

FIGURE 2.36 Class II phase diagram.

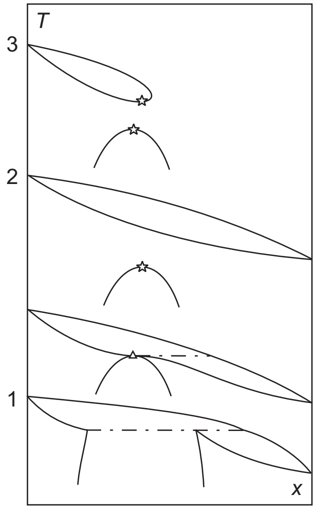

FIGURE 2.37 Corresponding *Tx* cross sections.

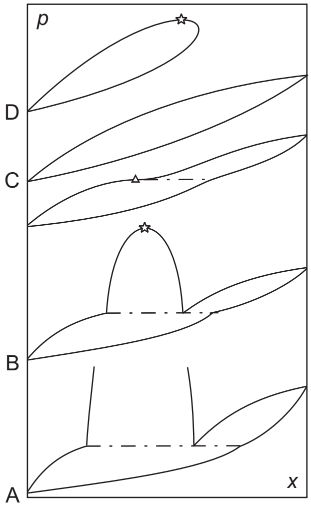

FIGURE 2.38 Corresponding *px* cross sections.

on the shape of the l=l critical curve, one can distinguish several subclasses. In the subclass shown in Fig. 2.36, the l=l critical curve has a negative slope in the *pT* projection. The corresponding *Tx* and *px* cross sections are displayed in Figs 2.37 and 2.38, respectively.

- In the *Tx* cross section at low pressure (section 1 in Fig. 2.37), a vapor–liquid coexistence region "overlaps" with a liquid–liquid phase equilibrium coming up from low temperatures. A three-phase line llg (more precisely: l_1l_2g) splits the vapor–liquid region in two parts, l_1g and l_2g. The two parts are connected to the boiling points of the pure components at $x=0$ and $x=1$.
- With increasing temperature, the liquid–liquid coexistence region detaches from the vapor–liquid region at a critical endpoint.
- In cross section 2, the two regions are separated.

- Above the critical point of the more volatile substance, there are merely regular vapor–liquid phase equilibria. The vapor–liquid coexistence region terminates in a binary critical point l=g (cross section 3).

The *px* cross sections show an analogous development:

- In cross section A at low temperature, the vapor–liquid coexistence region is split into two parts by a llg three-phase state. The liquid–liquid immiscibility region in the middle is either open toward high pressures or may reach the l=l critical curve at a very high pressure beyond the scale of the phase diagram (Fig. 2.36).
- At somewhat higher temperature, in cross section B, the liquid–liquid region is closed and terminated by a critical point at the top. If the temperature is increased further, the liquid–liquid immiscibility region shrinks until it finally vanishes at a critical endpoint.
- Beyond that point, a regular vapor–liquid phase coexistence remains (cross section C), which develops a critical point l=g (cross section D) as in class I.

It should be noted that the region of liquid–liquid immiscibility is always on the low-temperature side of the l=l critical curve in *pT* phase diagrams. In *Tx* cross sections, the critical points of the liquid–liquid immiscibility are always above the two-phase region; they are called upper critical solution points or – for historical reasons – upper critical solution temperatures (UCST). Consequently, the critical endpoint of a class II system is an *upper critical endpoint*. Its phase symbol is l=lg.

The critical endpoint is not the end of the l=l critical curve in the sense that there is nothing beyond it; it is merely the end of the stable part of the critical curve. There exists a metastable continuation, which can even be followed with proper experimental techniques. We defer the discussion of this to Section 5.6.3

2.2.2.1 *Variants of Class II:* l=l *Critical Curves with Positive Slopes*

Another type of class II phase behavior contains an l=l critical curve with a positive slope (Fig. 2.39). The *Tx* cross sections are topologically the same as for class II with negative slope, but the *px* cross sections are different. As shown in Fig. 2.40, the liquid–liquid coexistence region detaches from the vapor–liquid coexistence region with increasing temperature, whereas it is pulled into it in the regular case (Fig. 2.38). An experimental example for this subclass is {methane + tetrafluoromethane} [15, 16].

2.2.2.2 *Variants of Class II:* l=l *Critical Curves with a Temperature Minimum*

A third type of class II behavior has a liquid–liquid critical curve with a temperature minimum (Fig. 2.41). Again, the *Tx* cross sections are the same as those of the previously mentioned subclasses, but the *px* cross sections differ.

In cross section B of Fig. 2.42, the liquid–liquid coexistence region consists of two parts, each having a critical point. If the temperature is decreased,

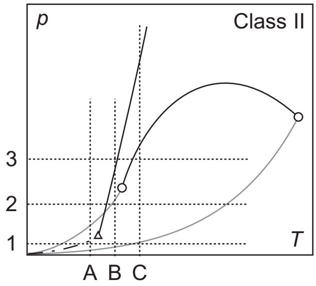

FIGURE 2.39 Class II phase diagram with an ll-critical curve having a positive slope.

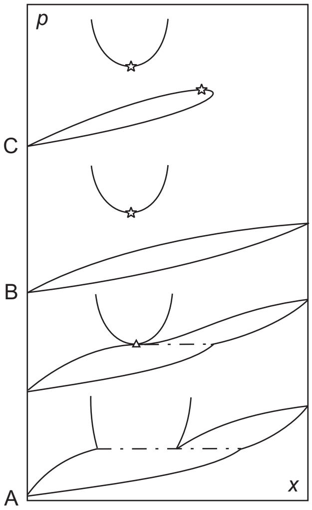

FIGURE 2.40 Corresponding *px* cross sections.

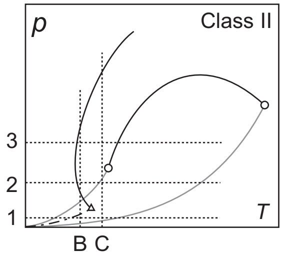

FIGURE 2.41 Class II phase diagram with a temperature minimum in the ll-critical curve. The curvature of the l=l critical curve has been exaggerated for clarity.

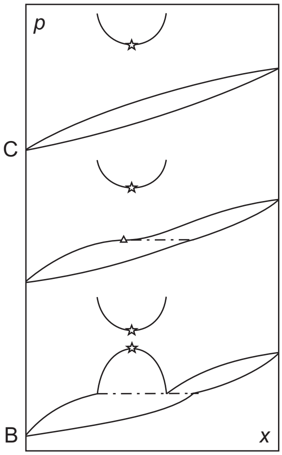

FIGURE 2.42 Corresponding *px* cross sections.

the two critical points meet. This happens at the temperature minimum in the *pT* projection (Fig. 2.41). With increasing temperature, one liquid–liquid coexistence region vanishes in a critical endpoint, while the other liquid–liquid coexistence region remains (cross section C). Examples for this kind of behavior are {tetrafluoromethane + propane} or {sulfur hexafluoride + octane} [16, 17].

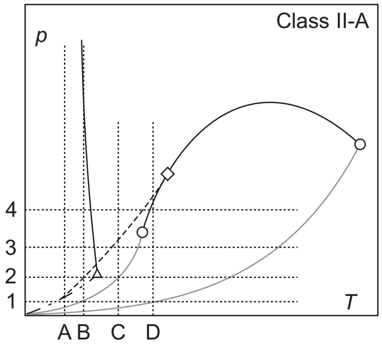

FIGURE 2.43 Class II-A phase diagram.

2.2.2.3 *Variants of Class II: Azeotropy*

Azeotropy can appear in connection with class II, too. In the *pT* projection (Fig. 2.43), the three-phase curve is located above the vapor pressure curve of the more volatile substance. Azeotropy starts somewhere along the three-phase curve and terminates at the critical curve in a critical azeotrope.

- The *px* cross section A at low temperature (Fig. 2.44) contains two vapor–liquid coexistence regions connected to a liquid–liquid coexistence region at higher pressure; between them, a three-phase state lgl is formed. Cross section type A is called *heteroazeotropic*.

  In a heteroazeotropic system, there are two distinct liquid–gas phase equilibrium regions at a given pressure and temperature, like in a regular azeotropic system. At the highest possible pressure (or the lowest possible temperature) for vapor–liquid equilibria, however, these two regions merge to form a three-phase state lgl. This is in contrast to a regular azeotropic system (cf. Fig. 2.45 curve C), where the vapor–liquid equilibrium with the highest pressure (lowest temperature) is reached in an azeotropic two-phase state $(\mathsf{lg})^{\mathrm{az}}$.
- With increasing temperature, the vapor–liquid region at high mole fraction develops an azeotrope connected to the three-phase line. Such an $\mathsf{l}(\mathsf{lg})^{\mathrm{az}}$ three-phase state is called an *azeotropic endpoint*. As for a regular azeotrope, the slopes of both phase boundary curves are here zero.
- In cross section B, above that temperature, the vapor–liquid coexistence region exhibits a regular azeotrope connected to the other two coexistence regions through a three-phase state.
- With increasing temperature, the liquid–liquid immiscibility region shrinks and and finally terminates in a critical endpoint l=lg.
- In cross section C (Fig. 2.45), a regular vapor–liquid azeotrope exists.
- If the critical azeotrope lies at a higher temperature than the critical point of the more volatile component, first a vapor–liquid critical point appears at

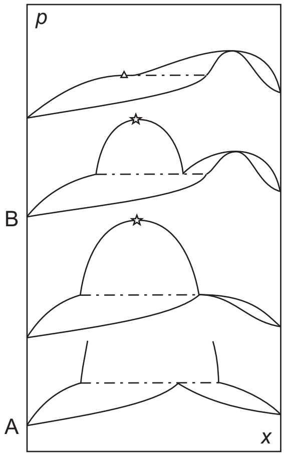

FIGURE 2.44 Class II-A: corresponding *px* cross sections.

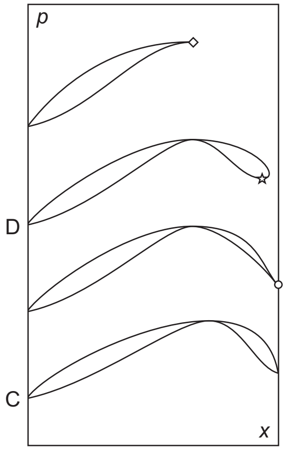

FIGURE 2.45 More corresponding *px* cross sections.

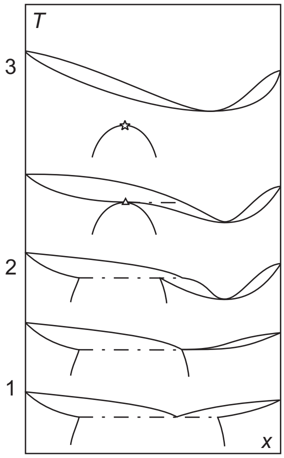

FIGURE 2.46 *Tx* cross sections of class II-A.

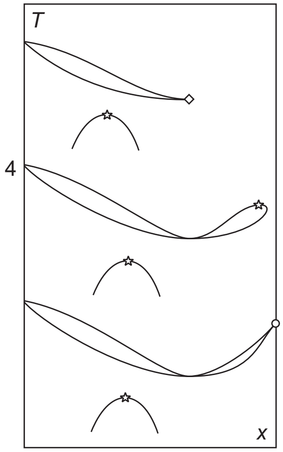

FIGURE 2.47 More *Tx* cross sections.

high mole fraction (cross section D) before the azeotropic curve ends in a critical azeotrope.

The *Tx* cross sections of class II-A (Figs 2.46 and 2.47) behave similarly as the *px* sections, although with the difference that the liquid–liquid immiscibility region is detached from the vapor–liquid region at the critical endpoint. Between cross sections 1 and 2, three-phase states and azeotropy occur together. Above cross section 4, there is a cross section with a critical azeotrope, and at still higher pressures, the cross sections are similar to those of class I.

An experimentally known example for this phase diagram subclass is {pentane + dodecafluoropentane}.

It is conceivable, of course, that the vapor–liquid critical curve has a temperature minimum. In this case, *px* phase envelopes in the critical region have to be "borrowed" from Fig. 2.27.

2.2.3 Class III

Class III phase diagrams also consist of l=g critical and l=l critical curves, but their connection is different from that of class II. In contrast to classes I and II, there is no continuous critical curve connecting the critical points of the pure components (see Fig. 2.48). The l=g critical curve originating at the critical point of the more volatile substance is usually rather short and terminates in an upper critical endpoint.[9] In the *pT* projection, an llg three-phase curve is located slightly below the vapor pressure curve. It runs from the critical endpoint to absolute zero (or rather, to solidification).

Another critical curve starts at the critical point of the less volatile substance. It begins as a l=g critical curve, but changes its character to l=l on its way to higher pressures. Finally, it runs toward the fictive jamming point at infinite pressure. As in class II, this critical curve is in reality terminated by the solidification of the system at high pressure.

The above description of class III phase behavior is rather general. As for the other phase diagram classes, there are subclasses.

The first discussed here is class $\mathrm{III_m}$. The subscript "m" indicates that the major critical curve passes through a maximum and a minimum. The minimum may be at higher pressures than the short critical curve, as in Fig. 2.48, but can also be below it. The evolution of the phase envelopes with temperature is illustrated in Fig. 2.49 for the *px* cross sections.

- At low temperatures (cross section A), as in class II, a liquid–liquid phase equilibrium intersects a vapor-liquid equilibrium, thus creating a three-phase line.
- Here, however, the critical point of the more volatile substance is reached first, causing the detachment of the vapor–liquid coexistence region from the ordinate at $x = 1$. Hence, in cross section B, an l=l critical point and an l=g critical point belonging to the short critical curve exist at the same time.
- On further heating, the vapor–liquid two-phase region contracts and vanishes at the critical endpoint; its symbol is, therefore, ll=g. A regular vapor–liquid coexistence region is formed.
- Above this temperature, the cross sections look like those of class I.

---

[9] For a discussion of its metastable continuation, see Section 5.6.3.

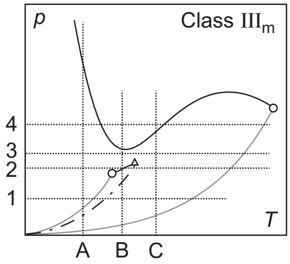

FIGURE 2.48 Class III$_m$ phase diagram.

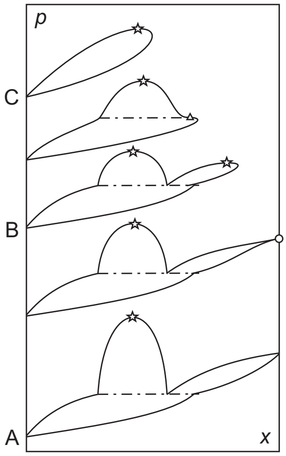

FIGURE 2.49 Corresponding *px* cross sections.

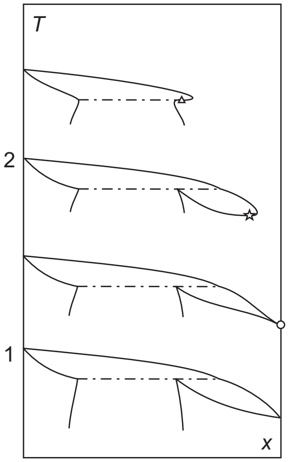

FIGURE 2.50 Corresponding *Tx* cross sections.

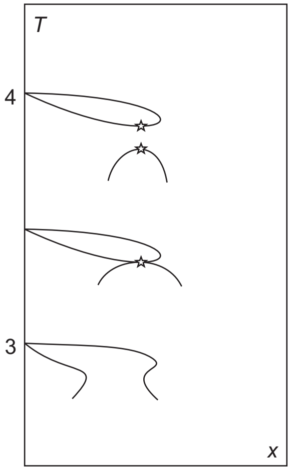

FIGURE 2.51 More *Tx* cross sections.

The development of the *Tx* cross sections with increasing pressure is summarized in Figs 2.50 and 2.51:

- Cross section 1 is a typical diagram with a three-phase state connecting three 2-phase coexistence regions.
- With increasing pressure, one vapor–liquid region detaches from the ordinate at $x = 1$ and contracts, until it vanishes in the critical endpoint.
- In Section 3, the vapor–liquid coexistence region has merged with the liquid–liquid region at lower temperatures. The coexistence region forms a

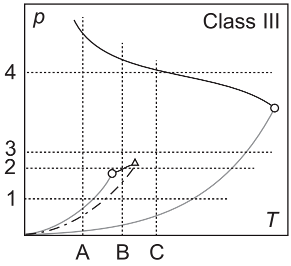

FIGURE 2.52 Class III phase diagram.

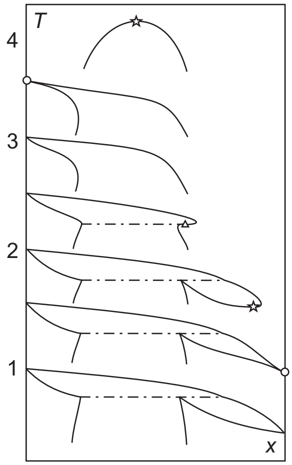

FIGURE 2.53 Corresponding *Tx* sections.

waistline that shrinks to a point. This point is a *hyperbolic minimum pressure critical point* [9].[10]

- Beyond the pressure minimum critical point, in section 4, one can see the separate vapor–liquid and the liquid–liquid coexistence regions with their corresponding critical points.

Typical representatives of this class are {carbon dioxide + squalane} and {carbon dioxide + hexadecane} [18].

2.2.3.1 Variants of Class III: Monotonously Decreasing Major Critical Curve

The regular class III phase diagram does not exhibit any extrema in the major critical curve, as shown in Fig. 2.52. The *px* cross sections are topologically identical to those of class $\mathrm{III_m}$. In the *Tx* cross sections, shown in Fig. 2.53, the behavior at high pressures differs from that of class $\mathrm{III_m}$. Because there is no minimum in the critical curve in class III, there is only one coexistence region above the pressure of the critical endpoint.

Examples for this kind of behavior are the systems {methane + toluene} [19], {ethane + *N*,*N*-dimethyl formamide}, or {carbon dioxide + water}.

2.2.3.2 Variants of Class III: Gas–Gas Equilibria

Further variants of class III are systems with so-called gas–gas equilibria. Their *pT* phase diagrams are shown in Fig. 2.54. Here, the major critical curve runs

---

[10] This is the IUPAC nomenclature recommendation. In the literature, the point is sometimes called "homogeneous double plait point" or "hypercritical point of the second kind."

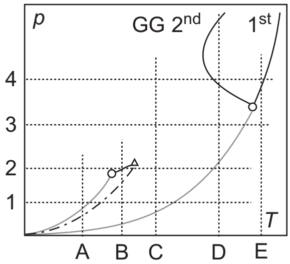

FIGURE 2.54 Class III with gas–gas equilibria of first and second kind.

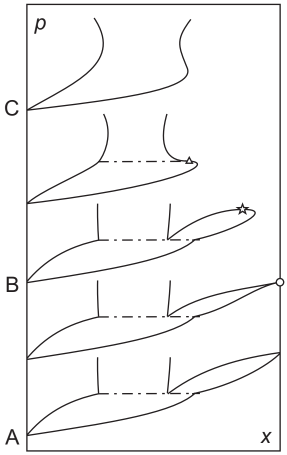

FIGURE 2.55 Corresponding *px* cross sections.

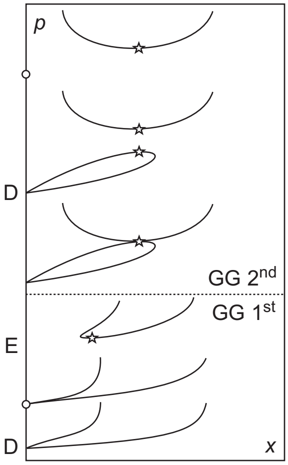

FIGURE 2.56 More *px* cross sections.

from the critical point of the less volatile component to high temperatures and high pressures (possibly through a temperature minimum) not to low temperatures. The *px* sections shown in Figs 2.55 and 2.56 are similar to those of regular class III, with the exception that the gas–gas equililibria systems have an open two-phase region at high pressure, whereas in regular class III, it is closed at some pressure by a critical point. This critical point is not present in gas–gas equililibria systems because the critical curve maintains a positive slope (in the *pT* projection).

There are two versions of gas–gas equilibria, namely the so-called first and second kind. In the *pT* projection, the major critical curve of the latter type starts at the critical point of the less volatile pure component with a negative slope and passes through a temperature minimum. The first kind has a positive slope everywhere. The corresponding *px* sections for the two versions are shown in Fig. 2.56. The *Tx* sections are topologically the same as those of class III.

The name "gas–gas equilibrium" alludes to the fact that here a phase separation can occur even beyond the critical temperature of the heavier component.

The phenomenon had been predicted already in 1906 by van Laar from the van der Waals equation of state but was at that time believed to be an artifact of the theory. The first experimental evidence of a gas–gas equilibrium was found by Krichevsky and Tsiklis around 1942 for the system {nitrogen + ammonia}. Nowadays, many other systems are known; For instance, helium shows gas–gas equilibria with practically all other substances. The best-documented systems are perhaps {helium + xenon} [20] for a first-kind and {neon + krypton} [21] for a second-kind gas–gas equilibrium. Gas–gas equilibria can cause unexpected problems during handling of helium- or hydrogen-containing gas mixtures.

2.2.3.3 Variants of Class III: Critical Curve with a Pressure and a Temperature Minimum

This subclass combines the features of subclass $\mathrm{III_m}$ and gas–gas equilibria of the second kind: In the *pT* diagram, the major critical curve passes through a pressure maximum and a pressure minimum as for class $\mathrm{III_m}$, but then it exhibits a temperature minimum and approaches the jamming point with a positive slope (cf. Fig. 5.9). The *Tx* and *px* cross sections are similar to those of class $\mathrm{III_m}$ (Figs 2.49–2.51), except that in the *px* sections at low temperatures and high pressures an ll two-phase region appears, as shown in Fig. 2.42 or 2.56 (upper curve D).[11]

This type of phase diagram is rather common. The examples are {tetrafluoromethane + alkane} for alkane carbon numbers of 4 and higher and {sulfur hexafluoride + alkane} for alkane carbon numbers of 11 and higher [16].

2.2.3.4 Variants of Class III: Azeotropy and Heteroazeotropy

There are two variants of class III with azeotropic or heteroazeotropic behavior. One of them, the regular azeotropic subclass, is similar to that of classes I and II; it is called class III-A. A *pT* projection is shown in Fig. 2.57. Two major differences to the regular class III exist, namely the three-phase curve is located above the vapor pressure curve of the more volatile substance, and an azeotropic curve lies at slightly higher pressures. The latter starts at an azeotropic endpoint on the three-phase curve and ends in a critical azeotrope on the minor critical curve.

The *Tx* cross section 1 in Fig. 2.58 at low pressure is the same as for the regular class III. When the temperature is increased, the azeotrope appears at the three-phase state, so that an azeotropic endpoint $\mathrm{l(lg)^{az}}$ results. Dew and bubble point curves meet here with zero slope. Beyond this endpoint, in cross section 2, the vapor–liquid coexistence region at high mole fraction exhibits an azeotrope. This coexistence region then detaches from the rest of the phase diagram at a critical endpoint. In cross section 3, an l=g critical point exists,

---

[11] In the earlier literature, this two-phase region was sometimes called a "gas–gas equilibrium of the third kind." But the term "gas–gas" equilibrium should be reserved for cases where the high-pressure part of the major critical curve comes close to $T_{c,2}$.

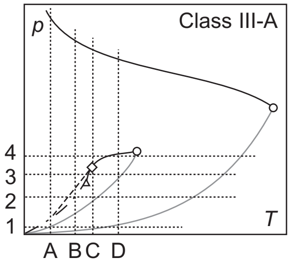

FIGURE 2.57 Class III-A phase diagram.

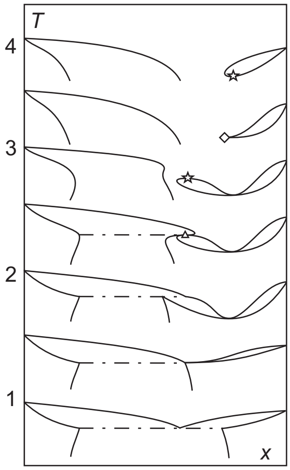

FIGURE 2.58 Corresponding *Tx* cross sections.

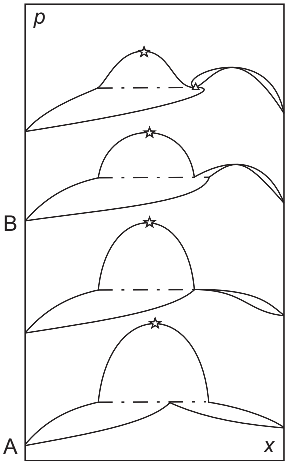

FIGURE 2.59 Corresponding *px* cross sections.

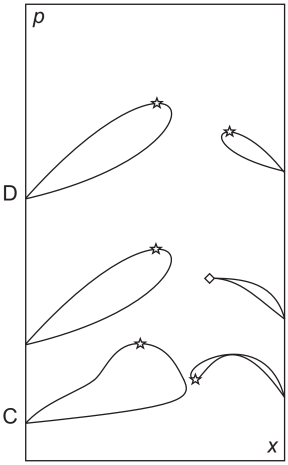

FIGURE 2.60 More *px* cross sections.

which moves toward the azeotropic point with increasing pressure and finally vanishes in a critical azeotropic point.

The sequence of *px* cross sections is similar but contains a liquid–liquid immiscibility region at high pressures. In Figs 2.59 and 2.60, the development via the appearance of the azeotrope at a three-phase state, the detachment of the vapor–liquid region at the critical endpoint, and the approach to the critical azeotropic point are summarized.

Below the azeotropic endpoint, the *px* and *Tx* phase diagrams show heteroazeotropic behavior.

2.2.3.5 Variants of Class III: Heteroazeotropy without Azeotropy

The second azeotropic class III phase behavior is the so-called heteroazeotropic class III-H. The term "heteroazeotropy" has already been introduced in the context of class II-A. Heteroazeotropic cross sections appear in some temperature and pressure ranges of classes II-A and III-A. Class III-H differs from these classes by having no azeotropic states at all (Fig. 2.61). In contrast to the regular class III, the three-phase curve is located above the vapor pressure curve of the more volatile substance. The *Tx* and *px* cross sections, shown in Figs 2.62 and 2.63, respectively, can be obtained from those of class III-A straightforwardly by omitting the azeotrope.

This subclass is technically important, for it includes many {water + alkane} systems [22] (see Fig. 9.26).

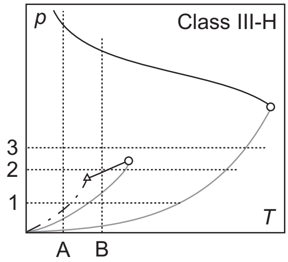

FIGURE 2.61 Class III-H phase diagram.

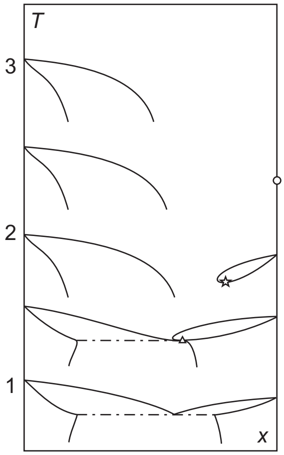

FIGURE 2.62 Corresponding *Tx* cross sections.

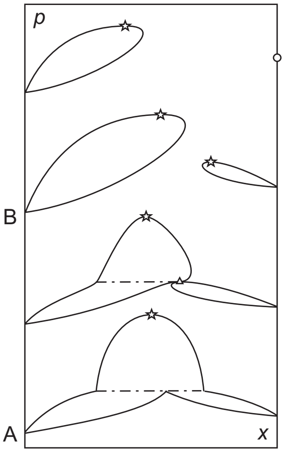

FIGURE 2.63 Corresponding *px* cross sections.

2.2.4 Class IV

Class IV phase diagrams can be obtained from class II by inserting a three-phase curve that interrupts the vapor–liquid critical curve. An example for a *pT* projection of class IV behavior is shown in Fig. 2.64. It contains three critical endpoints and two 3-phase curves. One three-phase curve starts at the origin of the diagram and ends in an upper critical endpoint at a liquid–liquid critical curve running to infinite pressure. The second three-phase curve runs between an upper and a lower critical endpoint. As will be shown in Chapter 9, the two 3-phase curves are rather two pieces of one curve, which is interrupted by the critical curve. Similar to the class III behavior, the critical curve starting at the critical point of the less volatile substance changes from a vapor–liquid to a liquid–liquid critical curve in the region where it interrupts the three-phase curve. Due to the many features present in class IV phase behavior, it gives a rich variety of cross sections.

As can be seen in Figs 2.65–2.67, the *Tx* cross sections look like those of class II at low pressure (cross section 1). At higher pressures, the three-phase

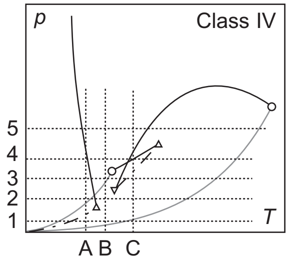

FIGURE 2.64 Class IV phase diagram.

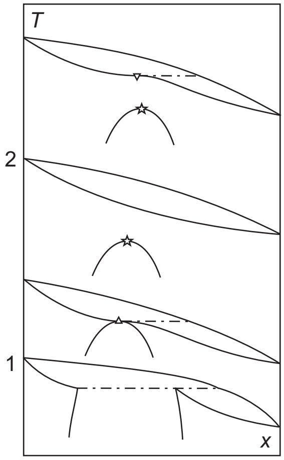

FIGURE 2.65 Corresponding *Tx* cross sections.

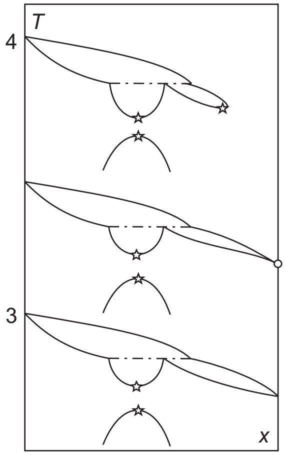

FIGURE 2.66 More *Tx* cross sections.

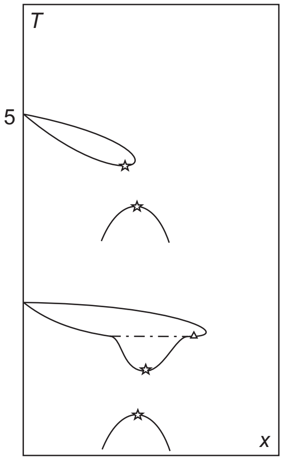

FIGURE 2.67 More *Tx* cross sections of class IV systems.

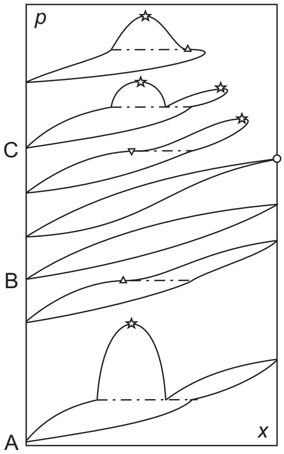

FIGURE 2.68 *px* cross sections of class IV systems.

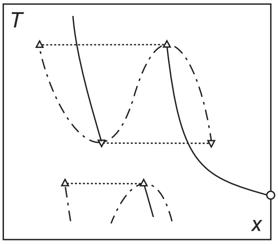

FIGURE 2.69 Projection of three-phase states and critical states onto the *Tx* plane.

state **llg** vanishes and then reappears (from cross sections 1 to 2 and 2 to 3). At the third critical endpoint, between cross sections 4 and 5 (Fig. 2.67), the three-phase state vanishes again. The *px* cross sections shown in Fig. 2.68 exhibit a similar sequence of the disappearing, the reappearing, and the final disappearing of the three-phase state.

It should be noted that the lowest and the highest critical endpoints in Fig. 2.64 are upper critical endpoints, whereas the middle endpoint is a lower critical endpoint. The critical curve originating from this endpoint has – at least in the beginning – the two-phase region on its right (high-temperature) side. The critical points forming this curve are called lower critical solution points or lower critical solution temperatures (LCST).

Fig. 2.69 shows the projections of the phase boundaries and critical curves onto the *Tx* plane; this diagram can be constructed from Figs 2.65–2.67 by marking the locations of critical points and three-phase states. Its most striking feature is the S-shaped curve connecting the loci of the phases of three-phase states. This S-shape is always found in the vicinity of "swallow tail" regions, i.e., the regions where two critical curves cross in the *pT* projection and terminate at the ends (critical endpoints) of a three-phase curve. Swallow tails, and therefore S-shaped critical-endpoint loci, also appear in some phase diagram classes discussed below.

Experimental examples for this class are rare, as far as truly binary mixtures are concerned; a known case is {methane + hexane} [23]. Class IV behavior is often found for polymer systems. For instance, many {solvent + polystyrene} mixtures belong to this class [24] (see Section 2.5).

2.2.5 Class V

Class V can be derived from other phase diagram classes in various ways: one can simply remove the liquid–liquid critical curve from a class IV phase diagram or introduce a three-phase curve into the critical curve of a class I phase diagram. A schematic class V phase diagram is shown in Fig. 2.70. In this particular case, the three-phase curve is relatively short and does not reach temperatures below the critical temperature of the more volatile substance. The corresponding cross sections are depicted in Figs 2.71 and 2.72. Similar as for

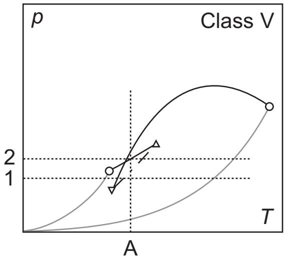

FIGURE 2.70 Class V phase diagram.

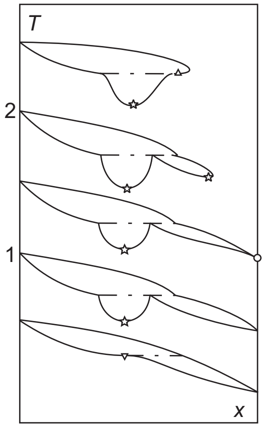

FIGURE 2.71 Corresponding *Tx* cross sections.

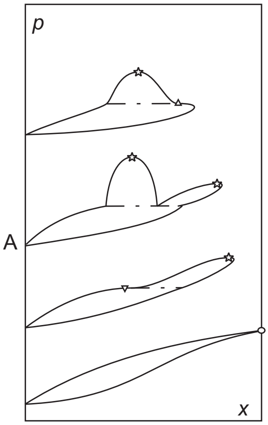

FIGURE 2.72 Corresponding *px* cross sections.

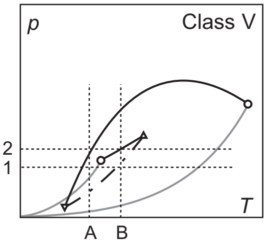

FIGURE 2.73 Class V phase diagram with an lower critical endpoint at low temperature.

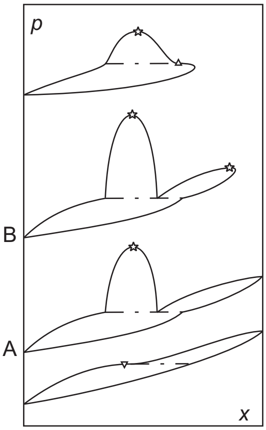

FIGURE 2.74 Corresponding *Tx* cross sections.

the *pT* diagram, the cross sections can be obtained from those of class IV by removing the liquid–liquid phase equilibrium at low temperature and all related transition states.

It is also possible that the three-phase curve of a class V systems has its lower endpoint at a temperature below the critical temperature of component 1, as shown in Fig. 2.73. This leads to a different sequence of transition states in the *px* cross sections, as shown in Fig. 2.74. Here, first, a three-phase state appears at low pressure (cross section A), followed by the detachment of the vapor–liquid phase equilibrium from the ordinate at $x = 1$, i.e., at the critical point of component 1. At higher temperatures, the cross sections of the two class V variants are the same.

The mixtures of methane with some hexane isomers have been reported to belong to class V [25].[12]

2.2.6 Class VI

Class VI phase behavior differs from the ones discussed before in one major feature, namely the existence of a closed-loop liquid–liquid immiscibility region in the *Tx* cross sections. Closed vapor–liquid immiscibility regions are commonly found in binary phase diagrams, for example, of class I (cf. Fig. 2.18). They always exist if an l=g critical curve exhibits a pressure maximum. In class VI, however, the closed-loop coexistence curve surrounds a liquid–liquid coexistence region.

---

[12] It is possible that some class V systems belong in fact to class IV, but their low-temperature l=l critical curve was overlooked for technical reasons or is obscured by solidification.

There are several variants of class VI. Figure 2.75 shows the most prominent class VI phase diagram. It is a combination of a class I phase diagram and a liquid–liquid critical curve having a pressure maximum. Both ends of this critical curve lie at low pressure on the same three-phase curve. The *px* cross sections (Fig. 2.77) do not exhibit special features besides the appearance and vanishing of a regular liquid–liquid coexistence region at a lower and an upper critical endpoint, respectively. The *Tx* cross section 2 in Fig. 2.76 shows the liquid–liquid closed-loop immiscibility. Its domains ends at high temperature in an upper critical solution point and at low temperature in a lower critical solution point.

Three possible variants of class VI phase behavior are shown in Figs 2.78–2.80. These subclasses have different numbers and connectivities of l=l critical curves at low temperature: The phase diagram in Fig. 2.78 has an additional l=l

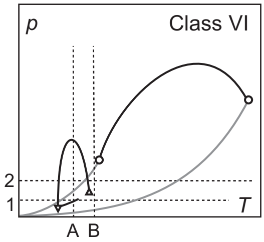

FIGURE 2.75 Class VI phase diagram.

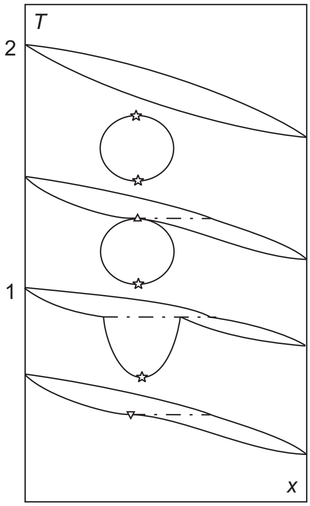

FIGURE 2.76 Corresponding *Tx* cross sections.

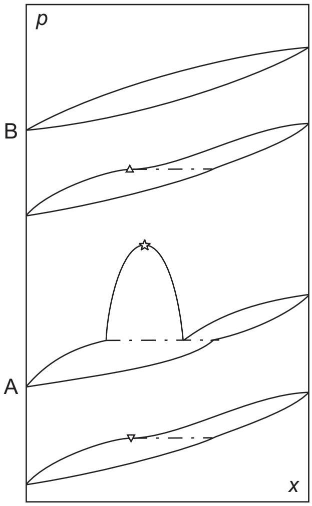

FIGURE 2.77 Corresponding *px* cross sections.

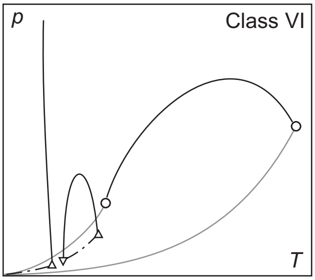

FIGURE 2.78 Class VI phase diagram with additional ll-critical curve at low temperatures.

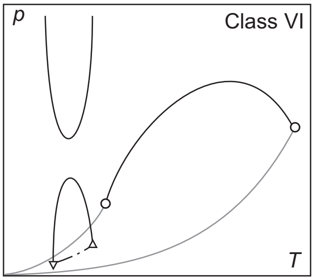

FIGURE 2.79 Class VI phase diagram with additional ll-critical curve at high pressures.

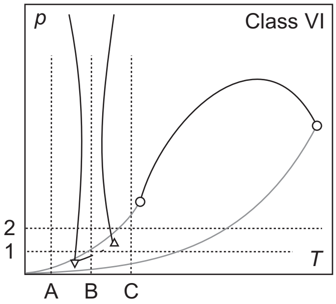

FIGURE 2.80 Class VI phase diagram with two ll-critical curves going to high pressures.

critical curve running to high pressures. In the phase diagram Fig. 2.79, there is an additional U-shaped l=l critical curve at high pressures.

The class VI phase diagram shown in Fig. 2.80 can be understood as the result of merging the minimum and the maximum of the liquid–liquid critical curves of Fig. 2.79, which creates a tube-like liquid–liquid immiscibility region between two critical curves. For the latter case, the *px* and *Tx* sections are shown in Figs 2.81 and 2.82, respectively. The *px* cross sections comprise the appearance and vanishing of a three-phase state, which is connected to the appearance and vanishing of a liquid–liquid immiscibility region. At some temperatures, this liquid–liquid immiscibility region merges with another liquid–liquid immiscibility region located at high pressures (cross section B). With increasing temperature, the two liquid–liquid immiscibility regions come apart again, exactly at the temperature minimum of the critical curve between section B and C in Fig. 2.80.

The "transitional" phase diagram between Figs 2.79 and 2.80 is one in which the two critical curves just touch in a so-called a *hypercritical point*.

The *Tx* cross sections are essentially the same as for the regular class VI (Fig. 2.75), but with one exception: at pressures above cross section 2 in

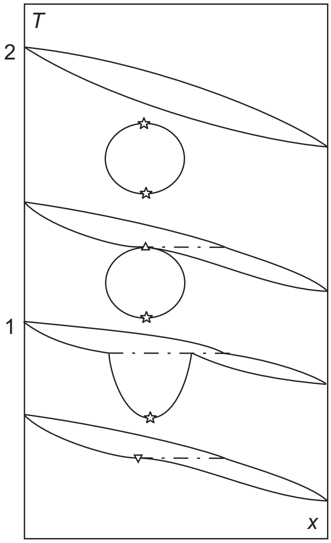

FIGURE 2.81 Corresponding *Tx* cross sections.

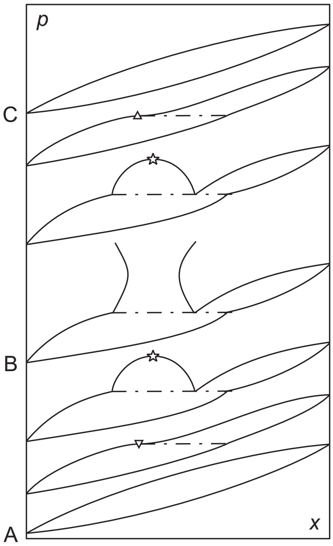

FIGURE 2.82 Corresponding *px* cross sections.

Fig. 2.75, the liquid–liquid immiscibility region vanishes in one point corresponding to the pressure maximum of the liquid–liquid critical curve in Fig. 2.75, whereas it does not vanish in the case of Fig. 2.80.

2.2.7 Class VII

Classes VI and VII differ by an additional three-phase curve interrupting the vapor–liquid critical curve. As shown in the *pT* projection, Fig. 2.83, the class VII phase diagram contains two 3-phase curves that are basically two pieces of one larger three-phase curve intersected by the critical curve. The resulting *px* cross sections depicted in Fig. 2.84 are combinations of the class VI behavior at low temperatures (below cross section B) and class V behavior at high temperatures (above cross section B). Similarly, the *Tx* sections shown in Figs 2.85 and 2.86 are combinations of the class VI type closed-loop liquid–liquid immiscibility with the liquid–liquid and liquid–gas phase equilibria of class V.

For class VII, similar subclasses exist as for class VI. For example, in Fig. 2.87, a class VII phase diagram with an additional l=l critical curve at low temperatures is shown. In this phase diagram, five critical endpoints terminate three 3-phase curves. Actually, the courses of the three-phase curves suggest that they are three pieces of the same curve. This curve is interrupted two times by a l=l critical curve.

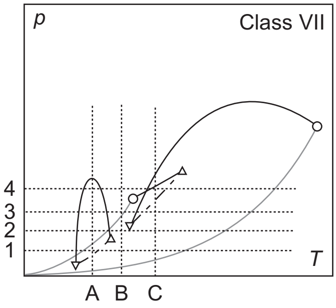

FIGURE 2.83 Class VII phase diagram.

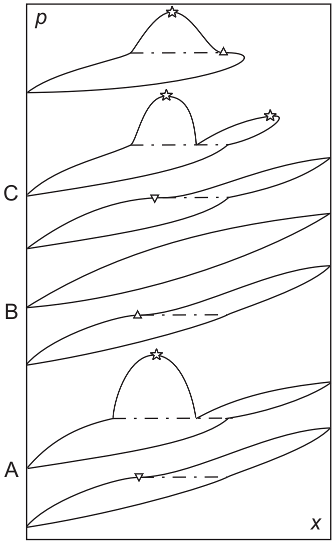

FIGURE 2.84 Corresponding *px* cross sections.

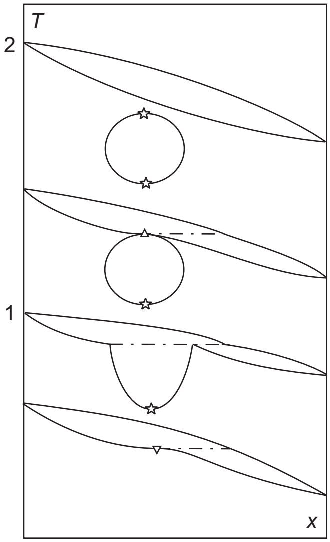

FIGURE 2.85 Corresponding *Tx* cross sections.

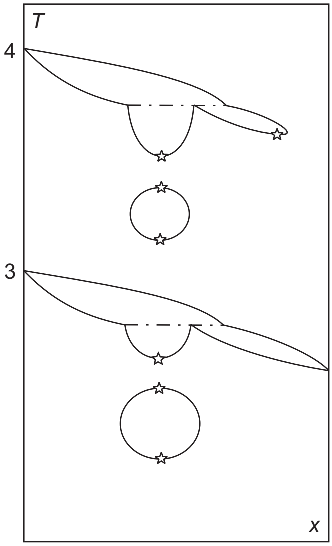

FIGURE 2.86 More *Tx* cross sections.

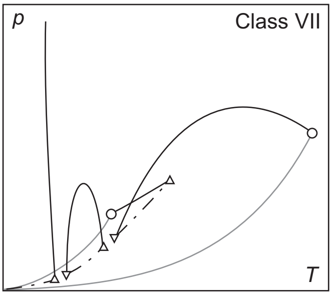

FIGURE 2.87 Class VII phase diagram with an additional l=l critical curve at low temperatures.

At this point, we have to point out that class VI was not part of the original catalog of classes found by Scott and van Konynenburg [26]. It was added later and is clearly a misnomer; its many variants are not merely subclasses, but differ in the number and connectivity of the critical curves, and therefore should have become classes of their own. Once the class VI had been established in the literature, however, the discoverers of class VII and other classes had to accept the numbering.

There are numerous experimental cases for closed-loop liquid–liquid immiscibility; the most famous probably being {nicotine + water} [27]. Schneider found that the {D_2O + 2-methylpyridine} system has a liquid–liquid immiscibility region at low pressure and one beyond 300 MPa, with a region of complete miscibility in between [28, 29] (Fig. 2.79), whereas in the {D_2O + 3-methylpyridine}, the two immiscibility regions have merged (Fig. 2.80). {H_2O + 3-methylpyridine} exhibits the high-pressure immiscibility region only. Visak *et al.* [30] showed that for this system, the low-pressure demixing region exists, too, but at negative pressures. By changing the H/D ratio or by adding small amounts of salts, it was possible to achieve transitions between the various subclasses. A summary of experimental evidence for closed-loop immicibility regions was given by Schneider [31].

The possible existence of the low-temperature l=l critical curve in phase diagrams of classes VI and VII had been predicted already by Boshkov in 1987 [32]. Such a behavior was found experimentally for mixtures of trichloromethane and the ionic liquid [$C_n$mim][Ntf_2] [33].

Shifting the critical curves in Fig. 2.87 toward higher pressures and above the three-phase curve leads to class III_m phase diagram with a pressure maximum in the liquid–liquid equilibrium region (see Fig. 2.88). An example for such a system is {butan-2-ol + water}, which was reported by Schneider [31]. This discovery supports the view that class VII is the result of a "collision" of a wriggling class III critical curve with a three-phase curve and that the l=l critical curves of a class VII phase diagram are parts of a single critical curve.

The problem with all these experiments is, however, that they cannot distinguish between class VI and class VII. Such a distinction can only be based on

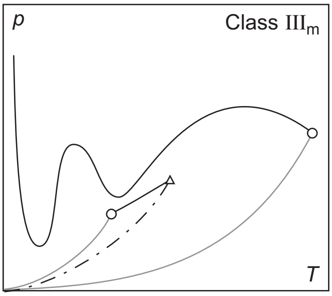

FIGURE 2.88 Class III phase diagram with two pressure maxima.

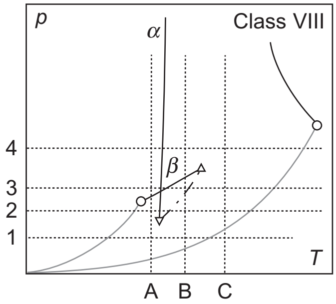

FIGURE 2.89 Class VIII phase diagram. The labels α and β are meant to facilitate the identification of the critical points in the Figs 2.90 and 2.91.

the behavior of the l=g critical curves of these systems, which has never been studied yet. But many of the experimentally known class VI systems are highly asymmetric mixtures, and for these, an uninterrupted l=g critical curve seems unlikely.

2.2.8 Class VIII

Although there are many more classes of binary phase behavior in theory, we list here only one more class, because experimental evidence has been found for it [34], i.e., class VIII, which may be constructed from class V by moving the maximum of the l=g critical curve to infinite pressure. Figure 2.89 shows that in class VIII diagrams, there exist a high-temperature critical curve similar to that of the gas–gas equilibrium subclass and an l=l critical curve that also runs to high pressures. This l=l critical curve lies at relatively high temperatures, usually above the critical temperature of the volatile component. It ends in a critical endpoint on a three-phase curve, which in turn is connected to the short l=g critical curve originating from the critical point of the volatile component.

The *Tx* and *px* cross sections shown in Figs 2.90 and 2.91, respectively, are combinations of cross sections known from other phase diagram types. For their

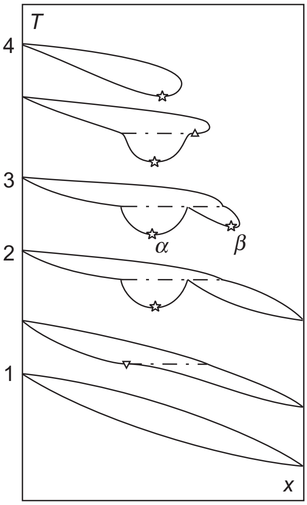

FIGURE 2.90 Corresponding *Tx* cross sections.

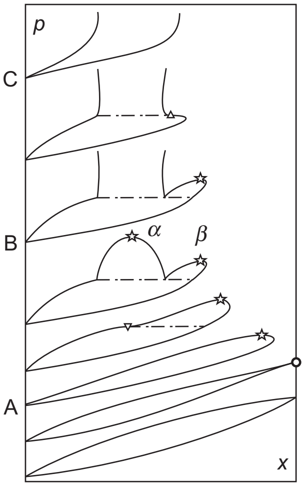

FIGURE 2.91 Corresponding *px* cross sections.

construction, it is important to remember that the l=l critical curve of class VIII is a curve of *lower* critical points.

2.3 RATIONAL NOMENCLATURE OF PHASE DIAGRAM CLASSES

The nomenclature for the phase diagram classes used in the previous section goes back to van Konynenburg and Scott, who simply assigned Roman numerals to the classes in the order of their discovery.[13] The main classes are determined by the topology of the critical curves. Special features, such as azeotropy, are indicated by tags such as "–A." Although this historically grown nomenclature is still widely used, it has turned out to be inefficient for several reasons. So it is not clear which features set apart main classes; e.g., the appearance of a liquid–liquid immiscibility distinguishes class II from class I, or class IV from class V, but for classes VI and VII, it creates new subclasses only (cf. Figs 2.75 and 2.78–2.80). The old nomenclature cannot distinguish these subclasses.

Furthermore, systematic theoretical studies of phase diagram classes (see Chapter 9) revealed the existence of many more classes. These were handled by adding tags like "*" or "**" to the class number, which are clearly not very descriptive.

---

[13] Van Konynenburg's Ph.D. thesis lists classes I–V only, plus their azeotropic and heteroazeotropic subclasses. Class VI was added later.

In contrast to this, the rational nomenclature of Bolz *et al.* [9] is based on the connectivity of the critical curves. Hence, the pT projection of a binary phase diagram can be deduced directly from its rational class symbol. Such a symbol is constructed in four steps:

1. We observe that critical curves sometimes form sequences, i.e., a critical curve ends in a critical endpoint on a three-phase curve, and this runs to another endpoint. Here, a second critical curve starts, which then runs to another critical endpoint, etc. We define the count of a critical curve sequence as the number of critical curves in it. An uninterrupted critical curve has the segment count 1.

   The critical points of the pure components are always starting points of critical curve sequences. First, the critical curve sequence originating at the critical point of the substance with the *higher* critical temperature is considered. It can run toward the following targets:

   P – The critical point of the other pure component
   C – A compact state at infinite pressure, the so-called jamming point
   Z – A critical endpoint on a three-phase curve running to absolute zero
   Q – A critical endpoint on a three-phase curve running to a liquid–liquid–liquid–vapor quadruple point

   The first part of the rational class symbol is the segment count with the target as a superscript, as illustrated in Fig. 2.92. For example, class I is 1^P (Fig. 2.18) in the rational nomenclature, and class V is 2^P (Fig. 2.70), because here the critical curve is interrupted by a three-phase curve.
2. The second part of the rational class symbol describes the connectivity of the critical curve sequence starting at the critical point of the substance with the *lower* critical temperature in the same fashion as the first part. It can be

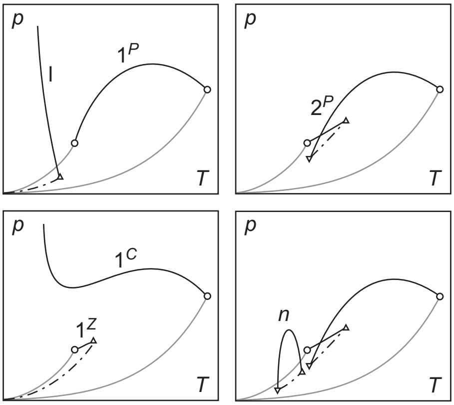

FIGURE 2.92 The rational nomenclature of fluid-phase diagrams: schematic representation of the major critical-curve sequences and types. See the text for explanations.

omitted if this critical point is reached by a sequence of critical curves from the other critical point, so that the sequence has been considered already.

3. For critical curves that do not originate from a pure-component critical point, the following symbols are introduced, which are meant to graphically represent their shapes:
    - l – A critical curve starting at an endpoint and running to a compact state or jamming point at infinite pressure (In real systems, solidification takes place before this state can be reached.)
    - n – A critical curve with a pressure maximum and two critical endpoints
    - u – A critical curve with a pressure minimum, coming from and running to compact states
    - o – A closed-loop critical curve

    These symbols are given in the order of decreasing temperature. If necessary, the formation of sequences can be indicated with parentheses.
4. Special features are indicated by the following symbols:
    - A – Azeotropic behavior
    - H – Heteroazeotropic behavior
    - M – Pressure maxima, their number is specified by a superscript
    - Q – Presence of a quadruple point
    - W – Pressure minima, their number is specified by a superscript

    The symbols follow the critical curve descriptor to which they belong.

These are the main elements of the rational nomenclature, which can, in principle, describe all known fluid-phase diagrams. If necessary, it can be extended, e.g., to account for the presence of solid phases.

The advantage of the rational nomenclature can be demonstrated with the various subclasses of class VI as mentioned above. The plain class VI, as shown in Fig. 2.75, has an l=g critical curve that starts from the critical point of the less volatile component and runs to the critical point of the other component without interruption. This curve is represented in the class symbol by 1^P. The l=l critical curve terminates at two critical endpoints; hence, it is represented by n. The total rational name is, therefore, $1^P n$. The class VI phase diagram shown in Fig. 2.78 is named $1^P nl$, because it contains an additional l=l critical curve running to the compact state, or jamming point, at high pressure. The naming of the other two class VI variants is straightforward: the phase diagram shown in Fig. 2.79 is classified as $1^P nu$, and the one in Fig. 2.80 as $1^P ll$ or, more precisely, as $1^P (ll)$. In the latter example, the parentheses indicate that the two l critical curves form a sequence.

This application of the rational nomenclature to “class VI” is one example of many showing that it is descriptive and much more useful for the discussion and accurate representation of a specific phase behavior. In Table 2.1, the new names are given for the phase diagram classes from the previous section.

TABLE 2.1 Translation Table Between the Old and the Rational Nomenclature of Phase Diagram Classes

Old	New	Figure
I	1^P	2.18
I	1^P, $1^P MW$	2.21
I-A	$1^P A$	2.23
II-A	$1^P Al$	2.43
III	$1^C 1^Z$	2.52
III_m	$1^C 1^Z$, $1^C W 1^Z$	2.48
III-A	$1^C 1^Z A$	2.57
III-H	$1^C 1^Z H$	2.61
IV	$2^P l$	2.64
V	2^P	2.70
VI	$1^P n$	2.75
VI	$1^P nl$	2.78
VI	$1^P nu$	2.79
VI	$1^P ll$, $1^P (ll)$	2.80
VII	$2^P n$	2.83
VII	$2^P nl$	2.87
VIII	$1^C 2^C$	2.89

Finally, we wish to point out that the rational nomenclature resolves a problem of experimentalists: A phase diagram class symbol can be assigned to a mixture only after the mixtures has been studied at all possible temperatures and pressures. But the meaning of "all possible" evidently depends on the available technology and resources. If a mixture is found to have an uninterrupted l=g critical curve and therefore classified as "I," but later a liquid–liquid immiscibility is discovered at low temperatures, the former classification is proven wrong and must be changed to "II."

With the rational nomenclature, however, the first classification is 1^P, and the discovery of the low-temperature demixing turns this into $1^P l$, thus showing the older work to be not wrong but merely incomplete.

2.4 TERNARY PHASE DIAGRAMS

Many aspects of the fluid-phase behavior of multicomponent mixtures can be related to the phase behavior of binary systems. In technical applications, real multicomponent systems are often quantitatively modeled as quasi-binary systems by means of pseudocomponents (see Section 8.10.2).

However, in many applications, it is necessary to go beyond binary systems. Examples are extractions, where a substance is distributed between two phases having different compositions of two solvents, rectifications with an entrainer, or oil–water–surfactant systems. Here, the mixtures in question must be treated as (at least) ternary systems.

A ternary system consists of three binary subsystems, of which each can belong to one of the binary phase diagram classes listed above. The resulting number of ternary phase diagram classes is staggering. Listing them all would go beyond the scope of this book. Instead, it is our intention to give the reader the tools to read and construct ternary phase diagrams for a specific case than discussing all possible cases.

This section focuses on cross sections, mainly isothermal–isobaric ones. As for binary systems, solid phases are omitted here, too. For further information on ternary phase diagrams, the reader is referred to the literature, e.g., an overview on 464 CO_2-containing ternary systems with liquid–liquid immiscibility has been published by Francis [35, 36] and a study of ternary phase diagrams including solid phases by Valyashko [37].

For the discussion of ternary phase behavior, it is important to have adequate graphical presentations. The additional mole fraction requires an additional coordinate. The most commonly employed graphical representation is the Gibbs phase triangle. In this equilateral triangle, the corners represent the pure components. The mole fractions correspond to ratios of the distances from the edges to the height of the triangle. For each component, the mole fraction can, therefore, vary between 1 (on its corner) and 0 (on the opposite edge), but the sum of all mole fractions cannot exceed 1. Fig. 2.93 shows an example.

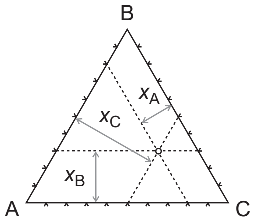

FIGURE 2.93 Composition of a mixture in ternary Gibbs phase triangle. The composition of the marked mixture is $x_A = 0.2$, $x_B = 0.3$, and $x_C = 0.5$.

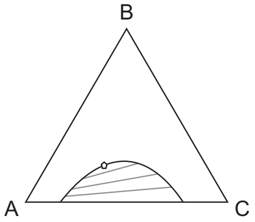

FIGURE 2.94 Isothermal–isobaric section of a ternary phase diagram with one partially immiscible subsystem. ⬠: ternary critical point; grey lines: connodes.

2.4.1 One Immiscible Binary Subsystem

The simplest possible ternary cross section[14] is obtained for a system consisting of two miscible binary subsystems and one having a miscibility gap.[15] The resulting ternary phase diagram is shown in Fig. 2.94. The two-phase region of the subsystem {A + C} extends from the edge into the Gibbs triangle. It shrinks and finally vanishes with increasing concentration of substance B, because the other two subsystems {A + B} and {B + C} are completely miscible. The system {water + phenol + methanol} exhibits such behavior at ambient pressure and temperature [38].

The connodes, the lines connecting two coexisting phases in this diagram, are usually not parallel. They shrink with increasing distance from the edge; finally, they attain zero length at the ternary critical point. In principle, the critical point may be anywhere along the coexistence curve. Its position depends on the symmetry of the interactions of the three components.

2.4.2 Two Immiscible Binary Subsystems

In case of two immiscible binary subsystems, there are several options for the phase behavior. First, a simple juxtaposition of two 2-phase areas leads to the Gibbs triangle as shown in Fig. 2.95. This kind of behavior has been found for the system {methyl phthalate + heptane + carbon dioxide} [35].

The sizes and shapes of the two-phase regions change with temperature and pressure. It can happen that the two 2-phase areas "collide." In such a case, the two ternary critical points meet in one point, as shown in Fig. 2.96. A further shift of temperature or pressure then lets the two 2-phase regions merge into a band (Fig. 2.97). In this case, the connodes have to change continuously from the connodes of the subsystem {A + C} to those of the subsystem {A + B}.

---

[14] Aside from a completely miscible system.

[15] Or having a vapor–liquid phase separation. We do not distinguish between lg and ll phase equilibria in this section.

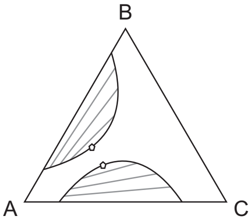

FIGURE 2.95 Cross section of a ternary phase diagram with two partially immiscible subsystems.

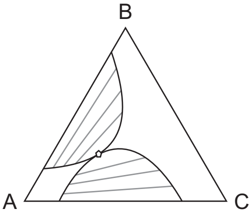

FIGURE 2.96 Cross section of a ternary phase diagram with two partially immiscible subsystems, with the two-phase regions touching at their critical points.

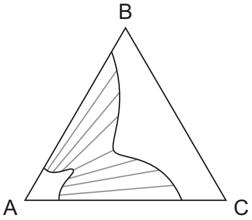

FIGURE 2.97 Cross section of a ternary phase diagram with two partially immiscible subsystems, with the two-phase regions forming a continuous band.

Of course, the actual shape of the two-phase region may look different for real systems; it may, e.g., not be as curvy as the contour depicted in Fig. 2.97. An example for this kind of phase diagram topology is the system {1-chloro-2-hydroxy-ethane + heptane + carbon dioxide} [35].

There is another ternary phase diagram type with two immiscible subsystems that contains a three-phase region (Fig. 2.98). This region implies the existence of an additional two-phase region, which is oriented toward the {B + C} subsystem and terminates in a ternary critical point. The three-phase triangle in the center of the cross section is discussed below.

2.4.3 Three Immiscible Binary Subsystems

Finally, it is possible to have three immiscible binary subsystems. In this case, there are again several topological options for the ternary phase diagrams. The

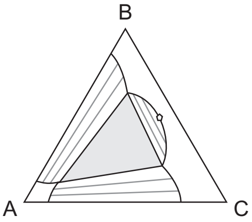

FIGURE 2.98 Cross section of a ternary phase diagram with two partially immiscible subsystems, with a three-phase region (shaded area) and an additional two-phase region terminated by a critical point.

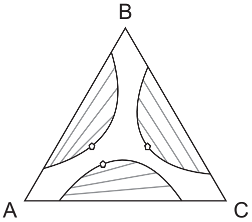

FIGURE 2.99 Cross section of a ternary phase diagram with three partially immiscible subsystems.

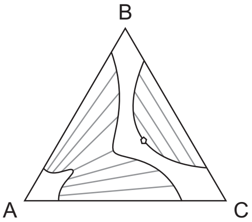

FIGURE 2.100 Cross section of a ternary phase diagram with three partially immiscible subsystems, with two 2-phase regions merged into a band.

first is again a simple juxtaposition of three 3-phase areas that are not connected to each other (Fig. 2.99). The second option is a phase diagram with two connected two-phase areas (a band) and one unconnected, as shown in Fig. 2.100. Finally, if all three 2-phase areas are connected, a three-phase triangle appears somewhere inside the phase diagram (Fig. 2.101). At ambient conditions, the system {perfluoro-tributylamine + nitroethene + 2,2,4-trimethylpentane} exhibits such a phase behavior with three-phase coexistence [36].

2.4.4 No Immiscible Binary Subsystems

If none of the three subsystems exhibits an immiscibility, the ternary system is usually completely miscible. But "usually" is not the same as "always": it is

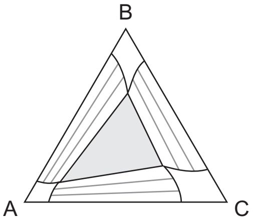

FIGURE 2.101 Cross section of a ternary phase diagram with three partially immiscible subsystems, with a three-phase region in the center (shaded area).

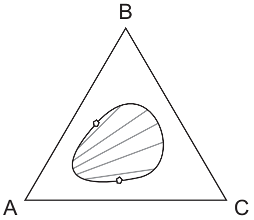

FIGURE 2.102 Closed-loop coexistence curve in an isothermal–isobaric cross section of a ternary phase diagram.

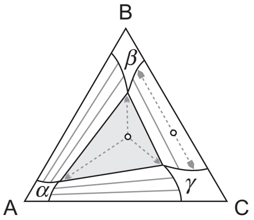

FIGURE 2.103 Illustration of the lever rule in ternary phase diagrams. In the two-phase regions, the lever rule for binary systems, Eq. (2.11), is valid. In the three-phase region, the system decomposes into three phases represented by its corners.

possible – depending on the interactions between the three components – that a two-phase immiscibility region appears within the Gibbs triangle, which has no connection to the border systems. Such a case is depicted in Fig. 2.102. This system exhibits a closed coexistence curve with two ternary critical points. An example for such mixture is the system {heptane + o-toluidine + acetic acid} [36].

2.4.5 The Ternary Lever Rule

Fig. 2.103 illustrates the separation of a mixture with an overall composition inside the triangular three-phase region: the mixture decomposes into three phases that are represented in the diagram by the corners of the triangle. The amounts of these phases for a given overall composition can be calculated with an extension of the lever rule, Eq. (2.11), to three-phase equilibrium[16]:

$$n'(x_i' - x_i) + n''(x_i'' - x_i) + n'''(x_i''' - x_i) = 0 \quad i = 1, 2, 3 \tag{2.15}$$

Again, the mechanical analogy is evident: The "weights" attached to the corners of the three-phase triangle, n', n'', and n''', must be chosen in such a way that $\vec{x}$ is its center of gravity.

2.4.6 Three-Dimensional Representations

The Gibbs triangles discussed so far are cross sections of the total ternary phase diagrams at constant pressure and constant temperature. As the contours and sizes of the two-phase and three-phase regions in these cross sections depend on temperature and pressure, and can even undergo drastic changes of topology, it is often important to look at the evolution of the Gibbs triangles with these variables. Because the graphical representation of both temperature and pressure is rather difficult, usually isothermal or isobaric ternary phase prisms are depicted.

Figure 2.104 shows an isobaric prism for a system that changes with increasing temperature from cross sections with two immiscible subsystems to cross sections with one immiscible subsystem. The band connecting the two-phase regions at low temperature disintegrates at higher temperatures into two separate two-phase regions. If the temperature is increased further, one of the two-phase regions shrinks to a point at the prism face belonging to the {A + C} subsystem. This point is actually a binary critical point of this subsystem. Above this temperature, only one two-phase region exists, which finally vanishes at a binary critical point of the {A + B} subsystem.

The curve connecting the ternary critical points in the phase prism is the ternary critical curve; it is a (one-dimensional) curve in this isobaric cross section of the total ternary phase diagram. In the full pTx_1x_2 representation of the ternary phase behavior, this curve is an element of a critical surface.

The ternary critical curve is usually not a straight line; instead, it is often found to "sag," or even to have a minimum. The practical consequence is that even if two mixtures {A + B} and {A + C} show a phase separation, {A + B + C} may be miscible. This phenomenon is called *cosolvency effect* [39].

2.4.7 Miscibility Windows and Cosolvency

As stated above already, the number of ternary phase diagram classes that can be obtained merely by combining three binary phase diagram classes is large. Herein, we will discuss only one subclass of ternary mixtures, for which some systematic work has been done, namely quasi-binary mixtures.

---

[16] See Problem 2.

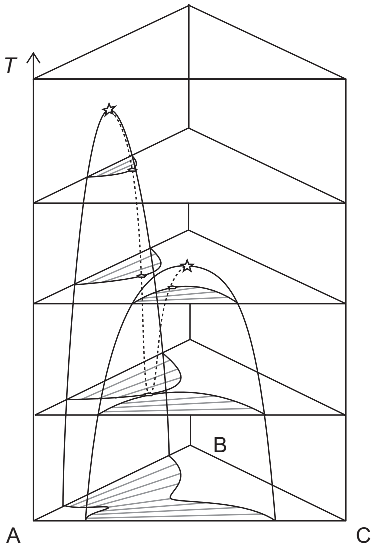

FIGURE 2.104 Isobaric phase prism showing the influence of the temperature on the ternary phase behavior. ····: ternary critical curve.

With this term, we denote ternary mixtures, of which two components are very similar, {A + B_1 + B_2}; in particular, the subsystems {A + B_1} and {A + B_2} must belong to the same binary phase diagram class or at least similar classes.[17]

For such systems, another kind of graphical representation of the phase behavior has been found useful, namely the phase cube. This is a three-dimensional representation in pTx^* space, where x^* is a reduced mole fraction reflecting the amounts of the B_1 and B_2 components only:

$$x^* = \frac{x_{B_1}}{x_{B_1} + x_{B_2}}. \tag{2.16}$$

Two opposite faces of the cube contain the binary pT phase diagrams of the subsystems {A + B_1} and {A + B_2}.

Then the ternary critical surfaces can be constructed by connecting the binary critical curves of one subsystem with their partner curves in the other subsystem. An example is shown in Fig. 2.105.

It should be noted, however, that ternary critical surfaces are usually not planar, and this can lead to some interesting (and sometimes surprising) effects. An example is the system {carbon dioxide + docosane + tetradecanoic acid} [39]: docosane and tetradecanoic acid are fully miscible; the other two subsystems belong to class III_m ($1^C W 1^Z$). Because of the cosolvency effect, the

---

[17] More accurately: neighbor classes in the global phase diagram (see Section 9).

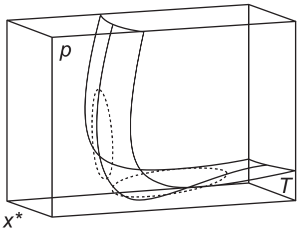

FIGURE 2.105 Ternary phase cube for a system with two class $\mathrm{III_m}$ and one class I subsystems (after [40]). The isobaric and isochoric cross sections (dotted loops) indicate miscibility windows.

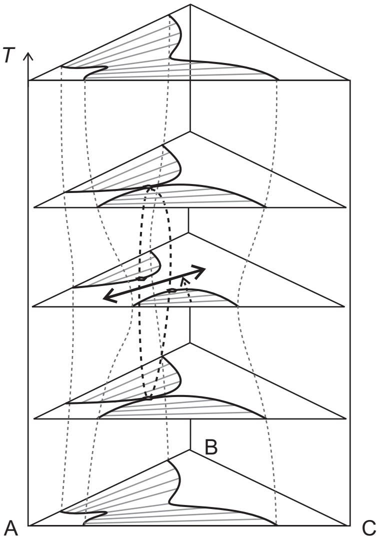

FIGURE 2.106 Ternary phase prism for a system with a miscibility window (after [40]). ··········: phase boundaries of binary subsystems; •••: critical curve, border of the miscibility window. The dotted arrow indicates the cosolvency effect. The bold arrow indicates a path through the triangle without phase separation.

addition of a small amount of tetradecanoic acid to docosane enhances the miscibility with carbon dioxide. In this specific ternary mixture, the cosolvency effect can be smaller at lower or higher temperatures. This situation is illustrated in Fig. 2.105: In the phase cube, the ternary critical surface resembles a chair. Because of the cosolvency effect, the "seat" of the chair has got a pressure minimum. Consequently, isobaric cross sections of the cube just above this minimum contain a closed loop of a critical curve that encloses a one-phase region. Such a loop is called a *miscibility window*.

Likewise, it is possible to have temperature minima in the "back" of the chair-like critical surface. These lead to isothermal miscibility windows.

Fig. 2.106 shows the formation of miscibility window at constant pressure in a phase prism. At high and low temperatures, there is a band-like two-phase region. The cosolvency effect makes this band contract and eventually come apart at intermediate temperatures. The two separate two-phase regions terminate in critical points; the locus of all these critical points is an oval critical loop, the miscibility window. Through this window, it is possible to traverse a phase triangle without a phase separation.

Miscibility windows can be of practical importance: Just by changing the composition, i.e., adding a substance, one can transform an immiscible system to a miscible system. It is also possible to enhance the miscibility by entering a miscibility window.

The opposite phenomenon, the appearing of an immiscibility region in a quasi-binary system where the binary subsystems are all miscible, can occur, too; it is called a *miscibility island* [39].

A more detailed discussion of the shapes of ternary critical surfaces and especially of the phase behavior of quasi-binary systems will be given in Chapter 9.

2.5 PHASE DIAGRAMS OF POLYMER SOLUTIONS

Polymer solutions are a rather special case for three reasons: First, polymers are usually polydisperse, i.e., mixtures of chemically similar chain molecules with a range of molar masses. A solution of a polymer in a (pure) solvent of low molar mass is, therefore, not really a binary mixture, but at best a quasi-binary mixture. Second, polymer solutions are very asymmetric mixtures. This has direct consequences for the phase diagrams. The phase equilibrium regions, e.g., are very asymmetric having a critical point at a very low polymer mole fraction. Third, polymer solutions are often rather viscous. Phase separations, which take place on the millisecond scale in ordinary mixtures, may now require minutes or hours. Consequently, metastable states may be important for polymer systems and should be included in phase diagrams.

Fig. 2.107 shows some schematic Tx cross sections for polymer solutions where the polymers are assumed to be monodisperse. Depending on the system, a liquid–liquid immiscibility can occur at low as well as high temperatures. The immiscibility regions vanish at the upper critical solution temperature (UCST) or the lower critical solution temperature (LCST).

Figure 2.107 also shows the influence of the molar mass of the polymer: the longer the polymer chains, the more asymmetric the immiscibility region becomes. An increase of the chain length shifts the UCST and LCST to lower polymer mole fractions. At the same time, usually the miscibility decreases, and hence, the UCST and the LCST move closer toward each other. Whether the two critical points merge at some high molar mass of the polymer or not depends on the interactions between the polymer and the solvent molecules. In the limit of infinite polymer mass, the UCST or the LCST converges against a *tricritical point* at $x_{\text{poly}} = 0$, which is also called a Θ point [41].

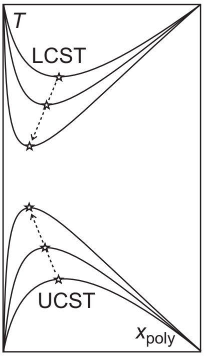

FIGURE 2.107 *Tx* cross sections of polymer solutions in a low-molecular solvent for different molar mass of the polymer. The molar mass increases in the direction of the arrows.

For the description of the phase behavior of polymer solutions, it is common to use volume fractions rather than mole fractions. These can be defined in various ways, e.g.,

$$\varphi_i = \frac{n_i N_{\text{seg},i}}{\sum_k n_k N_{\text{seg},k}}, \tag{2.17}$$

where n_k denotes the amount of substance of species k and $N_{\text{seg},k}$ its number of segments; for the solvent, $N_{\text{seg},1} = 1$.[18] The experimental definition of volume fractions is based on the mass, the mass density of the pure polymer, d_{poly}, and the volume of the solution,

$$\varphi_{\text{poly}} = \frac{m_{\text{poly}}}{d_{\text{poly}} V}. \tag{2.18}$$

The plots of phase envelopes against volume fractions appear less asymmetric than plots against mole fractions, and this is perhaps a practical reason for using volume fractions. As polymers tend to be very large molecules, mole fractions and volume fractions differ very much.

Often only the liquid–liquid immiscibility region is shown for polymer solutions. This is usually sufficient, because the liquid–liquid equilibria dominate the phase behavior. A detailed view can be deduced from the general phase diagrams of class IV or III_m. In Fig. 2.108, a partial class IV diagram is shown in the region of the vapor pressure curve of the solvent [42]. Typically, polymers have very low vapor pressures and very high critical temperatures (depending on their molar masses). In fact, their critical points are often hypothetical only, because they decompose before the critical temperature is reached.

---

[18] More accurately: This equation defines a segment fraction in the context of a lattice model like the Flory–Huggins theory, which is then interpreted as a volume fraction.

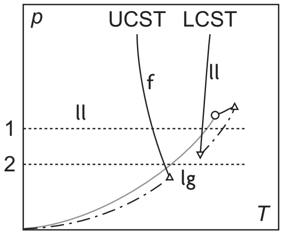

FIGURE 2.108 Schematic phase diagram of a polymer solution in the vicinity of the solvent vapor pressure curve [42] .

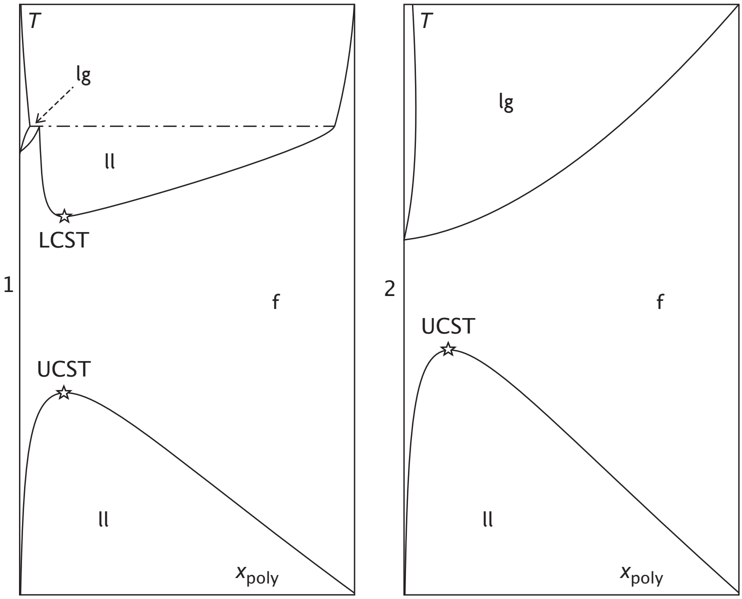

FIGURE 2.109 Corresponding *Tx* cross sections [42].

Between the two liquid–liquid immiscibility regions (ll), a fluid region (f) of complete miscibility is located. The detailed *Tx* cross section 1 in Fig. 2.109 reveals the existence of a very small vapor–liquid two-phase region close to the solvent vapor pressure. Cross section 2 shows the phase diagram at a pressure between the two critical endpoints. In this situation, the coexistence region at high temperature is a vapor–liquid coexistence region. With increasing pressure, the liquid–liquid region reappears at the lower critical endpoint of the short three-phase curve.

Figure 2.110 shows the two classes IV and III_m in the context of polymer–solvent systems. While the main critical curve of class III_m has a minimum and does not intersect the three-phase curve, the critical curve of class IV runs to such low pressures that it interferes with the three-phase curve. As a

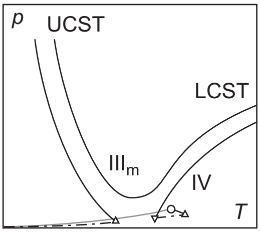

FIGURE 2.110 Class IV and class III phase behavior of polymer solutions [42] .

consequence, in the *Tx* cross section, the LCST and the UCST merge with decreasing pressure for class III_m, whereas for class IV, the LCST and the UCST still exist separately at the vapor pressure of the solvent. Actually, the UCST at the vapor pressure of the solvent is very close to the upper critical endpoint (UCEP). Similarly, the LCST at the vapor pressure of the solvent is very close to the lower critical endpoint (LCEP).

Continuous transitions from class IV to III behavior could be achieved experimentally for {solvent + polystyrene} mixtures by varying the chain length [43].

As mentioned above, polymers usually do not have a single, well-defined molar mass but rather a molar mass distribution. This polydispersity is related to the reaction kinetics of the polymerization process. The growth of polymer chains by, e.g., a radical mechanism can be terminated any time during the reaction and therefore does not depend on the length of a polymer chain or its molecular mass. The resulting polymer consists of relatively few, but rather long chain molecules with a characteristic chain length distribution, whereas polymers obtained by a polycondensation mechanism tend to consist of more, but shorter chain molecules.

The effect of polydispersity on the phase behavior can be best explained by treating the polymer as a mixture of two well-defined components with slightly different chain lengths. Together with the solvent, a ternary system is thus formed. Its liquid–liquid immiscibility region can be represented in a Gibbs triangle. In the quasi-binary approximation, the ratio of the two polymers is constant; hence, the locus of the polymer solution in the Gibbs triangle is a straight line from the corner of the pure solvent to the opposite edge.

In the Tx_1x_2 Gibbs prism, this line expands to a plane intersecting the (now three-dimensional) two-phase region. The resulting contour, the quasi--binary cross section, is called *cloud point curve* (cpc). The maximum of this cloud point curve is not necessarily a critical point but usually lies at a somewhat higher temperature, as can be seen in Fig. 2.111; it is called *precipitation threshold*.

For a state on the cloud point curve, the coexisting equilibrium phase is not on the cloud point curve, too, because in a ternary mixture, the connodes may have arbitrary directions. Instead, the locus of the coexisting phases is another

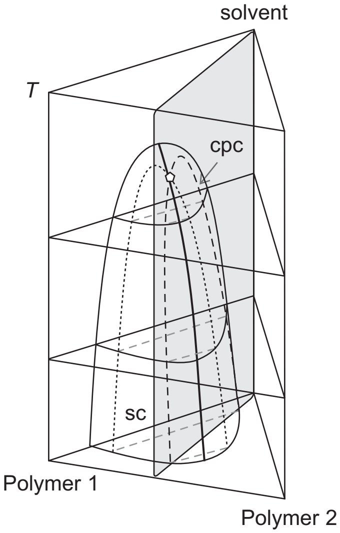

FIGURE 2.111 Phase prism for a system consisting of two polymers (mimicking a polydisperse system) and one solvent. Grey plane: quasi-binary section for a fixed mass ratio of the two polymers; – – : cloud point curve (cpc), intersection of this plane with the phase envelope; ··········: shadow curve (sc), locus of phases in equilibrium with those on the cloud point curve; ⬠: ternary critical point (after [44]).

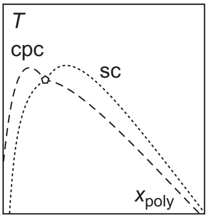

FIGURE 2.112 Cross section at fixed polymer mass ratio through the phase prism in Fig. 2.111. – – : cloud point curve (cpc); ··········: shadow curve (sc); ⬠: ternary critical point; x_{poly}: total polymer mole fraction.

curve, the so-called *shadow curve*, which is outside the quasi-binary cross section through the Gibbs prism and not accessible experimentally. Figure 2.112 shows its projection onto the quasi-binary cross section.

With decreasing polydispersity, the cloud point curve and the shadow curve approach each other, and the precipitation threshold approaches the critical point.

In real polymer mixtures, the cloud point curve can have a more complicated shape. It is possible, for instance, for this curve to have two maxima [45, 46].

2.6 PROBLEMS

1. Consider a vessel containing gaseous ammonia, gaseous hydrogen chloride, and solid ammonium chloride. How many thermodynamic degrees of freedom does the system have? Does it matter whether the gas phase inside the vessel is prepared by mixing the two pure gases or by heating an amount of ammonium chloride? Does it matter that chlorine is a mixture of two isotopes, ^{35}Cl and ^{37}Cl?

2. Extend the lever rule, Eq. (2.11), to an N-component system in a k-phase equilibrium ($k=2,\ldots N$)!

3. Can this phase diagram be correct? (see Section 5.5.6)

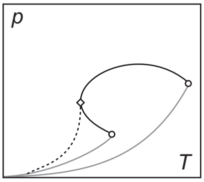

4. Consider two class I binary mixtures of the most common type, i.e., with a pressure maximum along the critical curve (and no other complications), where in one case component 1 has the lower critical pressure, in the other case component 2. Do the *px* and *Tx* phase diagrams of these systems have qualitatively different shapes?

5. Construct some isopleths for the azeotropic phase diagrams shown in Figs 2.23 and 2.26; compare them with the isopleths of a nonazeotropic class I mixture.

6. Is it possible for a class II system to have its critical endpoint at a higher temperature than the critical temperature of the more volatile component? Construct possible cross sections.

7. Construct the *px* and *Tx* cross sections for a class II-A system where the vapor–liquid critical curve has a temperature minimum.

Chapter 3

Experimental Observation of Phase Equilibria

This book focuses on the interpretation and calculation of fluid phase diagrams. It would be incomplete, however, without at least a short overview of the experimental methods. The choice of the experimental method is one of the factors that determine the accuracy and the reliability of the experimental data.

This may seem like a trivial statement, but one must keep in mind that there is no experimental method that is always superior to all others; instead, all methods have their merits, but also their blind spots.

The ultimate goal of phase diagram calculations is the prediction of diagrams within the experimental uncertainty. Evidently, it is advisable to know what the experimental uncertainty is!

3.1 WARNING

Before fitting parameters of an equation of state to a set of experimental data or optimising such an equation, one should check whether the data are worth the effort.

This advice might sound provoking and, in a book on computational methods, perhaps even inappropriate, for theories and computational methods should strive to match the experimental data, but not the data the theories. Still, one must not forget that experimental data are usually not exact, but have an uncertainty.

Modern electronic devices can produce accurate temperature and pressure readings in a fraction of a second where, only a few decades ago, scientists had to work with cumbersome compensation circuitry and manually switched resistor arrays. But there is one aspect where electronics does not help, and where the "stone age" is still present: sample purity. Chemical analysis and purification still require time, effort, and chemical knowledge.

If an experimental publication contains a statement like "compound X was purchased from supplier Y with 99% purity and used as delivered", the

High-Pressure Fluid Phase Equilibria. DOI: 10.1016/B978-0-444-56347-7.00003-7

reported data should not be trusted, unless it has been demonstrated that the 1% impurities will not significantly interfere with the experiment. For example, the presence of 1 mole-% 4-methylpentanol in hexanol would probably not affect the vapor–liquid equilibria of the system {hexane + hexanol} significantly,[1] but the presence of 1% water would.

3.2 OVERVIEW

In most cases the main experimental problem is not the determination of pressure or temperature, but the determination of phase compositions or concentrations of the equilibrium phases. Two main classes of experimental methods can be distinguished: *analytical methods* measure the compositions of the equilibrium phases, whereas *synthetic methods* work with samples of known (predetermined) compositions.

A further distinction can be made between true equilibrium methods and transient techniques. The latter do not establish a true phase equilibrium, but achieve it approximately. The approximation, however, can be good, and transient methods may have some practical advantages over true equilibrium methods for some applications.

Here, only a superficial overview can be given. Interested readers should look up the bibliography of Dohrn *et al.* [47], which contains not only references to experimental data, but also a classification scheme for experimental techniques. Furthermore, another excellent overview over experimental techniques – not only for phase equilibria – can be found in the IUPAC monograph series on experimental thermodynamics [48, 49]. A recent publication of Richon [50] not only shows some advanced experimental equipment for the determination of phase equilibria, but also contains some thoughts about the importance of experiments that are worthwhile reading.

3.3 SYNTHETIC METHODS

Synthetic methods circumvent the problem of measuring the composition of coexisting phases by preparing samples of known composition and then bringing about a phase separation by varying pressure or temperature. A (p, T) combination at which the phase separation just sets in is evidently a point on the phase envelope at the fixed composition, i.e., the synthetic methods primarily yield isopleths. Isothermal or isobaric phase diagrams have then to be constructed from a set of isopleths by making cross sections at $T=$const or $p=$const, respectively (see Fig. 3.1).

Synthetic methods are more or less restricted to binary mixtures, because only here points on the phase envelope with the same pressure and temperature

---

[1] … but would have a strong effect on viscosity!

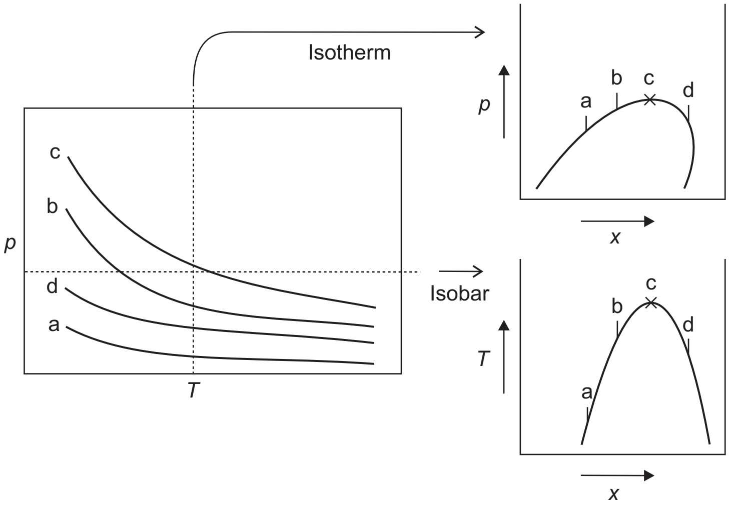

FIGURE 3.1 Construction of isothermal or isobaric phase diagrams from a set of isopleths with different compositions.

must be in equilibrium. For multicomponent mixtures, it would not be possible to determine the composition of the phase coexisting with the fixed phase.

The typical setup for the synthetic method is shown in Fig. 3.2. The central piece is a pressure vessel equipped with temperature and pressure controls as well as a stirrer. The vessel can be transparent (e.g., made from synthetic sapphire) or equipped with windows to permit optical detection of the phase separation. For turbid or colored mixtures, detection can be made by photometry at a suitable wavelength or by light scattering.

The reliability of the synthetic method depends on the ability to determine the onset of phase separation. Lowering the pressure by a small amount for mixture (c) in Fig. 3.1 would, because of the lever rule, result in nearly equal amounts of the coexisting phases, and consequently the phase separation would be easy to see. Lowering the pressure for mixture (d) would result in a very small amount of one of the phases. According to Murphy's Laws, this small amount of phase would probably form a thin film on the walls or a droplet in a corner of the vessel, which could easily escape detection. In other words: the phase separation would be detected deeper inside the two-phase region only, where the amount of the newly formed phase is large enough to be seen.

The systematic pressure error can be estimated from the lever rule Eq. (2.11): very close to the phase boundary, the lever of the majority phase, $x_i - x_i'$, can be approximated by $\delta p/(\mathrm{d}p/\mathrm{d}x_1)$, the ratio of the pressure error and the slope of the phase boundary. On the right hand side of the lever rule, there is n'', the minimum amount of the newly formed phase that can be detected, and its lever, $x_i'' - x_i$, which has a value between 0 and 1. Then, the lever rule can be

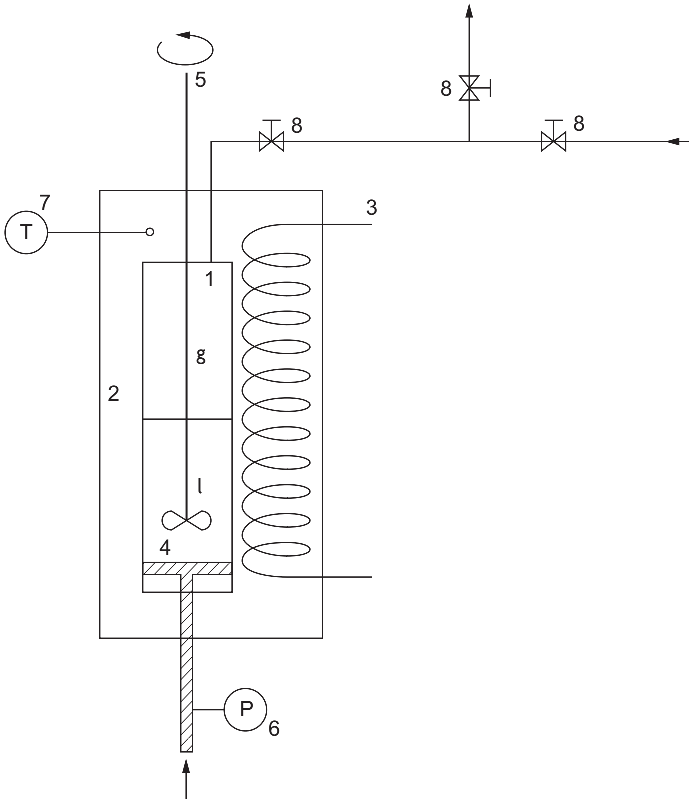

FIGURE 3.2 Schematic representation of an apparatus for the determination of fluid phase equilibria with the synthetic method. (1) Sample space, (2) pressure vessel, (3) heater, (4) piston, (5) stirrer, (6) manometer, (7) thermometer, and (8) valves.

rearranged to yield

$$\delta p \leq \frac{n''}{n'} \frac{\mathrm{d}p}{\mathrm{d}x_1} \,. \tag{3.1}$$

Consequently, the systematic pressure error of the synthetic method is very small in the vicinity of critical points, but can get rather large when the phase boundaries are very steep.

If the coexisting phases have the same refraction indices, the synthetic method with optical detection cannot be applied.

An important variant of the synthetic method is the isochoric technique. Here, a sample of known overall composition is placed in a vessel with constant volume, and the pressure is recorded as a function of temperature. A phase transition can be recognized from a change of the slope of the $p(T)$ isochore. Pressure vessels for this technique do not need moving parts for the pressure control. However, there are compositions at which the change of the slope is hard to detect (see Appendix B.2).

Another variant of the method makes use of pressure vessels, which allow the determination of the phase volumes. If the same (p, T) equilibrium state can be reached with two different overall compositions, the mole fractions of the coexisting phases can be calculated from the material balance equations [51, 52] (see also Problem 1).

3.4 ANALYTIC METHODS

The overall composition of the fluid sample does not have to be known for experiments based on the analytic method. Here, temperature and pressure are adjusted until phase separation occurs, and then the compositions of the coexisting phases can be analyzed. A typical setup is shown in Fig. 3.3.

The apparatus shown here is of the "double recirculation" design, which means that each phase is pumped through the other one with a recirculation pump. This not only provides rapid equilibration, but also makes it easy to

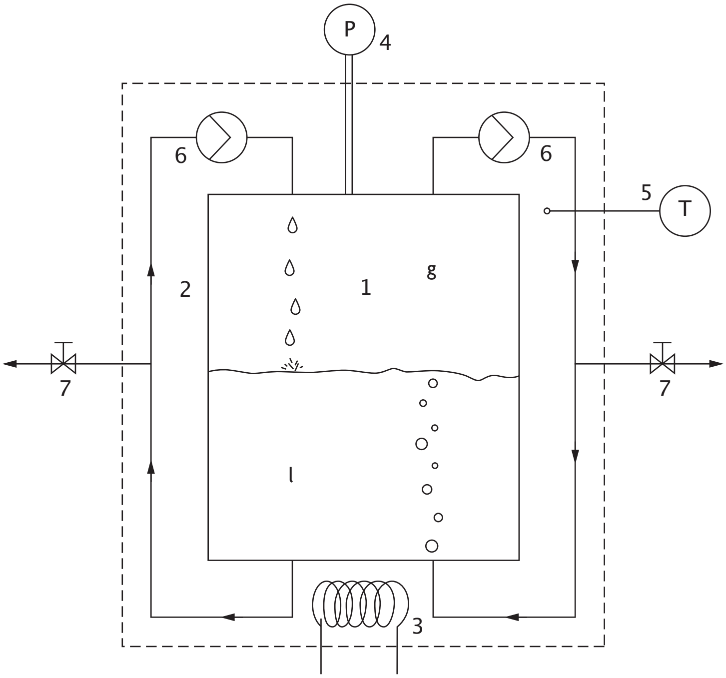

FIGURE 3.3 Schematic representation of an apparatus for the determination of fluid phase equilibria with the analytic method. (1) Sample space, (2) pressure vessel, (3) heater, (4) manometer, (5) thermometer, (6) recirculation pumps, and (7) valves.

divert fractions of the recirculation flows to the analytic device, usually a gas chromatograph.

Removing samples from the system disturbs the phase equilibrium. In order to minimize this effect, analytic phase equilibrium apparatus must be designed in such a way that the amount of substance in the equilibrium vessel is much larger than the size of the sample. This condition sets a minimum useful vessel size, and traditionally analytic apparatus tended to be much larger than synthetic apparatus for the same pressure and temperature range. Nowadays, however, electromagnetically operated valves can reproducibly withdraw samples of less than 1 mg [53]. Still, pressure or temperature fluctuations can be a problem whenever the slope of phase equilibrium isotherms or isobars is small. This behaviour is just the opposite to that of synthetic methods.

In principle, the phase compositions can also be determined in situ by means of spectroscopy, thus avoiding the problem of withdrawing samples. But then one has to make sure that the components of the mixture have nonoverlapping spectral bands.

In the past, IR, UV/Vis, and Raman spectroscopy have been successfully applied. A difficulty with IR spectroscopy is that many compounds have such large extinction coefficients that the optical pathlength cannot exceed a few micrometers. To keep such a pathlength constant in spite of large temperature and pressure variations is a technical challenge. The problem can be circumvented, however, by using NIR (near infrared) spectroscopy, where the extinction coefficients are much smaller, or by using ATR (attenuated total reflection) techniques.

The contours of IR and Raman peaks are affected by molecular collision rates, conformer equilibria, and association effects, and thus show pronounced pressure and temperature dependencies, which necessitate complicated calibrations. UV/Vis spectra reflect electronic structures of the molecules and are therefore less dependent on external parameters. But sometimes the presence of other molecules, especially of polar solvents, shifts the absorption bands; this effect is known as solvatochromy.

Analytic methods rely on the *spatial* separation of phases. They cannot be applied to systems where the phases do not segregate, which can happen if barotropic inversion occurs.

The great advantage of the analytical methods over the synthetic ones is their applicability to multicomponent mixtures.

3.5 TRANSIENT METHODS

3.5.1 Methods Using Flow of Matter

Transient methods are often employed for the determination of vapor pressures and/or sublimation pressures of compounds with a very low volatility, or for the measurement of solubilities of compounds, which are present in traces only.

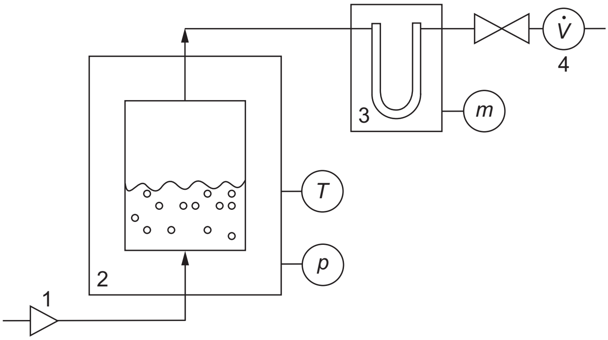

FIGURE 3.4 Schematic representation of an apparatus for the determination of fluid phase equilibria using a material flow method. (1) Compressor, (2) pressure vessel, (3) cold collector attached to precision scale, and (4) flow meter.

Figure 3.4 shows a typical setup: The carrier gas (or supercritical fluid) is compressed to the desired pressure and passed through a vessel filled with the low-volatile compound. After getting saturated with this compound, the fluid is passed through a cold trap, where the low-volatile compound is deposited. The mass loss of the saturation vessel or the mass gain of the cold trap, together with the flow rate, allow the computation of the solubility.

Related techniques are thermogravimetry, where either the sample tray or a cold collector plate is connected to a balance, and Knudsen effusion. The latter has been used to obtain vapor or sublimation pressures of compounds with a *very* low volatility. Then it is advisable to measure the gas density with a mass spectrometer in order to eliminate impurities. Otherwise trace amounts of volatile impurities could easily ruin the experiment.

A flowing inert gas can used to dilute and safely transport the vapor phase of a vapor–liquid equilibrium experiment to the analytical instruments. This so-called stripping technique has been used to study phase equilibria in the limit of infinite dilution [54].

3.5.2 Methods Using Heat Flow

Typical methods of this kind are differential thermal analysis, DTA, and differential scanning calorimetry, DSC. Both techniques subject the sample and a reference system to a slowly increasing or decreasing temperature. As phase transitions are usually accompanied by a change of enthalpy, they cause a temperature difference between the sample and the reference (DTA) or an additional heat flow (DSC), which can be detected.

The disadvantage of these methods is that, because of finite heat conductivity, the samples may contain temperature gradients, so that it is difficult to assign a signal to a sharp temperature value. On the other hand, these methods can work reliably with rather small amounts of substance.

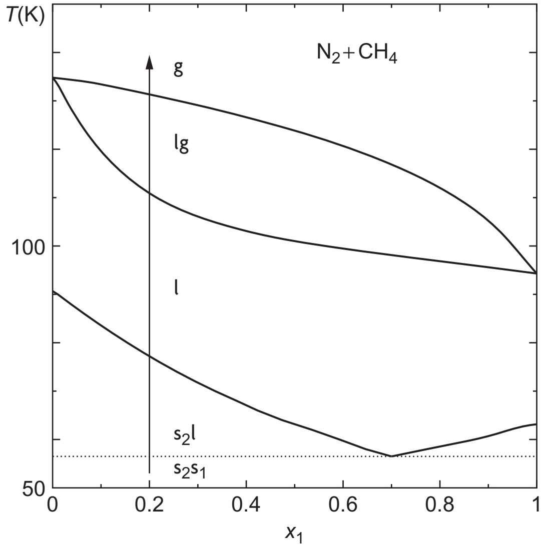

FIGURE 3.5 Isobaric phase diagram of the {nitrogen (1) + methane (2)} system at 0.5 MPa. ——: phase boundaries and ⋯⋯: three-phase (eutectic) equilibrium.

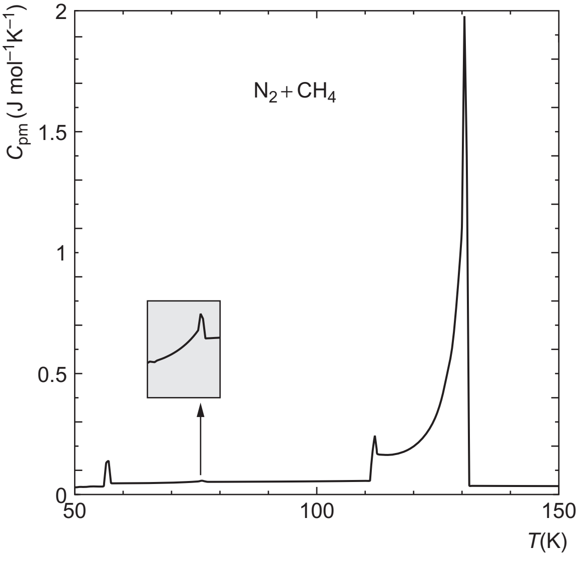

FIGURE 3.6 Theoretical DSC or transitiometry trace for the system {nitrogen (1) + methane (2)} at 0.5 MPa and $x_1 = 0.2$. The peak at 56 K marks the eutectic point ($s_1s_2 \rightarrow s_2l$; s_2 = solid phase of methane) and the tiny peak at 76 K marks the end of the s_2l region ($s_2l \rightarrow l$). The large peak is caused by passing through the lg two-phase region, with the spikes marking the entry ($l \rightarrow lg$) and exit ($lg \rightarrow g$).

DSC can also be applied to mixtures. Here, however, phase transitions usually span a temperature range; in this range, the heat flow is mostly caused by changes of the amounts of the coexisting phases as given by the lever rule. As an example, Fig. 3.5 shows an isobaric phase diagram of the {nitrogen + methane} system, and Fig. 3.6 the simulated[2] trace (heat flow vs. time) of a DSC experiment on this system. A more detailed discussion is given in Section 5.9.

Transitiometry may be regarded as an advanced DSC technique, where not only the temperature, but also the pressure of the sample is controlled. Thus a transitiometer can also record isothermal phase transitions (i.e., phase changes brought about by pressure variation), or even transitions along arbitrary paths in (p, T) space [55–57].

3.6 PROBLEMS

1. A binary mixture consisting of $n_{1,\mathrm{A}}$ moles of component 1 and $n_{2,\mathrm{A}}$ moles of component 2 splits into two phases at the pressure p and the temperature T; the absolute volumes of these phases are measured. The experiment is repeated with a mixture consisting of $n_{1,\mathrm{B}} + n_{2,\mathrm{B}}$ moles of the two components (at the same pressure and temperature!). How can the mole fractions and molar volumes of the coexisting phases be calculated?[3]
2. Why are the beginning and the end of the vapor–liquid transition in Fig. 3.6 marked by spikes? Calculate the overall heat capacity of the sample, using the lever rule, Eq. (2.11) for the two-phase region.

---

[2] Due to the lack of experimental data.

[3] Experimental technique used by Specovius *et al.* and Fontalba *et al.* [51, 52].

Chapter 4

Thermodynamic Variables and Functions

Before discussing phase diagrams and methods for computing them, it is necessary to introduce some thermodynamic concepts and functions. As this book does not focus on thermodynamic fundamentals, this chapter is rather compact. It is not meant as a substitute for a textbook of thermodynamics. Still, this chapter is necessary to establish the nomenclature and to present the relations between some thermodynamic quantities that will be used later.

4.1 FUNDAMENTALS

Thermodynamic quantities can be divided into several categories:

- *Extensive quantities:* quantities that are proportional to the system size, e.g., which double if the system size is doubled by an identical copy process
- *Intensive quantities:* quantities that do not depend on the system size; these can again be divided into two categories:
  - *Fields:* quantities that must be the same in all coexisting phases under equilibrium conditions and in absence of external fields
  - *Densities:* quantities that can have different values in coexisting phases under equilibrium conditions

Examples for field quantities are the temperature T, the pressure p, or the chemical potentials μ_i. Examples for density variables are the molar volume, the molar enthalpy, or the molar heat capacity. These latter properties are intensive, whereas their nonmolar counterparts (total) volume, enthalpy, or heat capacity are extensive.

The most important variables are introduced by the Laws of thermodynamics:

- The *Zeroth Law of thermodynamics* states that there is an energy form called heat, which has the tendency to spread through a system, and a variable called temperature that measures this tendency: heat flows from the regions of high temperature to the regions of low temperature only.

High-Pressure Fluid Phase Equilibria. DOI: 10.1016/B978-0-444-56347-7.00004-9

This statement may seem trivial, but it is necessary, because without this law the other laws of thermodynamics cannot be defined properly.

- The *First Law of thermodynamics* is usually given in the form

$$\mathrm{d}U = đq + đw, \tag{4.1}$$

where q and w are the heat and the work flowing into or out of a system; their sum is reflected in the change of the internal energy U, which is defined by this law. This is practically the law of the conservation of energy.

When dealing with phase equilibria of liquids and gases, it is usually sufficient to consider volumetric work only, i.e., $đw = -p\,\mathrm{d}V$. If other forms of energy play a role (e.g., surface energy, electric energy), the definition of $đw$ has to be extended.

We note in passing that q and w are not state functions, but U is (hence the "đ" differential operator in Eq. (4.1)).

- The *Second Law of thermodynamics* states that there is a state function called entropy defined by

$$\mathrm{d}S = \frac{đq}{T}, \tag{4.2}$$

where $đq$ denotes reversibly exchanged heat. In isolated systems, processes that make the entropy decrease are forbidden. When equilibrium has been reached, the entropy is at its maximum.

- The *Third Law of thermodynamics* states that the entropy of a pure substance in a perfect crystalline state at zero temperature is zero.

Although the second law gives thermodynamic processes a direction, it is seldomly used directly, because its condition – a system perfectly isolated from its environment – is not what is usually needed. Instead, a set of alternative criteria for equilibrium states has been derived:

- $U \rightarrow$ min (internal energy), if $S, V, n = \mathrm{const}$
- $H \rightarrow$ min (enthalpy), if $S, p, n = \mathrm{const}$
- $A \rightarrow$ min (Helmholtz energy), if $T, V, n = \mathrm{const}$
- $G \rightarrow$ min (Gibbs energy), if $p, T, n = \mathrm{const}$

The conditions under which minima of these four energies constitute equilibrium states define their *natural variables*. Of course one can express each energy with each set of variables, if desired; this is discussed in Section 4.4.

Combining Eqs. (4.1) and (4.2) then gives the total differential of the internal energy (tacitly assuming that all changes and processes are carried out reversibly, i.e., all intermediate states of the system are equilibrium states, and all work is volume work, $\mathrm{d}w = -p\,\mathrm{d}V$):

$$\mathrm{d}U = T\,\mathrm{d}S - p\,\mathrm{d}V + \sum_{i=1}^{N} \mu_i\,\mathrm{d}n_i \tag{4.3}$$

The third term on the right-hand side is required for mixtures; it accounts for changes of amounts of substance. The summation includes all components of the mixture.

It should be noted that U, H, A, and G are derived from each other by means of Legendre transformations. The underlying principle is that of an integration by parts to switch variables:

$$\int y\,\mathrm{d}x = xy - \int x\,\mathrm{d}y \tag{4.4}$$

A more detailed explanation is given in Appendix B.1.

Application to the thermodynamic energy functions of mixtures gives the following definitions and total differentials:

- Enthalpy

$$H \equiv U + pV \tag{4.5}$$

$$\begin{aligned} \mathrm{d}H &= T\,\mathrm{d}S - p\,\mathrm{d}V + \sum_{i=1}^{N} \mu_i\,\mathrm{d}n_i + p\,\mathrm{d}V + V\,\mathrm{d}p \\ &= T\,\mathrm{d}S + V\,\mathrm{d}p + \sum_{i=1}^{N} \mu_i\,\mathrm{d}n_i \end{aligned} \tag{4.6}$$

- Helmholtz energy

$$A \equiv U - TS \tag{4.7}$$

$$\mathrm{d}A = -S\,\mathrm{d}T - p\,\mathrm{d}V + \sum_{i=1}^{N} \mu_i\,\mathrm{d}n_i \tag{4.8}$$

- Gibbs energy

$$G \equiv H - TS \tag{4.9}$$

$$\mathrm{d}G = -S\,\mathrm{d}T + V\,\mathrm{d}p + \sum_{i=1}^{N} \mu_i\,\mathrm{d}n_i \tag{4.10}$$

If natural variables other than p, V, T or S are needed, an appropriate energy function can be generated with this method [58].[1]

It should be noted that the "chemical term" is always the same, which means that the chemical potential does not depend on the system of variables

---

[1] This is not an exotic concept at all. Working with a fixed pH is equivalent to specifying the chemical potential of protons in solution, $\mu_{\mathrm{H^+(aq)}}$. In electrochemical applications, it may be useful to have the voltage as a natural variable.

chosen:

$$\mu_i = \left(\frac{\partial U}{\partial n_i}\right)_{S,V,n_{j\neq i}} = \left(\frac{\partial H}{\partial n_i}\right)_{S,p,n_{j\neq i}} = \left(\frac{\partial A}{\partial n_i}\right)_{T,V,n_{j\neq i}} = \left(\frac{\partial G}{\partial n_i}\right)_{T,p,n_{j\neq i}} \tag{4.11}$$

Switching from $U(S, V)$ to $G(p, T)$ has an important side effect: S_m and V_m are density variables, i.e., they can be different in coexisting phases, whereas p and T are field variables. As these are the same in all coexisting phases, there may be states of different density (and hence different G_m value) for one (p, T) combination. Hence, G_m is no longer a true, monovalent function, but a relation. This has consequences for the formulation of the criteria of phase equilibrium and for their implementation in computer programs, as will be shown later.

Another consequence of using field variables is that the integration of Eq. (4.10) at constant pressure and temperature, $\mathrm{d}p = 0$ and $\mathrm{d}T = 0$, and at constant overall composition amounts to an identical copy process of the original infinitesimal system. Because of the extensivity of G, the result is

$$G(p, T, \vec{x}) = \sum_{i=1}^{N} \mu_i(p, T, \vec{x}) n_i. \tag{4.12}$$

An analogous integration of the Helmholtz energy differential Eq. (4.8) at constant temperature and total volume would lead to a more complicated result, for changing the amount of substance at constant volume implies a compression or expansion.

How are the thermodynamic energy functions measured? It turns out that usually they can be determined neither directly nor absolutely, and that at best one can measure their change during a process. This makes the thermodynamic energy functions somewhat fuzzy quantities; only their differences and derivatives are well-defined.

Whenever U_m, H_m, A_m, or G_m are used, they are calculated with respect to some reference state. There is some freedom of choice of this reference state: for nonreacting systems a state in the ideal gas region might be appropriate, whereas for chemically reacting systems the reference states of enthalpies are defined by chemical elements under standard conditions, and of entropies by the Third Law. Whatever the choices of the reference states are, the numerical values of the energy functions depend on them, and their users are well advised to make sure that their choices do not influence the results of their calculations.

4.2 ENERGY FUNCTIONS AND THE EQUATION OF STATE

While the Helmholtz energy and the Gibbs energy are usually not directly measurable, the equation of state[2] $p(V_\mathrm{m}, T, \vec{x})$ is. Eqs. (4.7) and (4.9) can be used to construct A_m and G_m from it. The procedure is as follows:

---

[2] More accurately: the *thermal* equation of state. The function $U_\mathrm{m}(V_\mathrm{m}, T)$ is sometimes called the *caloric* equation of state.

- It is assumed that all components of the mixture are at first separate and at such a low pressure $p^{\ominus}$ that they can be considered ideal gases. The ideal gas state is in principle attainable for each substance. Then the Gibbs energy of the system is

  $$G^{\ominus} = \sum_{i=1}^{N} n_i G^{\ominus}_{\mathrm{m},i}(T). \tag{4.13}$$

  The $G^{\ominus}_{\mathrm{m},i}(T)$ are intrinsic properties of the species. They depend on their chemical constitutions and can be obtained from ideal gas heat capacities:

  $$\begin{aligned} G^{\ominus}_{\mathrm{m},i}(T) &= H^{\ominus}_{\mathrm{m},i}(T) - TS^{\ominus}_{\mathrm{m},i}(T) \\ \text{with } H^{\ominus}_{\mathrm{m},i}(T) &= H^{\ominus}_{\mathrm{m},i}(T^{\ominus}) + \int_{T^{\ominus}}^{T} C^{\ominus}_{p\mathrm{m},i}(T)\,\mathrm{d}T \\ S^{\ominus}_{\mathrm{m},i}(T) &= S^{\ominus}_{\mathrm{m},i}(T^{\ominus}) + \int_{T^{\ominus}}^{T} \frac{1}{T} C^{\ominus}_{p\mathrm{m},i}(T)\,\mathrm{d}T \end{aligned} \tag{4.14}$$

  The previous two equations are applications of Kirchhoff's laws [cf. Eq. (6.25)].

  The heat capacities vary slowly with temperature and can be conveniently represented by cubic spline interpolations of experimental data. However, they are only required when nonisothermal processes are considered; they are not needed for isothermal processes or phase equilibrium calculations, because here coexisting phases must have the same temperature.

  The reference enthalpies, $H^{\ominus}_{\mathrm{m},i}(T^{\ominus})$, as well as reference entropies, $S^{\ominus}_{\mathrm{m},i}(T^{\ominus})$, are needed for chemical reactions only. For plain phase equilibrium calculations without chemical reactions, they as well as $G^{\ominus}_{\mathrm{m},i}(T)$ need not be considered, because they cancel in the relevant equations.
- Now the components are mixed, which creates the ideal mixing entropy. The contribution to the Gibbs energy is

  $$\Delta_{\mathrm{mix}} G = \sum_{i=1}^{N} n_i RT \ln x_i. \tag{4.15}$$

  It should be noted that this contribution depends on the mole fractions of the species, not on surface or volume fractions.
- Finally, the mixture is compressed to the desired pressure:

  $$\Delta_{\mathrm{comp}} G = \int_{p^{\ominus}}^{p} V(p, T, \vec{n})\,\mathrm{d}p \tag{4.16}$$

Therefore the Gibbs energy of the system can be written as the sum of these three contributions:

$$G(p,T,\vec{n})=\sum_{i=1}^{N} n_i\left(G_{\mathrm{m},i}^{\ominus}(T)+RT\ln x_i\right)+\int_{p^{\ominus}}^{p} V(p,T,\vec{n})\,\mathrm{d}p \tag{4.17}$$

As the volume is sometimes not a true, monovalent function of pressure, it is better to switch to a volume-dependent formulation by means of a partial integration:

$$G(p,T,\vec{n})=\sum_{i=1}^{N} n_i\left(G_{\mathrm{m},i}^{\ominus}(T)+RT\ln x_i\right)+pV-p^{\ominus}V^{\ominus}-\int_{V^{\ominus}}^{V} p(V,T,\vec{n})\,\mathrm{d}V. \tag{4.18}$$

Here $V^{\ominus}=nRT/p^{\ominus}$ is the volume of the system in the ideal gas state at $p^{\ominus}$. Because of $G=A+pV$, the resulting equation for the molar Helmholtz energy is

$$A_{\mathrm{m}}(V_{\mathrm{m}},T,\vec{x})=\sum_{i=1}^{N} x_i\left(G_{\mathrm{m},i}^{\ominus}(T)+RT\ln x_i\right)-RT-\int_{V_{\mathrm{m}}^{\ominus}}^{V_{\mathrm{m}}} p(V_{\mathrm{m}},T,\vec{x})\,\mathrm{d}V_{\mathrm{m}}. \tag{4.19}$$

This is the master equation for all thermodynamic calculations of mixture properties based on equations of state.

4.3 RESIDUAL, EXCESS, AND PARTIAL MOLAR QUANTITIES

4.3.1 Residual Quantities

A *residual quantity* is the difference between a property of a real fluid and the same property of an ideal gas at the same density, temperature, and composition:

$$X^{\mathrm{r}}=X(V_{\mathrm{m}},T,\vec{x})-X^{\mathrm{id}}(V_{\mathrm{m}},T,\vec{x}) \tag{4.20}$$

Residual quantities are well-defined and do not depend on reference states.

An important example is the residual Helmholtz energy. The full Helmholtz energy equation, Eq. (4.19), contains an integral $\int p\,\mathrm{d}V_{\mathrm{m}}$. Now all real-gas equations of state contain a term RT/V_{m}, which causes a $\ln(V_{\mathrm{m}}/V_{\mathrm{m}}^{\ominus})$ contribution to A_{m}. This contribution, however, diverges for low densities ($V_{\mathrm{m}}\to\infty$). Although such divergent terms pose no algebraic problems, they are a nuisance in computer programming. Using the residual Helmholtz energy avoids these problems. In order to obtain it, the Helmholtz energy of the ideal gas,

$$A_{\mathrm{m}}^{\mathrm{id}}(V_{\mathrm{m}},T,\vec{x})=\sum_{i=1}^{N} x_i\left(G_{\mathrm{m},i}^{\ominus}(T)+RT\ln x_i\right)-RT-\int_{V_{\mathrm{m}}^{\ominus}}^{V_{\mathrm{m}}} \frac{RT}{V_{\mathrm{m}}}\,\mathrm{d}V_{\mathrm{m}}, \tag{4.21}$$

has to be subtracted from the full Helmholtz energy, Eq. (4.19), giving

$$\begin{aligned}A_\mathrm{m}^\mathrm{r}(V_\mathrm{m},T,\vec{x}) &= -\int\limits_{V_\mathrm{m}^{\ominus}}^{V_\mathrm{m}} \left(p(V_\mathrm{m},T,\vec{x})-\frac{RT}{V_\mathrm{m}}\right)\mathrm{d}V_\mathrm{m}\\ &= -\int\limits_{\infty}^{V_\mathrm{m}} \left(p(V_\mathrm{m},T,\vec{x})-\frac{RT}{V_\mathrm{m}}\right)\mathrm{d}V_\mathrm{m} + \int\limits_{\infty}^{V_\mathrm{m}^{\ominus}} \left(p(V_\mathrm{m},T,\vec{x})-\frac{RT}{V_\mathrm{m}}\right)\mathrm{d}V_\mathrm{m}.\end{aligned} \tag{4.22}$$

Now $V_\mathrm{m}^{\ominus}$ is by definition a molar volume beyond which the system behaves as an ideal gas. Therefore, the last integral in the previous equation is zero, and the residual Helmholtz energy can be written as

$$A_\mathrm{m}^\mathrm{r}(V_\mathrm{m},T,\vec{x}) = -\int\limits_{\infty}^{V_\mathrm{m}} \left(p(V_\mathrm{m},T,\vec{x})-\frac{RT}{V_\mathrm{m}}\right)\mathrm{d}V_\mathrm{m}, \tag{4.23}$$

or, using the molar density $\rho = 1/V_\mathrm{m}$ instead of the molar volume, as

$$A_\mathrm{m}^\mathrm{r}(\rho,T,\vec{x}) = +\int\limits_{0}^{\rho} \frac{p(\rho,T,\vec{x})-RT\rho}{\rho^2}\,\mathrm{d}\rho = +RT\int\limits_{0}^{\rho} \frac{Z-1}{\rho}\,\mathrm{d}\rho. \tag{4.24}$$

The latter function is well-defined for $\rho = 0$: $A_\mathrm{m}^\mathrm{r}(0,T,\vec{x}) = 0$

From it or the equation of state, respectively, all other thermodynamic functions needed for phase equilibrium calculations can be derived:

$$G_\mathrm{m}(V_\mathrm{m},T,\vec{x}) = A_\mathrm{m}(V_\mathrm{m},T,\vec{x}) + pV_\mathrm{m} \tag{4.25}$$

or

$$\frac{G_\mathrm{m}^\mathrm{r}}{RT} = \frac{A_\mathrm{m}^\mathrm{r}}{RT} + Z - 1, \tag{4.26}$$

$$\frac{U_\mathrm{m}^\mathrm{r}}{RT} = -T\left(\frac{\partial(A_\mathrm{m}^\mathrm{r}/RT)}{\partial T}\right)_{V_\mathrm{m},x_k}, \tag{4.27}$$

$$\frac{S_\mathrm{m}^\mathrm{r}}{R} = \frac{U_\mathrm{m}^\mathrm{r}}{RT} - \frac{A_\mathrm{m}^\mathrm{r}}{RT}, \tag{4.28}$$

$$\frac{H_\mathrm{m}^\mathrm{r}}{RT} = \frac{U_\mathrm{m}^\mathrm{r}}{RT} + Z - 1, \tag{4.29}$$

$$Z = \frac{pV_\mathrm{m}}{RT} = -V_\mathrm{m}\left(\frac{\partial(A_\mathrm{m}^\mathrm{r}/RT)}{\partial V_\mathrm{m}}\right)_T + 1, \tag{4.30}$$

residual isochoric heat capacity:

$$\frac{C^{\mathrm{r}}_{V\mathrm{m}}}{R} = -2T\left(\frac{\partial(A^{\mathrm{r}}_{\mathrm{m}}/RT)}{\partial T}\right) - T^2\left(\frac{\partial^2(A^{\mathrm{r}}_{\mathrm{m}}/RT)}{\partial T^2}\right) \tag{4.31}$$

residual isobaric heat capacity:

$$\frac{C^{\mathrm{r}}_{p\mathrm{m}}}{R} = \frac{C^{\mathrm{r}}_{V\mathrm{m}}}{R} + \frac{T\alpha_p^2}{R\rho\kappa_T} - 1 \tag{4.32}$$

For the previous equation we need some additional derivatives, namely the tension coefficient:

$$\beta_V = \left(\frac{\partial p}{\partial T}\right)_{V_\mathrm{m}} \tag{4.33}$$

the isothermal compressibility:

$$\kappa_T = -\frac{1}{V}\left(\frac{\partial V}{\partial p}\right)_T = \left[\rho\left(\frac{\partial p}{\partial \rho}\right)_T\right]^{-1} \tag{4.34}$$

the isobaric expansion coefficient:

$$\alpha_p = \frac{1}{V}\left(\frac{\partial V}{\partial T}\right)_p = \kappa_T\beta_V \tag{4.35}$$

and the internal pressure:

$$\pi_T = \left(\frac{\partial U}{\partial V}\right)_T = T\beta_V - p \tag{4.36}$$

4.3.2 Excess Quantities

An *excess quantity* is the difference between the property of a real mixture and that of an ideal mixture at the same pressure, temperature, and composition:

$$X^{\mathrm{E}} = X(p, T, \vec{x}) - X^{\mathrm{idmix}}(p, T, \vec{x}) \tag{4.37}$$

Excess quantities are useful for mixtures only; they are zero for pure fluids.

In contrast to residual quantities, excess quantities take the pressure as their natural variable. Furthermore, the reference state can also be a liquid.

Ideal mixtures – irrespective of their state of aggregation – have no heat of mixing; their molar volumes are linear mole fraction averages of the molar volumes of their pure components, but of course they do have a mixing entropy:[3]

$$H_{\mathrm{m}}^{\mathrm{idmix}} = \sum_{i=1}^{N} x_i H_{\mathrm{m},i}(p,T) \tag{4.38}$$

$$V_{\mathrm{m}}^{\mathrm{idmix}} = \sum_{i=1}^{N} x_i V_{\mathrm{m},i}(p,T) \tag{4.39}$$

$$S_{\mathrm{m}}^{\mathrm{idmix}} = \sum_{i=1}^{N} x_i S_{\mathrm{m},i}(p,T) - R\sum_{i=1}^{N} x_i \ln x_i \tag{4.40}$$

The last term, the mixing entropy term, can be derived from Eq. (4.15).

With these definitions of ideal mixing, the definitions of the most important excess functions become

$$H^{\mathrm{E}} = H_{\mathrm{m}}(p,T,\vec{x}) - \sum_{i=1}^{N} x_i H_{\mathrm{m},i}(p,T), \tag{4.41}$$

$$V^{\mathrm{E}} = V_{\mathrm{m}}(p,T,\vec{x}) - \sum_{i=1}^{N} x_i V_{\mathrm{m},i}(p,T), \tag{4.42}$$

$$S^{\mathrm{E}} = S_{\mathrm{m}}(p,T,\vec{x}) - \left(\sum_{i=1}^{N} x_i S_{\mathrm{m},i}(p,T) - R\sum_{i=1}^{N} x_i \ln x_i\right). \tag{4.43}$$

$$G^{\mathrm{E}} = G_{\mathrm{m}}(p,T,\vec{x}) - \left(\sum_{i=1}^{N} x_i G_{\mathrm{m},i}(p,T) + RT\sum_{i=1}^{N} x_i \ln x_i\right) \tag{4.44}$$

$$\mu_i^{\mathrm{E}} = \mu_i(p,T,\vec{x}) - \big(G_{\mathrm{m},i}(p,T) + RT\ln x_i\big) \tag{4.45}$$

For other excess quantities the definition has to be derived from these equations (see Problem 3). *It is not safe to assume that an excess quantity is the difference between the property of the real mixture and the linear mole fraction average of the properties of the pure components.*

The excess enthalpy is equal to the heat of mixing under isothermal–isobaric conditions. The excess volume is equal to the volume contraction or expansion under these conditions.

The historical motivation for the definition of the excess quantities was the realization that, for mixtures of chemically similar compounds, the ideal-mixture model represents the experimental data already rather well, and that the excess quantities are small, have no complicated dependence on composition,

---

[3] In Chapter 2, we had called mixtures ideal if they obey Raoult's law. This is in agreement with the present definition; the proof will be given in Section 5.5.2.

and can sometimes even be related to the chemical structures of the components. *This, however, is only true if all pure components of the mixture have the same state of aggregation at the given pressure and temperature.*[4] It is mathematically possible to define the excess functions of a mixture where some pure components are liquids and the others gases. But this is not done in practice, for the resulting excess quantities would neither be small nor easily interpretable.

Consequently, excess functions are not very useful for work involving mixtures of sub- and supercritical components.

For the mathematical modeling of excess quantities several empirical functions have been proposed. By definition, excess quantities are zero for pure components. The simplest possible function fulfilling this requirement is a parabolic symmetric function known as Porter's function:

$$X^{\mathrm{E}} = 4X^{\mathrm{E}}_{\mathrm{max}} x_1 x_2 \tag{4.46}$$

The Redlich–Kister function is a straightforward extension of Porter's function that can also describe asymmetric excess functions:

$$X^{\mathrm{E}} = x_1 x_2 \sum_{i=0}^{m} a_i (x_1 - x_2)^i \tag{4.47}$$

This ansatz is frequently used to fit experimental data.

4.3.3 Partial Molar Quantities

Partial molar quantities are derivatives with respect to the amount of substance at constant pressure and temperature:

$$X_i = \left(\frac{\partial X}{\partial n_i} \right)_{p,T,n_{j \neq i}} \tag{4.48}$$

They represent the change of a quantity when an infinitesimal amount of one of the components of a mixture is added or removed.

Partial molar quantities must not be confused with molar quantities. Partial molar quantities are strictly additive even for real mixtures, whereas molar quantities are not. For example, the molar volume of a mixture can be written as a sum of partial molar volumes,

$$V_{\mathrm{m}}(p,T,\vec{x}) = \sum_{i=1}^{N} x_i V_i(p,T,\vec{x}), \tag{4.49}$$

---

[4] For solid phases it may even be necessary to require the same crystal lattice type.

or as a sum of pure-fluid molar volumes,

$$V_{\mathrm{m}}(p,T,\vec{x}) = \sum_{i=1}^{N} x_i V_{\mathrm{m},i}(p,T) + V^{\mathrm{E}}(p,T,\vec{x}). \tag{4.50}$$

In the latter case the excess volume is needed to make the equation exact.

The chemical potential can be regarded as a partial molar Gibbs energy, hence

$$G_{\mathrm{m}}(p,T,\vec{x}) = \sum_{i=1}^{N} x_i \mu_i(p,T,\vec{x}). \tag{4.51}$$

Taking the differential of this equation gives

$$\mathrm{d}G_{\mathrm{m}} = \sum_{i=1}^{N} \mu_i \, \mathrm{d}x_i + \sum_{i=1}^{N} x_i \, \mathrm{d}\mu_i. \tag{4.52}$$

Comparison with the total differential of G_{m}, Eq.(4.10), at constant pressure and temperature ($\mathrm{d}T = \mathrm{d}p = 0$) leads to

$$\sum_{i=1}^{N} x_i \, \mathrm{d}\mu_i = 0, \tag{4.53}$$

which is the Gibbs–Duhem equation, a very useful relation underlying many proofs and consistency tests, e.g., the integral test of Herington [59].

Incidentally, the Gibbs–Duhem equation can also be regarded as the result of a Legendre transformation of Eq. (4.9).

For binary mixtures, it is possible to express partial molar quantities by means of derivatives with respect to the mole fraction[5]:

$$X_1 = \left(\frac{\partial (nX_{\mathrm{m}})}{\partial n_1}\right)_{p,T,n_2} = X_{\mathrm{m}} + n\left(\frac{\partial X_{\mathrm{m}}}{\partial x_1}\right)_{p,T} \frac{\mathrm{d}x_1}{\mathrm{d}n_1} = X_{\mathrm{m}} + x_2\left(\frac{\partial X_{\mathrm{m}}}{\partial x_1}\right)_{p,T}. \tag{4.54}$$

An analogous treatment for component 2 gives

$$X_2 = X_{\mathrm{m}} - x_1\left(\frac{\partial X_{\mathrm{m}}}{\partial x_1}\right)_{p,T}. \tag{4.55}$$

A generalization of these expressions to multicomponent mixtures has been given by Brown [60, 61]. If the mole fractions $x_1 \ldots x_{N-1}$ are treated as

---

[5] cf. Fig. 5.8 for a geometric interpretation.

independent variables, the partial molar properties are:

$$X_i = X_\mathrm{m} + \left(\frac{\partial X_\mathrm{m}}{\partial x_i}\right) - \sum_{i=1}^{N-1} x_k \left(\frac{\partial X_\mathrm{m}}{\partial x_k}\right), \quad i = 1, \ldots N-1 \tag{4.56}$$

$$X_N = X_\mathrm{m} - \sum_{i=1}^{N-1} x_k \left(\frac{\partial X_\mathrm{m}}{\partial x_k}\right) \tag{4.57}$$

4.4 JACOBIAN DETERMINANTS

Thermodynamic experiments are usually carried out at constant pressure. As will be seen in the next chapter, the stability criteria of fluid mixtures and phase equilibria are usually expressed in terms of derivatives of the *Gibbs energy* at constant pressure and temperature. Equations of state, fundamental equations, or other models obtained from statistical thermodynamics, however, usually make the *Helmholtz energy* available as a function of volume of temperature. Therefore, coordinate transformations from the state variables pressure and temperature to the variables volume and temperature are required. Such transformations can be carried out systematically by means of Jacobian determinants.

Jacobian determinants, also called functional determinants, are defined as follows:

$$\frac{\partial(x,y)}{\partial(u,v)} \equiv \begin{vmatrix} \left(\frac{\partial x}{\partial u}\right)_v & \left(\frac{\partial x}{\partial v}\right)_u \\ \left(\frac{\partial y}{\partial u}\right)_v & \left(\frac{\partial y}{\partial v}\right)_u \end{vmatrix} = \begin{vmatrix} x_{(u)} & x_{(v)} \\ y_{(u)} & y_{(v)} \end{vmatrix} = x_{(u)}y_{(v)} - x_{(v)}y_{(u)} \tag{4.58}$$

A very useful relation for Jacobian determinants is the so-called expansion theorem:

$$\frac{\partial(x,y)}{\partial(u,v)} = \frac{\partial(x,y)}{\partial(z,w)} \frac{\partial(z,w)}{\partial(u,v)} \tag{4.59}$$

Its proof is given in Appendix B.3.

The following equation could be called the reduction theorem; it is obtained from the definition of the Jacobian determinants, Eq.(4.58), by setting $y = v$:

$$\frac{\partial(x,y)}{\partial(u,y)} = \left(\frac{\partial x}{\partial u}\right)_y \underbrace{\left(\frac{\partial y}{\partial y}\right)_u}_{=1} - \left(\frac{\partial x}{\partial y}\right)_u \underbrace{\left(\frac{\partial y}{\partial u}\right)_y}_{=0} = \left(\frac{\partial x}{\partial u}\right)_y \tag{4.60}$$

These theorems can be used to obtain uncommon derivatives. First, we observe that any derivative can be written as a Jacobian determinant because of the reduction theorem:

$$\left(\frac{\partial x}{\partial u}\right)_y = \frac{\partial(x,y)}{\partial(u,y)} \tag{4.61}$$

Second, we can now use the expansion theorem to introduce two new auxiliary variables, r and s:

$$\left(\frac{\partial x}{\partial u}\right)_y = \frac{\partial(x,y)}{\partial(u,y)} = \frac{\dfrac{\partial(x,y)}{\partial(r,s)}}{\dfrac{\partial(u,y)}{\partial(r,s)}} = \frac{\begin{vmatrix} \left(\frac{\partial x}{\partial r}\right)_s & \left(\frac{\partial x}{\partial s}\right)_r \\ \left(\frac{\partial y}{\partial r}\right)_s & \left(\frac{\partial y}{\partial s}\right)_r \end{vmatrix}}{\begin{vmatrix} \left(\frac{\partial u}{\partial r}\right)_s & \left(\frac{\partial u}{\partial s}\right)_r \\ \left(\frac{\partial y}{\partial r}\right)_s & \left(\frac{\partial y}{\partial s}\right)_r \end{vmatrix}} \tag{4.62}$$

At a first glance, this transformation has achieved nothing more than replacing a simple expression with a complicated one. However, the advantage of the new equation lies in the fact that r and s can be chosen freely, and hence can be chosen in a way that simplifies the problem.

An example is the transformation of the derivative of an arbitrary thermodynamic property, w, with respect to mole fraction from $p = \text{const}$ to $V_\mathrm{m} = \text{const}$. For this operation, Eq.(4.62) is invoked with $r = V_\mathrm{m}$ and $s = x$ (mole fraction of component 1):

$$\begin{aligned} \left(\frac{\partial w}{\partial x}\right)_p &= \frac{\partial(w,p)}{\partial(x,p)} = \frac{\dfrac{\partial(w,p)}{\partial(V_\mathrm{m},x)}}{\dfrac{\partial(x,p)}{\partial(V_\mathrm{m},x)}} = \frac{\begin{vmatrix} \left(\frac{\partial w}{\partial V_\mathrm{m}}\right)_x & \left(\frac{\partial w}{\partial x}\right)_{V_\mathrm{m}} \\ \left(\frac{\partial p}{\partial V_\mathrm{m}}\right)_x & \left(\frac{\partial p}{\partial x}\right)_{V_\mathrm{m}} \end{vmatrix}}{\begin{vmatrix} \left(\frac{\partial x}{\partial V_\mathrm{m}}\right)_x & \left(\frac{\partial x}{\partial x}\right)_{V_\mathrm{m}} \\ \left(\frac{\partial p}{\partial V_\mathrm{m}}\right)_x & \left(\frac{\partial p}{\partial x}\right)_{V_\mathrm{m}} \end{vmatrix}} \\ &= \frac{-w_{(V)}A_{(Vx)} + w_{(x)}A_{(2V)}}{0 \times (-A_{(Vx)}) + 1 \times A_{(2V)}} = \frac{1}{A_{(2V)}}\left(-w_{(V)}A_{(Vx)} + w_{(x)}A_{(2x)}\right) \end{aligned} \tag{4.63}$$

Here we have made use of

$$p_{(V)} = \left(\frac{\partial p}{\partial V_\mathrm{m}}\right)_T = -\left(\frac{\partial^2 A_\mathrm{m}}{\partial V_\mathrm{m}^2}\right)_{x,T} = -A_{(2V)} \tag{4.64}$$

and

$$p_{(x)} = \left(\frac{\partial p}{\partial x}\right)_{x,T} = -\left(\frac{\partial^2 A_\mathrm{m}}{\partial V_\mathrm{m} \partial x}\right) = -A_{(Vx)}. \tag{4.65}$$

Application of the transformation Eq.(4.63) to the molar volume, i.e., setting $w = V_\mathrm{m}$, then leads to

$$V_{(x)} = \left(\frac{\partial V_\mathrm{m}}{\partial x}\right)_p = \frac{1}{A_{(2V)}}\left[-\underbrace{\left(\frac{\partial V_\mathrm{m}}{\partial V_\mathrm{m}}\right)_x}_{=1} A_{(Vx)} + \underbrace{\left(\frac{\partial V_\mathrm{m}}{\partial x}\right)_{V_\mathrm{m}}}_{=0} A_{(2V)}\right] = -\frac{A_{(Vx)}}{A_{(2V)}}. \tag{4.66}$$

Substitution of this equation into Eq.(4.63) then gives the desired result for the transformation of a derivative of an arbitrary variable w at constant pressure to one at constant molar volume:

$$\left(\frac{\partial w}{\partial x}\right)_p = \left(\frac{\partial w}{\partial x}\right)_{V_\mathrm{m}} + \left(\frac{\partial w}{\partial V_\mathrm{m}}\right)_x \left(\frac{\partial V_\mathrm{m}}{\partial x}\right)_p \tag{4.67}$$

or

$$(w_{(x)})_p = (w_{(x)})_V + (w_{(V)})_x V_{(x)} \tag{4.68}$$

Another example for the application of Jacobian determinants is the derivation of the Joule–Thomson coefficient, which is the (differential) temperature change during an isenthalpic pressure change

$$\mu_\mathrm{JTh} = \left(\frac{\partial T}{\partial p}\right)_H . \tag{4.69}$$

Applying the expansion theorem with p and T as auxiliary variables gives:

$$\left(\frac{\partial T}{\partial p}\right)_H = \frac{\partial (T,H)}{\partial (p,H)} = \frac{\dfrac{\partial (T,H)}{\partial (p,T)}}{\dfrac{\partial (p,H)}{\partial (p,T)}} \tag{4.70}$$

Observing that $(\partial T/\partial T)_p = 1$, $(\partial T/\partial p)_T = 0$, and $(\partial H/\partial T)_p = C_p$ then leads to the well-known result

$$\mu_\mathrm{JTh} = \frac{1 \times \left(\dfrac{\partial H}{\partial p}\right)_T - 0 \times \left(\dfrac{\partial H}{\partial T}\right)_p}{0 \times \left(\dfrac{\partial H}{\partial p}\right)_T - 1 \times \left(\dfrac{\partial H}{\partial T}\right)_p} = \frac{1}{C_p}\left(\frac{\partial H}{\partial p}\right)_T . \tag{4.71}$$

4.5 VARIABLES OF HISTORICAL IMPORTANCE

The chemical potential of a mixture component can be obtained from the Helmholtz energy Eq. (4.19) by differentiating after the amount of substance, n_i. We write

$$\mu_i(V_\mathrm{m}, T, \vec{x}) = G^\ominus_{\mathrm{m},i} + RT \ln \frac{x_i V^\ominus_\mathrm{m}}{V_\mathrm{m}} + \mu_i^\mathrm{r}, \tag{4.72}$$

where the last term represents the derivative of the compression integral in Eq. (4.24). Taking the exponential of this equation gives

$$\exp\left(\frac{\mu_i}{RT}\right) = \frac{x_i V^\ominus_\mathrm{m}}{V_\mathrm{m}} \exp\left(\frac{G^\ominus_{\mathrm{m},i} + \mu_i^\mathrm{r}}{RT}\right), \tag{4.73}$$

which can be rearranged to

$$\frac{1}{V_{\mathrm{m}}^{\ominus}} \exp\left(\frac{\mu_i - G_{\mathrm{m},i}^{\ominus}}{RT}\right) = \exp\left(\frac{\mu_i^{\mathrm{r}}}{RT}\right) \frac{x_i}{V_{\mathrm{m}}}. \tag{4.74}$$

Multiplying both sides with RT and, on the right-hand side, substituting $RT/V_{\mathrm{m}} = p/Z$ (from the definition of the compression factor) and $px_i = p_i$ (Dalton's law) then yields

$$\frac{RT}{V_{\mathrm{m}}^{\ominus}} \exp\left(\frac{\mu_i - G_{\mathrm{m},i}^{\ominus}}{RT}\right) = \exp\left(\frac{\mu_i^{\mathrm{r}}}{RT}\right) \frac{p_i}{Z} \equiv f_i. \tag{4.75}$$

This equation defines the so-called fugacity of the component i, which can be interpreted as a partial pressure corrected for nonideality. The ratio of fugacity and partial pressure is the fugacity coefficient ϕ_i:

$$f_i = \phi_i p_i \quad \text{with} \quad \lim_{V_{\mathrm{m}} \to \infty} \phi_i = 1. \tag{4.76}$$

If a substance has the same fugacities in two phases at the same temperature, it also has the same chemical potentials. Therefore, the equality of fugacities can be used as an alternative criterion of phase equilibrium. However, fugacities should not be used in nonequilibrium situations, whereas chemical potentials are useful even then for the calculation of driving forces.

Another variable that sometimes appears in the context of mixture thermodynamics is the activity of a species, a_i, or its activity coefficient, $\gamma_i = a_i/x_i$. These variables were invented to "rescue" Raoult's law, Eq. (2.2), which is applicable to ideal mixtures only (chemically similar compounds), whereas the generalized version

$$p_i \phi_i = x_i^{\mathrm{l}} \gamma_i p_i^{\sigma} \tag{4.77}$$

can also be applied to nonideal cases. γ_i is a kind of "fudge factor" that makes this equation exact. It is related to the excess Gibbs energy, or the chemical potential, respectively:

$$G^{\mathrm{E}} = RT \sum_{i=1}^{N} x_i \ln \gamma_i \tag{4.78}$$

$$\mu_i^{\mathrm{E}} = RT \ln \gamma_i \tag{4.79}$$

As excess functions should only be used for mixtures where all pure components have the same state of aggregation, the application of activity coefficients to phase equilibria involving sub- and supercritical compounds can create some problems. So the vapor pressures of the supercritical compounds, which are needed in Eq. (4.77), do not exist and therefore have to be replaced by extrapolations.

Another complication with activity coefficients is that the choice of the reference state is ambiguous. Activity coefficients defined via Raoult's law approach 1 as the mole fraction approaches 1, $x_i \to 1 \Rightarrow \gamma_i \to 1$. But for compounds that do not exist in the pure state (at least not in the same state of aggregation) it is common to consider the infinitely dilute state as ideal, $x_i \to 0 \Rightarrow \gamma_i \to 1$. Examples are substances with high melting points or many biological molecules: one can have a dilute solution of NaCl in water at room temperature, but not a dilute solution of water in NaCl. It is then possible that both types of activity coefficients appear in the same model, which can be rather confusing.

In this book we will restrict ourselves to chemical potentials.

4.6 PROBLEMS

1. The excess Gibbs energy of a mixture is described by a first-order Redlich–Kister function [Eq. (4.47) with $m = 1$]. Derive the excess chemical potentials, μ_i^{E}. What is the limiting behavior for $x_i \to 1$?
2. Does it make sense to define an excess Helmholtz energy? Excess properties are differences between properties of real mixtures and ideal mixtures at the same pressure. Is it possible to use properties at the same molar volume?
3. What is the excess isothermal compressibility of a mixture?
4. Derive expressions for the Helmholtz energy and the isothermal compressibility for a gas obeying the truncated virial equation of state, $Z = 1 + B_2/V_{\mathrm{m}}$.
5. Use Jacobi transformations to obtain the difference between the isobaric and the isochoric heat capacity, $C_p - C_V$.
6. Use Jacobi transformations to derive an expression for the adiabatic compressibility, $\kappa_S = -V^{-1}(\partial V/\partial p)_S$.
7. Show that, for the Redlich–Kwong equation (Eq. (7.12)), the internal pressure π_T is proportional to the attraction term. Is this also true for other equations of state?

Chapter 5

Stability and Equilibrium

This chapter contains thermodynamic concepts and equations related to phase equilibria in general. It is assumed that the principal thermodynamic functions of the systems – the equation of state, the Helmholtz energy function, etc. – are known.

5.1 CRITERIA OF EQUILIBRIUM

What is equilibrium? The question may seem trivial; everybody has got an emotional understanding of what equilibrium is: balanced forces, things at rest, nothing changing . . .

But the criterion “nothing changes” is not sufficient. Consider a metal bar of which one end is cooled and the other end heated: after a while a temperature profile develops along the bar that does not change with time anymore. Still, the bar is not in an equilibrium state, but rather in a stationary state. This can be proven by isolating the bar from its environment, i.e., cutting off all flows of matter and energy, in particular of heat. Then the temperature gradient can no longer be maintained, and the bar relaxes toward its equilibrium state, in which all parts have the same temperature.

Note: It is necessary to distinguish between equilibrium states and stationary states. The former can be maintained indefinitely if the system is isolated from its environment.

Can we say that a system that does not change with time and that is or can be isolated is in an equilibrium state? An amount of liquefied natural gas in contact with its own vapor in an isolating container would be a good example of an equilibrium state – unless this container happens to be on a truck on a mountain road. Fortunately, the degree of freedom “altitude in a gravitational field” does not couple perceptibly with the thermodynamic degrees of freedom, at least not for small containers, and therefore can be omitted in thermodynamic considerations. It must be pointed out, however, that we are now no longer speaking about equilibrium in general, but equilibrium with respect to a chosen set of degrees of freedom.

High-Pressure Fluid Phase Equilibria. DOI: 10.1016/B978-0-444-56347-7.00005-0

For the definition of equilibrium it is necessary to specify its degrees of freedom.

In this book, we will only consider typical thermodynamic degrees of freedom, e.g., volume, amounts of substance, etc., but one should never forget that there may be other degrees of freedom – gravitational[1], electric, magnetic, chemical, and viscoelastic – which can interfere with the common thermodynamic degrees.

In the previous section, field quantities were defined as quantities that must have the same value everywhere in a system at equilibrium. The relevant field quantities for phase equilibrium studies are the temperature T, the pressure p, and the chemical potentials μ_i. Hence, the following criteria for two-phase equilibrium in a mixture of N components can be formulated:

$$\begin{aligned} T' &= T'' \\ p' &= p'' \\ \mu_i' &= \mu_i'' \quad i = 1, \ldots N \end{aligned} \tag{5.1}$$

These criteria represent the thermal, mechanic, and chemical equilibrium of all species between two phases (designated $'$ and $''$). A justification of these criteria is given below.

Fulfilling these criteria does not guarantee, however, that a stable phase equilibrium exists. In addition to these criteria each phase must be thermally stable, mechanically stable, and diffusionally stable, i.e., the isochoric heat capacity,[2] the isothermal compressibility,[3] and the diffusion coefficients must not be negative:

$$\begin{aligned} C_V &> 0 \\ \kappa_T &> 0 \\ D_{ij} &> 0 \quad i,j = 1, \ldots N \end{aligned} \tag{5.2}$$

These stability criteria are *local* conditions only. They guarantee the stability of a phase against small fluctuations of the local temperature, pressure, or composition. There are, however, some caveats to observe:

- The true stable state is characterized by a *global* extremum of the relevant thermodynamic potential, i.e., a global minimum of the total Gibbs energy of the system if pressure and temperature are kept constant. For isochoric–isothermal conditions, however, a minimum of the Helmholtz energy defines the stable state.

---

[1] An example is the density gradient that occurs in fluids in gravitational fields.

[2] The heat capacity of black holes is negative, which are therefore unstable. Massive black holes, however, like the one in the center of our galaxy, manage to stay unstable for a *very* long time.

[3] More precisely: the three-dimensional compressibility. It is possible to have materials with a negative compressibility in one dimension [62].

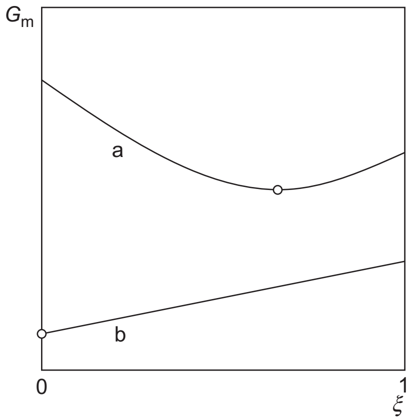

FIGURE 5.1 Gibbs energy of a system at $p, T = \text{const}$ as function of process extent (schematic): (a) typical shape if the process is a reversible chemical reaction and ξ its conversion ratio (local minimum of the Gibbs energy, $F = 0$ thermodynamic degrees of freedom) and (b) possible shape if the process is the evaporation of a pure fluid and ξ the fraction of substance in the vapor phase, and the applied pressure is higher than the vapor pressure (global minimum at $\xi = 0$ with $F = 0$: the liquid does not evaporate; $F = -1$ for $0 < \xi < 1$).

- The global minimum is simply the state with the lowest value. It is not necessary for the Gibbs energy function to be U-shaped in the vicinity of this minimum; in fact, it is not necessary for the Gibbs energy function to be differentiable at all. There are situations where searching for minima by locating zeros of the first derivative may lead to wrong results, as shown in Fig. 5.1, curve b.
- It can happen that the evaluation of the conditions of phase equilibrium for given pressure and temperature gives more than one solution; in such a case the solution that leads to the lowermost total Gibbs energy of the system is the stable solution, and all other solutions are at best metastable.

Overlooking multiple solutions and working with metastable solutions is one of the most common sources of errors in calculations of phase equilibria.

5.2 THERMODYNAMIC STABILITY AND EQUILIBRIUM CRITERIA BASED ON THE SECOND LAW

Here we briefly describe the derivation of the stability and equilibrium criteria from thermodynamic principles. Readers interested in a more detailed derivation are referred to the textbook of Kondepudi and Prigogine [63].

In Section 5.1, it has been pointed out that equilibrium states can be maintained in an isolated state, which distinguishes them from stationary states. “Isolation” in this context means that the system volume is constant, $\mathrm{d}V = 0$, and that there is no exchange of energy or matter with the environment, $\mathrm{d}U = 0$,

$\mathrm{d}n = 0$. Then we know from the second law of thermodynamics that such a system reaches equilibrium when its entropy is at its maximum.

Let $\delta\xi$ denote a perturbation of the equilibrium, i.e., a deviation from the state of maximum entropy maximum in an arbitrary direction. Then one can treat the entropy as a general function of $\delta\xi$. Expansion of this function into a Taylor series gives

$$S(\xi) = S_{\mathrm{eq}} + \frac{\mathrm{d}S}{\mathrm{d}\xi}\delta\xi + \frac{1}{2}\frac{\mathrm{d}^2 S}{\mathrm{d}\xi^2}(\delta\xi)^2 + \cdots. \tag{5.3}$$

Here S_{eq} is the entropy value at the maximum, corresponding to the equilibrium value; the derivatives are computed at the maximum. It can be shown that the first-order term of the expansion leads to the equilibrium criteria and the second-order term to the stability criteria. Here we briefly illustrate this for the variation of the internal energy.

We consider an isolated system consisting of a small subsystem $'$ and a large reservoir system $''$. The two subsystems each have constant volumes and constant amounts of substance, $\mathrm{d}V^{\alpha} = 0$, $\mathrm{d}n^{\alpha} = 0$, but can exchange energy. Hence, the perturbation that has to be considered is $\delta\xi = \mathrm{d}U$. The total entropy change, $\delta S = S - S_{\mathrm{eq}}$ with $S = S' + S''$, is then

$$\begin{aligned}\delta S = &\left(\frac{\partial S'}{\partial U'}\right)\delta U' + \left(\frac{\partial S''}{\partial U''}\right)\delta U'' \\ &+ \frac{1}{2}\left(\frac{\partial^2 S'}{\partial U'^2}\right)(\delta U')^2 + \frac{1}{2}\left(\frac{\partial^2 S''}{\partial U''^2}\right)(\delta U'')^2 + \cdots.\end{aligned} \tag{5.4}$$

As the whole system is isolated, $\delta U' = -\delta U'' \equiv \delta U$ must be fulfilled, and with

$$\left(\frac{\partial S}{\partial U}\right)_{V,n} = \frac{1}{T}, \tag{5.5}$$

the result

$$\delta S = \underbrace{\left(\frac{1}{T'} - \frac{1}{T''}\right)\delta U}_{=\delta^{(1)}S} + \underbrace{\frac{1}{2}\left[\frac{\partial}{\partial U'}\left(\frac{1}{T'}\right) + \frac{\partial}{\partial U''}\left(\frac{1}{T''}\right)\right](\delta U)^2}_{=\delta^{(2)}S} + \cdots \tag{5.6}$$

is obtained. The first-order variation, $\delta^{(1)}S$, has to vanish at a maximum. This immediately gives the criterion for thermal equilibrium,

$$T' = T''. \tag{5.7}$$

The derivatives in the second-order variation term can be written as

$$\left(\frac{\partial \frac{1}{T}}{\partial U}\right)_V = -\frac{1}{T^2}\left(\frac{\partial T}{\partial U}\right)_V = -\frac{1}{T^2 C_V}, \tag{5.8}$$

where C_V denotes the isochoric heat capacity. Furthermore, under isochoric conditions, $\delta U^\alpha = C_V^\alpha T^\alpha$ must hold. The second-order variation therefore becomes

$$\delta^{(2)}S = \frac{1}{2}\left(-\frac{1}{T'^2 C'_V} - \frac{1}{T''^2 C''_V}\right) C'^2_V (\delta T')^2. \tag{5.9}$$

With the thermal equilibrium condition $T' = T''$ and the fact that subsystem $'$ is much smaller than subsystem $''$ ($C'_V \ll C''_V$) we obtain

$$\delta^{(2)}S \simeq -\frac{C'_V(\delta T')^2}{2T'^2}. \tag{5.10}$$

As the entropy has a maximum at equilibrium, its second variation has to be negative. The equation above therefore yields the thermal stability criterion

$$C_V > 0. \tag{5.11}$$

Hence, a system is stable only if the isochoric heat capacity is positive, i.e., if an increase of temperature leads to an increase of its internal energy.

Analogous considerations can be made for perturbations of the volume or the amount of substance of the system. For perturbations of the volume, the first-order variation of the entropy yields the mechanical equilibrium criterion and the second-order variation yields the mechanical stability criterion:

$$p' = p'' \tag{5.12}$$

$$\kappa_T > 0, \tag{5.13}$$

and a perturbation of the amount of substance at constant internal energy and volume gives the criteria of two-phase equilibrium and diffusion stability, which for a binary mixture are[4]

$$\mu'_i = \mu''_i \tag{5.14}$$

$$G_{(2x)} > 0. \tag{5.15}$$

It should be noted that this method of deriving stability and equilibrium criteria is not limited to the "common" thermodynamic variables $p, T,$ and μ_i, but can be extended to electric and magnetic variables, elasticity parameters, or surface properties, if these should be relevant for the system under consideration.

---

[4] Fick's first law of diffusion, $(\partial n_i/\partial t) = -D\mathcal{A}(\partial\rho_i/\partial z)$($\mathcal{A}$: area, ρ_i: concentration, z: distance) seems to suggest that the concentration gradient is the driving force of diffusion. This, however, is not correct: the driving force must be a gradient of a field variable, in this case the chemical potential, $(\partial n_i/\partial t) = -D^*\mathcal{A}(\partial\mu_i/\partial z)$. Comparison of these two equations shows that Fick's diffusion constant is approximately $D = D^*(1-x_i)V_\mathrm{m}(\partial^2 G_\mathrm{m}/\partial x_i^2)$. Therefore, diffusion stability and the curvature of the Gibbs energy function are linked.

5.3 PHASE EQUILIBRIA OF PURE SUBSTANCES

5.3.1 Differential Equations

Along a phase boundary curve (e.g., vapor pressure curve) of a pure substance the phase equilibrium criterion $\mu_i' = \mu_i''$ must be fulfilled. Now for a pure substance, the chemical potential and the molar Gibbs energy are identical,

$$\mu = \left(\frac{\partial G}{\partial n}\right)_{p,T} = G_\mathrm{m}, \tag{5.16}$$

and therefore the equilibrium condition can be written, using the definition of the Gibbs energy, as

$$\mu' = G_\mathrm{m}' = H_\mathrm{m}' - TS_\mathrm{m}' = H_\mathrm{m}'' - TS_\mathrm{m}'' = G_\mathrm{m}'' = \mu''. \tag{5.17}$$

Rearrangement gives the relation between the entropy and the enthalpy of a phase transition:[5]

$$\Delta S_\mathrm{m} = S_\mathrm{m}'' - S_\mathrm{m}' = \frac{1}{T}(H_\mathrm{m}'' - H_\mathrm{m}') = \frac{\Delta H_\mathrm{m}}{T}. \tag{5.18}$$

Now the equilibrium condition, Eq. (5.17), must be fulfilled *at all points* of a phase boundary curve. Consequently, a small change of the chemical potential of one phase along the curve must be matched by the change of the chemical potential of the other phase. One can therefore conclude that

$$\mathrm{d}\mu' = \mathrm{d}\mu'' \tag{5.19}$$

must hold. Because of Eq. (5.16) it is possible to insert the total differential of G_m, Eq. (4.10), which gives

$$\mathrm{d}\mu' = -S_\mathrm{m}'\mathrm{d}T + V_\mathrm{m}'\mathrm{d}p = -S_\mathrm{m}''\mathrm{d}T + V_\mathrm{m}''\mathrm{d}p = \mathrm{d}\mu''. \tag{5.20}$$

Rearranging yields the following differential equation for the phase boundary curve:

$$\frac{\mathrm{d}p}{\mathrm{d}T} = \frac{S_\mathrm{m}'' - S_\mathrm{m}'}{V_\mathrm{m}'' - V_\mathrm{m}'} = \frac{\Delta S_\mathrm{m}}{\Delta V_\mathrm{m}} \tag{5.21}$$

Equation (5.18) can be used to replace the transition entropy, resulting in Clapeyron's equation,

$$\frac{\mathrm{d}p}{\mathrm{d}T} = \frac{\Delta H_\mathrm{m}}{T\Delta V_\mathrm{m}}. \tag{5.22}$$

---

[5] These properties should be written as $\Delta_\mathrm{trs}H_\mathrm{m}$, $\Delta_\mathrm{trs}S_\mathrm{m}$, T_trs. As this section is dealing with phase transitions only, we will omit the "trs" subscript for brevity.

This equation can be applied to all kinds of phase boundaries of pure substances – vapor pressure curves or sublimation pressure curves as well as melting pressure curves or solid–solid transitions.

In the special case that phase $'$ is a condensed phase, phase $''$ a gas phase, and

1. the molar volume of the latter is large in comparison to the molar volume of the former, $V''_\mathrm{m} \gg V'_\mathrm{m}$,
2. the gas phase can be treated as an ideal gas,
3. and the transition enthalpy does not depend on temperature (approximately true for small temperature intervals and far away from the critical point),

it is justified to assume $\Delta V_\mathrm{m} \approx V''_\mathrm{m} \approx RT/p$. Substitution into Eq. (5.22) and integration then yields the famous equation of Clausius and Clapeyron for vapor pressure and sublimation pressure curves:

$$\ln \frac{p}{p_0} = -\frac{\Delta H_\mathrm{m}}{R}\left(\frac{1}{T} - \frac{1}{T_0}\right) \tag{5.23}$$

Here (p_0, T_0) is a reference state on the vapor pressure or sublimation pressure curve. From this equation, one can conclude that a logarithmic plot of the vapor pressure versus T^{-1} should be linear.

Figures 5.2–5.5 illustrate this: Fig. 5.3 shows that the low-temperature end of the logarithmic plot is indeed approximately linear, and that even the deviations from the linear function at high temperatures are very small. In fact, the linearity is far better than it ought to be, for the enthalpy of vaporization is positively not constant (Fig. 5.4), and the difference of the molar volumes drops to zero as the critical point is approached. It turns out, however, that the enthalpy of vaporization and the molar volumes change in such a way that the deviations from constancy or the perfect gas law, respectively, cancel and thus do not affect the linearity of the logarithmic plot very much.

A plot of the densities of the coexisting phases, the so-called orthobaric densities, versus temperature (Fig. 5.5) looks almost like a horizontally oriented parabola at a first glance, but of course the branches of a parabola would run

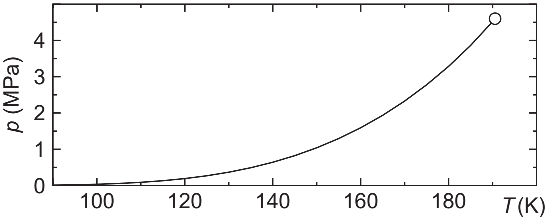

FIGURE 5.2 Vapor pressure curve of methane, calculated from the empirical equation of state of Setzmann and Wagner [64].

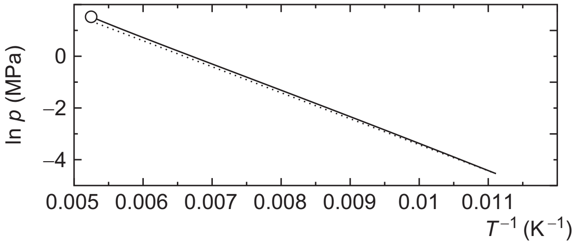

FIGURE 5.3 Vapor pressure curve of methane, logarithmic plot versus inverse temperature. ——: calculated from the empirical equation of state of Setzmann and Wagner [64] and ·········: linear extrapolation of the low-temperature part of the curve (shown for comparison only).

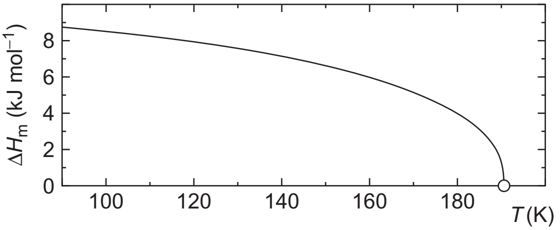

FIGURE 5.4 Vaporization enthalpy of methane, calculated from the empirical equation of state of Setzmann and Wagner [64].

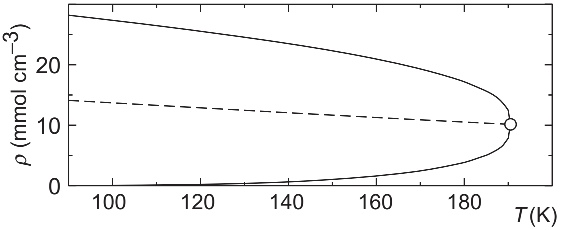

FIGURE 5.5 Molar density of methane as a function of temperature, calculated from the empirical equation of state of Setzmann and Wagner [64]. ——: orthobaric densities and – – : "rectilinear diameter".

toward ±∞, which cannot be expected for a density. Therefore the density diagram of a fluid is necessarily asymmetric.

The average density, $\bar{\rho} = (\rho' + \rho'')/2$ is called *rectilinear diameter*. Its plot versus temperature is an almost straight line for most substances, but a closer investigation shows that this is only approximately true, and that especially in the vicinity of the critical point this property shows a curvature.

Very close to the critical point, where the asymmetry of $\rho(T)$ is still negligible, it can be approximated with a power law:

$$\rho = \rho_c \pm B(T_c - T)^{\beta} \tag{5.24}$$

It can be shown that $\beta = 0.5$ must hold if the underlying equation of state is analytical. The experimentally observed value, however, is about 0.326. The deviation is caused by long-range fluctuations, which give a nonanalytical contribution to the equation of state (see Section 7.8).

For many fluids the entropy of vaporization at their normal boiling points is approximately $\Delta_{\text{vap}}S_{\text{m}} \approx 88\ \text{J mol}^{-1}\text{K}^{-1}$. This relation, which is known as Trouton's rule, is very useful for estimating the vaporization enthalpies of liquids. However, it cannot be used for associating liquids (e.g., water, alcohols, acids), salts, or metals.

The Clausius–Clapeyron equation can also be written as

$$\lg \frac{p}{p_0} = A + \frac{B}{\theta + C}, \tag{5.25}$$

where θ is the temperature in °C and $C = 273.15\text{K}$. If C is allowed to deviate from this value and to become substance-dependent, Eq. (5.25) is called Antoine equation [65]. It is a popular empirical equation for correlating vapor pressure curves.

5.3.2 Algebraic Equations

If a continuous equation of state is available that can describe the vapor and the liquid regime of a fluid, the criteria for phase equilibrium, Eq. (5.17), can be alternatively evaluated as follows:

$$\mu' = G'_{\text{m}} = A'_{\text{m}} + p^{\sigma} V'_{\text{m}} = A''_{\text{m}} + p^{\sigma} V''_{\text{m}} = G''_{\text{m}} = \mu'' \tag{5.26}$$

Here p^{σ} denotes the saturation vapor pressure. Because of

$$A_{\text{m}} = -\int p(V_{\text{m}}, T)\,\text{d}V_{\text{m}}, \tag{5.27}$$

the equilibrium criterion can be rearranged to yield

$$\int_{V'_{\text{m}}}^{V''_{\text{m}}} p(V_{\text{m}}, T)\,\text{d}V_{\text{m}} = p^{\sigma}(V''_{\text{m}} - V'_{\text{m}}). \tag{5.28}$$

$p(V_{\text{m}}, T)$ is the equation of state of the fluid. Equation (5.28) is also known as Maxwell's criterion. Combining Eq. (5.28) with the conditions

$$p(V'_{\text{m}}, T) = p(V''_{\text{m}}, T) = p^{\sigma}, \tag{5.29}$$

yields a set of nonlinear equations for the vapor pressure (It is assumed that the thermal equilibrium condition $T' = T''$ is already fulfilled.). Figure 5.6 shows the geometrical interpretation of this equation: the area under the isotherm given by the equation of state, $p(V_{\text{m}}, T)$, between the orthobaric molar volumes, V'_{m} and V''_{m}, must be equal to the area under the real isotherm (the straight line).

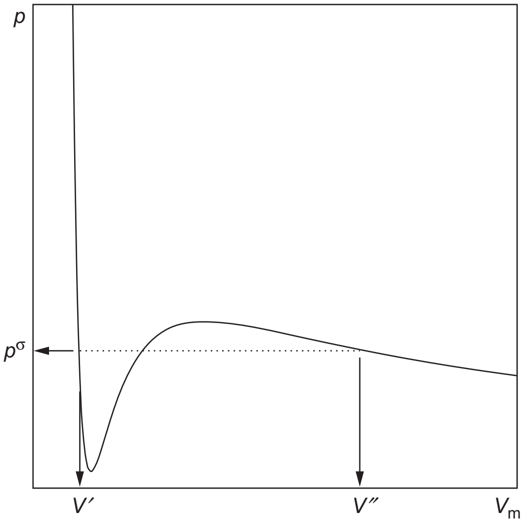

FIGURE 5.6 Schematic representation of Maxwell's criterion for the vapor–liquid equilibrium of a pure fluid. ——: isotherm as calculated with the equation of state and ············: real isotherm.

Figure 5.6 also shows the unstable part of the isotherm, the region of positive slope between the minimum and the maximum. These two extrema constitute the lower and the upper limit of (mechanical) stability: here the isothermal compressibility is infinite ($\kappa_T = \infty$ or $(\partial p/\partial V_\mathrm{m})_T = 0$); between them the compressibility is negative.

These considerations apply to a single isotherm. If the temperature is varied, the orthobaric volumes (the two volumes of the coexisting phases) and the volumes belonging to the extrema form two sets of curves, the connodal (or binodal) curve and the classical spinodal curve, respectively (see Fig. 5.7). The connodal curve encloses the spinodal curve. Outside the connodal curve the fluid is mechanically stable. Inside the spinodal curve it is mechanically unstable. In between it is metastable.

It has occasionally been argued that the extrema of the isotherms of equations of state (often nicknamed "van der Waals loops"[6]) have no physical basis, that the Maxwell construction for the determination of the vapor pressure is an artificial trick to "rescue" these equations, which would otherwise not be applicable to vapor–liquid equilibria, and that a physically correct equation of state should give horizontal isotherms in the 2-phase region. This is arguably true in the limit of infinite system size and infinite time. Still, it is an established experimental fact that liquids can be temporarily overheated or vapors undercooled in the regions that are metastable according to the equations of state. Superheated

---

[6] In fact, this concept was proposed by J. Thomson in 1871 [66], before van der Waals' work.

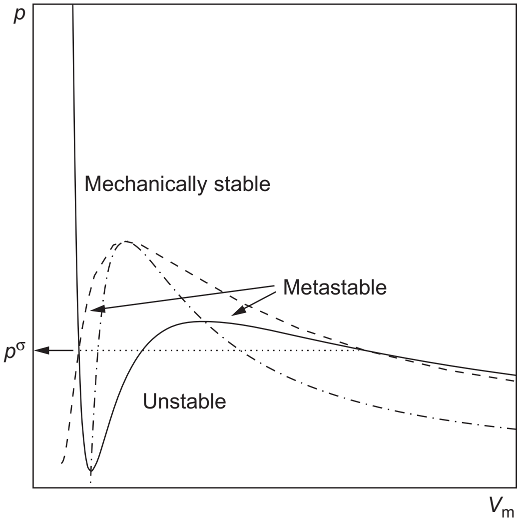

FIGURE 5.7 Schematic representation of the stability regions of an equation of state. ——: isotherm calculated with the equation of state, – – : the connodal curve (locus of equilibrium states) and –·–· : spinodal curve (locus of isotherm extrema).

liquids in the metastable region are likely to start boiling at the container walls or at dust particles; when the spinodal is approached, however, boiling starts everywhere, and as a result the thermal energy of the liquid can be released as a shock wave.[7]

When the temperature is increased, the spinodal as well as the connodal states approach each other; they coincide in the critical point, which for pure fluids is defined by the following criteria:

$$A_{(2V)} = -\left(\frac{\partial p}{\partial V_m}\right)_T = 0 \tag{5.30}$$

$$A_{(3V)} = -\left(\frac{\partial^2 p}{\partial V_m^2}\right)_T = 0. \tag{5.31}$$

Evidently, a critical point is an inflection point of a $p(V_m)$ isotherm with a horizontal tangent.

A vapor pressure curve cannot have a pressure or temperature maximum. A temperature maximum would imply $dT/dp = 0$, and would necessitate $\Delta V_m = 0$ because of Eq. (5.22). But for pure fluids at constant temperature and in absence

---

[7] Maxwell's criterion seems to imply that $p(V_m)$ exists and is integrable in the two-phase region. This, however, is not necessarily true, for the integration could also be carried out along an arbitrary path in the (V_m, T) plane running from the liquid state to the vapor state without entering the two-phase region.

of external fields all thermodynamic properties depend on the molar volume only, and this dependence is a monovalent function (e.g., the equation of state). Therefore, the molar volumes of the liquid and the vapor phase cannot become equal without all other properties becoming equal, too, and this can only happen at a critical point.

In an analogous way one can argue against pressure maxima of vapor pressure curves, which would require $\Delta S_\mathrm{m} = 0$.

Maxwell's criterion can be used to compute vapor pressure curves from equations of state, provided that an initial guess for the vapor pressure is available for which the equation of state gives distinct liquid and vapor densities. Algorithm 1 extrapolates initial values with the Clausius–Clapeyron equation, if possible. If Maxwell's criterion cannot be evaluated, it locates the two-phase region with a bisection method, i.e., it increases or decreases the initial pressure, depending on the curvature of the equation of state. Then it solves Maxwell's criterion by means of the Marquardt–Levenberg method. The enthalpy of vaporization, which is required for the extrapolation of initial values, is at first estimated with Trouton's rule, but then recalculated from vapor pressure points as soon as they become available.

An alternative algorithm will be discussed in Section 5.8.

5.4 CRITICAL POINTS OF PURE FLUIDS

Often the calculation of the critical data of a pure substance can be avoided, because they are given. In this case, however, it is necessary to calculate the parameters of the equation of state from them. In any case, the system of nonlinear equations $A_{(2V)} = A_{(3V)} = 0$ [Eqs (5.30) and (5.31)] has to be solved. For some simple equations of state analytic solutions exist, e.g., for the equation of van der Waals, Eq. (7.10):

$$p_\mathrm{c} = \frac{a}{27b^2} \qquad V_\mathrm{mc} = 3b \qquad T_\mathrm{c} = \frac{8a}{27bR} \tag{5.32}$$

For others the critical conditions have to be solved numerically. This can conveniently be done for example with the Marquardt–Levenberg method (see Appendix A.13).

There is a third critical condition, however, which can create problems, namely the condition that, at the critical point, the equation of state must return the critical pressure, $p(V_\mathrm{mc}, T_\mathrm{c}) = p_\mathrm{c}$.

Evidently, a two-parameter equation of state cannot match three critical conditions. Thus the van der Waals equation gives a fixed critical compression factor $Z_\mathrm{c} = p_\mathrm{c} V_\mathrm{mc} / RT_\mathrm{c}$ of 0.375, which is far too high. The famous Redlich–Kwong equation, Eq. (7.12), gives 0.333, which is also too high; the experimentally found values for most substances are between 0.23 and 0.29 (exceptions are strongly associating fluids, metals, salts, and quantum gases). But also many equations of state with three or more parameters cannot give Z_c

values in the experimental range. A selection of equations of state that have proven useful for the calculation of fluid properties as well as a discussion of their behavior at the critical point can be found in Chapter 7.

Algorithm 1: Vapor pressure curve of a pure compound

```
Input: equation of state: $p(\rho, T)$, fundamental equation: $A_\mathrm{m}(\rho, T)$
Data: critical data, $p_\mathrm{c}$ and $T_\mathrm{c}$, initial temperature $T_0$
Result: vapor pressure $p^\sigma(T), T = T_0, \dots T_\mathrm{c}$

function $y(p^\sigma, T)$ [Maxwell's criterion]:
    solve $p^\sigma = p(\rho, T)$ for $\rho$;
    if only 1 solution found then
        trigger exception;
    else
        assign solutions to $\rho^\mathrm{l}$ and $\rho^\mathrm{g}$;
        return $y := A_\mathrm{m}(\rho^\mathrm{g}, T) - A_\mathrm{m}(\rho^\mathrm{l}, T) + p^\sigma(1/\rho^\mathrm{g} - 1/\rho^\mathrm{l})$;
    end
end

$\Delta H_\mathrm{m} := T_0 \Delta S_\mathrm{m,Trouton}$ [use Trouton's rule as 1st estimation];
$p_0 := \frac{1}{2} p_\mathrm{c}$;
for $T := T_0, \dots T_\mathrm{c}$ do
    estimate $p := p_0 \exp\left(-\frac{\Delta H_\mathrm{m}}{R}\left(\frac{1}{T_0} - \frac{1}{T}\right)\right)$ [Eq. (5.23)];
    evaluate $y(p, T)$;
    if exception then
        $\delta p := 0$ [bisection search for a good initial pressure];
        repeat
            curvature $p_{(2\rho)} := (\partial^2 p(\rho, T)/\partial \rho^2)_T$;
            if $p_{(2\rho)} > 0$ then
                if $\delta p = 0$ then $\delta p := \frac{1}{2} p$;
                $p := p - \delta p$;
            else
                if $\delta p = 0$ then $\delta p := \frac{1}{2}(p_\mathrm{c} - p)$;
                $p := p + \delta p$;
            end
            $\delta p := \frac{1}{2} \delta p$;
            evaluate $y(p, T)$;
        until no exception;
    end
    solve $y(p) = 0$ by means of Marquardt–Levenberg method;
    if $T > T_0$ then $\Delta H_\mathrm{m} := R \ln(p/p_0) / \left(\frac{1}{T_0} - \frac{1}{T}\right)$
end
```

Users of an equation of state are advised to make sure that it can fulfill all three critical conditions before attempting to fit parameters to critical data or to compute thermodynamic data in the vicinity of the critical point.

5.5 PHASE EQUILIBRIA OF BINARY MIXTURES

5.5.1 Differential Equations

For the calculation of two-phase equilibria of binary mixtures it is necessary to consider not only pressure and temperature, but also the mole fractions x_1' and x_i'' of the coexisting phases. In analogy to Eq. (5.17), along the phase boundary the following equation must be fulfilled for both components:

$$\begin{aligned} \mathrm{d}\mu_i' &= -S_i'\,\mathrm{d}T + V_i'\,\mathrm{d}p + \left(\frac{\partial \mu_i'}{\partial x_1}\right)_{p,T} \mathrm{d}x_1' \\ &= -S_i''\,\mathrm{d}T + V_i''\,\mathrm{d}p + \left(\frac{\partial \mu_i''}{\partial x_1}\right)_{p,T} \mathrm{d}x_1'' = \mathrm{d}\mu_i'' \end{aligned} \tag{5.33}$$

S_i and V_i are *partial* molar entropies or volumes, respectively; they must not be confused with molar properties [see Eq. (4.48)]. Equation (5.33) is the extension of Eq. (5.20) to binary mixtures.

Combining terms with the same differentials gives

$$(S_i' - S_i'')\,\mathrm{d}T - (V_i' - V_i'')\,\mathrm{d}p = \left(\frac{\partial \mu_i'}{\partial x_1}\right)_{p,T} \mathrm{d}x_1' - \left(\frac{\partial \mu_i''}{\partial x_1}\right)_{p,T} \mathrm{d}x_1'' \quad i = 1, 2. \tag{5.34}$$

Multiplying this equation with x_1'' for $i = 1$ and with x_2'' for $i = 2$, and adding the results gives

$$\begin{aligned} &[x_1''(S_1' - S_1'') + x_2''(S_2' - S_2'')]\,\mathrm{d}T - [x_1''(V_1' - V_1'') + x_2''(V_2' - V_2'')]\,\mathrm{d}p \\ &= x_1''\left(\frac{\partial \mu_1'}{\partial x_1}\right) \mathrm{d}x_1' - x_1''\left(\frac{\partial \mu_1''}{\partial x_1}\right) \mathrm{d}x_1'' \\ &\quad + x_2''\left(\frac{\partial \mu_2'}{\partial x_1}\right) \mathrm{d}x_1' - x_2''\left(\frac{\partial \mu_2''}{\partial x_1}\right) \mathrm{d}x_1'' \end{aligned} \tag{5.35}$$

Because of the Gibbs–Duhem equation, Eq. (4.53),

$$x_1\left(\frac{\partial \mu_1}{\partial x_1}\right)_{p,T} + x_2\left(\frac{\partial \mu_2}{\partial x_1}\right)_{p,T} = 0, \tag{5.36}$$

the second and the fourth term on the right-hand side cancel. Furthermore, the Gibbs–Duhem equation can be used to express μ_2' with μ_1' in the third term:

$$[x_1''(S_1'-S_1'')+x_2''(S_2'-S_2'')]\,\mathrm{d}T-[x_1''(V_1'-V_1'')+x_2''(V_2'-V_2'')]\,\mathrm{d}p = \frac{x_1''-x_1'}{x_2'}\left(\frac{\partial\mu_1'}{\partial x_1}\right)\mathrm{d}x_1' \tag{5.37}$$

If Eq. (5.34) had not been multiplied with x_i'', but with x_i', the result would have been

$$[x_1'(S_1'-S_1'')+x_2'(S_2'-S_2'')]\,\mathrm{d}T-[x_1'(V_1'-V_1'')+x_2'(V_2'-V_2'')]\,\mathrm{d}p = \frac{x_1''-x_1'}{x_2''}\left(\frac{\partial\mu_1''}{\partial x_1}\right)\mathrm{d}x_1'' \tag{5.38}$$

Equations (5.37) and (5.38) can be used to determine the appropriate differential equation of a phase boundary for each cross section of a three-dimensional phase diagram. For example, for an isothermal cross section $\mathrm{d}T=0$ holds, and these equations can be transformed into the differential equations of the bubble point curve and the dew point curve in a px diagram:

$$\frac{\mathrm{d}p}{\mathrm{d}x_1'}=-\frac{x_1''-x_1'}{x_2'[x_1''(V_1'-V_1'')+x_2''(V_2'-V_2'')]}\left(\frac{\partial\mu_1'}{\partial x_1}\right) \tag{5.39}$$

$$\frac{\mathrm{d}p}{\mathrm{d}x_1''}=-\frac{x_1''-x_1'}{x_2''[x_1'(V_1'-V_1'')+x_2'(V_2'-V_2'')]}\left(\frac{\partial\mu_1''}{\partial x_1}\right) \tag{5.40}$$

Similarly, the differential equations of the liquid and the vapor branches of isopleths in a pT diagram ($\mathrm{d}x_1'=\mathrm{d}x_1''=0$) are obtained as

$$\frac{\mathrm{d}p}{\mathrm{d}T}=\frac{x_1''(S_1'-S_1'')+x_2''(S_2'-S_2'')}{x_1''(V_1'-V_1'')+x_2''(V_2'-V_2'')} \tag{5.41}$$

$$\frac{\mathrm{d}p}{\mathrm{d}T}=\frac{x_1'(S_1'-S_1'')+x_2'(S_2'-S_2'')}{x_1'(V_1'-V_1'')+x_2'(V_2'-V_2'')} \tag{5.42}$$

Equations (5.39) through (5.42) are called coexistence equations or Gibbs–Konowalow equations [67, 68].

Equations (5.39) and (5.40) can be further simplified by applying Equations (4.54) and (4.55) to the evaluation of the V_i as well as the μ_i; for the latter, the relation

$$\left(\frac{\partial\mu_1}{\partial x_1}\right)_{p,T}=x_2G_{(2x)} \tag{5.43}$$

Algorithm 2: Isothermal phase boundary curves of a binary mixture from the Gibbs–Konowalow equations

```
Input: equation of state $p(\rho, T)$, fundamental equation $A_\mathrm{m}(\rho, T)$
Data: temperature $T$, vapor pressure of pure component 2 $p_2^\sigma$
Result: bubble and dew point pressures
$p'(x_1), p''(x_1), x_1 = 0 \ldots 1$

function $\vec{y}(p', p'', x_1)$:
    for phases $\alpha := ', ''$ do
        solve $p^\alpha = p(\rho, T)$ for $\rho^\alpha$;
        $V_\mathrm{m}^\alpha := 1/\rho^\alpha$ (select appropriate density);
        calculate $V_{(x)}^\alpha$ using Eq. (4.66);
        calculate $G_{(2x)}^\alpha$ using Eq. (5.53);
    end
    if $\Delta x_1 \neq 0$ then
        $y_1 := -G'_{(2x)}/(V'_{(x)} - (\Delta V_\mathrm{m}/\Delta x_1))$ [Eq. (5.44)];
        $y_2 := -G''_{(2x)}/(V''_{(x)} - (\Delta V_\mathrm{m}/\Delta x_1))$;
    else
        $K_1 := \exp(-\Delta\mu_1^{\mathrm{r},\infty}) V''_\mathrm{m}/V'_\mathrm{m}$ [Eq. (5.73)];
        $y_1 := RT(K_1 - 1)/\Delta V_\mathrm{m}$ [Eq. (5.78)];
        $y_2 := y_1/K_1$;
    end
    return $(y_1, y_2)$;
end

$p' := p'' := p_2^\sigma$;
for $x_1 := 0 \ldots 1$ do
    apply Runge–Kutta method to $y(p', p'', x_1)$;
    print $x_1, p', p''$;
end
```

---

is obtained. Consequently, the isothermal Gibbs–Konowalow equations become[8]

$$\frac{\mathrm{d}p}{\mathrm{d}x'_1} = -\frac{G'_{(2x)}}{V'_{(x)} - \frac{V''_\mathrm{m} - V'_\mathrm{m}}{x''_1 - x'_1}} \tag{5.44}$$

$$\frac{\mathrm{d}p}{\mathrm{d}x''_1} = -\frac{G''_{(2x)}}{V''_{(x)} - \frac{V''_\mathrm{m} - V'_\mathrm{m}}{x''_1 - x'_1}}. \tag{5.45}$$

These equations constitute a system of ordinary differential equations for the (isothermal) bubble and dew point curves, with one of the pure-fluid vapor

---

[8] The limiting cases $x_i \to 0$ are discussed in Section 5.5.3.

pressures as the initial state. A possible realization is outlined in Algorithm 2. It is very fast and does not suffer from convergence problems as many other methods. It might fail, however, if the underlying functions $G_\mathrm{m}(p, x_1)$ and $V_\mathrm{m}(p, x_1)$ are discontinuous; this is indeed possible for vapor–liquid equilibria, and even unavoidable in case of azeotropy. Furthermore, this algorithm is not useful for liquid–liquid phase equilibria, because for them it is difficult to find an initial state, as there is no liquid–liquid phase separation for pure fluids.

5.5.2 Algebraic Equations Based on the Gibbs Energy

Because of Eqs (4.54) and (4.55), the chemical potentials for a binary mixture can be expressed as

$$\begin{aligned}\mu_1 &= \left(\frac{\partial G}{\partial n_1}\right)_{p,T,n_2} = G_\mathrm{m} + x_2\left(\frac{\partial G_\mathrm{m}}{\partial x_1}\right)_{p,T}\\ \mu_2 &= \left(\frac{\partial G}{\partial n_2}\right)_{p,T,n_1} = G_\mathrm{m} - x_1\left(\frac{\partial G_\mathrm{m}}{\partial x_1}\right)_{p,T}.\end{aligned} \tag{5.46}$$

Figure 5.8 gives a geometrical interpretation: when a tangent to a graph of the Gibbs energy function $G_\mathrm{m}(x_1)$ is constructed, the μ_i are the ordinate intercepts at $x_i = 0$ (curve 1). The criterion of phase equilibrium, $\mu_i' = \mu_i''$, is therefore

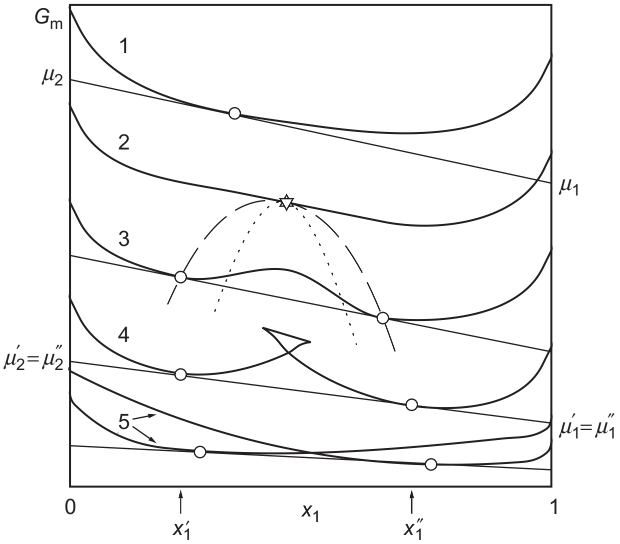

FIGURE 5.8 Schematic representation of the molar Gibbs energy of a binary mixture. Curve 1: stable case, a tangent, and the associated chemical potentials are indicated; curve 2: critical case; curve 3: two-phase equilibrium, the connodal and spinodal curves are indicated; curves 4 and 5: two-phase equilibrium, vapor–liquid equilibrium in the case of a Gibbs energy relation with three branches (the cusps mark the boundaries of mechanical stability).

equivalent to the construction of two tangents to the Gibbs energy function having the same ordinate intercepts or – as it is usually expressed – to the construction of a double tangent. This, however, is only possible if $G_\mathrm{m}(x_1)$ has a concave portion.

In such concave portions the molar Gibbs energy of the mixture with mole fraction x_i is larger than the average Gibbs energy of two adjacent states $x_i \pm \delta x$, i.e., the mixture is absolutely unstable against decomposition into two coexisting phases.

The stability limit is evidently at the inflection point of the $G_\mathrm{m}(x_1)$ function, where the curvature $G_{(2x)}$ is zero. The locus of the inflection points is called the binary spinodal.

As with the pure fluids, there are metastable regions ($G_\mathrm{m}(x_1)$ concave, but with positive curvature) between the spinodal states and the touching points of the double tangent (connodal states), which are the true phase equilibrium states.

If two inflection points coincide, so that the concave region between them vanishes, a critical point occurs; its mathematical conditions are

$$G_{(2x)} = G_{(3x)} = 0, \quad G_{(4x)} > 0 \tag{5.47}$$

The inequality ensures that the global curvature of the Gibbs energy function remains positive.[9] This is discussed in more detail in Chapter 9.

Figure 5.8, curve 4, also demonstrates an alternative shape of the Gibbs energy curve. As fluids can sometimes have more than one molar volume for a given pressure and temperature (see Fig. 5.6), the Gibbs energy curve can have *two* stable branches, and then it may be possible to construct a double tangent between them. The stable branches are connected by a mechanically unstable branch. There are inflection points on the stable branches, usually very close to the cusps. A computer program that returned the lowermost (= most stable) Gibbs energy only might never access the concave regions (regions of negative curvature), so that a phase equilibrium calculation based on an analysis of the local curvature might fail. If the cusps are outside the physically possible mole fraction range, curve pair 5 results: one curve for the liquid and one for the vapor, both convex.

Gibbs energy curves with more than one branch always occur in connection with azeotropy.

Critical points and their vicinity deserve some special attention. Let us assume that the molar volume along the phase boundary can be represented by a Taylor series (this is not possible for $x_i \to 1$!),

$$V_\mathrm{m} = V_\mathrm{m}^\mathrm{c} + V_{(x)}^\mathrm{c}(x_1 - x_\mathrm{c}) + \frac{1}{2}V_{(2x)}^\mathrm{c}(x_1 - x_\mathrm{c})^2 + \cdots . \tag{5.48}$$

---

[9] More accurately: the first nonvanishing derivative of even order must be positive.

Then the denominator of the Gibbs–Konowalow Eq. (5.44) becomes

$$\begin{aligned} V'_{(x)} - \frac{V''_{\mathrm{m}} - V'_{\mathrm{m}}}{x''_1 - x'_1} &= V^{\mathrm{c}}_{(x)} + (x'_1 - x^{\mathrm{c}}_1)V^{\mathrm{c}}_{(2x)} + \cdots \\ - \frac{1}{x''_1 - x'_1}&\left((x''_1 - x'_1)V^{\mathrm{c}}_{(x)} + \frac{1}{2}\left(x''^2_1 - x'^2_1 - 2x^{\mathrm{c}}_1(x''_1 - x'_1)\right)V^{\mathrm{c}}_{(2x)} + \cdots\right) \\ &= -\frac{1}{2}(x''_1 - x'_1)V^{\mathrm{c}}_{(2x)} + \cdots . \end{aligned} \tag{5.49}$$

Similarly, Eq. (5.45) gives a result where the phase labels are exchanged. Forming the ratio of the two Gibbs–Konowalow equations and taking the limit $x'_1, x''_1 \rightarrow x^{\mathrm{c}}_1$ then results in

$$\lim_{x''_1, x'_1 \rightarrow x^{\mathrm{c}}_1} \frac{\mathrm{d}x''_1}{\mathrm{d}x'_1} = \frac{(x'_1 - x''_1)V^{\mathrm{c}}_{(2x)}}{(x''_1 - x'_1)V^{\mathrm{c}}_{(2x)}} = -1. \tag{5.50}$$

This explains not only the terminal slopes of phase equilibrium curves in McCabe–Thiele diagrams (cf. Fig. 2.11), but also the symmetrical shape of phase envelopes in the immediate vicinity of critical points, i.e., $x''_1 - x^{\mathrm{c}}_1 \approx x^{\mathrm{c}}_1 - x'_1$.

Using this symmetry, we can rewrite Eq. (5.44) for near-critical conditions as

$$\frac{\mathrm{d}p}{\mathrm{d}x'_1} \approx 2\frac{G^{\mathrm{c}}_{(2x)} + (x'_1 - x^{\mathrm{c}}_1)G^{\mathrm{c}}_{(3x)}}{((2x^{\mathrm{c}}_1 - x'_1) - x'_1)V^{\mathrm{c}}_{(2x)}}. \tag{5.51}$$

Because of the critical conditions $G_{(2x)} = G_{(3x)} = 0$, this equation and the analogous equation for the other phase yield a slope of $\mathrm{d}p/\mathrm{d}x = 0$ for the phase boundaries. Except for the case of $x_1 \rightarrow 1$ (discussed in Section 5.5.4), this means that critical points of binary mixtures must be local pressure minima or maxima of the phase boundaries in *px* diagrams. Similarly, critical points must be temperature extrema in *Tx* diagrams. This, however, is only true for binary mixtures.

We have to stress again that these derivatives of the Gibbs energy are calculated at constant pressure. As equations of state are usually pressure explicit, it is better to express these derivatives in terms of derivatives of the Helmholtz energy. This can conveniently be done with the help of Jacobian determinants.

Applying Eq. (4.63) immediately gives

$$G_{(x)} = \left(\frac{\partial(A_\mathrm{m} + pV_\mathrm{m})}{\partial x}\right)_p = \left(\frac{\partial A_\mathrm{m}}{\partial x}\right)_p + p\left(\frac{\partial V_\mathrm{m}}{\partial x}\right)_p \tag{5.52}$$

$$= A_{(x)} + A_{(V)}V_{(x)} - A_{(V)}V_{(x)} = A_{(x)}$$

$$G_{(2x)} = A_{(2x)} + A_{(Vx)}V_{(x)} \tag{5.53}$$

$$G_{(3x)} = A_{(3x)} + 3A_{(V2x)}V_{(x)} + 3A_{(2Vx)}V_{(x)}^2 + A_{(3V)}V_{(x)}^3 \tag{5.54}$$

$$G_{(4x)} = A_{(4x)} + 4A_{(V3x)}V_{(x)} + 6A_{(2V2x)}V_{(x)}^2 + 4A_{(3Vx)}V_{(x)}^3 + A_{(4V)}V_{(x)}^4 - \frac{3}{A_{(2V)}}\left(A_{(V2x)} + 2A_{(2Vx)}V_{(x)} + A_{(3V)}V_{(x)}^2\right)^2 \tag{5.55}$$

These relations can be used to discuss the stability or instability of mixtures. Mixtures are (locally) stable if $G_{(2x)} > 0$ (diffusion stability) and $A_{(2V)} > 0$ (mechanical stability). But which property, $G_{(2x)}$ or $A_{(2V)}$, becomes zero first when a phase separation occurs? This question can be answered with a gedankenexperiment: we assume that we have a fluid mixture in a stable state with $G_{(2x)} > 0$ and $A_{(2V)} > 0$. Now we manipulate the temperature, the pressure, or the composition in such a way that $A_{(2V)}$ decreases, i.e., we drive the fluid toward a region of mechanical instability. Because of Eqs (4.66) and (5.53), $G_{(2x)}$ can be expressed as

$$G_{(2x)} = A_{(2x)} - \frac{A_{(Vx)}^2}{A_{(2V)}}. \tag{5.56}$$

As $A_{(Vx)}^2$ cannot become negative, decreasing $A_{(2V)}$ lets the fraction on the right-hand side grow without bounds. If $A_{(2x)}$ remains finite, at one point of our path the right-hand side of the equation becomes negative, i.e., diffusion instability sets in, while $A_{(2V)}$ is still positive.

We conclude from this gedankenexperiment that an arbitrary fluid mixture always exhibits diffusion instability before it becomes mechanically unstable.

The only exceptions from this rule are pure fluids and critical azeotropes; for the latter, the mathematical criteria of binary critical points cannot be used. But as azeotropes behave like pure substances, it is possible to use the critical conditions of pure fluids,

$$A_{(2V)} = A_{(3V)} = 0, \tag{5.57}$$

plus a condition for the exclusion of local concavity:

$$A_{(Vx)} = 0. \tag{5.58}$$

Because of this, in the gedankenexperiment $G_{(2x)}$, $A_{(2V)}$, and $A_{(Vx)}$ become zero simultaneously, so that the systems reaches the limits of mechanical stability and diffusion stability at the same time.

Now we come back to the computation of two-phase equilibria. For this we recall the equilibrium condition

$$\mu_i'(p,T,\vec{x}') = \mu_i''(p,T,\vec{x}'') \quad i=1,\dots N, \tag{5.59}$$

which constitutes a system of N nonlinear equations for the $2(N-1)$ independent mole fractions, pressure, and temperature; evidently there are more variables than equations, and it is up to the user to decide which quantities are kept fixed and which are calculated.

A frequently occurring task is the calculation of the vapor pressure and composition for a liquid of known composition at a prescribed temperature (or for the boiling point at a specified pressure). But especially for binary mixtures the calculation of the compositions of two coexisting phases at given temperature and pressure is also an important task.

The system of equations, Eq. (5.59), can be solved with several methods. One of the oldest approaches is a successive substitution scheme as outlined in Algorithm 3. It is based on the realization that the chemical potentials can be split into $\ln x_i$ terms, residual terms, and intrinsic terms; the latter must cancel in phase equilibrium calculations. Therefore Eq. (5.59) can be rewritten as

$$RT\ln K_i = RT\ln\frac{x_i''}{x_i'} = \mu_i^{\mathrm{r}\prime}(p,T,\vec{x}') - \mu_i^{\mathrm{r}\prime\prime}(p,T,\vec{x}'') + RT\ln\frac{V_\mathrm{m}''}{V_\mathrm{m}'}. \tag{5.60}$$

Algorithm 3: Successive-substitution method for the calculation of fluid phase equilibria of mixtures

```
Input: equation of state $p(V_\mathrm{m},\vec{x},T)$, fundamental equation $A_\mathrm{m}(V_\mathrm{m},\vec{x},T)$
Data: mole fractions of the fixed phase: $\vec{x}'$; estimates of the results
Result: equilibrium pressure $p$, composition of the other phase $\vec{x}''$

function $\vec{K}(\vec{x}',\vec{x}'',p,T)$:
    for phases $'$ and $''$ do
        calculate phase volume $V_\mathrm{m}(p,T,\vec{x})$;
        for components $i=1\dots n$ do $\mu_i^\mathrm{r} = \mu_i^\mathrm{r}(V_\mathrm{m},T,\vec{x})$
    end
    for components $i=1\dots n$ do $K_i = \exp((\mu_i^{\mathrm{r}\prime} - \mu_i^{\mathrm{r}\prime\prime})/RT)$
end

repeat
    $\vec{K} = \vec{K}(\vec{x}',\vec{x}'',p)$;
    for components $i=1\dots n$ do $x_i'' = K_i x_i'$;
    $p = p(V_\mathrm{m}'',T,\vec{x}'')$;
until convergence;
```

With a reasonably good estimate of the phase compositions it is thus possible to calculate the residual chemical potentials and thus the K factors. These can then be converted into (hopefully) better estimates for the mole fractions.

The convergence of this algorithm is sometimes slow. Acceleration schemes have been proposed in the literature. The direct application of a modern nonlinear equation solver, e.g., the Marquardt–Levenberg method (see Appendix A.13) is perhaps advantageous, but it is important to take precautions against this algorithm drifting into negative mole fractions.

Usually, the main problem is finding appropriate initial values. The algorithm sometimes fails to converge, particularly in the vicinity of critical points or three-phase states. A possible solution is "scanning" $G_\mathrm{m}(x)$ for concave portions and using their boundaries as initial values, but this brute force approach is very inefficient for multicomponent mixtures. Another disadvantage of Algorithm 3 and its variants is that the phase volumes have to be calculated at each iteration step.

The algorithm of Michelsen [69, 70] does not solve an algebraic equation like $\vec{\mu}' = \vec{\mu}''$, but tries to construct the tangent plane to the Gibbs energy surface with an efficient minimization method. It requires the calculation of molar volumes at every step, too.

An algorithm that finds initial values and solves the equilibrium conditions without volume calculations is proposed in Section 5.8.

In the special case of an ideal liquid mixture in equilibrium with an ideal-gas phase, Eq. (5.59) can be written as

$$G^\mathrm{l}_{\mathrm{m},i}(p,T) + RT\ln x^\mathrm{l}_i = G^\mathrm{g}_{\mathrm{m},i}(p^\sigma_i, T) + RT\ln\frac{p_i}{p^\sigma_i}. \tag{5.61}$$

The left-hand side follows immediately from Eq. (4.45) by setting the excess function to zero; the right-hand side follows from Eq. (4.18) after substituting the ideal-gas law. At the boiling point of the pure component i, the molar Gibbs energies of liquid and vapor must be equal (we tacitly assume $G_{\mathrm{m},i}(p,T) \approx G_{\mathrm{m},i}(p^\sigma_i, T)$ for liquids); therefore these term cancel. The result is

$$x^\mathrm{l}_i = \frac{p_i}{p^\sigma_i}. \tag{5.62}$$

This is Raoult's law again: an ideal mixture is therefore also ideal in the sense that it obeys Raoult's law.

5.5.3 Vapor–Liquid Equilibria at Infinite Dilution

Let us assume that a binary mixture consists mostly of component 2 and that component 1 is present in trace amounts only. Still, for the vapor–liquid equilibrium of the mixture the condition $\mu^\mathrm{l}_1 = \mu^\mathrm{g}_1$ must hold. Splitting the chemical potentials into intrinsic, ideal gas, and residual contributions gives

$$\mu_1^{\ominus} + RT\ln\frac{x_1^{\mathrm{l}} V_{\mathrm{m}}^{\ominus}}{V_{\mathrm{m}}^{\mathrm{l}}} + \mu_1^{\mathrm{r,l}} = \mu_1^{\ominus} + RT\ln\frac{x_1^{\mathrm{g}} V_{\mathrm{m}}^{\ominus}}{V_{\mathrm{m}}^{\mathrm{g}}} + \mu_1^{\mathrm{r,g}}. \tag{5.63}$$

The intrinsic terms cancel, of course. Rearrangement of terms leads to

$$\frac{x_1^{\mathrm{g}} V_{\mathrm{m}}^{\mathrm{l}}}{x_1^{\mathrm{l}} V_{\mathrm{m}}^{\mathrm{g}}} = \exp\left(\frac{\mu_1^{\mathrm{r,l}} - \mu_1^{\mathrm{r,g}}}{RT}\right). \tag{5.64}$$

Multiplying both sides of this equation with the pressure and observing that $p_1 = px_1^{\mathrm{g}}$ is the partial pressure of component 1 in the vapor phase (Dalton's law) then gives

$$\frac{p_1 V_{\mathrm{m}}^{\mathrm{l}}}{x_1^{\mathrm{l}} V_{\mathrm{m}}^{\mathrm{g}}} = p\exp\left(\frac{\mu_1^{\mathrm{r,l}} - \mu_1^{\mathrm{r,g}}}{RT}\right). \tag{5.65}$$

The limiting ratio of the fugacity of component 1, f_1, and its mole fraction in the liquid phase is called Henry's constant:

$$K_{\mathrm{H},12} \equiv \lim_{x_1^{\mathrm{l}} \to 0} \frac{f_1}{x_1^{\mathrm{l}}} \tag{5.66}$$

Substituting the definition of the fugacity, Eq. (4.75) yields

$$K_{\mathrm{H},12} = \lim_{x_1^{\mathrm{l}} \to 0}\left[\frac{p_1}{Zx_1^{\mathrm{l}}}\exp\left(\frac{\mu_1^{\mathrm{r,g}}}{RT}\right)\right] \tag{5.67}$$

Using Eq. (5.65) to eliminate p_1 finally leads to

$$K_{\mathrm{H},12} = \frac{RT}{V_{\mathrm{m},2}^{\mathrm{l}}}\exp\left(\frac{\mu_1^{\mathrm{r,l},\infty}}{RT}\right), \tag{5.68}$$

where the infinity symbol indicates that the chemical potential must be calculated in the limit of infinite dilution. This, however, is possible: *residual* chemical potentials do not diverge at infinite dilution, but retain finite values (cf. Section 4.3). In this limit, the molar volume of the liquid becomes the orthobaric liquid molar volume of the majority component 2.

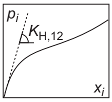

This equation is often used to predict gas solubilities from computer simulations, for there are efficient methods by which these can generate residual chemical potentials.

The values of Henry's constants are the results of a balance between the energy of solvation, the energy required to make a cavity large enough for the solute molecules, and the entropy associated with the solvent structure. For many (not chemically reacting) gas/solvent pairs, Henry's constant increases with temperature (i.e., the gas solubility decreases), but passes through a maximum at high temperatures.

Evaluating the equilibrium condition of component 2 leads – in analogy to Eq. (5.65) – to the following relation:

$$\frac{p_2 V_{\mathrm{m}}^{\mathrm{l}}}{x_2^{\mathrm{l}} V_{\mathrm{m}}^{\mathrm{g}}} = p \exp\left(\frac{\mu_2^{\mathrm{r,l}} - \mu_2^{\mathrm{r,g}}}{RT}\right). \tag{5.69}$$

Taking the logarithm and rearranging yields

$$RT \ln \frac{p_2}{x_2^{\mathrm{l}} p} = \mu_2^{\mathrm{r,l}} - \mu_2^{\mathrm{r,g}} + RT \ln \frac{V_{\mathrm{m}}^{\mathrm{g}}}{V_{\mathrm{m}}^{\mathrm{l}}}. \tag{5.70}$$

In the limit $x_2^{\mathrm{l}} \to 1$, the molar volumes become the pure-fluid molar volumes of component 2, and p its vapor pressure. Furthermore, the right-hand side of the previous equation becomes

$$\mu_2^{\mathrm{r,l}} - \mu_2^{\mathrm{r,g}} + RT \ln \frac{V_{\mathrm{m}}^{\mathrm{g}}}{V_{\mathrm{m}}^{\mathrm{l}}} \to G_{\mathrm{m},2}^{\mathrm{r,l}} - G_{\mathrm{m},2}^{\mathrm{r,g}} + RT \ln \frac{V_{\mathrm{m},2}^{\mathrm{g}}}{V_{\mathrm{m},2}^{\mathrm{l}}} = G_{\mathrm{m},2}^{\mathrm{l}} - G_{\mathrm{m},2}^{\mathrm{g}} = 0, \tag{5.71}$$

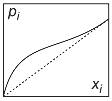

which is the phase equilibrium condition for pure component 2. Eq (5.69) therefore reduces to

$$\frac{p_2}{x_2^{\mathrm{l}}} = p_2^{\sigma}, \tag{5.72}$$

which is Raoult's law again.

Equation (5.64) can be used to express the K factor of component 1 at infinite dilution:

$$K_1^{\infty} = \frac{x_1^{\mathrm{g}}}{x_1^{\mathrm{l}}} = \frac{V_{\mathrm{m},2}^{\mathrm{g}}}{V_{\mathrm{m},2}^{\mathrm{l}}} \exp\left(\frac{\mu_1^{\mathrm{r,l},\infty} - \mu_1^{\mathrm{r,g},\infty}}{RT}\right). \tag{5.73}$$

From this equation, the limiting slopes of the phase boundary curves can be derived. For this we rewrite the isothermal Gibbs–Konowalow equations (5.44) and (5.45) as

$$\frac{\mathrm{d}p}{\mathrm{d}x_1^{\mathrm{l}}} = -\frac{(x_1^{\mathrm{g}} - x_1^{\mathrm{l}}) G_{(2x)}^{\mathrm{l}}}{(x_1^{\mathrm{g}} - x_1^{\mathrm{l}}) V_{(x)}^{\mathrm{l}} - (V_{\mathrm{m}}^{\mathrm{g}} - V_{\mathrm{m}}^{\mathrm{l}})} \tag{5.74}$$

and

$$\frac{\mathrm{d}p}{\mathrm{d}x_1^{\mathrm{g}}} = -\frac{(x_1^{\mathrm{g}} - x_1^{\mathrm{l}}) G_{(2x)}^{\mathrm{g}}}{(x_1^{\mathrm{g}} - x_1^{\mathrm{l}}) V_{(x)}^{\mathrm{g}} - (V_{\mathrm{m}}^{\mathrm{g}} - V_{\mathrm{m}}^{\mathrm{l}})}. \tag{5.75}$$

Now it is important to remember that, because of the definition of the excess Gibbs energy, Eq. (4.44),

$$G_\mathrm{m} = G_\mathrm{m}^{\ominus} + RT(x_1 \ln x_1 + x_2 \ln x_2) + G^\mathrm{E}, \tag{5.76}$$

the dominating and diverging part of $G_{(2x)}$ at small concentrations of x_1 is

$$G_{(2x)} \simeq \frac{RT}{x_1}. \tag{5.77}$$

Using this observation to eliminate $G^\mathrm{l}_{(2x)}$ or $G^\mathrm{g}_{(2x)}$, respectively, substituting $x_1^\mathrm{g} = K_1^\infty x_1^\mathrm{l}$, and taking the limit $x_1 \to 0$ leads to

$$\left.\frac{\mathrm{d}p}{\mathrm{d}x_1^\mathrm{l}}\right|_{x_1 \to 0} = \frac{RT(K_1^\infty - 1)}{V_\mathrm{m}^\mathrm{g} - V_\mathrm{m}^\mathrm{l}}. \tag{5.78}$$

and

$$\left.\frac{\mathrm{d}p}{\mathrm{d}x_1^\mathrm{g}}\right|_{x_1 \to 0} = \frac{RT(1 - 1/K_1^\infty)}{V_\mathrm{m}^\mathrm{g} - V_\mathrm{m}^\mathrm{l}}, \tag{5.79}$$

where K_1^∞ is taken from Eq. (5.73) or, for ideal mixtures, from Eq. (2.8). The last two equations represent the initial and final slopes of bubble and dew point curves.

5.5.4 Mixtures in the Vicinity of Pure-Fluid Critical Points

Another application of the Gibbs–Konowalow equations is the calculation of the limiting slope of phase boundary curves for $x_1 \to 1$. For this we start from the isothermal Gibbs–Konowalow equation for the bubble point curve, Eq. (5.44), and express $G'_{(2x)}$ and $V'_{(x)}$ with derivatives of the Helmholtz energy, Eqs (5.56) and (4.66):

$$\frac{\mathrm{d}p}{\mathrm{d}x_1'} = -\frac{G'_{(2x)}}{V'_{(x)} - \frac{V''_\mathrm{m} - V'_\mathrm{m}}{x''_1 - x'_1}} = -\frac{A_{(2x)} - \frac{A^2_{(Vx)}}{A_{(2V)}}}{-\frac{A_{(Vx)}}{A_{(2V)}} - \frac{V''_\mathrm{m} - V'_\mathrm{m}}{x''_1 - x'_1}} = \frac{A_{(2V)} A_{(2x)} - A^2_{(Vx)}}{A_{(Vx)} + A_{(2V)} \frac{V''_\mathrm{m} - V'_\mathrm{m}}{x''_1 - x'_1}}. \tag{5.80}$$

On approaching the critical point along the phase boundary, V'_m and V''_m become equal. Consequently, the $V_\mathrm{m}(x_1)$ curve touches the V_m axis with a vertical tangent (see Fig. 2.16). Alternatively, we can state that the function $x_1(V_\mathrm{m})$ has got a zero slope. The Taylor expansion of this function must therefore have the general shape

$$x'_1 = 1 + \alpha(\Delta V'_\mathrm{m})^2 + \cdots \quad x''_1 = 1 + \alpha(\Delta V''_\mathrm{m})^2 + \cdots \\ \text{with } \Delta V_\mathrm{m} = V_\mathrm{m} - V_{\mathrm{mc},1}, \tag{5.81}$$

where α is a negative parameter. Consequently[10],

$$\frac{\Delta V''_\mathrm{m}}{\Delta V'_\mathrm{m}} = -\sqrt{\frac{1-x''_1}{1-x'_1}} = -\sqrt{K_2} \tag{5.82}$$

and

$$\begin{aligned} x''_1 - x'_1 &= \alpha(\Delta V''_\mathrm{m} + \Delta V'_\mathrm{m})(V''_\mathrm{m} - V'_\mathrm{m}) \\ &= \alpha(1-\sqrt{K_2})\Delta V'_\mathrm{m}(V''_\mathrm{m} - V'_\mathrm{m}). \end{aligned} \tag{5.83}$$

Inserting this into Eq. (5.80) gives

$$\left.\frac{\mathrm{d}p}{\mathrm{d}x'_1}\right|_{x_1\to 1} = \frac{A_{(2V)}A_{(2x)} - A^2_{(Vx)}}{A_{(Vx)} + A_{(2V)}\frac{1}{\alpha(1-\sqrt{K_2})\Delta V'_\mathrm{m}}}. \tag{5.84}$$

Now K_2 usually runs to a value different from 1 for $x_1 \to 1$ (cf. Fig. 2.7). Furthermore, all equations of state show an at least third-order behavior close to the critical point, so that $A_{(2V)} = -p_{(V)}$ should vanish with $(\Delta V_\mathrm{m})^2$. So, we can conclude that the second term in the denominator of Eq. (5.84) vanishes with $(\Delta V_\mathrm{m})^1$ when the pure-fluid critical point is approached. Then Eq. (5.84) reduces to

$$\left.\frac{\mathrm{d}p}{\mathrm{d}x'_1}\right|_{x_1\to 1} = \frac{A_{(2x)}A_{(2V)} - A^2_{(Vx)}}{A_{(Vx)}} \tag{5.85}$$

or, as $A_{(2V)} = 0$ at a pure-fluid critical point, to

$$\left.\frac{\mathrm{d}p}{\mathrm{d}x'_1}\right|_{x_1\to 1} = -A_{(Vx)}. \tag{5.86}$$

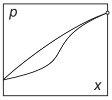

This result is also known as Krichevsky's parameter, and it is perhaps surprising: a pure-fluid critical point is an endpoint of a critical curve of a mixture, and binary critical points are minima or maxima of phase boundary curves; hence one might expect $\mathrm{d}p/\mathrm{d}x_1$ to be zero. But this is evidently not the case (see also Fig. 2.14). The limiting slope at a pure-fluid critical point is zero only in case of border azeotropy.

An analogous analysis can be made for the limiting slope of a dew point curve at a pure-fluid critical point, with the same result: consequently, the dew point curve and the bubble point curve have the same slope at the pure-fluid critical point, thus forming a cusp.

---

[10] We assume $V''_\mathrm{m} > V_{\mathrm{mc},1}$, $V'_\mathrm{m} < V_{\mathrm{mc},1}$. Hence $\Delta V''_\mathrm{m}$ and $\Delta V'_\mathrm{m}$ must have opposite signs.

5.5.5 The Isobaric Phase Diagram of an Ideal Mixture

The evaluation of the phase equilibrium criterion $\mu_i' = \mu_i''$ usually leads to systems of algebraic equations which can be solved numerically only. In the case of an ideal mixture, however, an analytical solution can be given.

For an ideal mixture, the only contribution to the Gibbs energy of mixing comes from the ideal mixing entropy [cf. Eq. (4.44)]:

$$G_\mathrm{m}(p,T,\vec{x}) = \sum_{i=1}^{N} x_i G_{\mathrm{m},i}(p,T) + RT \sum_{i=1}^{N} x_i \ln x_i \tag{5.87}$$

Then the chemical potential of component i is

$$\mu_i(p,T,x_i) = G_{\mathrm{m},i}(p,T) + RT \ln x_i. \tag{5.88}$$

From now on we will omit the pressure from the function arguments, for we are dealing with isobaric conditions. The phase equilibrium conditions then become

$$\begin{aligned} \mu_i^\mathrm{g}(T,x_i^\mathrm{g}) &= G_{\mathrm{m},i}^\mathrm{g}(T) + RT \ln x_i^\mathrm{g} \\ &= G_{\mathrm{m},i}^\mathrm{l}(T) + RT \ln x_i^\mathrm{l} = \mu_i^\mathrm{l}(T,x_i^\mathrm{l}), \end{aligned} \tag{5.89}$$

or, after some rearrangements,

$$K_i = \frac{x_i^\mathrm{g}}{x_i^\mathrm{l}} = \exp\left(\frac{G_{\mathrm{m},i}^\mathrm{l}(T) - G_{\mathrm{m},i}^\mathrm{g}(T)}{RT}\right). \tag{5.90}$$

For the difference of the Gibbs energies of pure component i we can write

$$\begin{aligned} G_{\mathrm{m},i}^\mathrm{l}(T) - G_{\mathrm{m},i}^\mathrm{g}(T) &= \left(H_{\mathrm{m},i}^\mathrm{l}(T) - TS_{\mathrm{m},i}^\mathrm{l}(T)\right) - \left(H_{\mathrm{m},i}^\mathrm{g}(T) - TS_{\mathrm{m},i}^\mathrm{g}(T)\right) \\ &= -\Delta_\mathrm{vap} H_{\mathrm{m},i}(T) + T\Delta_\mathrm{vap} S_{\mathrm{m},i}(T). \end{aligned} \tag{5.91}$$

As the temperature variation in an isobaric vapor–liquid phase diagram is usually not very large, we can approximate $\Delta_\mathrm{vap} H_{\mathrm{m},i}(T)$ by its value at the boiling temperature of the pure component, $T_{\mathrm{b},i}$; the corresponding entropy of evaporation is $\Delta_\mathrm{vap} S_{\mathrm{m},i}(T_{\mathrm{b},i}) = \Delta_\mathrm{vap} H_{\mathrm{m},i}(T_{\mathrm{b},i})/T_{\mathrm{b},i}$. Thus, the Gibbs energy difference becomes

$$\begin{aligned} G_{\mathrm{m},i}^\mathrm{l}(T) - G_{\mathrm{m},i}^\mathrm{g}(T) &\approx -\Delta_\mathrm{vap} H_{\mathrm{m},i}(T_{\mathrm{b},i}) + T\Delta_\mathrm{vap} S_{\mathrm{m},i}(T_{\mathrm{b},i}) \\ &= -\Delta_\mathrm{vap} H_{\mathrm{m},i}(T_{\mathrm{b},i}) + \frac{T}{T_{\mathrm{b},i}} \Delta_\mathrm{vap} H_{\mathrm{m},i}(T_{\mathrm{b},i}). \end{aligned} \tag{5.92}$$

Inserting this into Eq. (5.90) gives

$$K_i(T) = \exp\left[\frac{\Delta_\mathrm{vap} H_{\mathrm{m},i}(T_{\mathrm{b},i})}{R}\left(\frac{1}{T_{\mathrm{b},i}} - \frac{1}{T}\right)\right]. \tag{5.93}$$

Evidently, the logarithms of the K factors are linear functions of the reciprocal temperature.

Incidentally, the exponential term represents the equation of Clausius and Clapeyron, so that it is possible to write

$$K_i(T) = \frac{p_i^\sigma(T)}{p_i^\sigma(T_{\mathrm{b},i})}, \tag{5.94}$$

where $p_i^\sigma(T)$ is the vapor pressure of component i.

The conversion of the K_i to x_i is a linear problem. For a binary mixture, the bubble point curve is given by

$$x_1^{\mathrm{l}} = \frac{K_2 - 1}{K_2 - K_1} \tag{5.95}$$

and the dew point curve by

$$x_1^{\mathrm{g}} = \frac{K_1(K_2 - 1)}{K_2 - K_1}. \tag{5.96}$$

In contrast to the isothermal phase diagram (cf. Section 2.1.2), none of these curves is linear.

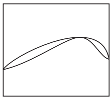

5.5.6 Azeotropy

At an azeotropic point the coexisting phases have the same composition, $x_1' = x_1''$; in this case the Gibbs–Konowalow Eqs (5.39) and (5.40) reduce to

$$\frac{\mathrm{d}p}{\mathrm{d}x_1'} = \frac{\mathrm{d}p}{\mathrm{d}x_1''} = 0. \tag{5.97}$$

An azeotropic point is evidently an extremum of both the bubble point curve and the dew point curve; both curves come together with zero slope, they "osculate."[11] Equations (5.41) and (5.42) reduce to

$$\left.\frac{\mathrm{d}p}{\mathrm{d}T}\right|_{\mathrm{az}} = \frac{x_1 S_1' + x_2 S_2' - x_1 S_1'' - x_2 S_2''}{x_1 V_1' + x_2 V_2' - x_1 V_1'' - x_2 V_2''} = \frac{S_\mathrm{m}' - S_\mathrm{m}''}{V_\mathrm{m}' - V_\mathrm{m}''} = \frac{\Delta S_\mathrm{m}}{\Delta V_\mathrm{m}}, \tag{5.98}$$

i.e., azeotropic curves in a pT projection obey the Clausius–Clapeyron equation as do the vapor pressure curves of pure substances, and like these they can neither have temperature nor pressure extrema.

---

[11] From Latin, *osculare* = to kiss.

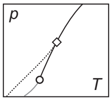

In order to deal with the special case of a *critical azeotropic point*, we expand the numerator and the denominator of Eq. (5.98):

$$\left.\frac{\mathrm{d}p}{\mathrm{d}T}\right|_{\mathrm{az}} = \frac{(S''_{\mathrm{m}}-S^{\mathrm{c,az}}_{\mathrm{m}})-(S'_{\mathrm{m}}-S^{\mathrm{c,az}}_{\mathrm{m}})}{(V''_{\mathrm{m}}-V^{\mathrm{c,az}}_{\mathrm{m}})-(V'_{\mathrm{m}}-V^{\mathrm{c,az}}_{\mathrm{m}})} = \frac{\dfrac{(S''_{\mathrm{m}}-S^{\mathrm{c,az}}_{\mathrm{m}})-(S'_{\mathrm{m}}-S^{\mathrm{c,az}}_{\mathrm{m}})}{x_1-x_1^{\mathrm{c,az}}}}{\dfrac{(V''_{\mathrm{m}}-V^{\mathrm{c,az}}_{\mathrm{m}})-(V'_{\mathrm{m}}-V^{\mathrm{c,az}}_{\mathrm{m}})}{x_1-x_1^{\mathrm{c,az}}}} \tag{5.99}$$

At a critical point the two phases become identical, hence the volume and entropy differences become zero. The slope at the critical azeotropic point can then be obtained by taking the limit $x_1 \to x_1^{\mathrm{c,az}}$ twice:[12]

$$\left.\frac{\mathrm{d}p}{\mathrm{d}T}\right|_{\mathrm{c,az}} = \lim_{x_1\to x_1^{\mathrm{c,az}}} \frac{\dfrac{S''_{\mathrm{m}}-S^{\mathrm{c,az}}_{\mathrm{m}}}{x_1-x_1^{\mathrm{c,az}}} - \dfrac{S'_{\mathrm{m}}-S^{\mathrm{c,az}}_{\mathrm{m}}}{x_1-x_1^{\mathrm{c,az}}}}{\dfrac{V''_{\mathrm{m}}-V^{\mathrm{c,az}}_{\mathrm{m}}}{x_1-x_1^{\mathrm{c,az}}} - \dfrac{V'_{\mathrm{m}}-V^{\mathrm{c,az}}_{\mathrm{m}}}{x_1-x_1^{\mathrm{c,az}}}} = \lim_{x_1\to x_1^{\mathrm{c,az}}} \frac{S''_{(x)}-S'_{(x)}}{V''_{(x)}-V'_{(x)}} = \frac{S_{(2x)}}{V_{(2x)}} \tag{5.100}$$

This, however, is also the result of Eq. (5.103). Evidently, the azeotropic curve and the critical curve have the same slope at the critical azeotropic point.

5.6 CRITICAL CURVES

5.6.1 Differential Equations

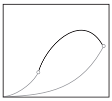

Information about the shape of critical curves can be obtained from the total differential of $G_{(2x)}$, which in turn can be obtained from the total differential of $G_{\mathrm{m}}(p,T,x_1)$ by two-fold differentiation:

$$\mathrm{d}G_{\mathrm{m}} = V_{\mathrm{m}}\,\mathrm{d}p - S_{\mathrm{m}}\,\mathrm{d}T + G_{(x)}\,\mathrm{d}x_1 \tag{5.101}$$

$$\underbrace{\mathrm{d}G_{(2x)}}_{=0} = V_{(2x)}\,\mathrm{d}p - S_{(2x)}\,\mathrm{d}T + \underbrace{G_{(3x)}\,\mathrm{d}x_1}_{=0} \tag{5.102}$$

Because of Eq. (5.47) the indicated terms vanish; the remaining terms can be rearranged to give

$$\left.\frac{\mathrm{d}p}{\mathrm{d}T}\right|_{\mathrm{c}} = \frac{S_{(2x)}}{V_{(2x)}} \tag{5.103}$$

---

[12] or by applying l'Hôpital's rule twice.

The left-hand side represents the slope of a critical curve in a pT projection. The shape of critical curves depends on curvatures of derivatives of the Gibbs energy.

Because of the definition of the Gibbs energy, Eq. (4.9), the curvature of the molar entropy is

$$S_{(2x)} = \frac{H_{(2x)}}{T} - \frac{G_{(2x)}}{T}. \tag{5.104}$$

Here, the second term can be omitted because of $G_{(2x)} = 0$ along critical curves. Together with Eq. (5.103), this leads to the following equation for the slope of a critical curve in a pT diagram:

$$\left.\frac{\mathrm{d}p}{\mathrm{d}T}\right|_{\mathrm{c}} = \frac{H_{(2x)}}{TV_{(2x)}} \tag{5.105}$$

Therefore, a pressure maximum or minimum of a critical curve implies $H_{(2x)} = 0$; likewise, a temperature minimum or maximum implies $V_{(2x)} = 0$, as shown in Fig. 5.9.

The second derivatives of the molar volume and enthalpy can in principle be related to excess functions. Because of Eq. (4.42), the molar volume of binary mixtures can be written as

$$V_{\mathrm{m}} = x_1 V_{\mathrm{m},1} + x_2 V_{\mathrm{m},2} + V^{\mathrm{E}}, \tag{5.106}$$

hence the second derivative is

$$V_{(2x)} = \left(\frac{\partial^2 V^{\mathrm{E}}}{\partial x_1^2}\right), \tag{5.107}$$

and analogous expressions are obtained for the enthalpy. These equations are formally exact. But, as mentioned in Section 4.3.2 already, excess functions should only be used if the two pure components at the given pressure and

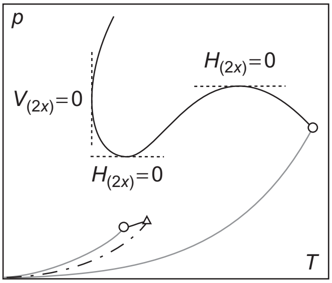

FIGURE 5.9 Schematic pT phase diagram of a class $\mathrm{III_m}$ system. The extrema of the critical curve correspond to zeros of the curvature of the molar volume function or the molar enthalpy function.

temperature have the same state of aggregation. In such a case, the excess functions can be approximated with a number of mathematical models and empirical functions. The simplest function for this purpose is that of Porter, Eq. (4.46), which for the molar volume is

$$V^{\mathrm{E}} = 4V^{\mathrm{E}}_{\max} x_1 x_2. \tag{5.108}$$

With this ansatz, the curvature of the second derivative of the molar volume becomes

$$V_{(2x)} = -8V^{\mathrm{E}}_{\max}. \tag{5.109}$$

An analogous treatment of the enthalpy gives

$$H_{(2x)} = -8H^{\mathrm{E}}_{\max}. \tag{5.110}$$

Consequently, the slope of a critical curve in a pT diagram becomes

$$\left.\frac{\mathrm{d}p}{\mathrm{d}T}\right|_{\mathrm{c}} \approx \frac{H^{\mathrm{E}}_{\max}}{TV^{\mathrm{E}}_{\max}}. \tag{5.111}$$

According to this equation, pressure extrema of critical curves are states where the excess enthalpy is zero, and temperature extrema states where the excess volume vanishes. We must stress, however, that this consideration is practically restricted to $\mathfrak{l}=\mathfrak{l}$ critical curves, and that Porter's function is usually a too crude approximation.

The slope of the critical curve in the Tx projection can be obtained from the total differential of the second critical condition, which must be zero for critical states:

$$\mathrm{d}G_{(3x)} = -S_{(3x)}\,\mathrm{d}T + V_{(3x)}\,\mathrm{d}p + G_{(4x)}\,\mathrm{d}x_1 = 0 \tag{5.112}$$

Using Eq. (5.103) to eliminate dp yields

$$\left.\frac{\mathrm{d}T}{\mathrm{d}x_1}\right|_{\mathrm{c}} = \frac{G_{(4x)}}{S_{(3x)} - V_{(3x)}\left.\frac{\mathrm{d}p}{\mathrm{d}T}\right|_{\mathrm{c}}} = \frac{G_{(4x)}}{S_{(3x)} - \frac{V_{(3x)}S_{(2x)}}{V_{(2x)}}}. \tag{5.113}$$

Alternatively dT can be eliminated, which gives

$$\left.\frac{\mathrm{d}p}{\mathrm{d}x_1}\right|_{\mathrm{c}} = \frac{G_{(4x)}}{-V_{(3x)} + S_{(3x)}\left.\frac{\mathrm{d}T}{\mathrm{d}p}\right|_{\mathrm{c}}} = \frac{G_{(4x)}}{-V_{(3x)} + \frac{S_{(3x)}V_{(2x)}}{S_{(2x)}}}. \tag{5.114}$$

The last two equations can be used to construct a fast method for the computation of critical curves, which does not suffer from the convergence problems

Algorithm 4: Critical curves from differential equations

```
Input: equation of state: $p(\rho, T, x_1)$, fundamental equation: $A_m(\rho, T, x_1)$
Data: pure-components critical data, $p_{c,i}$ and $T_{c,i}$
Result: critical curve(s) $p(x_1), T(x_1), x_1 = 0 \dots 1$

function $\vec{c}(p, T, x_1)$:
    calculate the density $\rho$ from the equation of state;
    calculate $A_{(2V)}, A_{(Vx)}, A_{(2x)}, A_{(3V)}, A_{(2Vx)}, \dots$;
    calculate $A_{(2VT)}, A_{(VxT)}, A_{(2xT)}, A_{(3VT)}, A_{(2VxT)}, \dots$;
    calculate $S_{(2x)}, V_{(2x)}, S_{(3x)}, V_{(3x)}, G_{(4x)}$;
    $c_1 = \frac{dT}{dx_1}$ (Eq. (5.113));
    $c_2 = \frac{dp}{dx_1}$ (Eq. (5.114));
end

$p^{(0)} := p_{c,2}, T^{(0)} := T_{c,2}$;
for $x_1 := 1 \dots 0$ do
    calculate $(p^{(i)}, T^{(i)})$ from $(p^{(i-1)}, T^{(i-1)})$ by applying the Runge–Kutta
    algorithm to $\vec{c}(p, T, x_1)$;
    if $p^{(i)}, T^{(i)} \leq 0$ or unreasonably large then terminate loop
end
if loop 1 terminated then
    $p^{(0)} := p_{c,1}, T^{(0)} := T_{c,1}$;
    for $x_1 := 0 \dots 1$ do
        calculate $(p^{(i)}, T^{(i)})$ from $(p^{(i-1)}, T^{(i-1)})$ by applying the Runge–Kutta
        algorithm to $\vec{c}(p, T, x_1)$;
        if $p^{(i)}, T^{(i)} \leq 0$ or unreasonably large then terminate loop
    end
end
```

of other methods (see the next section): Eqs (5.113) and (5.114) form a system of first-order differential equations, which can be solved numerically, using the pure-component critical points as initial values (see Algorithm 4). As there are phase diagram classes where there is no continuous critical curve connecting the pure-fluid critical points, it is advisable to start the calculation at $x_1 = 0$ as well as $x_1 = 1$. This approach, however, has got two important disadvantages:

- In some phase diagram classes there are critical curves that are not originating at the critical points of the pure components, e.g., the liquid–liquid critical curve of class II. These curves would not be found.
- It is not granted that the mole fractions increase or decrease monotonically along a critical curve. It might be necessary to make another variable the independent variable, or even to switch the independent variables automatically.

5.6.2 Algebraic Equations

The conditions of a binary critical point, $G_{2x} = 0$ and $G_{(3x)} = 0$, can be generalized for multicomponent mixtures:

$$D_2 \equiv \begin{vmatrix} \frac{\partial^2 G_\mathrm{m}}{\partial x_1^2} & \frac{\partial^2 G_\mathrm{m}}{\partial x_1 \partial x_2} & \cdots & \frac{\partial^2 G_\mathrm{m}}{\partial x_1 \partial x_{N-1}} \\ \frac{\partial^2 G_\mathrm{m}}{\partial x_2 \partial x_1} & \frac{\partial^2 G_\mathrm{m}}{\partial x_2^2} & \cdots & \frac{\partial^2 G_\mathrm{m}}{\partial x_2 \partial x_{N-1}} \\ \vdots & \vdots & \ddots & \vdots \\ \frac{\partial^2 G_\mathrm{m}}{\partial x_{N-1} \partial x_1} & \frac{\partial^2 G_\mathrm{m}}{\partial x_{N-1} \partial x_2} & \cdots & \frac{\partial^2 G_\mathrm{m}}{\partial x_{N-1}^2} \end{vmatrix} = 0 \tag{5.115}$$

$$D_3 \equiv \begin{vmatrix} \frac{\partial^2 G_\mathrm{m}}{\partial x_1^2} & \frac{\partial^2 G_\mathrm{m}}{\partial x_1 \partial x_2} & \cdots & \frac{\partial^2 G_\mathrm{m}}{\partial x_1 \partial x_{N-1}} \\ \frac{\partial^2 G_\mathrm{m}}{\partial x_2 \partial x_1} & \frac{\partial^2 G_\mathrm{m}}{\partial x_2^2} & \cdots & \frac{\partial^2 G_\mathrm{m}}{\partial x_2 \partial x_{N-1}} \\ \vdots & \vdots & \ddots & \vdots \\ \frac{\partial D_2}{\partial x_1} & \frac{\partial D_2}{\partial x_2} & \cdots & \frac{\partial D_2}{\partial x_{N-1}} \end{vmatrix} = 0 \tag{5.116}$$

$G_\mathrm{m}(p, T, \vec{x})$ is a function of pressure, whereas equations of state or fundamental equations that can be used to calculate G_m are usually functions of the molar volume. Moreover, G_m is not a true function, but may be multivalent: there can be more than one molar volume, and hence Gibbs energy value, for a given pressure (cf. Figs. 5.6 or 5.8). Therefore, the previous two equations are not very useful for practical calculations.

Using Eqs (5.53) and (5.54), these criteria can be expressed in terms of derivatives of the Helmholtz energy. For binary mixtures the results are:

$$G_{(2x)} = A_{(2x)} - \frac{A_{(Vx)}^2}{A_{(2V)}} = 0 \tag{5.117}$$

$$G_{(3x)} = A_{(3x)} - \frac{3A_{(V2x)}A_{(Vx)}}{A_{(2V)}} + \frac{3A_{(2Vx)}A_{(Vx)}^2}{A_{(2V)}^2} - \frac{A_{(3V)}A_{(Vx)}^3}{A_{(2V)}^3} = 0 \tag{5.118}$$

Multiplying with suitable powers of $A_{(2V)}$, which should be positive for stable states, then leads to

$$D_2 \equiv A_{(2x)}A_{(2V)} - A_{(Vx)}^2 = \begin{vmatrix} A_{(2x)} & A_{(Vx)} \\ A_{(Vx)} & A_{(2V)} \end{vmatrix} = 0 \tag{5.119}$$

$$\begin{aligned} D_3 \equiv{}& A_{(3x)}A_{(2V)}^3 - 3A_{(V2x)}A_{(Vx)}A_{(2V)}^2 + 3A_{(2Vx)}A_{(Vx)}^2A_{(2V)} \\ & - A_{(3V)}A_{(Vx)}^3 = \begin{vmatrix} A_{(2x)} & A_{(Vx)} \\ \frac{\partial D_2}{\partial x_1} & \frac{\partial D_2}{\partial V_\mathrm{m}} \end{vmatrix} = 0. \end{aligned} \tag{5.120}$$

Here we have introduced a notation with determinants, which renders the expressions more compact.

These criteria can also be extended to multicomponent mixtures; the results are:[13]

$$D_2 \equiv \begin{vmatrix} \frac{\partial^2 A_\mathrm{m}}{\partial x_1^2} & \frac{\partial^2 A_\mathrm{m}}{\partial x_1 \partial x_2} & \cdots & \frac{\partial^2 A_\mathrm{m}}{\partial x_1 \partial x_{N-1}} & \frac{\partial^2 A_\mathrm{m}}{\partial x_1 \partial V_\mathrm{m}} \\ \frac{\partial^2 A_\mathrm{m}}{\partial x_2 \partial x_1} & \frac{\partial^2 A_\mathrm{m}}{\partial x_2^2} & \cdots & \frac{\partial^2 A_\mathrm{m}}{\partial x_2 \partial x_{N-1}} & \frac{\partial^2 A_\mathrm{m}}{\partial x_2 \partial V_\mathrm{m}} \\ \vdots & \vdots & \ddots & \vdots & \vdots \\ \frac{\partial^2 A_\mathrm{m}}{\partial x_{N-1} \partial x_1} & \frac{\partial^2 A_\mathrm{m}}{\partial x_{N-1} \partial x_2} & \cdots & \frac{\partial^2 A_\mathrm{m}}{\partial x_{N-1}^2} & \frac{\partial^2 A_\mathrm{m}}{\partial x_{N-1} \partial V_\mathrm{m}} \\ \frac{\partial^2 A_\mathrm{m}}{\partial V_\mathrm{m} \partial x_1} & \frac{\partial^2 A_\mathrm{m}}{\partial V_\mathrm{m} \partial x_2} & \cdots & \frac{\partial^2 A_\mathrm{m}}{\partial V_\mathrm{m} \partial x_{N-1}} & \frac{\partial^2 A_\mathrm{m}}{\partial^2 V_\mathrm{m}} \end{vmatrix} = 0 \qquad (5.121)$$

$$D_3 \equiv \begin{vmatrix} \frac{\partial^2 A_\mathrm{m}}{\partial x_1^2} & \frac{\partial^2 A_\mathrm{m}}{\partial x_1 \partial x_2} & \cdots & \frac{\partial^2 A_\mathrm{m}}{\partial x_1 \partial x_{N-1}} & \frac{\partial^2 A_\mathrm{m}}{\partial x_1 \partial V_\mathrm{m}} \\ \frac{\partial^2 A_\mathrm{m}}{\partial x_2 \partial x_1} & \frac{\partial^2 A_\mathrm{m}}{\partial x_2^2} & \cdots & \frac{\partial^2 A_\mathrm{m}}{\partial x_2 \partial x_{N-1}} & \frac{\partial^2 A_\mathrm{m}}{\partial x_2 \partial V_\mathrm{m}} \\ \vdots & \vdots & \ddots & \vdots & \\ \frac{\partial^2 A_\mathrm{m}}{\partial x_{N-1} \partial x_1} & \frac{\partial^2 A_\mathrm{m}}{\partial x_{N-1} \partial x_2} & \cdots & \frac{\partial^2 A_\mathrm{m}}{\partial^2 x_{N-1}} & \frac{\partial^2 A_\mathrm{m}}{\partial x_{N-1} \partial V_\mathrm{m}} \\ \frac{\partial D_2}{\partial x_1} & \frac{\partial D_2}{\partial x_2} & \cdots & \frac{\partial D_2}{\partial x_{N-1}} & \frac{\partial D_2}{\partial V_\mathrm{m}} \end{vmatrix} = 0 \qquad (5.122)$$

The equations for the D_i can then be solved for the critical molar volume and temperature. Experience shows, however, that the straightforward application of a nonlinear root finder – even an advanced one like the Marquardt–Levenberg method – is rather hopeless: the range of convergence is rather small. Most reliable methods for the calculation of critical states of mixtures use sequential approaches.

Algorithm 5 scans the molar volume of a mixture with a given composition and solves $G_{(2x)} = 0$ for the temperature. Then it evaluates $G_{(3x)}$. If during the scan $G_{(3x)}$ changes its sign, the accurate critical molar volume is determined with a regula falsi method. For the critical coordinates thus established, the pressure is calculated; furthermore, various stability tests are made, e.g., the signs of $A_{(2V)}$ or $G_{(4x)}$ are checked. Finally, the results have to be assigned to critical curves and sorted.

The latter is not a trivial matter, as is possible in binary mixture calculations to have four or more critical points at one mole fraction. Furthermore, the stability tests deserve some considerations: stable critical points should have

- positive pressure, $p > 0$
- local mechanical stability, $A_{(2V)} > 0$,

---

[13] For criticism of these criteria, see Section 5.8.

Algorithm 5: Critical curves from algebraic equations (generally applicable method) [71]

```
Input: equation of state: $p(\rho, T, x_1)$, fundamental equation: $A_\mathrm{m}(\rho, T, x_1)$
Data: pure-components critical data, $p_{\mathrm{c},i}$ and $T_{\mathrm{c},i}$
Result: critical curve(s) $p(x_1), T(x_1), x_1 = 0 \dots 1$

function $D_2(V_\mathrm{m}, T, x_1)$:
    calculate $A_{(2V)}, A_{(Vx)}, A_{(2x)}$;
    return $D_2 := A_{(2V)} A_{(2x)} - A_{(Vx)}^2$;
end
function $D_3(V_\mathrm{m}, x_1)$:
    for $T := 1.5 T_{\mathrm{c},2} \dots 0.2 T_{\mathrm{c},1}$ do
        evaluate $D_2$;
        if change of sign then
            solve $D_2(T) = 0$ (regula falsi method);
            calculate $A_{(3V)}, A_{(2Vx)}, A_{(V2x)}, A_{(3x)}$;
            return $D_3$ [Eq. (5.120)];
        end
    end
end

for $x_1 := 0 \dots 1$ do
    estimate $V_\mathrm{min}, V_\mathrm{max}$ for volume scan;
    for $V_\mathrm{m} := V_\mathrm{max} \dots V_\mathrm{min}$ do
        evaluate $D_3$;
        if change of sign then
            solve $D_3 = 0$ (regula falsi method);
            apply stability criteria;
            store $x_1, V_\mathrm{m}, T$;
            resume volume scan;
        end
    end
end
for all critical points do
    find nearest neighbours in $p, T, x_1, V_\mathrm{m}$ space;
    group into critical curves;
end
```

- local diffusion stability, $G_{(4x)} > 0$,
- and global diffusion stability, $\sum x_i^\mathrm{n}(\mu_i^\mathrm{n} - \mu_i^\mathrm{c}) > 0$ for all x_i^n.

The last criterion considers the stability against a phase split into noncritical phases. This will be discussed in the next section.

Whether one should exclude unstable or metastable critical points from the results of the computation depends on the circumstances. For a comparison with experimental results they are usually not needed.[14] For the identification of critical curves and for the determination of phase diagram classes, however, they can be useful.

Algorithm 5 is good for binary mixtures only, although an extension to multicomponent mixtures is possible. It is very robust and locates all critical curves in one sweep, even liquid–liquid curves.

Only critical curves with almost constant mole fractions might pose a problem, namely if their mole fractions fall between the mole fractions of the x_1 search grid, which can sometimes happen with $\mathrm{l}=\mathrm{l}$ critical curves. It is therefore important to use a narrow x_1 spacing in regions of interest. Alternatively, one might do the V_m scan in the outer loop and the x_1 scan in the inner loop.

For some simple equations of state, like the van der Waals equation, all required derivatives have the common shape

$$A_{(iVjx)} = Tf_{ij}^{\mathrm{rep}}(V_\mathrm{m}) - f_{ij}^{\mathrm{att}}(V_\mathrm{m}). \tag{5.123}$$

In this case, the condition (5.119) reduces to a quadratic equation in T. For more complicated equations it is necessary to use an iterative scheme, but this is not a problem, for $G_{(2x)}(T)$ has got an approximately parabolic shape.

The algorithm of Heidemann and Khalil [72] is similar to the previous one, although it uses a different mathematical concept and was designed for multicomponent mixtures. It is based on a Taylor series of the Helmholtz energy at a state having the amounts of substances $\vec{n} = (n_1, n_2, \ldots)$:

$$\begin{aligned} A(V,T,\vec{n}) = A_0 &+ \sum_{i=1}^{N}\left(\frac{\partial A}{\partial n_i}\right)\Delta n_i + \frac{1}{2}\sum_{i=1}^{N}\sum_{j=1}^{N}\left(\frac{\partial^2 A}{\partial n_i \partial n_j}\right)\Delta n_i \Delta n_j \\ &+ \frac{1}{6}\sum_{i=1}^{N}\sum_{j=1}^{N}\sum_{k=1}^{N}\left(\frac{\partial^3 A}{\partial n_i \partial n_j \partial n_k}\right)\Delta n_i \Delta n_j \Delta n_k + \cdots \end{aligned} \tag{5.124}$$

The first two terms can be omitted from further considerations; they are not zero, but do not contribute to the curvature of the Helmholtz energy and are therefore not relevant for the phase stability.

For a stable state $\vec{n}$ each fluctuation $\Delta\vec{n}$ lets A increase. At the stability limit, the second-order term vanishes. For a mathematical formulation of the stability

---

[14] There are exceptions: so it is possible to realize negative pressures experimentally, although usually not for long periods of time.

criterion we consider the Hessian matrix

$$\boldsymbol{Q} = \begin{pmatrix} \frac{\partial^2 A}{\partial n_1^2} & \frac{\partial^2 A}{\partial n_1 \partial n_2} & \cdots & \frac{\partial^2 A}{\partial n_1 \partial n_N} \\ \frac{\partial^2 A}{\partial n_2 \partial n_1} & \frac{\partial^2 A}{\partial n_2^2} & \cdots & \frac{\partial^2 A}{\partial n_2 \partial n_N} \\ \cdots & \cdots & \cdots & \cdots \\ \frac{\partial^2 A}{\partial n_N \partial n_1} & \frac{\partial^2 A}{\partial n_N \partial n_2} & \cdots & \frac{\partial^2 A}{\partial n_N^2} \end{pmatrix} \tag{5.125}$$

For a stable state, $\det \boldsymbol{Q} > 0$ must be true. At the stability limit the determinant vanishes:

$$\det \boldsymbol{Q} = 0 \tag{5.126}$$

Consequently,[15] there must exist a nontrivial eigenvector, the so-called fluctuation vector, fulfilling the condition

$$\boldsymbol{Q} \cdot \Delta \vec{n} = 0. \tag{5.127}$$

$\Delta \vec{n}$ represents a fluctuation of the local composition away from the equilibrium state; at a critical point, such fluctuations encounter no "opposing forces". For a critical state, the third-order term of Eq. (5.124) must also vanish; hence, the fluctuation vector must also fulfill

$$A_3 = \sum_{i=1}^{N} \sum_{j=1}^{N} \sum_{k=1}^{N} \left(\frac{\partial^3 A}{\partial n_i \partial n_j \partial n_k} \right) \Delta n_i \Delta n_j \Delta n_k = 0. \tag{5.128}$$

The last three equations define the algorithm of Heidemann and Khalil, Algorithm 6.

5.6.3 Critical Endpoints

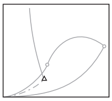

How does a critical curve behave when it runs from a stable or metastable region ($G_{(4x)} > 0$) to an unstable one ($G_{(4x)} < 0$)? Equation (5.103) does not depend on $G_{(4x)}$, hence the stable and the unstable branch come together in the pT projection with the same slope. Combining Eqs. (5.103) and (5.112) at $G_{(4x)} = 0$ leads to

$$\left. \frac{\mathrm{d}p}{\mathrm{d}T} \right|_{\mathrm{cc}} = \frac{S_{(3x)}}{V_{(3x)}} \tag{5.129}$$

(cc = critical cusp). Inserting this into Eq. (5.102) to eliminate dp leads to

$$\left. \frac{\mathrm{d}T}{\mathrm{d}x_1} \right|_{\mathrm{cc}} = \frac{G_{(3x)}}{S_{(2x)} - V_{(2x)} S_{(3x)} / V_{(3x)}}. \tag{5.130}$$

---

[15] Some useful relations of linear algebra are given in the Appendix.

Algorithm 6: Critical curves from algebraic equations (method of Heidemann and Khalil) [72]

```
Input: equation of state: $p(\rho, T, \vec{x})$, fundamental equation: $A_\mathrm{m}(\rho, T, \vec{x})$
Data: pure-components critical data, $p_{\mathrm{c},i}$ and $T_{\mathrm{c},i}$
Result: critical curve(s) $p(\vec{x}), T(\vec{x})$

function $q(V, T, \vec{n})$:
    calculate $Q_{ij} = \frac{\partial^2 A}{\partial n_i \partial n_j}$;
    return $\det \boldsymbol{Q}$;
end
function $A_3(V, T, \vec{n})$:
    solve $q(T) = 0$ (nonlinear problem);
    set one of the $\Delta n_i$ to 1;
    solve $\boldsymbol{Q}\Delta\vec{n} = 0$ for the remaining $\Delta n_i$ (linear problem);
    calculate $Q_{ijk} = \frac{\partial^3 A}{\partial n_i \partial n_j \partial n_k}$;
    return $A_3$ [Eq. (5.128)];
end

for all compositions $\vec{x}$ do
    estimate $V_\mathrm{min}, V_\mathrm{max}$ for volume scan;
    $\vec{n} := \vec{x}$;
    for $V_\mathrm{m} := V_\mathrm{max} \ldots V_\mathrm{min}$ do
        evaluate $A_3$;
        if change of sign then
            solve $A_3 = 0$ (regula falsi method);
            apply stability criteria;
            store results;
            resume volume scan;
        end
    end
end
for all critical points do
    find nearest neighbours in $p, T, x_1, V_\mathrm{m}$ space;
    group into critical curves;
end
```

Here, however, the numerator and the denominator both become zero. Applying l'Hôpital's rule then gives

$$\left.\frac{\mathrm{d}T}{\mathrm{d}x_1}\right|_\mathrm{cc} = \frac{G_{(4x)}}{S_{(3x)} - (V_{(3x)}^2 S_{(3x)} + V_{(2x)} V_{(3x)} S_{(4x)} - V_{(2x)} V_{(4x)} S_{(3x)})/V_{(3x)}^2} = \frac{G_{(4x)} V_{(3x)}^2}{V_{(2x)}(V_{(3x)} S_{(4x)} - V_{(4x)} S_{(3x)})} \tag{5.131}$$

In this equation the numerator is zero, but not necessarily the denominator. Consequently, the critical curve has an extremum in the Tx projection, and in the pT projection therefore appears to change its direction, thus forming a *critical cusp*.

A critical cusp should not be confused with a critical endpoint: at the critical endpoint a stable critical phase is in equilibrium with another, non-critical phase, i.e., here $G_{(4x)}$ is still positive. At the critical cusp $G_{(4x)}$ changes its sign, and G_m turns locally concave. If $G_{(4x)}$ runs from positive to negative values along a critical curve, this curve has first a stable portion, then passes through a critical endpoint to a metastable section, and finally through a critical cusp to the unstable branch, which then runs to negative pressure. This is illustrated in Fig. 5.10.

Figures 5.11 and 5.12 show the pT and the Tx projections of the critical curve of the {CO_2 + hexadecane} system in the vicinity of the critical endpoint. The cusp is evident in the pT diagram, but in the Tx diagram there is only a "smooth" maximum.

Figure 5.13 shows the underlying behavior of the Gibbs energy as we follow the $\mathrm{l} = \mathrm{g}$ critical curve in Fig. 5.11 from the stable portion to the unstable branch: In curve 1, the critical point is stable, and to the side of the phase diagram there is a stable equilibrium between two noncritical phases. At the critical endpoint (curve 2) there is an equilibrium between a critical and a noncritical phase. The curve 3 shows a stable equilibrium between two noncritical phases; the Gibbs energy of the critical point is above the double tangent, so that the critical point

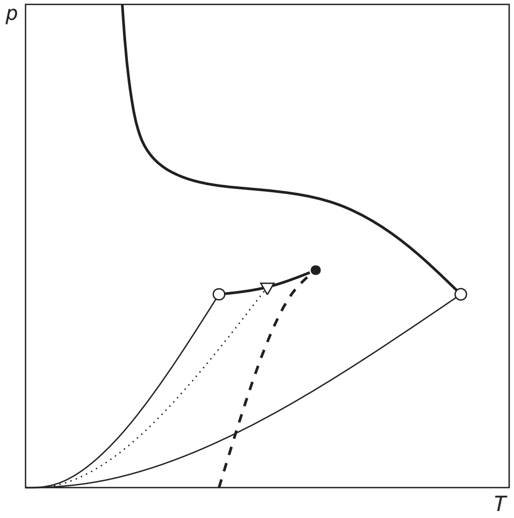

FIGURE 5.10 Metastable and unstable parts of a critical curve (schematic). ——: vapor pressure curves, ——: critical curves, – – : unstable critical curve, ··········: three-phase curve llg, ○: pure-substance critical point, ∇: (upper) critical endpoint, and ●: critical cusp.

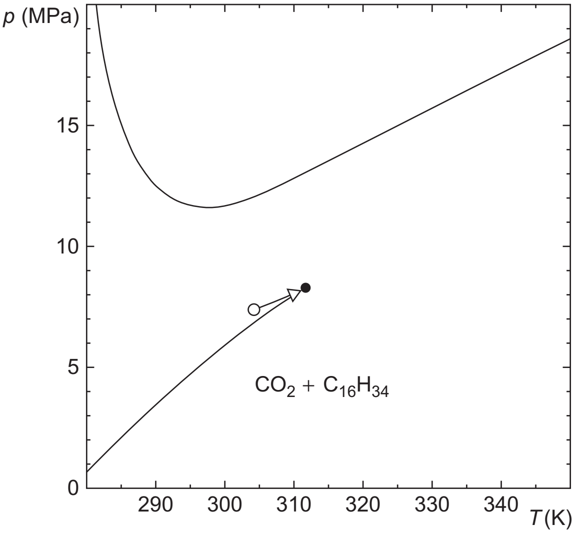

FIGURE 5.11 Critical curves (*pT* diagram) of the {carbon dioxide + hexadecane} system in the vicinity of the critical endpoint, calculated with the Redlich–Kwong equation of state. ○: pure-substance critical point; ∇: (upper) critical endpoint; and •: critical cusp.

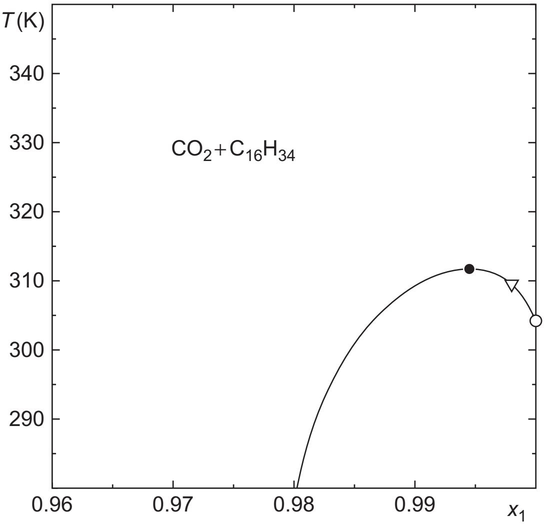

FIGURE 5.12 Corresponding *Tx* diagram of the {carbon dioxide + hexadecane} system.

is metastable. The fourth curve shows a critical point with $G_{(4x)} < 0$. The Gibbs energy curve exhibits a concave curvature in the vicinity of the critical point and is therefore unstable.

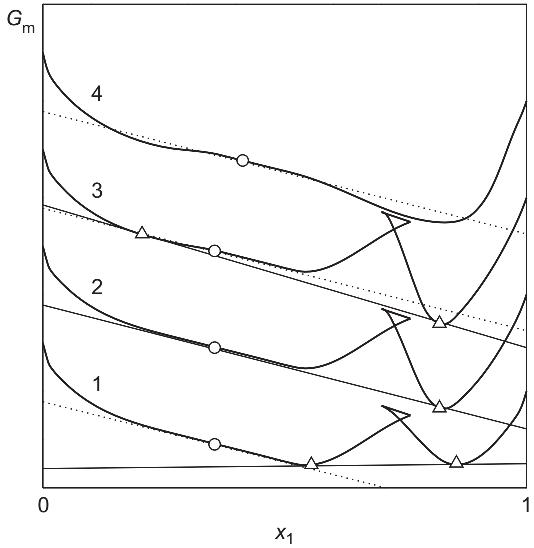

FIGURE 5.13 Schematic representation of the molar Gibbs energy in the vicinity of a critical endpoint. ——: molar Gibbs energy; ——: double tangent; and ··········: tangent at critical point. See the text for explanation of the curves.

For some (usually polymeric) systems and with the proper techniques, the metastable part of the l=g critical curve could even be determined experimentally [73].

Similarly, the l=l critical curves of class II or class IV systems also have metastable and unstable parts beyond their endpoints. Here the critical cusps exist, too, but usually at negative pressures. Again, for some polymer systems it was possible to follow the critical curves beyond the l=lg endpoint into the negative pressure domain [74].

The mathematical criteria for a critical endpoint (CEP) are easily derived: At a critical endpoint, a critical phase (c) is in equilibrium with a noncritical phase (n). For a binary mixture we can therefore write

$$G^{\mathrm{c}}_{(2x)} = G^{\mathrm{c}}_{(3x)} = 0, \tag{5.132}$$

$$\mu_1^{\mathrm{c}} = \mu_1^{\mathrm{n}} \quad \mu_2^{\mathrm{c}} = \mu_2^{\mathrm{n}}. \tag{5.133}$$

A direct numeric solution of this system of equations is not likely to succeed. Critical endpoints are probably located best by calculating a critical curve, monitoring the criterion

$$x_1^{\mathrm{n}}(\mu_1^{\mathrm{n}} - \mu_1^{\mathrm{c}}) + x_2^{\mathrm{n}}(\mu_2^{\mathrm{n}} - \mu_2^{\mathrm{c}}) = 0 \tag{5.134}$$

for all possible values of x_1^{n} and doing a regula falsi search when its sign changes.

5.7 THREE-PHASE CURVES

In order to derive an equation for three-phase curves of binary mixtures, we write the total differentials of the chemical potentials of both components from Eq. (5.46):

$$\begin{aligned}
\mathrm{d}\mu_1 &= \mathrm{d}\left(G_\mathrm{m} + x_2 G_{(x)}\right) \\
&= \mathrm{d}G_\mathrm{m} - G_{(x)}\,\mathrm{d}x_1 + x_2\,\mathrm{d}G_{(x)} \\
&= (-S_\mathrm{m}\,\mathrm{d}T + V_\mathrm{m}\,\mathrm{d}p + G_{(x)}\,\mathrm{d}x_1) - G_{(x)}\,\mathrm{d}x_1 \\
&\quad + x_2(-S_{(x)}\,\mathrm{d}T + V_{(x)}\,\mathrm{d}p + G_{(2x)}\,\mathrm{d}x_1) \\
&= -(S_\mathrm{m} + x_2 S_{(x)})\,\mathrm{d}T + (V_\mathrm{m} + x_2 V_{(x)})\,\mathrm{d}p + x_2 G_{(2x)}\,\mathrm{d}x_1 \\
\mathrm{d}\mu_2 &= -(S_\mathrm{m} - x_1 S_{(x)})\,\mathrm{d}T + (V_\mathrm{m} - x_1 V_{(x)})\,\mathrm{d}p - x_1 G_{(2x)}\,\mathrm{d}x_1
\end{aligned} \tag{5.135}$$

We note that in

$$d \equiv x_1\,\mathrm{d}\mu_1 + x_2\,\mathrm{d}\mu_2 = -S_\mathrm{m}\,\mathrm{d}T + V_\mathrm{m}\,\mathrm{d}p \tag{5.136}$$

all derivatives with respect to x_1 disappear. Forming $d'(x_1''' - x_1'') + d''(x_1' - x_1''') + d'''(x_1'' - x_1')$ and observing that each component of the mixture must have the same chemical potential in all phases,

$$\begin{aligned}
\mathrm{d}\mu_1' &= \mathrm{d}\mu_1'' = \mathrm{d}\mu_1''' \\
\mathrm{d}\mu_2' &= \mathrm{d}\mu_2'' = \mathrm{d}\mu_2''',
\end{aligned} \tag{5.137}$$

yields

$$\begin{aligned}
&-[S_\mathrm{m}'(x_1''' - x_1'') - S_\mathrm{m}''(x_1''' - x_1') + S_\mathrm{m}'''(x_1'' - x_1')]\,\mathrm{d}T \\
&+[V_\mathrm{m}'(x_1''' - x_1'') - V_\mathrm{m}''(x_1''' - x_1') + V_\mathrm{m}'''(x_1'' - x_1')]\,\mathrm{d}p = 0
\end{aligned} \tag{5.138}$$

and finally a differential equation for the slope of a three-phase curve, which we write here with determinants,

$$\left.\frac{\mathrm{d}p}{\mathrm{d}T}\right|_{3\Phi} = \frac{\begin{vmatrix} S_\mathrm{m}' & x_1' & 1 \\ S_\mathrm{m}'' & x_1'' & 1 \\ S_\mathrm{m}''' & x_1''' & 1 \end{vmatrix}}{\begin{vmatrix} V_\mathrm{m}' & x_1' & 1 \\ V_\mathrm{m}'' & x_1'' & 1 \\ V_\mathrm{m}''' & x_1''' & 1 \end{vmatrix}}. \tag{5.139}$$

It should be noted that there is a similarity to the Clapeyron equation, Eq. (5.21), for the two-phase coexistence curve of pure substances, which may also be written as

$$\left.\frac{\mathrm{d}p}{\mathrm{d}T}\right|_{2\Phi} = \frac{\Delta S_\mathrm{m}}{\Delta V_\mathrm{m}} = \frac{\begin{vmatrix} S'_\mathrm{m} & 1 \\ S''_\mathrm{m} & 1 \end{vmatrix}}{\begin{vmatrix} V'_\mathrm{m} & 1 \\ V''_\mathrm{m} & 1 \end{vmatrix}}. \tag{5.140}$$

These two equations are generally valid and can also be applied to solid–fluid phase equilibria.

At a *critical endpoint* there is a two-phase equilibrium between a critical phase (c) and a noncritical phase (n). Equation (5.135) then becomes

$$\begin{aligned} \mathrm{d}\mu_1^\mathrm{n} &= -(S_\mathrm{m}^\mathrm{n} + x_2^\mathrm{n} S_{(x)}^\mathrm{n})\,\mathrm{d}T + (V_\mathrm{m}^\mathrm{n} + x_2^\mathrm{n} V_{(x)}^\mathrm{n})\,\mathrm{d}p + x_2^\mathrm{n} G_{(2x)}^\mathrm{n}\,\mathrm{d}x_1 \\ \mathrm{d}\mu_1^\mathrm{c} &= -(S_\mathrm{m}^\mathrm{c} + x_2^\mathrm{c} S_{(x)}^\mathrm{c})\,\mathrm{d}T + (V_\mathrm{m}^\mathrm{c} + x_2^\mathrm{c} V_{(x)}^\mathrm{c})\,\mathrm{d}p. \end{aligned} \tag{5.141}$$

Analogous equations are obtained for component 2. For the critical phase $G_{(2x)}^\mathrm{c} = 0$ must hold. Elimination of the differentials of the molar fractions gives

$$\left.\frac{\mathrm{d}p}{\mathrm{d}T}\right|_\mathrm{CEP} = \frac{S_\mathrm{m}^\mathrm{c} - S_\mathrm{m}^\mathrm{n} - (x_1^\mathrm{c} - x_1^\mathrm{n}) S_{(x)}^\mathrm{c}}{V_\mathrm{m}^\mathrm{c} - V_\mathrm{m}^\mathrm{n} - (x_1^\mathrm{c} - x_1^\mathrm{n}) V_{(x)}^\mathrm{c}} = \frac{\begin{vmatrix} S_\mathrm{m}^\mathrm{n} & x_1^\mathrm{n} & 1 \\ S_\mathrm{m}^\mathrm{c} & x_1^\mathrm{c} & 1 \\ S_{(x)}^\mathrm{c} & 1 & 0 \end{vmatrix}}{\begin{vmatrix} V_\mathrm{m}^\mathrm{n} & x_1^\mathrm{n} & 1 \\ V_\mathrm{m}^\mathrm{c} & x_1^\mathrm{c} & 1 \\ V_{(x)}^\mathrm{c} & 1 & 0 \end{vmatrix}}, \tag{5.142}$$

i.e., the slope of a three-phase curve at a critical endpoint can be obtained by taking the derivatives of the determinants in Eq. (5.139).[16]

Equation (5.142) is useful for determining the initial values for a direct numerical solution of the phase equilibrium criteria: once a critical endpoint is known, one can chose a temperature in its vicinity, estimate the pressure of the three-phase curve by means of Eq. (5.142), and then solve the nonlinear system of equations

$$\begin{aligned} \mu'_1 &= \mu''_1 = \mu'''_1 \\ \mu'_2 &= \mu''_2 = \mu'''_2 \end{aligned} \tag{5.143}$$

with the Marquardt–Levenberg method.

---

[16] By subtracting two rows from each other and then invoking l'Hôpital's rule.

5.8 ISOCHORIC THERMODYNAMICS

As pressures and temperatures have to be the same in all coexisting phases, it is natural to formulate thermodynamic conditions and equations in terms of the Gibbs energy and to use pressures, temperatures, and mole fractions as primary variables.

$G_m(p, T, \vec{x})$, however, is not a true monovalent function, as explained in Section 5.5.2. In general, $G_m(p, T, \vec{x})$ consists of several branches connected through discontinuities, which makes the computerized solution of the phase equilibrium conditions difficult.

Statistical thermodynamical theories as well as most equations of state of fluids are formulated in terms of $(V_m, T, \vec{x})$, so that the problem of the discontinuities is practically avoided.

But still there is the problem that the variables that describe how much of the available space is occupied by matter – V_m and $\vec{x}$ – have different characters: the mole fractions are dimensionless quantities bounded between 0 and 1, whereas the molar volume has got the dimension m^3/mol and can assume arbitrary positive values above some minimal value. This lack of symmetry in the primary variables is not only an esthetic problem: the numerical solution of the phase equilibrium conditions or the evaluation of stability criteria may involve manipulations of matrices containing derivatives with respect to the molar volume and the mole fractions; an example is Eq. (5.121). But how does one compute the trace of a matrix in which the elements have different dimensions?

5.8.1 Isochoric Thermodynamics and Phase Equilibrium

This problem can be completely avoided by formulating the equilibrium conditions by means of *isochoric thermodynamics*. Here the primary variables of an N-component mixture are the N molar densities or concentrations

$$\rho_i = \frac{n_i}{V}, \tag{5.144}$$

where V is a constant reference volume that can be chosen freely (e.g., $1\,\mathrm{m}^3$) and which is never changed. Conversion to the conventional set of variables is accomplished by

$$\begin{gathered} \sum_{i=1}^{N} \rho_i = \rho = \frac{1}{V_m} \\ x_i = \frac{\rho_i}{\rho}. \end{gathered} \tag{5.145}$$

With these densities the chemical potential can then be expressed as

$$\mu_i = \left(\frac{\partial A}{\partial n_i}\right)_{V,T,n_{j\neq i}} = \left(\frac{\partial A}{\partial \rho_i}\right)_{\rho_{j\neq i},T} \left(\frac{\partial \rho_i}{\partial n_i}\right) = \frac{1}{V}\left(\frac{\partial A}{\partial \rho_i}\right)_{\rho_{j\neq i}}, \tag{5.146}$$

and therefore the phase equilibrium condition $\mu_i' = \mu_i''$ becomes

$$\left(\frac{\partial A'}{\partial \rho_i}\right) = \left(\frac{\partial A''}{\partial \rho_i}\right) \quad \text{with} \quad i = 1, \ldots N. \tag{5.147}$$

An expression for the pressure can be obtained from

$$G = A + pV, \tag{5.148}$$

which follows from the definitions of the thermodynamic energy functions, Eqs (4.5) through (4.9), and the relation

$$G = \sum_{i=1}^{N} n_i \mu_i, \tag{5.149}$$

which is obtained from Eq. (4.51). Combining these equations and dividing by the volume yields

$$-p = \frac{1}{V}\left(A - \sum_{i=1}^{N} n_i \mu_i\right) \tag{5.150}$$

or, with Eq. (5.146),

$$-p = \frac{1}{V}\left[A - \sum_{i=1}^{N} \rho_i \left(\frac{\partial A}{\partial \rho_i}\right)\right]. \tag{5.151}$$

Working with extensive functions and arbitrarily defined reference volumes is awkward and – at this stage – not necessary. Sengers and Levelt Sengers proposed to use the *Helmholtz energy density* $\Psi = A/V$ as central thermodynamic potential [75], which is of course an intensive function. With this definition the previous equation can be written as

$$-p = \Psi - \sum_{i=1}^{N} \left(\frac{\partial \Psi}{\partial \rho_i}\right) \rho_i, \tag{5.152}$$

and thus the equal-pressure criterion $p' = p''$ becomes

$$\sum_{i=1}^{N} \left(\frac{\partial \Psi''}{\partial \rho_i}\right) \rho_i'' - \sum_{i=1}^{N} \left(\frac{\partial \Psi'}{\partial \rho_i}\right) \rho_i' = \Psi'' - \Psi'. \tag{5.153}$$

The chemical potentials and their equality condition, Eqs (5.146) and (5.147) can be expressed in terms of Ψ as

$$\mu_i = \left(\frac{\partial \Psi}{\partial \rho_i}\right)_{\rho_{j \neq i}} \tag{5.154}$$

and hence

$$\left(\frac{\partial \Psi'}{\partial \rho_i}\right) = \left(\frac{\partial \Psi''}{\partial \rho_i}\right) \quad i = 1, \ldots N. \tag{5.155}$$

Because of this, the pressure criterion can be simplified to

$$\sum_{i=1}^{N} \left(\frac{\partial \Psi}{\partial \rho_i}\right) (\rho_i'' - \rho_i') = \Delta \Psi. \tag{5.156}$$

Here the phase indicators have been omitted for $(\partial \Psi / \partial \rho_i)$.

By switching to vector notation and using the gradient operator to indicate differentiation with respect to the densities of all components, the conditions of equal chemical potentials and equal pressures can be rendered as

$$\nabla \Psi'' = \nabla \Psi' \tag{5.157}$$

and

$$\nabla \Psi \cdot \Delta \vec{\rho} = \Delta \Psi, \tag{5.158}$$

respectively. Here $\Delta \vec{\rho} = \vec{\rho}\,'' - \vec{\rho}\,'$ is a vector that points from the composition of one phase to that of the other. Equation (5.157) specifies that both equilibrium phases must have the same Ψ gradients; Eq. (5.158) states that the equilibrium states have a common tangent (or a tangent plane in case of multicomponent mixtures).

Equations (5.157) and (5.158) together constitute a system of $N+1$ nonlinear equations. In a typical phase equilibrium calculation, one would keep the temperature and the mole fractions of one phase, $\vec{x}\,'$, constant and then use a nonlinear search algorithm to locate the $N+1$ unknown variables $\rho_1'', \ldots \rho_N''$ and $\rho' = \sum \rho_i'$. It should be noted that neither the pressure nor the orthobaric molar volumes appear in this formulation: there is no need to calculate molar volumes from pressure at every step of the iteration!

We now have to consider the problem of finding initial values for the phase equilibrium iteration. The total differential of Ψ can be derived from the one of A, Eq. (4.8), by dividing by the (constant!) volume:

$$\mathrm{d}\Psi = \mathrm{d}\left(\frac{A}{V}\right) = -\frac{S_\mathrm{m}}{V_\mathrm{m}}\,\mathrm{d}T + \sum_{i=1}^{N} \mu_i\,\mathrm{d}\rho_i \tag{5.159}$$

The ρ_i are the natural variables of Ψ. Using vector notation, this can be expressed as

$$\mathrm{d}\Psi = -\frac{S_\mathrm{m}}{V_\mathrm{m}}\,\mathrm{d}T + \nabla \Psi \cdot \mathrm{d}\vec{\rho}. \tag{5.160}$$

Integration between ρ' and ρ'' along an arbitrary path Ω at constant temperature then yields

$$\Delta\Psi = \int_{\Omega} \nabla\Psi\, \mathrm{d}\vec{\rho}. \tag{5.161}$$

In the limiting case of $\rho' \to \rho''$, the path integral becomes $\nabla\Psi \cdot \Delta\vec{\rho}$, and this is just the equal-pressure criterion, Eq. (5.158). Slightly away from this limiting case there will be a deviation from the linear approximation, and this deviation will depend on the size of $\Delta\vec{\rho}$. We therefore write to second order

$$\int_{\vec{\rho}'}^{\vec{\rho}''} \nabla\Psi\, \mathrm{d}\vec{\rho} = \nabla\Psi \cdot \Delta\vec{\rho} + \frac{\lambda}{2}(\Delta\vec{\rho})^2 = \Delta\Psi, \tag{5.162}$$

where λ is a scalar factor.

Calculating the gradient of this equation, forming the outer product on the left-hand side, gives

$$\nabla \cdot \nabla\Psi \cdot \Delta\vec{\rho} + \nabla\Psi + \lambda\Delta\vec{\rho} = \nabla(\Delta\Psi). \tag{5.163}$$

$\boldsymbol{\Psi} = \nabla \cdot \nabla\Psi$ is the Hessian matrix of the Helmholtz energy density:

$$\boldsymbol{\Psi} \equiv \begin{pmatrix} \Psi_{11} & \Psi_{12} & \ldots & \Psi_{1N} \\ \Psi_{21} & \Psi_{22} & \ldots & \Psi_{2N} \\ \vdots & \vdots & \ddots & \vdots \\ \Psi_{N1} & \Psi_{N2} & \ldots & \Psi_{NN} \end{pmatrix} \qquad \text{with} \quad \Psi_{ij} = \left(\frac{\partial^2\Psi}{\partial\rho_i\partial\rho_j}\right) \tag{5.164}$$

Let us assume that the gradient is formed with respect to $\vec{\rho}''$, i.e., $\nabla = \nabla_{\rho''}$. The right-hand side then reads $\nabla(\Delta\Psi) = \nabla_{\rho''}\Psi'' - \nabla_{\rho''}\Psi'$. The last term, however, is zero, for Ψ' does not depend on $\vec{\rho}''$. Consequently, Eq. (5.163) becomes

$$\boldsymbol{\Psi}\Delta\vec{\rho} + \lambda\Delta\vec{\rho} = 0. \tag{5.165}$$

This equation evidently constitutes an eigenvalue problem. If the state with the composition $\vec{\rho}'$ is thermodynamically stable, $\boldsymbol{\Psi}$ is symmetric and positive definite, and all of its eigenvalues must be real and positive. Let $\lambda_{\min}$ denote the smallest of these eigenvalues; then $\Delta\vec{\rho}_{\min}$, the eigenvector associated with $\lambda_{\min}$, points into the direction of the composition of the coexisting phase, $\vec{\rho}''$.

In the general case, i.e., equilibrium compositions $\vec{\rho}'$ and $\vec{\rho}''$ at arbitrary distances, the simplification Eq. (5.162) is no longer valid. But then the path can be broken up into small linear segments, for which this equation holds:

$$\int_{\vec{\rho}\,'}^{\vec{\rho}\,''} \nabla\Psi\,\mathrm{d}\vec{\rho} \to \sum_k \left(\nabla\Psi_k \cdot \Delta\vec{\rho}_k + \frac{\lambda_k}{2}(\Delta\vec{\rho}_k)^2 \right) = \sum_k \Delta\Psi_k = \Delta\Psi \tag{5.166}$$

Each segment k is associated with an eigenvalue equation.

Consequently, the path from one equilibrium state to the other is in general curved. In each segment k of this curve, the eigenvector belonging to the lowermost eigenvalue, $\lambda_{\mathrm{min},k}$, indicates the direction of the path. Conversely, a path that starts at one equilibrium phase and always follows the eigenvector will eventually lead to the other equilibrium phase. This is the theorem of Quiñones-Cisneros [6, 76].

5.8.2 Local Stability

In order to have local stability at a given location $\vec{\rho}$, $\Psi(\vec{\rho})$ must be a convex function: all radii of curvature must be positive. Now the curvatures of a surface are given by the eigenvalues of its Hessian matrix, and they are measured in the direction of the associated eigenvectors. Local stability therefore requires $\lambda_i > 0$ for all components i.

Evidently, the stability limit is reached when the lowest eigenvalue becomes zero,

$$\lambda_{\mathrm{min}} = 0, \tag{5.167}$$

while all other eigenvalues are positive. This is the first condition of a critical point (and at the same time the condition for a spinodal state. Then, however, Eq. (5.165) reduces to

$$\boldsymbol{\Psi}\Delta\vec{\rho} = 0. \tag{5.168}$$

This equation can have a nontrivial solution only if $\boldsymbol{\Psi}$ is singular. Hence

$$D_2 \equiv \det \boldsymbol{\Psi} = 0 \tag{5.169}$$

is an alternative criterion for critical states in multicomponent mixtures.

Here a word of caution is necessary: $\det \boldsymbol{\Psi} > 0$ does not necessarily indicate a stable state. Because of $\det \boldsymbol{\Psi} = \lambda_1 \lambda_2 \ldots \lambda_N$, this would also be true for an unstable state with an even number of negative eigenvalues. Criterion (5.169) is correct in the sense that it must be fulfilled at a critical point, but it is not as specific as criterion (5.167). A search for critical points based on (5.169) can return many solutions that later have to be discarded as unstable. This feature is common to all critical-point algorithms based on zeros of determinants.

The second criterion for a critical point can easily be derived from the fact that, along a stable path through the critical point, $\lambda_{\min}$ must be positive, but zero at the critical point itself, so that a local minimum is formed. Consequently, the second criterion is

$$\frac{\mathrm{d}\lambda_{\min}(\vec{\rho}+\alpha\vec{u}_{\min})}{\mathrm{d}\alpha}=0, \tag{5.170}$$

where α is a scalar quantity representing a displacement along $\vec{u}_{\min}$, the eigenvector belonging to $\lambda_{\min}$.

An alternative representation of this criterion is that the derivative of the determinant of $\boldsymbol{\Psi}$ must vanish:

$$D_3 \equiv \begin{vmatrix} \frac{\partial^2\Psi}{\partial\rho_1^2} & \frac{\partial^2\Psi}{\partial\rho_1\partial\rho_2} & \cdots & \frac{\partial^2\Psi}{\partial\rho_1\partial\rho_N} \\ \frac{\partial^2\Psi}{\partial\rho_2\partial\rho_1} & \frac{\partial^2\Psi}{\partial\rho_2^2} & \cdots & \frac{\partial^2\Psi}{\partial\rho_2\partial\rho_N} \\ \vdots & \vdots & \ddots & \vdots \\ \frac{\partial D_2}{\partial\rho_1} & \frac{\partial D_2}{\partial\rho_2} & \cdots & \frac{\partial D_2}{\partial\rho_N} \end{vmatrix} = 0 \tag{5.171}$$

But as with Eq. (5.169), the use of determinants creates additional zeros which merely confuse the equation solving algorithm.

A graphical interpretation of the equilibrium criteria is given in Fig. 5.14, which shows a contour diagram of $\rho_1, \rho_2 \to \Psi(\rho_1, \rho_2, T)$ for a binary mixture. This diagram is the analogon to Fig. 5.8. It corresponds to a vapor–liquid

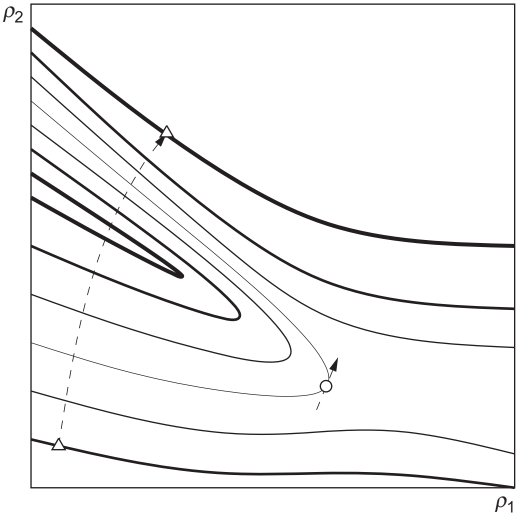

FIGURE 5.14 Schematic contour diagram $\rho_1, \rho_2 \to \Psi(\rho_1, \rho_2, T)$ for a supercritical binary mixture. The line thickness indicates the function value (bold curves = high values). △: coexisting phases and ○: critical point. The arrows indicate the direction of the relevant eigenvector (see text).

equilibrium where component 1 is supercritical and component 2 subcritical: the fold (concave portion of the surface on the left side of the diagram) touches the ρ_2 axis, but not the ρ_1 axis. It should be noted that Ψ surface is smooth and differentiable, as long as the underlying equation of state is differentiable: there are no switches between different branches as in the $x_1 \to G_\mathrm{m}(x_1, p, T)$ diagrams: fluid–fluid equilibria are *always* associated with a concave region of Ψ. Therefore, it is possible to apply differential geometry to locate coexisting phases: at a stable point, $\Psi(\vec{\rho})$ must be convex (i.e., all eigenvalues of the Jacobian are positive), and one of the eigenvectors points to the concave (two-phase) region, if such a region exists. This eigenvector is most likely the one belonging to the lowest eigenvalue.

Figure 5.15 shows a realistic Ψ map, computed for the system {CO_2 + decane} at 344 K with the Peng–Robinson equation of state. The map shows two regions of low Ψ values (dark), one close to the diagonal and corresponding to liquid states, and the other very close to the abscissa (CO_2 axis) and corresponding to gas states. The connodes running between these two regions span a ridge of positive curvature. The figure also shows how the connodes rotate when the pressure is increased, and finally contract when the critical point is reached.

Another interesting feature of the isochoric approach is that its equilibrium conditions can be applied to mixtures as well as pure components. Table 5.1 compares these conditions; it can be seen that the "local criterion" (equality of some derivatives) and the "global criterion" (common tangent or Maxwell criterion) switch their places.

For pure fluids, the stability criterion (5.169) reduces to $(\partial^2\Psi/\partial\rho^2) = 0$. It is easy to show that this is equivalent to $A_{(2V)} = 0$: in the Ψ-based formulation, the stability criterion reduces to the mechanical stability in a natural way (in contrast to the G_m-based formulation).

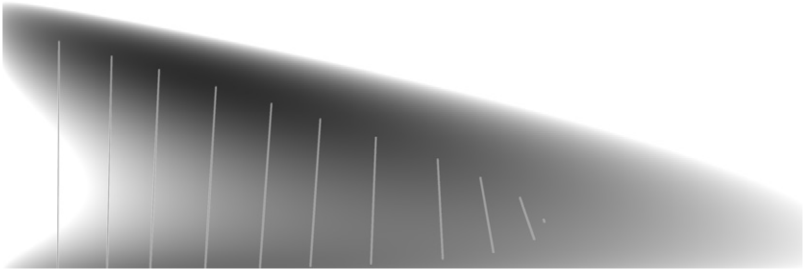

FIGURE 5.15 Pseudocolor map of the $\rho_1, \rho_2 \to \Psi(\rho_1, \rho_2, T)$ function for the system {carbon dioxide + decane} at 344 K, computed with the Peng–Robinson equation of state. A linear function was subtracted and the result scaled to achieve best contrast. Axes as in Fig. 5.14; dark regions: low Ψ values, white regions: high Ψ values or physically not accessible (above the diagonal), and straight lines: connodes.

TABLE 5.1 Criteria for Vapor–Liquid Equilibrium of a Pure Fluid, Classical Formulation versus Isochoric Formulation

Classical	Isochoric
$p' = p''$	$\left(\frac{\partial \Psi}{\partial \rho}\right)(\rho'' - \rho') = \Psi'' - \Psi'$
$p^\sigma (V''_\mathrm{m} - V'_\mathrm{m}) = A''_\mathrm{m} - A'_\mathrm{m}$	$\left(\frac{\partial \Psi'}{\partial \rho}\right) = \left(\frac{\partial \Psi''}{\partial \rho}\right)$

5.8.3 Mechanical Stability

The mechanical stability criterion for mixtures can be obtained from Eq. (5.152) by taking its total differential at constant temperature,

$$\mathrm{d}p = -\mathrm{d}\Psi + \sum_{i=1}^{N} \mu_i \, \mathrm{d}\rho_i + \sum_{i=1}^{N} \rho_i \, \mathrm{d}\mu_i, \tag{5.172}$$

and inserting Eq. (5.159); the result is

$$\mathrm{d}p = \sum_{i=1}^{N} \rho_i \, \mathrm{d}\mu_i = \sum_{i=1}^{N} \rho_i \left(\frac{\partial \mu_i}{\partial \rho_i}\right) \mathrm{d}\rho_i. \tag{5.173}$$

With $(\partial \mu_i / \partial \rho_i) = \Psi_{ii}$ [cf. Eq. (5.154)] and $\mathrm{d}\rho_i = \rho_i / \rho \, \mathrm{d}\rho$, this equation reduces to

$$\mathrm{d}p = \frac{1}{\rho} \sum_{i=1}^{N} \rho_i^2 \Psi_{ii} \, \mathrm{d}\rho, \tag{5.174}$$

which immediately leads to the criterion of mechanical stability:

$$-\left(\frac{\partial p}{\partial V}\right)_T = \rho^2 \left(\frac{\partial p}{\partial \rho}\right) = \rho \sum_{i=1}^{N} \rho_i^2 \Psi_{ii} \tag{5.175}$$

The right-hand side of this condition contains a sum that can be regarded as the trace of a matrix having the elements $\rho_i \rho_j \Psi_{ij}$, i.e., a matrix obtained from $\boldsymbol{\Psi}$ by multiplication with a diagonal matrix whose main-diagonal elements are the densities:

$$-\left(\frac{\partial p}{\partial V}\right)_T = \rho \, \mathrm{tr}\left(\mathrm{diag}(\vec{\rho}) \boldsymbol{\Psi} \mathrm{diag}(\vec{\rho})\right) \tag{5.176}$$

The matrix product represents a unitary transformation (cf. Section A.11), hence the eigenvalues of the product are the same as those of $\boldsymbol{\Psi}$. The trace of a matrix is also the sum of its eigenvalues:

$$-\left(\frac{\partial p}{\partial V}\right)_T = \rho\,\mathrm{tr}\,\boldsymbol{\Psi} = \rho\sum_{i=1}^{N}\lambda_i \tag{5.177}$$

The mechanical stability limit, $(\partial p/\partial V)_T = 0$, can only be reached if either all λ_i are zero or at least λ_{min} is negative. This, however, is a stronger requirement than the condition of diffusion stability, $\lambda_{\mathrm{min}} = 0$. Consequently, mixtures reach the limit of diffusion stability before they become mechanically unstable. Only for pure fluids and azeotropes these criteria coincide.

This extends the proof Eq. (5.56) to multicomponent mixtures.

5.8.4 Computation

Algorithm 7 illustrates a way to calculate the equilibrium pressure and the composition of the coexisting fluid phase for a fluid mixture of known composition. The algorithm proceeds in three steps: first, it varies the pressure until a thermodynamically stable state of the fixed[17] fluid phase is obtained. Then it performs a search along the eigenvectors for the density vector of the unknown phase, i.e., it computes the local eigenvectors, moves for some distance along one of them, computes new eigenvectors, etc. For the correct eigenvector, the search leads through an unstable domain and ends when "stable ground" has been reached again. In principle, the eigenvector associated with the lowest eigenvalue, $\vec{u}_{\mathrm{min}}$, should be chosen, but as the density of the fixed phase it not accurately known at this stage, it may be better to try the other eigenvectors, too[18]. Finally, a nonlinear solver is started.

For the calculation of a phase diagram, steps 1 and 2 have to be done for the first equilibrium state only. Once an equilibrium state has been calculated, initial values for the calculation of further equilibrium states at slightly different temperatures or compositions of the fixed phase can be obtained by extrapolation.

The algorithm can also be applied to pure fluids. In this case, of course, the calculation of the eigenvector is trivial, for there is only one density variable.

As mentioned above already, this algorithm is very fast, because it does not require the calculation of densities from pressure at every step. Another advantage is that it is not disturbed by azeotropes.

With Eqs (5.167) and (5.170) also a robust algorithm can be constructed that locates all critical states of a multicomponent mixture.

Algorithm 8 is essentially a modification, or perhaps even a simplification, of Algorithm 5 or 6. Its first step is the selection of the mole fraction. As there are

---

[17] Fixed with respect to the mole fractions: the densities still have to be determined.

[18] Follow them until their eigenvalues pass through a minimum, or until $\lambda_{\mathrm{min}} < 0$, then switch back to $\vec{u}_{\mathrm{min}}$.

Algorithm 7: Calculation of the equilibrium pressure and the composition of a coexisting phase for a fluid mixture of given composition with isochoric thermodynamics

```
Input: equation of state $p(\vec{\rho}, T)$, fundamental equation $A_\mathrm{m}(\vec{\rho}, T)$
Data: mole fractions of the fixed phase: $\vec{x}'$
Result: equilibrium pressure $p$, composition of the other phase $\vec{\rho}''$

function $\vec{y}(\vec{\rho}', \vec{\rho}'', T)$:
    for phases ′ and ″ do
        $\rho = \sum \rho_i$;
        $p = p(\vec{\rho}, T)$;
        $\vec{a} = \nabla_\rho (A^\mathrm{r}_\mathrm{m}(\vec{\rho}, T)\rho) + RT \ln \vec{\rho}$;
    end
    for components $i = 1 \ldots n$ do $y_i = a'_i - a''_i$;
    $y_0 = p' - p''$;
end

repeat
    calculate Hessian of $\Psi = A_\mathrm{m}\rho'$;
    solve eigenvalue problem, identify $\lambda_\mathrm{min}$;
    if $\lambda_\mathrm{min} < 0$ then modify $p$
until $\lambda_\mathrm{min} > 0$;
$\vec{\rho}'' := \vec{\rho}'$;
for all eigenvectors $\Delta\vec{\rho}_i$ do
    repeat
        $\vec{\rho}'' := \vec{\rho}'' + \alpha \Delta\vec{\rho}_i$;
        calculate Hessian of $\Psi = A_\mathrm{m}\rho''$;
        solve eigenvalue problem;
    until $\lambda_i < 0$ or $\lambda_i = \mathrm{min}$;
end
repeat
    $\vec{\rho}'' := \vec{\rho}'' + \alpha \Delta\vec{\rho}_i$;
    calculate Hessian of $\Psi = A_\mathrm{m}\rho''$;
    solve eigenvalue problem;
until $\lambda_\mathrm{min} > 0$ and $\vec{y}^2 = \mathrm{min}$;
solve $\vec{y} = 0$ for $\vec{\rho}', \vec{\rho}''$ with Marquardt–Levenberg method;
convert $\vec{\rho}''$ to mole fractions;
```

α is a conveniently chosen constant that lets the search pass through the unstable region. The search should be terminated if one of the ρ_i gets outside the permissible range.

two critical conditions only, Gibbs' phase rule allows to set the mole fractions freely (as long as they add up to 1). The user can vary one mole fraction and maintain the ratios of the others, or follow another path.

Algorithm 8: Critical curves by isochoric thermodynamics

```
Input: equation of state: $p(\vec{\rho}, T)$, fundamental equation: $\Psi(\vec{\rho}, T)$
Data: pure-components critical data, $p_{c,i}$ and $T_{c,i}$, $i = 1 \dots N$
Result: critical curve(s) $p(\vec{x}), T(\vec{x})$ for arbitrary vectors $\vec{x}$

function $f_1(\vec{\rho}, T)$:
    calculate $\mathbf{\Psi}(\vec{\rho}, T)$;
    calculate its eigenvalues;
    return $\lambda_{\min}$;
end

function $f_2(\vec{\rho})$:
    for $T := 1.5 \max(T_{c,i}) \dots 0.2 \min(T_{c,i})$ do
        evaluate $f_1$;
        if change of sign then
            solve $f_1(T) = 0$ (regula falsi method);
            calculate eigenvalues of $\mathbf{\Psi}(\vec{\rho} \pm \alpha \vec{u}_{\min}, T)$;
            return $(\lambda_{\min,+} - \lambda_{\min,-})/(2\alpha)$;
        end
    end
end

for all $\vec{x}$ do
    estimate $\rho_{\min}, \rho_{\max}$ for density scan;
    for $\rho := \rho_{\max} \dots \rho_{\min}$ do
        evaluate $f_2$;
        if change of sign then
            solve $f_2 = 0$ (regula falsi method);
            apply stability criteria;
            store $\vec{x}$, $\rho$, $T$;
        end
    end
end
for all critical points do
    find nearest neighbours in $\vec{\rho}, T$ space;
    group into critical curves;
end
```

The second part is a "scan" over the relevant density range. For each density, the critical temperature is estimated from Eq. (5.167) and then used to evaluate Eq. (5.170). A change of sign of the latter indicates a critical point.

Finally, the critical points have be sorted into critical curves.

Incidentally, it is also possible to solve Eqs (5.167) and (5.170) with a good nonlinear equation solver, e.g., the Marquardt–Levenberg method. Because of the way these equations were derived, i.e., from eigenvalue equations, the search direction of the Marquardt–Levenberg method is aligned with the main eigenvector, and this improves the convergence significantly. The disadvantage of such a direct, two-dimensional search is that one does not know to which critical point the search will converge if there is more than one for the fixed composition.

5.9 HEAT EFFECTS OF PHASE TRANSITIONS

Because of the second law of thermodynamics, the heat absorbed or generated by a reversible process can be expressed as $\mathrm{d}q = T\,\mathrm{d}S$[19]. For a process taking place at constant pressure and without changes of the amounts of the substances involved, the natural thermodynamic potential is the enthalpy, and because of Eq. (4.6) we can write $\mathrm{d}q = \mathrm{d}H$; for an isochoric process we would use $\mathrm{d}q = \mathrm{d}U$.

A differential scanning calorimeter (DSC) or a transitiometer in the isobaric scanning mode records the heat flow $\dot{q}$ to or from the sample that is required to maintain a constant heating or cooling rate, $\dot{T}$. If the sample is in a single-phase state (or in more than one phase, but with constant amounts of these phases), the heat flow can be expressed as

$$\dot{q} = \frac{\mathrm{d}q}{\mathrm{d}t} = \left(\frac{\partial H}{\partial T}\right)_{p,n_i} \frac{\mathrm{d}T}{\mathrm{d}t} = C_p \dot{T}, \tag{5.178}$$

i.e., a DSC apparatus records the isobaric heat capacity of the sample, or more accurately: the difference of the molar heat capacities of the sample and the reference.

For pure compounds, first-order phase transitions take place at a fixed temperature. The heat absorbed or liberated in the process is equal to the difference of the enthalpies (isobaric transition), $q = \Delta H = H'' - H'$. For the less common case of isochoric transitions, the analogous expression is $q = \Delta U$. For an ideal isobaric DSC experiment this implies $\dot{q} = \Delta H \delta(T - T_{\mathrm{tr}})$, where the second factor is Dirac's δ function located at the transition temperature, i.e., an infinitesimally narrow and infinitely high peak. In practical DSC experiments the peak is smeared out, but still its integral (after subtracting the baseline) represents the transition enthalpy:

$$\int\limits_{\mathrm{peak}} \dot{q}\,\mathrm{d}t = \Delta H = T\Delta S \tag{5.179}$$

It might be tempting to apply these equations to mixtures. Here, however, most phase transitions do not occur at a single, fixed temperature, but over a

---

[19] More accurately: $đq = T,\ \mathrm{d}S$, for q is not a state function (cf. Section 4.1). But the distinction is not relevant here.

temperature range. Moreover, the amounts of the components in the phases usually change over this temperature range. Now the total enthalpy of the sample in the two-phase state is the sum of the enthalpies of the two phases. The amounts of these phases can be determined from the lever rule, Eq. (2.11), which we write here as

$$n^\alpha = nf^\alpha, \alpha = {}', {}'' \\ \text{with}\, f' = \frac{x_1'' - x_1}{x_1'' - x_1'} \qquad f'' = \frac{x_1 - x_1'}{x_1'' - x_1'}, \tag{5.180}$$

where x_1 and n refer to the overall composition and amount of the sample, respectively, and x_1^α, n^α, and f^α to compositions, amounts, and fractions of the coexisting phases. Consequently, the total entropy is

$$S = \sum_{\alpha = ', ''} f^\alpha S_\mathrm{m}^\alpha \tag{5.181}$$

and the resulting heat flow (remembering that x_1' and x_1'' are functions of temperature) is given as follows.

$$\dot{q} = n\dot{T} \sum_{\alpha = ', ''} Tf^\alpha \left[\frac{C_{p,\mathrm{m}}^\alpha}{T} - \left(S_{(x)}^\alpha - \frac{S_\mathrm{m}'' - S_\mathrm{m}'}{x_1'' - x_1'} \right) \frac{\mathrm{d}x_1^\alpha}{\mathrm{d}T} \right]. \tag{5.182}$$

The $\mathrm{d}x_1^\alpha/\mathrm{d}T$ are the slopes of the phase boundaries.

Inserting the isobaric Gibbs–Konowalow equation,

$$\frac{\mathrm{d}T}{\mathrm{d}x_1^\alpha} = \frac{G_{(2x)}^\alpha}{S_{(x)}^\alpha - \frac{S_\mathrm{m}'' - S_\mathrm{m}'}{x_1'' - x_1'}}, \tag{5.183}$$

which is the analog of Eq. (5.44) or (5.45), finally leads to the result of Filippov and Chernik [77]:

$$\dot{q} = n\dot{T} \left[\sum_{\alpha = ', ''} f^\alpha C_{p,\mathrm{m}}^\alpha + \sum_{\alpha = ', ''} f^\alpha T G_{(2x)}^\alpha \left(\frac{\mathrm{d}x_1^\alpha}{\mathrm{d}T} \right)^2 \right]. \tag{5.184}$$

For practical purposes, it is probably better to evaluate the entropy equation and to differentiate it numerically. But, it is interesting to look at the last equation carefully: the first term in the brackets represents the change of the heat capacity (the baseline of a DSC trace) during a phase transition. The second term represents the enthalpy change due to the shift of the phase compositions. As $G_{(2x)} > 0$ for a stable phase, this term always increases the apparent heat capacity of the sample.

Figures 3.5 and 3.6 in the section on experimental methods show that even a simple system can have rather interesting DSC traces. Upon heating a solid mixture of nitrogen and methane, the system first reaches the eutectic temperature.

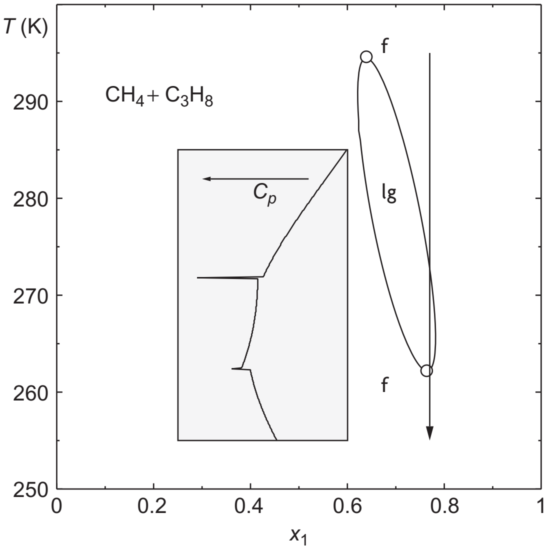

FIGURE 5.16 Isobaric phase diagram of the {methane + propane} system at 10 MPa, calculated with the Peng–Robinson equation of state. ——: phase boundaries and ○: binary critical points. Inset: predicted DSC trace (arbitrary units) for a path along the arrow.

Here the nitrogen crystals melt, thus giving rise to a sharp peak. Then the system passes through a two-phase region, s_2l, where the methane gradually melts. As the "lever" of the liquid phase shortens rapidly upon approaching the phase boundary, a small peak occurs. Then the system passes through a one-phase liquid state, where incidentally the heat capacity is higher than in the solid or partially solid state. Finally, the system evaporates, giving rise to a huge signal, because under the present conditions the vaporization enthalpy is much larger than the fusion enthalpy. Again, the vanishing of a lever upon entering or leaving a two-phase region produces a spike.

Figure 5.16 shows a supercritical isobaric phase diagram of a class I binary system (cf. Fig. 2.19) with the DSC trace along the indicated path, i.e., at a pressure and composition where retrograde behavior occurs. Entering the two-phase region corresponds to the precipitation, leaving it to the evaporation of a liquid phase. Still, both phase changes produce a positive spike in accordance with Eq. (5.184).

Chapter 6

Solid–Fluid Equilibrium

Toward low temperatures or high pressures, fluid-phase equilibria are bounded by solid–fluid equilibria. Here we will treat the basic thermodynamic modeling of solid phases as well as the calculation of phase equilibria that appear in the context of supercritical fluid extraction and related technologies. For an exhaustive discussion of the topologies of solid–fluid phase diagrams or mixtures, the reader should consult other textbooks, particularly textbooks of mineralogy.

6.1 THERMODYNAMIC FUNCTIONS OF SOLIDS

The calculation of the thermodynamic functions of fluid phases — liquids, gases, or supercritical states — can be done with Eq. (4.19). If the target phase is a liquid, the integration required by this equation has to be carried out through the unstable region of the equation of state, but as long as this is continuous, there is no problem.

This is different for solids: there is no continuous equation of state that describes the fluid *and* the solid state. Hence, the problem arises to connect the thermodynamic properties of solids to those of fluids in a thermodynamically consistent way.

A possible way to achieve a consistent connection of the solid state to the fluid state is as follows (see Fig. 6.1):

- We begin with the same reference state as for fluids, namely a state at very low pressures in the ideal-gas range. Its Gibbs energy is $G_\mathrm{m}^\mathrm{f}(p^\ominus, T)$.
- We integrate the fluid equation of state up to the sublimation pressure p^sg:

$$\Delta G_\mathrm{m}^\mathrm{f} = \int\limits_{p^\ominus}^{p^\mathrm{sf}} V_\mathrm{m}^\mathrm{f}(p, T)\,\mathrm{d}p$$

- At the sublimation pressure, the molar Gibbs energies of the solid and the gas phase are equal, $G_\mathrm{m}^\mathrm{f}(p^\mathrm{sf}, T) = G_\mathrm{m}^\mathrm{s}(p^\mathrm{sf}, T)$.

High-Pressure Fluid Phase Equilibria. DOI: 10.1016/B978-0-444-56347-7.00006-2

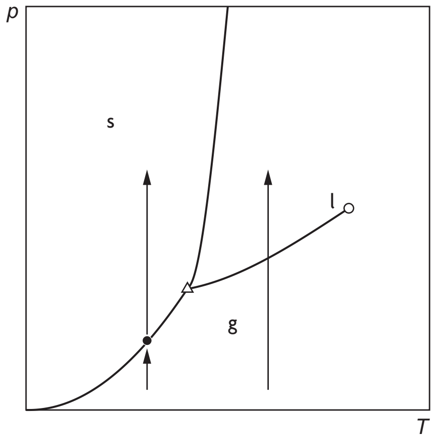

FIGURE 6.1 Illustration of the calculation of the Gibbs energy of liquids and solids: for liquids, the equation of state can be integrated from the reference state to the desired final pressure; for solids, it is necessary to integrate first the fluid equation of state to the sublimation pressure curve and then the solid equation of state from there to the final pressure.

- Finally, the equation of state of the solid is integrated up to the desired pressure:

$$\Delta G_\mathrm{m}^\mathsf{s} = \int_{p^\mathsf{sf}}^{p} V_\mathrm{m}^\mathsf{s}(p,T)\,\mathrm{d}p$$

The resulting master equation of the Gibbs energy of a solid is therefore

$$G_\mathrm{m}^\mathsf{s}(p,T) = G_\mathrm{m}^\mathsf{f}(p^\ominus,T) + \int_{p^\ominus}^{p^\mathsf{sf}} V_\mathrm{m}^\mathsf{f}(p,T)\,\mathrm{d}p + \int_{p^\mathsf{sf}}^{p} V_\mathrm{m}^\mathsf{s}(p,T)\,\mathrm{d}p \tag{6.1}$$

or, expressing the fluid term with the Helmholtz energy according to Eq. (4.19),

$$\begin{aligned} G_\mathrm{m}^\mathsf{s}(p,T) &= G_\mathrm{m}^\mathsf{f}(p^\ominus,T) + p^\mathsf{sf} V_\mathrm{m}^\mathsf{f}(p^\mathsf{sf},T) - RT + A_\mathrm{m}^{\mathsf{r,f}}(V_\mathrm{m}^{\mathsf{f,sf}},T) \\ &\quad + \int_{p^\mathsf{sf}}^{p} V_\mathrm{m}^\mathsf{s}(p,T)\,\mathrm{d}p. \end{aligned} \tag{6.2}$$

These equations make use of the equation of state of the solid, for which several approximations are possible:

- The simplest approximation is to treat the solid phase as incompressible, $V_\mathrm{m}^\mathsf{s} = \text{constant}$. This, however, is only permissible if small pressure changes are considered. Many organic solids have compressibilities that are comparable to those of liquids. The resulting contribution to the Gibbs energy of the solid the integral in Eq. (6.2) is then

$$\Delta G_{\mathrm{m}}^{\mathrm{s}} = V_{\mathrm{m}}^{\mathrm{s}}(p - p^{\mathrm{sf}}). \tag{6.3}$$

- A better approximation is obtained if the compressibility of the solid is assumed to be positive and constant,

$$\kappa_T^{\mathrm{s}} = -\frac{1}{V_{\mathrm{m}}^{\mathrm{s}}}\left(\frac{\partial V_{\mathrm{m}}^{\mathrm{s}}}{\partial p}\right)_T = \text{const.} \tag{6.4}$$

  This is an ordinary differential equation for $V_{\mathrm{m}}^{\mathrm{s}}$. Its solution is

$$V_{\mathrm{m}}^{\mathrm{s}}(p) = V_{\mathrm{m}}^{\mathrm{s}}(p^{\mathrm{sf}}) \exp\left(-\kappa_T^{\mathrm{s}}(p - p^{\mathrm{sf}})\right). \tag{6.5}$$

  Integration with respect to pressure gives the Gibbs energy contribution:

$$\Delta G_{\mathrm{m}}^{\mathrm{s}} = \frac{V_{\mathrm{m}}^{\mathrm{s}}(p^{\mathrm{sf}})}{\kappa_T^{\mathrm{s}}}\left(1 - \exp\left(-\kappa_T^{\mathrm{s}}(p - p^{\mathrm{sf}})\right)\right). \tag{6.6}$$

- A superior equation of state for solids is the Murnaghan equation, which makes use of the experimentally established relation

$$\frac{1}{\kappa_T^{\mathrm{s}}(p)} = \frac{1}{\kappa_T^{\mathrm{s}}(0)} + \lambda p, \tag{6.7}$$

  where λ is a substance-dependent parameter. The expression $1/\kappa_T^{\mathrm{s}}(p)$ is often referred to as *bulk modulus*. The resulting equation of state is then

$$V_{\mathrm{m}}^{\mathrm{s}}(p) = V_{\mathrm{m}}^{\mathrm{s}}(p^{\mathrm{sf}})\left(1 + \lambda(p - p^{\mathrm{sf}})\kappa_T^{\mathrm{s}}(p^{\mathrm{sf}})\right)^{-1/\lambda}, \tag{6.8}$$

  and the Gibbs energy contribution is

$$\Delta G_{\mathrm{m}}^{\mathrm{s}} = \frac{V_{\mathrm{m}}^{\mathrm{s}}(p^{\mathrm{sf}})}{\lambda \kappa_T^{\mathrm{s}}(p^{\mathrm{sf}})}\left(\left(1 + \lambda(p - p^{\mathrm{sf}})\kappa_T^{\mathrm{s}}(p^{\mathrm{sf}})\right)^{1-1/\lambda} - 1\right). \tag{6.9}$$

  For most substances, the sublimation pressures are rather small and negligible against the pressures required to achieve a significant compression.[1] Then the last two equations can be simplified to

$$V_{\mathrm{m}}^{\mathrm{s}}(p) = V_{\mathrm{m}}^{\mathrm{s}}(0)\left(1 + \lambda \kappa_T^{\mathrm{s}}(0) p\right)^{-1/\lambda} \tag{6.10}$$

  and

$$\Delta G_{\mathrm{m}}^{\mathrm{s}} = \frac{V_{\mathrm{m}}^{\mathrm{s}}(0)}{\lambda \kappa_T^{\mathrm{s}}(0)}\left(\left(1 + \lambda \kappa_T^{\mathrm{s}}(0) p\right)^{1-1/\lambda} - 1\right). \tag{6.11}$$

---

[1] CO_2 is an exception: $p_{\mathrm{trp}} = 0.5185$ MPa.

In addition to data of the fluid phase, the calculation of the Gibbs energy of a solid phase at a given temperature merely requires the molar volume of the solid, the sublimation pressure, and — if high pressures are considered — the compressibility and eventually the Murnaghan parameter of the solid. Once these data are available, the computation of phase equilibria involving this phase is no longer a problem.

In practice, the calculation of phase diagrams involving solid phases is not a very rewarding task, for reliable experimental molar volumes and sublimation pressures of solids are scarce. A "solid" obtained from cooling down a liquid may not be in its equilibrium state, but perhaps be a glass state or a high-temperature solid modification that still needs to relax to the stable modification. The measurement of low sublimation pressures requires a considerable experimental effort and awareness of chemical sources of trouble: volatile trace impurities or decomposition products can (and sometimes did) shift the sublimation pressure by several orders of magnitude.

The equations given above can also be applied to polymorphic solids. In such a case, there are several solid phases, each having its own molar volume and sublimation pressure curve.[2] In such a case, the Gibbs energy of each one must be calculated, and the phase with the lowest value is the stable one.

It is not safe to choose the solid phase with the smallest sublimation pressure, as can be seen from the following example:

Tetracosane (n-$C_{24}H_{50}$) has got two solid modifications, a "normal" low-temperature modification s_β with a high density and a high-temperature modification s_α with an almost liquid-like density and compressibility. The phase diagram (Fig. 6.2) shows that the solid–solid transition curve is inclined, and that the low-temperature modification becomes the only stable modification at high pressures [57, 78].

It should be noted that, as soon as the fluid equation of state has been chosen and the solid phase characteristics (molar volume, sublimation pressure, solid compressibility) are known, the melting pressure curve is completely determined; there are no more free parameters left. Therefore, the prediction of the melting pressure curve from sublimation data is a rather severe test for fluid equations of state.

In a pT phase diagram, melting pressure curves are usually very steep. For their calculation, it is therefore advantageous to set the pressure and solve the equilibrium condition

$$G_\mathrm{m}^\mathsf{s}(p,T) = G_\mathrm{m}^\mathsf{l}(p,T) \tag{6.12}$$

---

[2] more accurately: … and phase boundary curve with another phase whose Gibbs energy is known: some substances have high-pressure modifications that have equilibria with other solid phases only, but not with a gas phase. But if at least one of these other solid phase regions has a boundary with a fluid-phase region, the Gibbs energies of the solid phases can be computed.

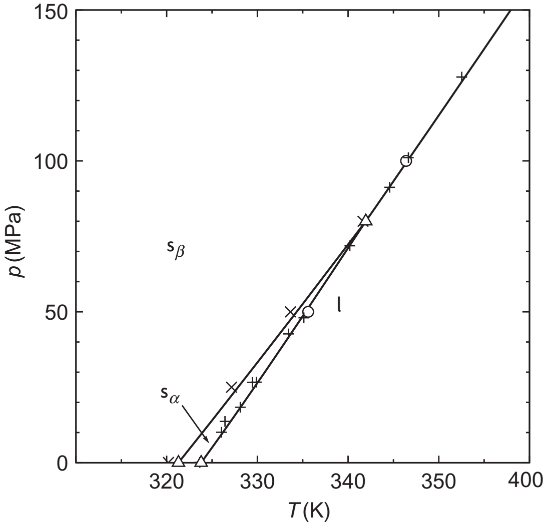

FIGURE 6.2 Low-temperature part of the phase diagram of tetracosane. ——: phase boundaries between the two solid modifications and the liquid, calculated with the Peng–Robinson equation of state, △: triple points (calculated), and other symbols: experimental results [78]. (*Reprinted from Supercritical Fluids as Solvents and Reaction Media, G. Brunner (ed.), Ch. 1.8: U. K. Deiters, "Correlation and prediction of high-pressure phase equilibria and related thermodynamic properties of simple fluid mixtures", pp. 185–209, © 2004, with permission from Elsevier*)

for the temperature. This can be very efficiently done with a *regula falsi* algorithm (see Section A.3).

Algorithm 9: The melting pressure curve of a pure substance.

```
Input: equation of state: $p(\rho, T)$, fundamental equation: $A_\mathrm{m}(\rho, T)$,
       Gibbs energy of the solid phase: $G^\mathrm{s}_\mathrm{m}(p, T)$
Data: triple point temperature $T_\mathrm{trp}$
Result: melting temperature $T(p), p = p_\mathrm{min} \cdots p_\mathrm{max}$

function $y(p, T)$:
    $y := G^\mathrm{l}_\mathrm{m}(p, T) - G^\mathrm{s}_\mathrm{m}(p, T)$;
end function

for $p := p_\mathrm{min} \cdots p_\mathrm{max}$ do
    $T_0 := T_\mathrm{trp}$;
    repeat $T_0 := T_0/f$ with $f \approx 1.1$ until $y(p, T_0) \geq 0$;
    $T_1 := T_\mathrm{trp}$;
    repeat $T_1 := T_1 f$ until $y(p, T_1) \leq 0$;
    perform regula falsi search on $y(p, T)$ between $T_0$ and $T_1$
end
```

6.2 EQUILIBRIUM OF A PURE SOLID AND MIXED FLUID PHASE

The general equilibrium criterion, (Eq. 5.1), holds for solid–fluid equilibria too. In the special case of a pure solid phase in presence of a fluid mixture, the equilibrium condition for the chemical potentials can be written as

$$G^{\mathrm{s}}_{\mathrm{m},2} = \mu^{\mathrm{f}}_{2} , \tag{6.13}$$

assuming that component 2 of the system forms the solid, and component 1 acts as the solvent. The situation is illustrated in Fig. 6.3: the task of finding the phase equilibrium is equivalent to constructing a tangent to the $G_{\mathrm{m}}(x_1)$ function of the fluid mixture that passes through the Gibbs energy of the solid. As long as $G^{\mathrm{s}}_{\mathrm{m},2}$ is lower than the end point of the curve of the fluid, $G^{\mathrm{f}}_{\mathrm{m},2}$, such a tangent can always be constructed, and therefore, the phase equilibrium must exist.

Complications can arise if the Gibbs energy function of the fluid has a concave portion or multiple branches. In such a case, more than one tangent can be constructed; the lowermost tangent represents the stable equilibrium.

If the crystallizing compound has more than one modification, care must be taken to use the modification with the lowest molar Gibbs energy at the given pressure and temperature.

The equilibrium condition given above can immediately be used to construct an algorithm for the calculation of phase equilibria. The Gibbs energy of the fluid mixture can be obtained from an equation of state using Eqs (4.18) and (4.19) that of the solid from Eqs (6.3) through (6.9). If the solid phase is stable, its molar Gibbs energy is lower than the chemical potential of the crystallizing

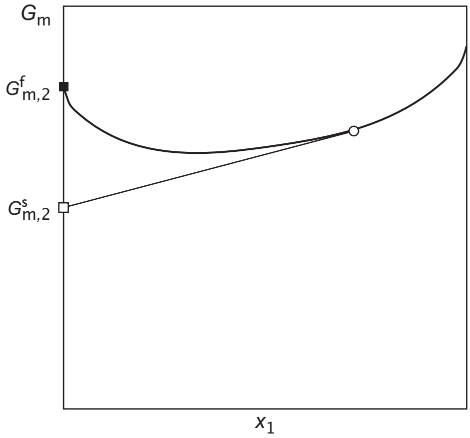

FIGURE 6.3 Determination of the phase equilibrium between a pure solid and a fluid mixture from the molar Gibbs energies of the phases. ——: molar Gibbs energy of the fluid, ■: molar Gibbs energy of pure fluid (liquid or gaseous) component 2, □: molar Gibbs energy of the solid, ——: tangent, and ○: fluid equilibrium phase.

component 2 in the pure fluid state ($x_2 = 1$). But as this chemical potential runs toward $-\infty$ for $x_2 \to 0$, there must be a mole fraction at which the difference becomes zero.

Algorithm 10: Calculation of a solid–fluid equilibrium.

```
Input: fluid equation of state: $p(\rho, T, x_1)$, fundamental equation:
        $A_\mathrm{m}(\rho, T, x_1)$, solid Gibbs energy $G^\mathrm{s}_{\mathrm{m},2}(p, T)$
Data: pressure $p$, temperature $T$
Result: solid–fluid equilibrium mole fraction $x^\mathrm{f}_2(p, T)$

function $\Delta\mu_2(p, T, x_1)$:
    calculate $\rho^\mathrm{f}$ from equation of state;
    $\Delta\mu_2 := \mu^\mathrm{f}_2(p, T, 1 - x_1) - G^\mathrm{s}_{\mathrm{m},2}(p, T)$;
end function

if $\Delta\mu_2(p, T, 0) < 0$ then no solid–fluid equilibrium possible, exit;
$x_2 := 1$;
repeat $x_2 := 0.1x_2$ until $\Delta\mu_2(p, T, x_1) < 0$;
perform a regula falsi search on $\Delta\mu_2$ between $x_1 = 0$ and $x_1 = 1 - x_2$;
```

The equilibrium condition, Eq. (6.13), can be analyzed further if some simplifying assumptions are made: if the sublimation pressure of the solid is so low that the vapor phase can be treated as an ideal gas ($p^\mathrm{sf}_2 V^\mathrm{f,\,sf}_\mathrm{m} = RT$, $A^\mathrm{r,f}_\mathrm{m}(V^\mathrm{f,\,sf}_\mathrm{m}, T) = 0$) and the solid phase as incompressible, the left-hand side reduces to

$$G^\mathrm{s}_\mathrm{m} = G^\mathrm{f}_\mathrm{m}(p^\ominus, T) + RT \ln \frac{p^\mathrm{sf}}{p^\ominus} + pV^\mathrm{s}_{\mathrm{m},2} \tag{6.14}$$

because of Eqs. (6.2) and (6.3). The right-hand side can be written as

$$\mu^\mathrm{f}_2 = G^\mathrm{f}_\mathrm{m}(p^\ominus, T) + RT \ln \frac{x^\mathrm{f}_2 p \phi_2}{p^\ominus}, \tag{6.15}$$

using the definitions of the fugacity and the fugacity coefficient Eqs (4.75) and (4.76). Combining these two equations yields

$$\ln x^\mathrm{f}_2 = \ln \frac{p^\mathrm{sf}_2}{p\phi_2} + \frac{pV^\mathrm{s}_{\mathrm{m},2}}{RT}. \tag{6.16}$$

This equation for the mole fraction of the heavy component in the fluid phase can be found in many textbooks [79]. It shows that the mole fraction of the solid compound in the fluid phase depends to a large extent on its sublimation pressure. The second term, which contains the molar volume of the solid phase, contributes at high pressures. The fugacity coefficient ϕ_2 reflects the "solvation power" of the fluid phase. Of course, ϕ_2 depends on x^f_2. Hence, this equation has to be solved iteratively, and thus does not offer any real advantage over Eq. (6.13).

Another important application of Eq. (6.13) is checking whether a fluid–fluid phase equilibrium is metastable with respect to the crystallization of one of the components. If the fluid–fluid phase equilibrium has been computed, the chemical potentials μ_i^{f} of all components are available (and are the same for both phases). Then one has to test for

$$G^{\mathrm{s}}_{\mathrm{m},i} > \mu_i \quad i = 1, \ldots N. \tag{6.17}$$

If the criterion is fulfilled for all components i, the fluid–fluid phase equilibrium is stable; otherwise (at least) component i will crystallize, and it is necessary to perform a solid–fluid equilibrium calculation.

It is particularly interesting to discuss the influence of pressure in solid–fluid equilibria: in Fig. 6.3, a change of the pressure will usually not affect the Gibbs energy of the solid very much. If the solvent is a supercritical fluid or gas, however, the $G_{\mathrm{m}}(x_1)$ curve of the fluid mixture can be shifted considerably, and this changes the solubility of the solid. This is the principle underlying the so-called supercritical fluid extraction technology, which uses supercritical fluids to dissolve or mobilize low-volatile compounds.

An example is given in Fig. 6.4, which contains a solid–fluid equilibrium curve for the {carbon dioxide + adamantane} system. Adamantane is a solid

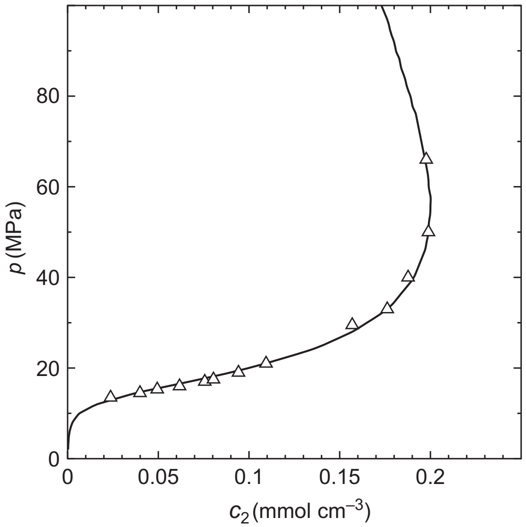

FIGURE 6.4 Solid–fluid equilibrium of the {carbon dioxide + adamantane} system at 343.15 K. ——: calculated (equation of state: Eq. (7.44) [80, 81] with density-dependent mixing rules, Eqs (8.18) and (8.19) [82]) and △: experimental.

under the experimental conditions. The equilibrium curve of the system has several portions:

- If the pressure is very low, the presence of the carbon dioxide does not influence the adamantane very much. The adamantane concentration in the gas phase is determined by its sublimation pressure, which is very low.
- When the critical pressure of the carbon dioxide (c. 73.8 MPa) is approached, its density increases markedly, so that it can solubilize the adamantane molecules. As a consequence, the adamantane concentration in the gas phase increases by several orders of magnitude.
- At very high pressures, much energy is required to create vacancies for the adamantane molecules in the carbon dioxide phase, and so the adamantane concentration decreases.

The increase of the concentration at and above the critical pressure of the carbon dioxide is technically important: here the pressure can be used to control the solubilities of dissolved species efficiently and rapidly. By dropping the pressure, the solutes can be recovered very easily; no solvent evaporation or distillation process is necessary. By expanding supercritical solutions of heavy compounds adiabatically through nozzles (RESS = rapid expansion of supercritical solutions), it is sometimes possible to produce solid phases with special particle-size distributions or unusual crystal morphologies [83, 84].

The interaction of fluid–fluid and solid–fluid phase equilibria can give rise to rather complicated phase diagrams. In this book, we restrict ourselves to technically important asymmetric systems consisting of a volatile component (solvent) and a heavy, crystallizing component of low volatility. Fig. 6.5 shows such a case, namely the phase diagram of {ethene + naphthalene}. With regard to the fluid-phase equilibria, the system belongs to class III_m: the critical curve originating at the critical point of the heavy component runs toward a compact state, passing through a pressure minimum. However, it intersects the three-phase curve $\mathsf{s_2lg}$ close to the minimum and thus terminates in a critical endpoint $\mathsf{s_2l{=}g}$. On the left (cold) side of this three-phase curve there are solid–fluid equilibria only, whereas on the right (warm) side there are fluid–fluid equilibria. The resulting *px* cross sections are discussed below (Fig. 6.9). Depending on the initial conditions, a RESS experiment starting in the one-phase region above the critical curve can therefore either enter the solid–fluid equilibrium region directly or pass through a vapor–liquid equilibrium first. The morphology of the resulting precipitates can be quite different.

6.3 REMARKS ON PHASE DIAGRAMS OF BINARY MIXTURES

The *pT* phase diagram of a pure compound contains a sublimation pressure curve (**sg**), a melting pressure curve (**sl**), and a vapor pressure curve (**lg**). These

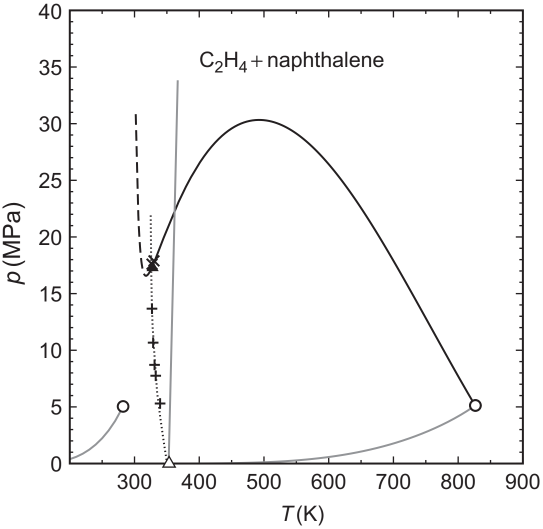

FIGURE 6.5 Phase diagram of the {ethene + naphthalene} system [78]. Gray curves: pure-fluid vapor pressure and melting pressure curves, ○: pure fluid critical point, △: triple point, ——: binary critical curve (stable part), – –: metastable part, ······: three-phase curve slg, +: experimental slg data, and ▲: experimental critical endpoint. Equation of state: Eq. (7.44) [80, 81] with density-dependent mixing rules, Eqs (8.18–8.19) [82]. (*Reprinted from Supercritical Fluids as Solvents and Reaction Media, G. Brunner (ed.), Ch. 1.8: U. K. Deiters, "Correlation and prediction of high-pressure phase equilibria and related thermodynamic properties of simple fluid mixtures", pp. 185–209, © 2004, with permission from Elsevier*).

curves meet at the triple point. If there is more than one solid phase, additional curves and triple points appear, but we will disregard this complication for now.

A simple binary mixture of class I, where there is no miscibility in the solid state and complete miscibility in the liquid state, can evidently have four phases: s_1, s_2, l, and g. Consequently, there will be one *quadruple point* $s_1s_2$lg somewhere below the triple point of component with the lower melting temperature and, emerging from it, four three-phase curves, namely

s_1s_2g – This is a generalized sublimation curve for mixtures (two solids in the presence of one mixed gas phase). It runs toward absolute zero (if no solid–solid transitions complicate the issue).

s_1s_2l – This is the eutectic curve of the system. It runs toward high pressures, roughly parallel to the $(\mathrm{sl})_1$ melting pressure curve.

$s_1$lg – This curve runs toward the triple point $(\mathrm{slg})_1$. It represents the shifting of the pure-fluid triple point due to the presence of small amounts of component 2.

$s_2$lg – This is the analogous curve for component 2.

Figs 6.6 and 6.7 show possible phase diagrams for this simple case. The $s_2$lg curve may stay at low pressures, but it may also, depending on the system, run

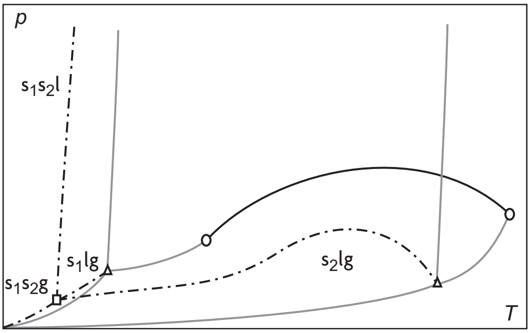

FIGURE 6.6 Schematic phase diagram of a class I system with solidification (no miscibility in the solid state) – simple case: the s_2lg curve not interfering with the critical curve.

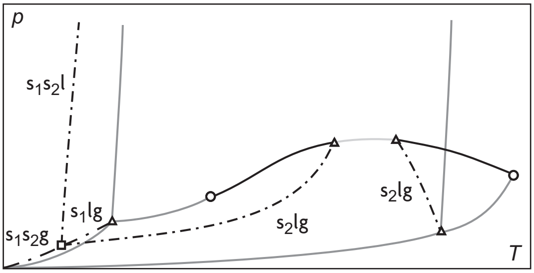

FIGURE 6.7 Schematic phase diagram of a class I system with solidification (no miscibility in the solid state) – complicated case: the s_2lg curve intersecting the critical curve; light gray — metastable portion of a critical curve.

to pressures high enough to let it interfere with the critical curve. Thus, Fig. 6.7 contains two critical endpoints $s_2l{=}g$.

Similar subtypes can be constructed for all phase diagram classes mentioned in Section 2.2. This can lead to rather interesting phase diagrams. An example is class III, for which there is a complicated case (again with the s_2lg curve intersecting the critical curve) and an even more complicated case.

The first case is shown in Fig. 6.8; it is similar to the previous case, Fig. 6.7, with the s_2lg curve cutting through both critical curves, thus generating two critical endpoints $s_2l{=}g$. Here liquid–liquid immiscibility of class III is effectively hidden by the crystallization. Fig. 6.9 shows some typical *px* cross sections: cross section A on the “cold side” of the s_2lg three-phase curve contains a solid–fluid equilibrium region only, whereas B and C contain a solid–fluid region and a vapor–liquid region, separated by the three-phase curve. At higher pressures and lower temperatures, the vapor–liquid region contracts and finally vanishes in a critical endpoint $s_2l{=}g$; at lower pressures and higher temperatures, the three-phase curve ends at the triple point $(slg)_2$ of component 2 (cut D). Beyond this point, there are regular class III vapor–liquid equilibria only (cf. Fig. 2.48).

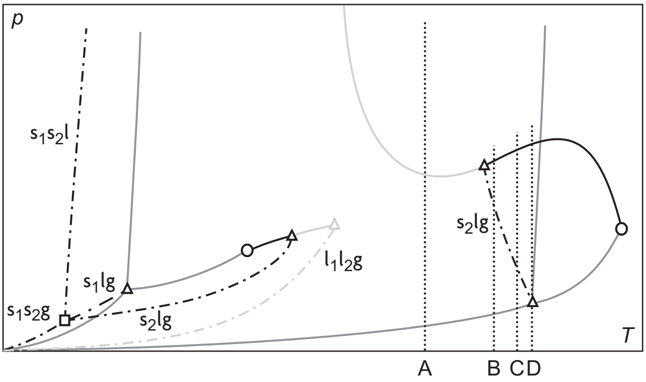

FIGURE 6.8 Schematic phase diagram of a class III system with solidification (no miscibility in the solid state) – complicated case: the s_2lg curve intersecting both critical curves; light gray -··-, —: metastable curves.

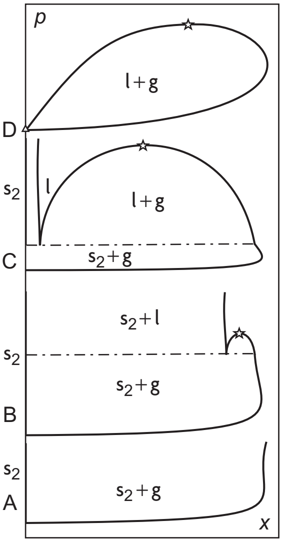

FIGURE 6.9 Isothermal *px* cross sections of Fig. 6.8.

But if the s_2lg curve "misses" the $l_1{=}gl_2$ critical endpoint, an even more complicated case results Fig. (6.10), for now the s_2lg curve must intersect the l_1l_2g three-phase curve, thus creating quadruple point $Q_2 = s_2l_1l_2g$. From here, an $s_2l_1l_2$ three-phase curve runs toward high pressures, and an s_2l_1g three-phase curve to a second quadruple point, $Q_1 = s_1s_2lg$. From this quadruple point, a three-phase curve s_1lg runs to the triple point of component 1, a eutectic curve s_1s_2l to high pressures, and a binary sublimation three-phase curve s_1s_2g to absolute zero. The high-temperature branch of the s_2lg three-phase curve may or may not interrupt the critical curve issuing from the critical point of component 2.

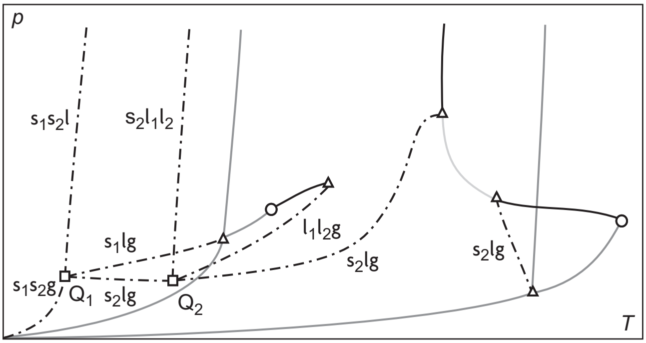

FIGURE 6.10 Schematic phase diagram of a class III system with solidification (no miscibility in the solid state) – awful case: the s_2lg curve missing the minor critical curve.[3]

The discussion of high-pressure fluid-/solid-phase diagrams can evidently get rather complicated. We can, however, observe some principles:

- The three-phase curve originating at the triple point of the heavier component is of the type s_2lg.
- The three-phase sublimation curve is s_1s_2g.
- Four three-phase curves issue from a quadruple point.
- These curves differ in one phase, i.e., by passing through a quadruple point one can exchange one phase for another.

Evidently, it takes one quadruple point to go from s_2lg to s_1s_2g, and this explains Fig. 6.8.

In Fig. 6.10, the intersection of the s_2lg and the l_1l_2g three-phase curves creates a quadruple point $Q_2 = s_2l_1l_2g$. From here, it is impossible to reach the s_1s_2g curve in one step. But it can be accomplished if a second quadruple point is used, as shown in this figure.

By starting from another fluid-phase diagram class than I or III or by varying the shapes of the three-phase curves, phase diagrams of an even higher complexity can be generated. There is evidently a huge variety. Still, even the most complicated phase diagram is based on simple rules, and a systematic minimization of the Gibbs energy of the system, taking all possible phases into account, will eventually lead to the correct diagram.

6.4 IMPURE SOLIDS

Most publications dealing with the calculation of solid–fluid phase equilibria contain the statement “it is assumed that the solid phase is pure,” or something similar to this effect.

Why are solid phases always pure compounds?

---

[3] When two liquid phases coexist, we distinguish them by writing l_1 and l_2. Both are mixtures, with l_1 having a higher mole fraction of component 1.

Of course, they are not! Admittedly, the solubilities of foreign substances in crystalline phases are usually very low; this is the reason why purification techniques like recrystallization and zone melting are so effective. Furthermore, the experimental evidence concerning solubilities in crystalline phases is meagre: even if an impurity is detected, it is often very difficult to distinguish a component truly dissolved in a crystalline phase from one adsorbed at the crystal boundaries, or occluded during crystallization.

But there are some cases in which the solid phases are known to contain significant amounts of other substances.

6.4.1 Continuous Miscibility

Continuous miscibility in the sense that two compounds can occupy lattice sites of the same crystal lattice is a rare phenomenon. Evidently, the pure compounds must have the same crystal structure and very similar lattice parameters to do so. A well-known example is the system {silver + gold}.

For thermodynamic modeling of this case, one can invoke (Eq. 6.2) for both compounds and then calculate the total Gibbs energy of the mixed solid from

$$G_{\mathrm{m}}^{\mathrm{s}}(p,T,\vec{x}^{\mathrm{s}}) = \sum_{i=1} x_i^{\mathrm{s}}\left(G_{\mathrm{m},i}^{\mathrm{s}}(p,T) + RT\ln x_i^{\mathrm{s}}\right) + G^{\mathrm{E,s}}(p,T,\vec{x}^{\mathrm{s}}). \tag{6.18}$$

The summation extends over all compounds making up the solid phase. For the excess term, a suitable function has to be chosen, but as the compounds have very similar sizes as well as chemical constitutions to achieve miscibility in the solid state, a Porter ansatz, Eq. (4.46), is usually sufficient.

In principle, one needs to know the temperature and pressure dependence of the excess function, but the authors are not aware of any published work on this topic.

If the ansatz, Eq. (6.18), is also applicable to the liquid phase (with different parameters, of course), the phase diagram can be calculated with an extension of the method presented in Section 5.5.5.

It should be noted that a large excess term can lead to "solid azeotropy" and limited miscibility in the solid state. A systematic survey of the solid–liquid phase diagrams that can be generated with this simple model has been given by van Pelt [85]; the number of phase diagrams is impressive.

6.4.2 Continuous Solubility on Interstitial Sites (Clathrates)

Miscibility in a solid phase can also occur if one component can occupy vacancies or interstitial sites in the crystal lattice of the other. An important example are clathrates: here the host component is usually a species capable of hydrogen bonding, like water, and the guest component is a nonpolar or weakly polar species, like methane, ethane, or carbon dioxide.

Clathrates can be described, in principle, with the model of van der Waals and Platteeuw [86]. In its simplest form, it assumes that the interstitial sites are all of the same quality and can be occupied by one guest molecule only;

furthermore, the guest molecules do not interact with each other. This model is in fact a three-dimensional analogon of the Langmuir adsorption model. If N_1 and N_2 denote the numbers of guest and host molecules, respectively, and $M = \alpha N_2$ denotes the number of interstitial sites, this model gives the following lattice filling ratio:

$$\theta = \frac{N_1}{M} = \frac{\lambda_1 q_1}{1 + \lambda_1 q_1}, \tag{6.19}$$

where q_1 denotes the partition function of a free guest molecule and $\lambda_1 = \exp(-\epsilon_{L1}/k_B T)$ the Boltzmann factor of the absorption process; ϵ_{L1} denotes the energy[4] required to transfer a molecule 1 from the vacuum into the crystal lattice. The resulting Gibbs energy of the impure crystal is therefore

$$G_{\mathrm{m}}^{\mathrm{s}} = G_{\mathrm{m},2}^{\mathrm{s}} + x_1 \epsilon_{\mathrm{L1}} + RT(x_1 \ln x_1 + (\alpha x_2 - x_1)\ln(\alpha x_2 - x_1) - \alpha x_2 \ln(\alpha x_2)). \tag{6.20}$$

Evidently, the largest possible mole fraction of the guest component is $x_{1,\max}^{\mathrm{s}} = \alpha/(\alpha+1)$, e.g., $x_{1,\max}^{\mathrm{s}} = 0.5$ for $\alpha = 1$ (one interstitial site per host molecule). The second term in the equation above, the energetic contribution to the Gibbs energy, is a rather steep linear function, for ϵ_{L1} represents an interaction energy of the guest molecule with all host molecules lining its cavity. The size of the third term, the entropic contribution, is merely of the order of magnitude of RT. The resulting situation is depicted in Fig. 6.11:

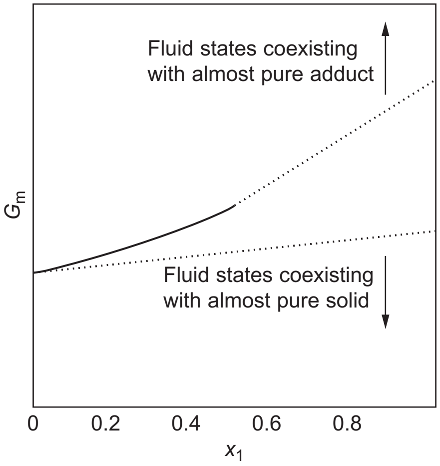

FIGURE 6.11 Molar Gibbs energy of a clathrate according to the van der Waals–Platteeuw model. ——: Eq. (6.20), for $\alpha = 1$ and $\epsilon_{\mathrm{L1}} = 5RT$, and ··········: tangent lines indicating the equilibrium with a fluid phase, for $x_1^{\mathrm{s}} = 0.001$ and 0.499.

---

[4] more accurately: the free energy; the entropic contribution, however, is often small.

- For all Gibbs energy values of the fluid below the lower dotted line, the solid equilibrium phase is an almost pure host phase. Eq. (6.20) gives infinite slopes at both ends of the G_m^s curve, so that the solid phase cannot be exactly pure, but the amount of component 1 dissolved in the host lattice is very small.
- For all Gibbs energies of the fluid above the upper dotted line, the solid equilibrium phase has almost all its vacancies occupied. It would appear to the experimentalist as an adduct phase with a stoichiometric composition, "compound $1 \cdot \alpha$ compound 2".
- Only in the narrow range between the two dotted lines, the composition of the solid would perceptibly change with the Gibbs energy or the pressure of the fluid phase.

Just as the van der Waals equation of state captures the essentials of fluid behavior qualitatively, but is not good for accurate quantitative work, the van der Waals–Platteeuw model gives a qualitative explanation of the behavior of clathrates, but not a good quantitative description. In practice, clathrate compounds may contain more than one cavity type, larger cavities may contain more than one guest molecule, and there may be interactions between guest molecules. Readers interested in these compounds will find several advanced models in the literature, which are better but also much more complicated.

6.4.3 Formation of Stoichiometric Compounds

Sometimes, two compounds can form a new compound that crystallizes in pure form (*cum granulo salis*) in a crystal phase of its own. Whether the new compound is formed by a chemical reaction, e.g.,

$$\mathrm{CaO} + \mathrm{CO_2} \rightleftharpoons \mathrm{CaCO_3},$$

or is merely an adduct, e.g.,

$$\mathrm{CaSO_4} + 2\,\mathrm{H_2O} \rightleftharpoons \mathrm{CaSO_4} \cdot 2\,\mathrm{H_2O},$$

is irrelevant. What matters is that there is a new compound with a well-defined, fixed composition.

This case is often found in connection with small, polar, or hydrogen-bonding molecules like water or hydrogen chloride, but sometimes larger molecules form adducts, too. A well-known example is tartaric acid, which has got two enantiomeric forms (and one meso diastereomer); the racemic mixture of the enantiomers has a crystal structure of its own.

The calculation of the phase equilibrium has to account for the chemical reaction equilibrium:

$$\sum_{i=1}^{N} \nu_i \mu_i = 0. \tag{6.21}$$

Here the ν_i are the *stoichiometric coefficients* for the chemical reaction (positive for products, negative for educts). For the calcination equilibrium mentioned above, we can assume that the two solid phases and the fluid phase are pure; therefore, the chemical potentials can be replaced by molar Gibbs energies, and the central equation becomes

$$G^{\mathsf{s}}_{\mathrm{m,CaCO_3}}(T) - G^{\mathsf{s}}_{\mathrm{m,CaO}}(T) - G^{\mathsf{f}}_{\mathrm{m,CO_2}}(p,T) = 0. \tag{6.22}$$

Here it has already been assumed that the Gibbs energies of the solid phases do not significantly depend on pressure.

The Gibbs energies of the solid phases are their absolute Gibbs energies, which can be found in thermodynamic tables. The Gibbs energy of the carbon dioxide is its standard Gibbs energy plus the Gibbs energy of compression from the standard pressure of the thermodynamic table to p.

Here a word of caution is in order: the reference state that appears in many thermodynamic equations of this book, $(p^{\ominus}, V^{\ominus}_{\mathrm{m}}, T)$, is in the ideal-gas regime: $V^{\ominus}_{\mathrm{m}}$ is so large that $p^{\ominus}V^{\ominus}_{\mathrm{m}} = RT$ holds. The reference state of thermochemical tables is the standard state, the most stable phase at the standard temperature T° (usually 298.15 K) and the standard pressure p° (usually 0.1 MPa). It is not necessarily an ideal gas. We denote its molar volume by V°_{m}.

The Gibbs energy balance then becomes

$$\begin{aligned} 0 &= G^{\mathsf{s}}_{\mathrm{m,CaCO_3}}(T) - G^{\mathsf{s}}_{\mathrm{m,CaO}}(T) - G^{\mathsf{f}}_{\mathrm{m,CO_2}}(p^{\circ},T) \\ &\quad - (G^{\mathsf{f}}_{\mathrm{m,CO_2}}(p,T) - G^{\mathsf{f}}_{\mathrm{m,CO_2}}(p^{\circ},T)) \\ &= \Delta_{\mathrm{r}}G^{\ominus}_{\mathrm{m}}(p^{\circ},T) - pV_{\mathrm{m}} + p^{\circ}V^{\circ}_{\mathrm{m}} - A^{\mathrm{r}}_{\mathrm{m,CO_2}}(V_{\mathrm{m}},T) + A^{\mathrm{r}}_{\mathrm{m,CO_2}}(V^{\circ}_{\mathrm{m}},T) \\ &\quad + RT\ln\frac{V_{\mathrm{m}}}{V^{\circ}_{\mathrm{m}}}. \end{aligned} \tag{6.23}$$

Here p and V_{m} refer to the fluid phase (carbon dioxide). $\Delta_{\mathrm{r}}G^{\ominus}_{\mathrm{m}}$ is the standard Gibbs energy of the reaction. Eq. (6.23) is a nonlinear equation with one variable, p, which can be solved with one of the methods listed in the appendix.

If the fluid phase is an ideal gas, the residual Helmholtz energy terms can be neglected, and Eq. (6.23) turns into

$$RT\ln\frac{p}{p^{\circ}} = \Delta_{\mathrm{r}}G^{\ominus}_{\mathrm{m}}. \tag{6.24}$$

Fig. 6.12 shows the carbon dioxide equilibrium pressure of the calcination equilibrium, computed with Eq. (6.23) and a reference equation of state for the gas phase [87].

It must be pointed out that this is a rather simple case. In general, the solid compounds might dissolve in the fluid phase. Eq. (6.21) is still valid in such a case, but then more complicated expressions for the chemical potentials are required.

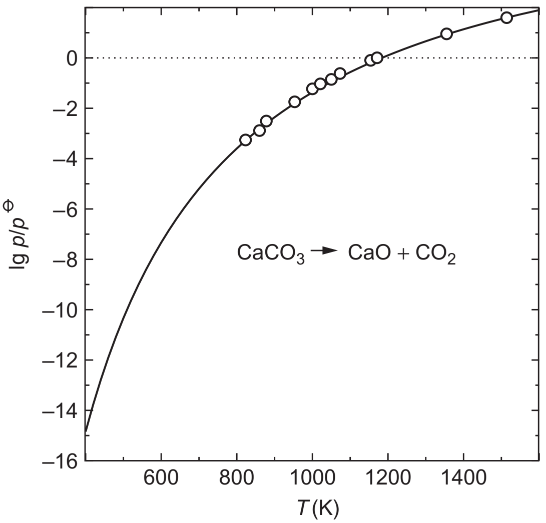

FIGURE 6.12 Carbon dioxide equilibrium pressure of the calcination reaction. —— calculated with Eq. (6.23), ·········: reference pressure, and ○: experimental data.

The standard Gibbs energies of reaction depend on the temperature. Some thermodynamic tables list the $\Delta_r G_m^{\ominus}$ directly or even give interpolation functions. Other tables list standard enthalpies and entropies only and expect the user to perform the integrations by means of Kirchhoff's laws:

$$
\begin{aligned}
H_m(T) &= H_m(T^\circ) + \int_{T^\circ}^{T} C_{pm}(T)\,\mathrm{d}T \\
S_m(T) &= S_m(T^\circ) + \int_{T^\circ}^{T} \frac{C_{pm}(T)}{T}\,\mathrm{d}T.
\end{aligned}
\tag{6.25}
$$

The isobaric heat capacity, $C_{pm}(T)$, usually varies slowly with temperature. Experimental values can be interpolated with low-order polynomials or cubic spline functions.

6.5 PROBLEMS

1. A solid has the sublimation pressure p^{sg}. The space above the solid is filled with an inert gas at pressure $p_1 > p_2^{sg}$. At this pressure, the gas phase is adequately described by the ideal-gas law. The solid can be considered incompressible. Does the presence of the gas affect the partial pressure of component 2?

2. Consider the formation of gypsum from gypsum hemihydrate,

$$\mathrm{CaSO_4 \cdot 0.5\,H_2O + 1.5\,H_2O \rightleftharpoons CaSO_4 \cdot 2\,H_2O}$$

at 25°C. Calculate the equilibrium pressure of water in the vapor phase (molar Gibbs energies at 0.1 MPa, $\mathrm{CaSO_4 \cdot 2\,H_2O}$: −2080.5 kJ/mol, $\mathrm{CaSO_4 \cdot 0.5\,H_2O}$: −1615.6 kJ/mol, water: $\mathrm{H_2O}$: −306.69 kJ/mol; vapor pressure of pure water: 3.17 kPa; the vapor phase can be treated as an ideal gas).

3. Construct *px* cross sections for phase diagram Fig. 6.10 at temperatures slightly below and above quadruple point Q_1.

Chapter 7

Equations of State for Pure Fluids

In the previous chapters, we have discussed fluid phase behavior qualitatively and then shown how phase boundaries are related to thermodynamic functions like the Helmholtz energy function, $A_\mathrm{m}(V_\mathrm{m}, T, \vec{x})$, or the Gibbs energy function, $G_\mathrm{m}(p, T, \vec{x})$, which in turn are related to the equation of state, $p(V_\mathrm{m}, T, \vec{x})$. But until now we did not say what this function actually is.

In this chapter, we will describe some equations of state that have been found useful for the calculation of fluid phase equilibria. We will first treat equations of state for pure fluids and then, in the next chapter, their generalization to mixtures.

7.1 FUNDAMENTALS

As shown in the previous chapters, the criteria of phase equilibrium and phase stability can be conveniently formulated with the Helmholtz energy function, $A_\mathrm{m}(V_\mathrm{m}, T, \vec{x})$. This function is also called the fundamental equation of a fluid.

A_m is not directly measurable but can be obtained from the experimentally accessible pressure function, $p(V_\mathrm{m}, T, \vec{x})$, which is called the equation of state for historical reasons. More accurately, this function is called the *thermal* equation of state, in contrast to the *caloric* equation of state, $U_\mathrm{m}(V_\mathrm{m}, T, \vec{x})$. The latter function, however, is rarely used.

In this chapter, we will consider thermal equations of state for pure substances, i.e., the function $p(V_\mathrm{m}, T)$, and its associated fundamental equations, $A_\mathrm{m}(V_\mathrm{m}, T)$. These two functions are related by

$$\begin{aligned} p(V_\mathrm{m}, T) &= -\left(\frac{\partial A_\mathrm{m}(V_\mathrm{m}, T)}{\partial V_\mathrm{m}}\right)_T \\ A_\mathrm{m}(V_\mathrm{m}, T) &= A_\mathrm{m}(V_\mathrm{m}^{\ominus}, T) - \int_{V_\mathrm{m}^{\ominus}}^{V_\mathrm{m}} p(V_\mathrm{m}, T)\,\mathrm{d}V_\mathrm{m}. \end{aligned} \tag{7.1}$$

High-Pressure Fluid Phase Equilibria. DOI: 10.1016/B978-0-444-56347-7.00007-4

7.2 THE IDEAL GAS

Thermal equations of state go back to the compression and expansion experiments of Boyle and Mariotte at the end of the 17th Century, which can be summarized as

$$p \propto \frac{1}{V}, \tag{7.2}$$

on condition that the amount of substance and the temperature are constant. About a 100 years later, Charles, Amontons, and Gay-Lussac discovered the relations

$$V \propto T \tag{7.3}$$

at constant pressure and amount of substance and

$$p \propto T \tag{7.4}$$

at constant volume and amount of substance. The combination of these empirical results gives the ideal-gas law, which is historically the first equation of state:

$$pV = nRT \tag{7.5}$$

or

$$pV_{\mathrm{m}} = RT. \tag{7.6}$$

Here $R = 8.314472\ \mathrm{J\ K^{-1}\ mol^{-1}}$ denotes the universal gas constant.

Later, with the development of quantum mechanics and statistical thermodynamics, it became possible to derive the ideal-gas law from first principles. This gave an insight into various assumptions and approximations limiting its applicability. Ideal behavior results if the gas molecules do not interact with each other; in particular, this means

- the absence of attractive forces between the molecules,
- an infinitesimally small size of the molecules,
- and no quantum mechanical restrictions with regard to wave-function symmetry or the number of accessible states.

This explains why the ideal-gas law is valid for gases at low pressures (large molar volumes) only, for only under this condition the average distances between the molecules are so large that the interactions become negligible. Conversely, each gas can be made to behave like an ideal gas if it is expanded sufficiently. Therefore, the ideal-gas law is the limiting law for all equations of state:

$$\lim_{V_{\mathrm{m}} \to \infty} p(V_{\mathrm{m}}, T)V_{\mathrm{m}} = RT. \tag{7.7}$$

It should be noted that this equation describes the high-volume/low-pressure limiting behavior. *The analogous relation for the high-temperature limit is not true: a gas does not necessarily conform to the ideal-gas law if it is heated to high temperatures at constant density.*

Another consequence of the conditions of the ideal-gas law is that it does not predict fluid-phase equilibria.

7.3 THE VIRIAL EQUATION OF STATE

The virial equation of state was probably proposed first by Thiesen in 1885 [88] and intensively studied by Kamerlingh Onnes at the beginning of the previous century as an empirical extension of the ideal-gas law. It is a series expansion of the compression factor either with respect to pressure,

$$Z = 1 + B_2' + B_3' p^2 + B_4' p^3 + \cdots, \tag{7.8}$$

or with respect to molar volume,

$$Z = 1 + \frac{B_2}{V_\mathrm{m}} + \frac{B_3}{V_\mathrm{m}^2} + \frac{B_4}{V_\mathrm{m}^3} + \cdots. \tag{7.9}$$

The virial coefficients B_i' of the pressure series can be computed from those of the volume series, B_i, and vice versa.

The virial coefficients depend on temperature. Experimental data for the second virial coefficient have been tabulated for many substances. Experimental data for $B_3(T)$ and higher virial coefficients, however, are rather scarce.

A truncated virial equation of state containing the B_2 and the B_3 terms only is theoretically able to represent van der Waals loops. But such an equation would describe the pVT behavior of liquids and dense gases rather badly. In fact, the mathematical structure of the volume-based virial equation, a polynomial in V_m^{-1}, is not well adapted to the behavior of real fluids, which show a strong divergence of the pressure at high densities. Unless a rather large number of terms is used, the virial equation of state is not useful for phase equilibrium calculations.

Still, virial coefficients play an important role in the theory of equations of state. It can be shown that the virial coefficient B_i is related to i-body interactions in a fluid and can, in principle, be calculated from statistical thermodynamics.

7.4 CUBIC EQUATIONS OF STATE

7.4.1 The van der Waals Equation of State

A major step in the development of equations of state was accomplished by van der Waals in 1873 [89, 90]. His equation of state accounts for interactions between molecules:

$$p = \underbrace{\frac{RT}{V_m - b}}_{p_{rep}} - \underbrace{\frac{a}{V_m^2}}_{p_{att}} . \tag{7.10}$$

The equation consists of a repulsion term, p_{rep}, which (approximately) reflects the decrease of the accessible volume by the volume occupied by the molecules, and an attraction term, p_{att}, which describes the decrease of the pressure because of attractive forces acting between the molecules. It contains two parameters, the attraction parameter a and the so-called covolume parameter b.

This equation of state was the first one that could be used for the calculation of vapor–liquid phase equilibria of pure fluids. It generates a qualitatively correct vapor–liquid coexistence curve that terminates in a critical point. In the two-phase region, the isotherms of this equation of state pass through one minimum on the liquid side and one maximum on the vapor side. This back-and-forth movement is called a van der Waals loop (cf. Fig. 5.6).

While the development of the van der Waals equation was historically a milestone for the modelling of fluid-phase equilibria, this equation is not very accurate. It can be used for general discussions of features of fluids, but it should not be used for accurate phase-diagram calculations. One indicator of its insufficiency is the critical compression factor $Z_c = p_c V_{mc}/RT_c$, which has the value 0.375 for this equation of state, whereas the experimental values typically fall below 0.3 for most substances. Therefore, many empirical and theoretical improvements were proposed afterwards.

Multiplying the van der Waals equation, Eq. (7.10), with its denominator expressions and rearrangement leads to a cubic polynomial in V_m,

$$pV_m^3 + (-pb - RT)V_m^2 + aV_m - ab = 0 \tag{7.11}$$

(see also Section C.1). Because of this transformability into a cubic polynomial, the van der Waals equation is called a *cubic equation of state*; in fact, it is the first and simplest member of a large class of equations of state having this characteristic.

The van der Waals equation and cubic equations of state in general have several desirable properties:

- A polynomial degree of at least 3 is necessary for the formation of van der Waals loops. Cubic equations are, therefore, the simplest equations that can be used for fluid-phase equilibrium calculations.
- With a polynomial degree of 3, only one van der Waals loop can occur (one maximum–minimum pair along a $p(V)$ isotherm); classical spinodals can be clearly defined, and there are no spurious metastable states within the unstable portion of an isotherm.

- The calculation of molar volumes for given pressure and temperature is an algebraic problem for which reliable and fast algorithms exist (see Appendix A.5) If there is more than one real solution (no more than three can exist), the solution with the smallest molar volume is usually considered to belong to a liquid phase, the solution with the largest molar volume to a vapor phase, and the intermediate solution to an unstable state.

  This identification is strictly correct for the van der Waals equation only!

Due to these mathematical characteristics, their simplicity, and their low computer-time requirements, cubic equations of state are frequently used for phase equilibrium calculations.

However, one must not confuse ease of use with correctness. Cubic equations of state have been proven to give physically meaningless results for some caloric and phase diagram properties at very high pressures [91, 92].

The quantitative inadequacy of the van der Waals equation led to the empirical development of other equations of state that still preserve the "cubic quality," but agree better with experimental data. In these equations, typically the attraction term is varied, whereas the van der Waals repulsion term is maintained.

7.4.2 The Redlich–Kwong Equation

In 1949, Redlich and Kwong published a very successful improvement of the van der Waals equation [93], where the attraction term had been modified in two ways: First, Redlich and Kwong found from an analysis of experimental data that the attraction term had a temperature dependence that could be represented approximately by a power law with an exponent close to –0.5. The second change in the attraction term concerned its dependence on the molar volume and led to a lower critical compression factor. The resulting Redlich–Kwong equation of state is given by

$$p=\frac{RT}{V_\mathrm{m}-b}-\frac{a}{\sqrt{T}V_\mathrm{m}(V_\mathrm{m}-b)} \tag{7.12}$$

(see also Section C.2).

The critical compression factor Z_c is 1/3 for this equation of state, which is still somewhat too high for most substances, but much closer to the typical experimental range than the Z_c of the van der Waals equation of state.

It should be noted that, at very high pressures, the calculation of molar volumes for given pressures can produce unphysical values that are smaller than the covolume parameter [94].

7.4.3 The Redlich–Kwong–Soave Equation

In 1972, Soave created a variant of the Redlich–Kwong equation with an improved empirical temperature dependence [95]:

$$p=\frac{RT}{V_\mathrm{m}-b}-\frac{a_\mathrm{c}\alpha(T)}{V_\mathrm{m}(V_\mathrm{m}-b)}$$
$$\text{with } \alpha(T)=\left(1+m\left(1-\sqrt{\frac{T}{T_\mathrm{c}}}\right)\right)^2. \tag{7.13}$$

a_c is the value of the attraction parameter at the critical temperature; evidently, $\alpha(T_\mathrm{c})=1$. The temperature function $\alpha(T)$ is shown in Fig. 7.4. The parameter m is related to Pitzer's acentric factor ω [96, 97]:

$$m=0.480+1.574\omega-0.176\omega^2. \tag{7.14}$$

The acentric factor relates the vapor pressure of a fluid at a reduced temperature $\tilde{T}=T/T_\mathrm{c}=0.7$ to its critical pressure:

$$\omega=\lg\frac{p_\mathrm{c}}{p^\sigma(\tilde{T}=0.7)}-1. \tag{7.15}$$

ω has been tabulated for many substances [98]; the value for argon is approximately zero.

Although the choice of the reference fluid is arbitrary, the acentric factor is often understood as a measure of the deviation of the molecular shape from a sphere.

Soave's temperature function significantly improves the prediction of vapor pressure curves, which is not surprising, because the ω parameter is directly related to vapor pressures. At very high temperatures, however, it can cause unphysical results (cf. Fig. 7.4).

7.4.4 The Peng–Robinson Equation

Another famous cubic equation of state was proposed in 1976 by Peng and Robinson [99]. The temperature dependence of its attractive term is similar to that of Soave, but its density dependence is slightly different:

$$p=\frac{RT}{V_\mathrm{m}-b}-\frac{a(T)}{V_\mathrm{m}(V_\mathrm{m}+b)+b(V_\mathrm{m}-b)}$$
$$a(T)=a_\mathrm{c}\left(1+\kappa\left(1-\sqrt{\frac{T}{T_\mathrm{c}}}\right)\right)^2 \tag{7.16}$$
$$\kappa=0.37464+1.54226\omega+0.26992\omega^2.$$

In spite of its simplicity, this equation has been found to give remarkably good results especially for alkanes and other nonpolar compounds.

7.4.5 Generalized Cubic Equations of State

Between 1970 and 2000, many more cubic equations of state were published, which can be summarized as

$$p = \frac{RT}{V_\mathrm{m} - b} - \frac{a_\mathrm{c}\alpha(T)}{V_\mathrm{m}^2 + c_1 V_\mathrm{m} + c_0}. \tag{7.17}$$

This equation is called a generalized cubic equation of state. Evidently, for $c_0 = c_1 = 0$ and $\alpha(T) = \text{constant}$, the van der Waals equation is recovered. Other choices for the c_i give the Redlich–Kwong or the Peng–Robinson equation. Optimal choices for the c_i and $\alpha(T)$ have been published for many classes of chemical compounds; the reader is referred to the original literature.

In order to correct the notoriously bad representation of liquid molar volumes, Martin [100] and Péneloux *et al.* [101] introduced the concept of "volume translation": an equation of state in which V_m is replaced by $V_\mathrm{m} + \Delta V_\mathrm{m}$ has the same vapor pressure curve (ΔV_m cancels in Maxwell's criterion, Eq. (5.28), but evidently the orthobaric volumes are shifted by ΔV_m). If ΔV_m is made temperature dependent, simultaneously a good representation of liquid densities and critical compression factors should be possible; this, however, is seldom attempted. In fact, for such an approach, caution is advised, because it is known that a temperature-dependent volume translation or covolume can lead to isotherm crossing at high densities [91, 102, 103].

A modern equation of state using this feature is the "volume-translated Peng–Robinson equation" by Ahlers and Gmehling [104]. At this point, it should be mentioned that some modern equations of state are coupled with group contribution methods that allow the user to derive the substance-dependent parameters from the chemical constitution.

By a suitable redefinition of its constants, a volume-translated cubic equation of state can always be turned into a generalized cubic equation of state.

As mentioned above, these equations can be inverted by finding the roots of a cubic polynomial. If there are three real roots, it is generally *not* safe to assume that the root with the smallest molar volume represents a liquid state; it may belong to an unphysical state with a density beyond the dense-packing limit or even with a negative density. *For most cubic equations of state except the van der Waals equation, it is important to implement appropriate tests in the computer programs.*

7.5 EQUATIONS OF STATE BASED ON MOLECULAR THEORY

Van der Waals already used microscopic considerations for the development of his equation of state, such as the ideas of a molecular volume (covolume) leading to a repulsive contribution and of attraction forces acting between molecules. However, his approach was intuitive rather than fundamental, because at his time statistical mechanics had not progressed far enough.

Equations of state based on molecular theory start from well-defined molecular interaction potentials and use statistical thermodynamics to generate the required thermodynamic functions. Here we will summarize some of the modern concepts very shortly.

Fluids are homogeneous in the sense that, in absence of external fields, at any location the average number of molecules (time average) in a volume element $\mathrm{d}V$ is $\mathrm{d}\mathcal{N} = \hat{\rho}\,\mathrm{d}V$, where $\hat{\rho} = \mathcal{N}/V$ is the overall number density[1]. This does not mean, however, that fluids have no structure: in dense fluids, molecules form "coordination shells" around each other and thus develop a kind of local order. The deviation of the local density from the overall value is then described with a correction factor, the radial distribution function $g(r)$. For a system consisting of spherical molecules, the number of molecules found on average in a spherical shell of thickness $\mathrm{d}r$ at the distance r from a given molecule is

$$\mathrm{d}\mathcal{N} = 4\pi r^2 \hat{\rho} g(r)\mathrm{d}r\,. \tag{7.18}$$

$g(r)$ is sketched in Fig. 7.1. It is 0 at close distance, because molecules cannot overlap, and it is 1 at long distances, because there the molecules do not "feel" the influence of the given molecule. At intermediate distances, however, maxima and minima indicate the formation of coordination shells.

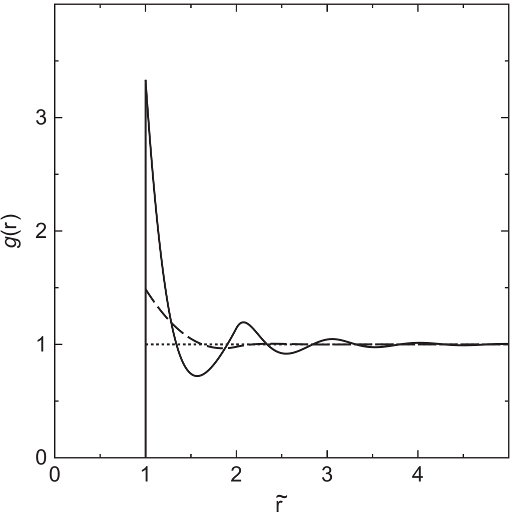

FIGURE 7.1 Radial distribution function $g(\tilde{r})$ of hard spheres ($\tilde{r} = r/\sigma$: reduced distance). ⋯⋯: reduced density $\xi = 0$, – – : $\xi = 0.15$, and ——: $\xi = 0.4$.

---

[1] not to be confused with the molar density $\rho = V_\mathrm{m}^{-1} = \hat{\rho}/N_\mathrm{A}$

The radial distribution function also depends on density and temperature: the extrema become more pronounced with increasing density or lower temperature. For low densities, the radial distribution function converges against the Boltzmann factor of the pair potential:

$$\lim_{\hat{\rho}\to 0} g(r) = \exp\left(-\frac{u(r)}{k_{\mathrm{B}}T}\right). \tag{7.19}$$

Here $u(r)$ represents the pair potential function, i.e., the energy of a pair of molecules separated by the distance r, with $u(\infty)=0$.

The calculation of the radial distribution function is complicated and cannot be treated here. Fortunately, for many applications, it is not necessary to know $g(r)$ explicitly or over the whole range of distances. We give here, without further proofs, some relations between the radial distribution function and some thermodynamic functions:

- the energy equation, i.e., the contribution of intermolecular interactions to the configurational internal energy:

$$U_{\mathrm{conf}} = 2\pi\,\hat{\rho}\mathcal{N}\int_0^\infty g(r)u(r)r^2\,\mathrm{d}r. \tag{7.20}$$

- the pressure equation:

$$Z = 1 - \frac{2\pi}{3}\frac{\hat{\rho}}{k_{\mathrm{B}}T}\int_0^\infty g(r)\frac{\mathrm{d}u(r)}{\mathrm{d}r}r^3\,\mathrm{d}r. \tag{7.21}$$

  The integral represents the so-called virial, a statistical average of the product of intermolecular force, $\mathrm{d}u(r)/\mathrm{d}r$, and intermolecular distance, r.
- the compressibility equation:

$$\hat{\rho}k_{\mathrm{B}}T\kappa_T = 1 + 4\pi\,\hat{\rho}\int_0^\infty (g(r)-1)r^2\,\mathrm{d}r. \tag{7.22}$$

For the energy and the pressure equation, it is assumed that the intermolecular interactions are pairwise additive, whereas the compressibility equation can be used even for nonadditive interaction potentials. All three equations are written here for spherical molecules; for nonspherical molecules, additional integrations over orientation angles must be performed.

Substituting Eq. (7.19) into Eq. (7.22) and comparing the result with the virial series, Eq. (7.9), leads to an expression for the second virial coefficient (again assuming that the pair potential has no angle dependence):

$$B_2(T) = -2\pi \int_0^\infty \left[\exp\left(-\frac{u(r)}{k_B T}\right) - 1\right] r^2\,\mathrm{d}r. \tag{7.23}$$

As mentioned above, the higher virial coefficients B_3, B_4, … represent three-, four-, …-body interactions. These can be approximately broken down into combinations of two-body interactions by means of the superposition approximation. So the third virial coefficient contains three terms stemming from three two-body interactions that are possible between three particles. But there is also a contribution that vanishes if one of the three particles is removed, the so-called three-body term. This latter contribution, however, is often neglected or approximated with an Axilrod–Teller term [105]. In the end, the calculation of higher order virial coefficients amounts to the evaluation of multidimensional integrals over Boltzmann factors of the interaction potentials [106].

7.5.1 Hard-Sphere Equations of State

A simple but important interaction potential is the hard-sphere potential: two hard spheres do not interact if their distance is larger than their diameter; but if their distance is smaller than their diameter, the potential energy becomes infinite, which means that the spheres cannot penetrate (Fig. 7.2):

$$u(r) = \begin{cases} \infty & r < \sigma \\ 0 & r \geq \sigma \end{cases}. \tag{7.24}$$

The radial distribution function of the hard-sphere fluid is shown in Fig. 7.1. As the pair potential is either zero or infinite, the zero-density limit of $g(r)$ is simply a step function. At higher densities, a peak forms at $r = \sigma$. It should be noted that this peak is not caused by attraction forces (which do not exist for this model) but entirely by geometric effects.

These effects exist in all real fluids, regardless of their temperatures or intermolecular attraction. Therefore, the hard-sphere fluid is a popular and important reference system.

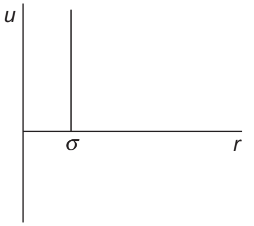

FIGURE 7.2 Interaction potential of hard spheres.

The equation of state of the hard-sphere fluid can be derived from the virial expansion. For the second, third, and fourth virial coefficients of the hard-sphere fluid, analytical solutions are available, whereas the higher order coefficients were calculated by numerical methods [107, 108]. Inserting these coefficients into the virial expansion gives

$$\begin{aligned}Z = 1 + \frac{b}{V_\mathrm{m}} + \frac{5}{8}\left(\frac{b}{V_\mathrm{m}}\right)^2 + 0.28695\left(\frac{b}{V_\mathrm{m}}\right)^3 + 0.1103\left(\frac{b}{V_\mathrm{m}}\right)^4 \\ + 0.0386\left(\frac{b}{V_\mathrm{m}}\right)^5 + \cdots,\end{aligned} \tag{7.25}$$

where $b = (2\pi/3)N_\mathrm{A}\sigma^3$ is the van der Waals covolume parameter.

For further manipulations of this equation, it is convenient to introduce the packing fraction $\xi = b/(4V_\mathrm{m}) = (\pi/6)N_\mathrm{A}\sigma^3/V_\mathrm{m}$, which leads to

$$Z = 1 + 4\xi + 10\xi^2 + 18.3648\xi^3 + 28.2368\xi^4 + 39.5264\xi^5 + \cdots. \tag{7.26}$$

Carnahan and Starling [109] realized that the coefficients of the series are close to integer numbers, and that their values can be represented by $n^2 + n - 2$. This allows to summate the series:

$$Z = 1 + \sum_{n=2}(n^2 + n - 2)\xi^{n-1} = 1 + \sum_{n=0}(n^2 + 3n)\xi^n. \tag{7.27}$$

With the assumption that the general expression for the virial coefficients is valid for arbitrary n, the sum can be transformed into

$$Z = \frac{1 + \xi + \xi^2 - \xi^3}{(1 - \xi)^3}. \tag{7.28}$$

This is the well-known Carnahan–Starling equation of state for the hard-sphere fluid. It represents the properties of the hard-sphere fluid quite well up to liquid-like densities of about $\xi = 0.5$.

For higher densities, this equation shows deviations from Monte Carlo simulations. These are related to the increasingly inaccurate description of the higher virial coefficients by Eq. (7.27). In particular, the inadequate treatment of their limiting behaviour is the reason why the Carnahan–Starling equation of state diverges at $\xi \to 1$ and not at the close-packing limit of $\xi = 0.74$ or the random-close-packing limit of about $\xi = 0.69$.

The comparison of the virial series of the Carnahan–Starling equation,

$$Z_\mathrm{CS} = 1 + 4\xi + 10\xi^2 + 18\xi^3 + 28\xi^4 + 40\xi^5 + \cdots, \tag{7.29}$$

and the repulsion term of the van der Waals equation of state,

$$Z_\mathrm{vdW,rep} = 1 + 4\xi + 16\xi^2 + 64\xi^3 + 256\xi^4 + 1024\xi^5 + \cdots, \tag{7.30}$$

shows that already the third virial coefficient of the van der Waals equation is far off the mark. Therefore, a logical improvement of the van der Waals equation of state is the replacement of the repulsion term by the Carnahan–Starling term, leading to the Carnahan–Starling–van der Waals (CSvdW) equation of state:

$$p = \frac{RT}{V_\mathrm{m}} \frac{1+\xi+\xi^2-\xi^3}{(1-\xi)^3} - \frac{a}{V_\mathrm{m}^2}. \tag{7.31}$$

There are various other hard-sphere equations of state, derived by different statistical-mechanics methods, of which some are even more accurate [110]. Still, the Carnahan–Starling equation is the most widely used equation of state for the hard-sphere fluid, probably for esthetic reasons.

It can be shown that the ratio of two subsequent virial coefficients is related to the location of the pole of the hard-sphere equation of state [111]:

$$\xi_\mathrm{max} = \lim_{i\to\infty} \frac{B_i}{B_{i+1}}. \tag{7.32}$$

By taking the first virial coefficient from the hard-sphere series but calculating the higher ones from $B_{i+1} = B_i/\xi_\mathrm{max}$, it is possible to create equations of state that combine a correct behavior at low densities with a physically reasonable behavior at very high densities. An example is given as follows:

$$Z = \frac{3+5\xi+6\xi^2}{(1-\xi)(3-4\xi)}, \tag{7.33}$$

which evidently has $\xi_\mathrm{max} = 0.75$, close to the close-packing limit [112].

7.5.2 Attraction Terms

Like the repulsion term, the attraction term of the van der Waals equation is merely a first approximation and can be improved. An inspection of Eq. (7.21) in connection with Eq. (7.19) shows that the long-distance part of the integral must give a temperature-dependent contribution to the pressure, at least at low densities. The van der Waals equation with its temperature-independent attraction term, a/V_m^2, is compatible with Eq. (7.21) only if an attractive pair potential of infinite range, but infinitesimal strength is assumed: for such a pair potential, the internal energy of a fluid would not depend on the configuration. This, however, is not a good approximation for the molecules of this universe.

A more realistic model potential, which is similar to the hard-sphere potential in the sense that it has discrete sections, is the square-well potential (Fig. 7.3). The attraction is described by a constant negative energy value $-\epsilon$ in the range from the contact of two particles at the diameter σ to a $\lambda\sigma$. Beyond

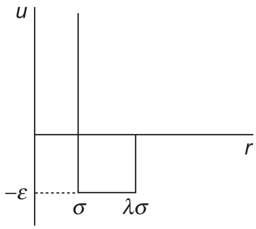

FIGURE 7.3 Interaction potential of the square-well fluid.

this distance, the interaction between the two particles is zero:

$$u(r) = \begin{cases} \infty & r < \sigma \\ -\epsilon & \sigma \le r < \lambda\sigma \, . \\ 0 & r \ge \lambda\sigma \end{cases} \tag{7.34}$$

A typical value for λ is 1.5. It is possible to derive an analytic expression for the second virial coefficient of the square-well potential from Eq. (7.23):

$$B_2 = b\left[1 - (\lambda^3 - 1)\left(\exp\left(\frac{T^*}{T}\right) - 1\right)\right]. \tag{7.35}$$

Here $T^* = \epsilon / k_\mathrm{B}$ is the characteristic temperature. The first term is again the (positive) hard-sphere second virial coefficient, whereas the second term is the (negative) contribution of the attractive well. Inserting Eq. 7.35 into the truncated virial series

$$p = \frac{RT}{V_\mathrm{m}}\left(1 + \frac{B_2}{V_\mathrm{m}}\right) \tag{7.36}$$

gives

$$p = \frac{RT}{V_\mathrm{m}} + \frac{RTb}{V_\mathrm{m}^2} - \frac{(\lambda^3 - 1)RTb}{V_\mathrm{m}^2}\left(\exp\left(\frac{T^*}{T}\right) - 1\right). \tag{7.37}$$

This exponential temperature dependence of the attraction is present in several equations of state. In the limit of high temperatures, this attraction term approaches the van der Waals attraction term $p_\mathrm{att} \rightarrow (\lambda^3 - 1)RT^* b / V_\mathrm{m}^2 \propto a / V_\mathrm{m}^2$. This behavior suggests that a physically sound temperature dependence of an attraction term is monotonically decreasing toward a nonzero, positive limiting value at high temperatures. In Fig. 7.4, the exponential temperature dependence is plotted and compared to some empirical temperature functions used in cubic equations of state such as the Peng–Robinson or Soave–Redlich–Kwong equations (PR), the Redlich–Kwong equation (RK), and the van der Waals equation

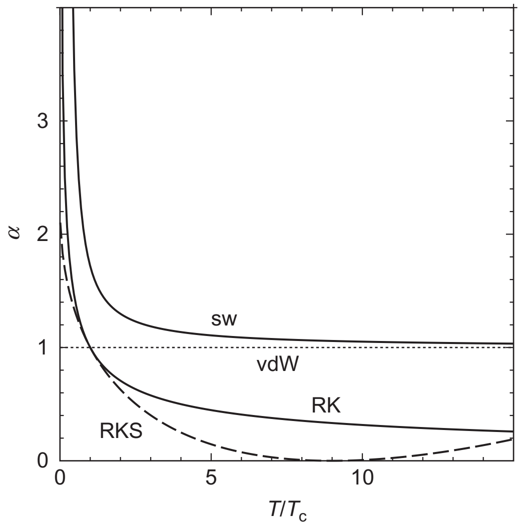

FIGURE 7.4 Temperature dependence of the attraction term. RKS: Peng–Robinson or Redlich–Kwong–Soave, RK: Redlich–Kwong, sw: square well, and vdw: van der Waals.

(vdW). The square-root dependence of the Redlich–Kwong equation of state is monotonically decreasing, but the limiting value at high temperature is zero. The Soave temperature function used in many cubic equations of state exhibits a minimum at around $9T_c$. Above that temperature, the function increases again; this behavior is not physically justified and can, in principle, lead to artifacts. Of course, for most substances, $9T_c$ is an unrealistically high temperature. But for hydrogen or neon, this corresponds to normal handling conditions. Therefore, such cubic equations of state should be used for light gases with caution.

7.5.3 Perturbed-Hard-Chain Theories

The translational partition function of an ideal gas consisting of $\mathcal{N}$ molecules can be written as

$$Q^{\mathrm{id}} = \frac{1}{\mathcal{N}!}\left(\frac{V}{\Lambda^3}\right)^{\mathcal{N}} q_{\mathrm{int}}^{\mathcal{N}}, \tag{7.38}$$

where Λ is the thermal de Broglie wavelength and q_{int} is the molecular partition function pertaining to the internal degrees of freedom, e.g., rotation and vibration. q_{int} does not depend on density, and therefore, this term does not contribute to the equation of state.

In order to proceed from here to the partition function of a real gas, the following modifications have to be made:

- Because of intermolecular repulsion (the molecules have a finite volume), the volume has to be replaced by the free volume.
- Intermolecular attraction has to be represented by a density-dependent Boltzmann factor.
- At higher densities, rotations and vibrations are hindered, which makes a density-dependent correction to q_{int} necessary.

In the perturbed-hard-chain theory, the density-dependent contributions to q_{int} are treated as additional translational degrees of freedom:

$$Q=\frac{1}{\mathcal{N}!}\left(\frac{V_{\text{f}}}{\Lambda^3}\right)^{\mathcal{N}c} q_{\text{int}}^{\mathcal{N}} \exp\left(-\frac{\langle U_{\text{att}}(V)\rangle}{RT}\right), \tag{7.39}$$

Here c is an empirical correction factor to the number of the translational degrees of freedom; for spherical molecules it is $c=1$. For the energetic term, a plausible assumption has to be made.

The free volume is related to repulsive interactions. For a fluid without energetic interactions, having the same internal degrees of freedom as a reference ideal gas, the partition function is

$$Q=\frac{1}{\mathcal{N}!}\left(\frac{V_{\text{f}}}{\Lambda^3}\right)^{\mathcal{N}} q_{\text{int}}^{\mathcal{N}}. \tag{7.40}$$

Dividing by the expression for an ideal gas, Eq. (7.38), and computing the logarithm yields

$$\ln\frac{Q}{Q^{\text{id}}}=\mathcal{N}\ln\left(\frac{V_{\text{f}}}{V}\right)=\frac{A}{k_{\text{B}}T}-\frac{A^{\text{id}}}{k_{\text{B}}T}=\frac{A^{\text{r}}}{k_{\text{B}}T}. \tag{7.41}$$

A^{r}, the residual Helmholtz energy, can be calculated from a repulsive equation of state. If the Carnahan–Starling equation for hard spheres, Eq. (7.28), is used, the free volume is

$$V_{\text{f}}=V\exp\left(-\frac{4\xi-3\xi^2}{(1-\xi)^2}\right). \tag{7.42}$$

This is the free volume term that perturbed-hard-chain theories use.

An important example for this class of equations is the "simplified perturbed-hard-chain equation of state" (SPHCT) [113]. The attractive term combines features of the Redlich–Kwong equation and the theory of square-well molecules (cf. Section C.6):

$$
\begin{aligned}
Z &= 1 + c\frac{4\xi - 2\xi^2}{(1-\xi)^3} - \frac{18c\xi f}{1+\xi f} \\
\text{with } f &= \frac{1}{\tau}\left(\exp\left(\frac{1}{2\tilde{T}}\right) - 1\right) \\
\text{and } \tau &= \frac{\pi}{6}\sqrt{2}, \quad \tilde{T} = \frac{k_\mathrm{B} T}{\epsilon}.
\end{aligned}
\tag{7.43}
$$

A more complicated member of this family is

$$
Z = 1 + cc_0\frac{4\xi - 2\xi^2}{(1-\xi)^3} - \frac{6}{\pi\sqrt{2}}\frac{\xi}{c\tilde{T}} I_1(\xi, \tilde{T}, c),
\tag{7.44}
$$

where I_1 is a polynomial expansion [80, 81]. This equation of state is one of a few equations that can match the Z_c of real fluids.

Today, the perturbed-hard-chain theory has been superseded by the statistical associating fluid theory (see Section 7.5.4.5).

7.5.4 Perturbation Theories

There are many theory-derived and molecular-based equations of state which cannot all be described here. The interested reader is referred to recent reviews, e.g., the book of Sengers *et al.* [114], or the textbook of Gray and Gubbins [115]. Here we summarize some approaches that have become popular in recent decades.

Thermodynamic perturbation theory goes back to Pople [116, 117] and was later extended to the modelling of various fluids such as dipolar or quadrupolar fluids, ionic fluids, or softly repulsive fluids. Perturbation theory can be regarded as an expansion, in a sense similar to a Taylor expansion, around the properties of a well-investigated reference fluid.

The general idea is to write the internal energy of the system as a sum of the internal energy of the reference fluid and a "perturbation term":

$$
U(\lambda) = U_0 + \lambda U_1.
\tag{7.45}
$$

λ is the so-called coupling parameter: $\lambda = 0$ lets Eq. (7.45) return the properties of the reference system, and $\lambda = 1$ of the system with the full energy function.

The standard statistical thermodynamic expression for the residual Helmholtz energy is

$$
A^\mathrm{r} = -k_\mathrm{B} T \ln Q_\mathrm{C},
\tag{7.46}
$$

where Q_C is the configuration integral of an $\mathcal{N}$-particle system,

$$
Q_\mathrm{C} = V^{-\mathcal{N}} \int \exp\left(-\frac{U(\vec{r}^{\mathcal{N}}, \Omega^{\mathcal{N}})}{k_\mathrm{B} T}\right) \mathrm{d}\Omega^{\mathcal{N}}\, \mathrm{d}\vec{r}^{\mathcal{N}}.
\tag{7.47}
$$

The integration is carried out over all locations and orientations of all molecules. The difference of the Helmholtz energies of the fluid with the perturbed potential and the reference fluid is then

$$A^{\mathrm{r}}(\lambda)-A_0^{\mathrm{r}}=-k_{\mathrm{B}}T\ln\frac{Q_{\mathrm{C}}(\lambda)}{Q_{\mathrm{C}}(0)}=-k_{\mathrm{B}}T\ln\left\langle\exp\left(-\frac{\lambda U_1(\vec{r}^{\mathcal{N}},\Omega^{\mathcal{N}})}{k_{\mathrm{B}}T}\right)\right\rangle_0 . \tag{7.48}$$

The subscript “0” indicates a canonical average over the reference system. Expanding the logarithm and the exponential into Taylor series, collecting terms with equal powers of λ, and finally setting $\lambda=1$ gives

$$\begin{aligned}
A^{\mathrm{r}}&=A_0^{\mathrm{r}}+A_1^{\mathrm{r}}+A_2^{\mathrm{r}}+A_3^{\mathrm{r}}+\ldots\\
A_1^{\mathrm{r}}&=\langle U_1\rangle_0\\
A_2^{\mathrm{r}}&=-\frac{1}{2}\left(\frac{1}{k_{\mathrm{B}}T}\right)\left\langle(U_1-\langle U_1\rangle_0)^2\right\rangle_0\\
A_3^{\mathrm{r}}&=-\frac{1}{6}\left(\frac{1}{k_{\mathrm{B}}T}\right)^2\left\langle(U_1-\langle U_1\rangle_0)^3\right\rangle_0 .
\end{aligned} \tag{7.49}$$

A_0^{r} is, of course, a property of the reference system, and thus known by definition.

This equation is known as the λ *expansion*. It is formally applicable to all kinds of energy models, provided that a reference system exists whose properties are known.

7.5.4.1 Nonspherical Pair Potentials

In practice, often the hard-sphere fluid serves as a reference fluid, because its properties, including the pair correlation function, are well known. Another option is the Lennard-Jones fluid. Both interaction potentials are spherical.

In order to obtain the Helmholtz energy of a fluid with a nonspherical interaction potential, the following ansatz is made [116]:

$$u(r,\Omega_1,\Omega_2)=u_0(r)+\lambda u_{\mathrm{a}}(r,\Omega_1,\Omega_2). \tag{7.50}$$

Here r denotes the distance between the molecules 1 and 2; Ω_1 and Ω_2 are their orientations. If the spherical reference potential is defined as

$$u_0(r)=\langle u(r,\Omega_1,\Omega_2)\rangle_{\Omega_1,\Omega_2}, \tag{7.51}$$

the orientational average of the anisotropic part of the pair potential vanishes:

$$\langle u_{\mathrm{a}}(r,\Omega_1,\Omega_2)\rangle_{\Omega_1,\Omega_2}=0. \tag{7.52}$$

Consequently, $\langle U_1\rangle_0=0$, and the first-order term of the λ expansion vanishes.

The A_2^{r} term represents two-body interactions, the even more complicated A_3^{r} term three-body interactions. The latter are usually resolved by means of the superposition approximation. In order to obtain analytical equations, the integrals are often evaluated numerically and then fitted to suitable functions.

Not unexpected, the calculation of the high-order perturbation terms beyond A_3^r is rather complicated and, at some point, not worth the effort. Moreover, the perturbation series does not converge very well. Since perturbation theories are per definition valid for small deviations from the reference state only, a slow convergence means an even narrower range of applicability.

Replacing the summation in Eq. (7.49) by suitable Padé approximants has been found to improve the convergence significantly [118]:

$$A^\mathrm{r} = A_0^\mathrm{r} + \frac{A_2^\mathrm{r}}{1 - \frac{A_3^\mathrm{r}}{A_2^\mathrm{r}}}. \tag{7.53}$$

Examples for the application of thermodynamic perturbation theory are the treatment of multipolar and ionic fluids based on the hard-sphere reference fluid [119] or the accounting for soft repulsion (discussed in Section 7.5.4.3). Gray *et al.* [120] showed that perturbation theory can be applied to arbitrary anisotropic intermolecular potentials; this includes polar interactions and polarizability.

7.5.4.2 Scaled-particle Theory

Scaled-particle theory (SPT) may be regarded as a perturbation theory as well: Where standard thermodynamic perturbation theory gradually turns on a contribution to a pair potential, scaled particle theory “turns on” a particle of the same type in a cavity of the fluid. Scaled-particle theory had originally been developed by Reiss *et al.* [121] for the hard-sphere fluid in order to obtain an expression for the value of its pair correlation function at contact of the hard spheres. They introduced a coupling parameter in the potential model which allowed increasing a sphere from a point to full size. Integration over the coupling parameter yielded an expression for the chemical potential of the hard-sphere fluid.

Gibbons generalized that approach to particles of arbitrary shape [122] by implementing the expression for the excluded volume of convex bodies by Kihara [123] and others, and so obtained a Percus–Yevick equation[2] for the hard-convex-body fluid. In the limit of a spherical pair potential, the Percus–Yevick equation for hard spheres is recovered. Boublík developed an equation of state for hard convex bodies that has the Carnahan–Starling equation as its spherical limit [124], Eq. (7.55).

7.5.4.3 Soft Repulsion

Real molecules do not really behave like hard spheres, but they can interpenetrate to some extent if they collide with high speeds. For many practical

---

[2] The Percus-Yevick equations of state for the hard-sphere fluid can be regarded as predecessors for the Carnahan–Starling equation.

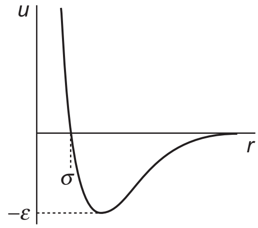

FIGURE 7.5 Lennard-Jones interaction potential.

applications, intermolecular or interatomic interactions are reasonably well described by the Lennard-Jones pair potential, which is sketched in Fig. 7.5. Perturbation theory assumes that a soft-sphere fluid can be modelled essentially as a hard-sphere fluid, but with a temperature-dependent collision diameter. Specifically, the Barker–Henderson theory [106, 125] proposes

$$\sigma_{\mathrm{eff}} = \int_0^\infty \left(1 - \exp\left(-\frac{u(r)}{k_{\mathrm{B}}T}\right)\right) \mathrm{d}r. \tag{7.54}$$

The Weeks–Chandler–Andersen perturbation theory [126] goes beyond the Barker–Henderson theory and takes also pressure effects on the effective collision diameter into account.

Consequently, an effective covolume parameter is obtained which, for the Barker–Henderson approach, depends on temperature; for the Weeks–Chandler–Andersen approach, it also depends on density. For a repulsive soft-sphere model, the effective diameter of the hard sphere becomes smaller with increasing temperature.

It should be noted that perturbation theories are valid only for small perturbations of the reference systems. How small the perturbation has to be in order to still give reasonable results depends on the problem. In the case of the virial series of the hard-sphere system, the description becomes the more accurate the more virial coefficients are correctly included in the model. This affects not only the values of the calculated pressure, but also the maximum packing fraction [111, 112]. The Barker–Henderson perturbation theory is valid for low densities only, roughly up to the critical density. At higher densities, isotherm crossing can appear [103]. Hence, not only empirical equations of states, but also theory-based equations of state should be evaluated before using them over wide ranges of state variables.

7.5.4.4 Hard Convex Bodies

Nonspherical shapes can be accounted for by perturbation theories too. A simple nonspherical molecular model is the hard convex body. “Convex” in this context means that any straight line connecting two points of a molecule lies entirely within this molecule. Examples for convex bodies are ellipsoids and spherocylinders; fused-hard-sphere molecules are generally not convex.

Therefore, hard convex bodies are rather good models for small, rigid molecules like hydrogen or nitrogen but not for complicated or even flexible molecules like hexane.

The derivation of an equation of state for hard convex bodies of Boublík, for example, gives an equation resembling the Carnahan–Starling equation of state [124, 127]:

$$Z_{\mathrm{hcb}} = \frac{1+(3\alpha-2)\xi+(\alpha^2+\alpha-1)\xi^2-\alpha(5\alpha-4)\xi^3}{(1-\xi)^3}. \tag{7.55}$$

Here α is a nonsphericity parameter. For a spherical shape, it has the value one. Consequently, the insertion of $\alpha = 1$ into Eq. (7.55) gives the Carnahan–Starling equation Eq. (7.28).

7.5.4.5 Hard Flexible Chains

The model of hard convex bodies is appropriate for small, rigid molecules only. For larger and typically more flexible molecules, models for flexible chains of spheres should be employed. The first approach to an equation of state for flexible chains is the well-known Flory–Huggins lattice theory. In 1984, Wertheim developed the thermodynamic perturbation theory for chain molecules, called TPT1 [128, 129], which subsequently was used for the chain contributions of the SAFT (statistical association fluid theory) equation of state [130]. The term “association” might seem out of context for an equation of state for chain molecules, but Wertheim first derived the fundamental equation for association and then – by taking the limit of infinite association strength, which is equivalent to a covalent bond between two segments of a molecule – obtained the chain term. Due to the rich phase behavior of polymers and their industrial importance, equations of state for chain molecules and especially the SAFT approach have been further developed and extended in various ways. Therefore, today many different versions of SAFT equations of state exist in the literature.

The SAFT equation of state can be written in terms of the residual free Helmholtz energy as:

$$\begin{aligned} A^{\mathrm{r}} =& A_{\mathrm{seg}}(m,\rho,T,\sigma,\epsilon)+A_{\mathrm{chain}}(\rho,\sigma,m) \\ &+A_{\mathrm{assoc}}(\rho,T,\epsilon_{\mathrm{assoc}},\kappa_{\mathrm{assoc}}). \end{aligned} \tag{7.56}$$

Here A_{seg} is the contribution of the chain segments (repulsive as well as attractive contributions). For an attracting hard-sphere reference fluid or for a Lennard-Jones reference fluid, a segment is described by the attraction parameter ϵ and the diameter of the spherical segment σ. It furthermore depends on the temperature and the segment density, i.e., the density of the chain molecules times the chain length parameter m. Since the fluid is actually not a system of segments, the connectivity has to be accounted for. This is accomplished by the chain term A_{chain}. It depends on the density, the chain length parameter m, and the segment diameter σ. Finally, SAFT is able to describe the association of molecules, for example hydrogen bonding, with the third term, A_{assoc}, which depends on temperature and density. Two additional parameters are required for the association, namely the attraction parameter and the covolume parameter of the association site. In case of a hard-sphere reference fluid, the association site is placed on the surface of the segment; in case of a soft-sphere Lennard-Jones type reference fluid, the association site may penetrate the reference segment.

The segment term is basically the reference fluid equation of state. In case of a hard-sphere reference, usually the Carnahan–Starling equation Eq. (7.28) is employed, which can be written as

$$Z = 1 + \frac{4\xi - 2\xi^2}{(1-\xi)^3}\,. \tag{7.57}$$

Here ξ is the reduced segment density, $(\pi/6) m N_{\text{A}} \sigma^3$. The relation

$$Z = 1 + 4\xi g(\sigma) \tag{7.58}$$

establishes the connection between the equation of state and the value of the radial distribution function at the contact of two spheres $g(\sigma)$. For the Carnahan–Starling equation, this leads to

$$g(\sigma) = \frac{1-\xi/2}{(1-\xi)^3}\,. \tag{7.59}$$

With this contact value, the chain term, which lowers the Helmholtz free energy of the unconnected segments, can be expressed as

$$A_{\text{chain}} = RT(1-m)\ln g(\sigma)\,. \tag{7.60}$$

Insertion into Eq. (7.56) and differentiation with respect to density give the SAFT equation of state for chains of attractive hard spheres:

$$Z = 1 + m\frac{4\xi - 2\xi^2}{(1-\xi)^3} + (m-1)\frac{2\xi^2 - 5\xi}{(2-\xi)(1-\xi)} - m\frac{a}{bRT}4\xi\,. \tag{7.61}$$

The last term is the van der Waals attraction term, multiplied with the number of segments m in the molecules.

The association term of SAFT requires a detailed balance of species in the system, because association lowers the number of free molecules. The Helmholtz energy of the association is obtained as

$$A_{\text{assoc}} = RT\sum_{a=1}^{M}\left(\ln X_a - \frac{X_a}{2}\right) + \frac{M}{2}\,. \tag{7.62}$$

Here M is the number of association sites of a molecule, a an index of an association site, and X_a the mole fraction of the molecules not attached to this site.

The number of unattached (free) sites a is given by

$$X_a = \frac{1}{1 + \hat{\rho} \sum_b X_{b \neq a} \Delta_{ab}}\,. \tag{7.63}$$

$\hat{\rho}$ is the number density before association. The summation over b includes all other sites except site a. The so-called association strength is defined as

$$\Delta_{ab} \equiv 4\pi \int_0^{r_c} \left[\exp\left(\frac{\epsilon_{ab}}{k_B T}\right) - 1\right] r^2 g(r)\,\mathrm{d}r\,. \tag{7.64}$$

This expression can be approximated as

$$\Delta_{ab} = \sigma^3 g(\sigma) \kappa_{ab}, \tag{7.65}$$

where κ_{ab} is a substance-dependent parameter. For $g(\sigma)$, the same value as for the hard-sphere reference fluid is used.

The extension of the SAFT equation of state to mixtures is straightforward. The chain term is summated in terms of the Helmholtz free energy, the segment term is extended by the one-fluid mixing theory as discussed in Section 8.3, and the association term requires an extension to a double summation over the mole fraction and the sites of each substance.

Today, there is an impressive number of SAFT versions and applications. It is possible to extend the theory to copolymers [131] or to chemically reacting systems, for instance in the context of carbon dioxide capture [132]. SAFT has also successfully been used in computational schemes for surface tensions [133] or corrections for nonanalytic behavior at the critical point (see Section 7.8).

7.5.4.6 Polar Molecules

Perturbation theories have also been developed for attractive contributions beyond the van der Waals attraction. For electrostatic interactions, the second- and third-order perturbation contributions have been calculated and extrapolated to higher order by Padé approximation. In this way, one can derive equations of state not only for dipolar, but also for quadrupolar and octupolar fluids [115, 119, 134].

Such approaches have been based on the hard-sphere as well as on the soft-sphere reference fluid.

For some simple molecular geometries, there are ready reference equations of state, e.g., for dipolar Lennard-Jones molecules [135, 136].

7.5.5 Chemical Association Theories

In some chemical compounds, the molecules can reversibly associate and form dimers or even oligomers. Therefore, small carbonic acids are known to form stable dimers in the vapor phase. Many alkanols and amines can form linear or cyclic oligomers. Water molecules, of course, can build spatial networks. In all these cases, the association is caused by hydrogen bonding, but there are also some other causes, like the formation of charge-transfer complexes.

Now "association" is a somewhat fuzzy concept. Two argon atoms can associate and form what is frequently called a van der Waals dimer, i.e., a pair loosely held together by dispersion forces. Ethene molecules can associate and form the very stable polymer polyethylene. In fluid thermodynamics, the term "associating fluid" usually refers to something in the middle between these extremes: typical associating fluids have chemical binding forces significantly stronger than dispersion interactions. On the other hand, the binding forces are weak enough to permit thermal dissociation and rapid equilibration. The latter is perhaps the most significant point: typical associating fluids are equilibrium mixtures of monomers, dimers, etc., and it is not possible to separate them, for instance by distillation.

Association naturally affects the equation of state. It can be accounted for by chemical association models, which are either single association models,

$$\mathrm{A} + \mathrm{A} \rightleftharpoons \mathrm{A}_2$$

or chain association models,

$$\begin{gathered} \mathrm{A} + \mathrm{A} \rightleftharpoons \mathrm{A}_2 \\ \mathrm{A}_2 + \mathrm{A} \rightleftharpoons \mathrm{A}_3 \\ \vdots \end{gathered}$$

The latter is, of course, useful for the modelling of alkanols or amines.

The set of chemical equilibria yields a set of chemical balance equations (mass actions laws),

$$\frac{z_{i+1}}{z_1 z_i} = K_{x,i} \quad i = 1, 2, \ldots \tag{7.66}$$

where the z_i are the mole fractions of the oligomers and the $K_{x,i}$ the appropriately defined chemical equilibrium constants. With the assumptions that all $K_{x,i}$ are the same, that there is no volume effect of association (covolume $b_i = ib_1$, with $i = 1$ denoting the monomer), and a few other simplifications, Heidemann and Prausnitz derived a closed-form solution that can be coupled, in principle, with any van der Waals-type equation of state [137]. If the compression factor of a nonassociating fluid is

$$Z = Z_{\mathrm{rep}} + Z_{\mathrm{att}}\,, \tag{7.67}$$

the compression factor of a fluid exhibiting chain association is

$$Z = \frac{2Z_{\mathrm{rep}}}{1+\sqrt{1+4K_x V_{\mathrm{m}}^{\ominus}\rho}} + Z_{\mathrm{att}}$$
$$\text{with } K_x = \exp\left(-\frac{\Delta_{\mathrm{assoc}}H_{\mathrm{m}} - T\Delta_{\mathrm{assoc}}S_{\mathrm{m}}}{RT}\right). \tag{7.68}$$

Here $\Delta_{\mathrm{assoc}}H_{\mathrm{m}}$ and $\Delta_{\mathrm{assoc}}S_{\mathrm{m}}$ are the enthalpy and the entropy, respectively, of the association reaction. They are adjustable parameters.

It is possible to account for a covolume change of the association reaction. This improves the behavior of the model at elevated pressures but requires an additional iteration [138].

Assuming the same equilibrium constant K_x for all oligomers is of course not very realistic. Furthermore, the formation of cyclic oligomers, branching, and (in mixtures) cross association need to be accounted for. For these matters, the reader is referred to the work of Heintz [139], the review of Economou and Donohue [140], or the textbook of Malanowski and Anderko [141].

Nowadays, many chemical association models have been superseded by SAFT variants (see Section 7.5.4.5), because these combine the association concept with modern statistical thermodynamics.

Working with chain length–dependent association constants naturally leads to a proliferation of substance-dependent, adjustable parameters in the equation of state. This made the advanced chain association models rather unattractive in the beginning. But nowadays, it is possible to calculate at least the energies of association ab initio with quantum mechanical methods, so that the number of adjustable parameters can be kept reasonably low [142, 143].

7.6 REFERENCE EQUATIONS OF STATE

For many applications, the accuracy given by the above mentioned empirically or theoretically derived equations of state is sufficient. In some cases, however, extremely accurate data are required. To give an example, the calorific value of a fuel is directly related to its mass. In gas pipelines, usually the volume flow rate is measured and then transformed into the mass flow rate for billing purposes. The mass flow rate can be calculated from the density, which is obtained from an equation of state for given temperature and pressure. In such a case, depending on the state region of the fuel, small inaccuracies in the equation of state may lead to large changes in price. Another example is the calibration of experimental apparatus requiring very precise equations of state for a reference substance. For such purpose, much effort has been spent on the development of reference equations of state.

Reference equations of state are typically developed for single specific fluids only. These are simple fluids such as argon or methane, or important fluids such as water. In order to achieve the desired accuracy, many adjustable parameters are necessary. Early reference equations employed more than 100 parameters for a given substance. By using an evolution technique in combination with an assessment of the statistical significance of terms, the group of Wagner managed to reduce the number of parameters to the range from 30 to 60 depending on the desired accuracy.

An example is the Setzmann–Wagner equation of state for methane [64], which is given here as equation of the residual Helmholtz energy:

$$\begin{aligned}\frac{A_\mathrm{m}^\mathrm{r}}{RT} &= \sum_i f_{1i}\omega^{o_{1i}}\tau^{t_{1i}} + \sum_i f_{2i}\omega^{o_{2i}}\tau^{t_{2i}} \exp\left(-\omega^{e_i}\right) \\ &\quad + \sum_i f_{3i}\omega^{o_{3i}}\tau^{t_{3i}} \exp\left(-a_i(\omega - c_i)^2 - b_i(\tau - d_i)^2\right) \qquad (7.69) \\ &\quad \text{with}\, \tau = \frac{T_\mathrm{c}}{T} \,\text{and}\, \omega = \frac{\rho}{\rho_\mathrm{c}}.\end{aligned}$$

The number of the terms, the coefficients f_{ki}, a_i, and b_i, the exponents o_{ki}, t_{ki}, and e_i, and the parameters c_i and d_i depend on the substance. This equation can be regarded as an extension of the earlier reference equations of Benedict, Webb, and Rubin, of Bender, and of Jacobsen and Stewart.

This approach does not claim any microscopic physical background; in fact, it is rather a very precise correlation of experimental data. In this context, it should be kept in mind that the experimental data included in the correlation are all for the stable single phase or for the vapor–liquid equilibrium. Therefore, extrapolations into the metastable region should be made with caution [144].[3]

Especially, equations of the Setzmann–Wagner type are known to oscillate wildly in the two-phase region: the pressure maxima can even exceed the critical pressure by more than an order of magnitude. Such equations cannot be used to describe properties of the metastable fluid. Moreover, during the numerical calculation of molar volumes for given temperature and pressure, care must be taken to avoid the regions of oscillations.

7.7 THE CORRESPONDING-STATES PRINCIPLE

The $p(V_\mathrm{m}, T)$ equations of state of different substances are different although some features are common for all substances. The corresponding-states principle is the principle – or rather the wish – that the equations of real gases can be mapped onto each other by a proper scaling of the variables. More specifically, the principle assumes that there exists a universal equation of state, which is

---

[3] Recent experimental work on metastable water showed the Wagner–Pruß reference equation [145] to be correct down to –26 MPa [146].

expressed in terms of reduced properties:

$$\tilde{p} = \tilde{p}(\tilde{V}, \tilde{T})$$
$$\text{with} \quad \tilde{p} = \frac{p}{p_c} \quad \tilde{V} = \frac{V_m}{V_{mc}} \quad \tilde{T} = \frac{T}{T_c}. \tag{7.70}$$

The reduction parameters are the critical properties of the fluid.

This principle makes it possible to apply an equation of state for one substance to another one. The equation of state can be a reference equation. The scaling of the variables is simple and requires no complicated parameter estimation.

The disadvantage of this approach is that the corresponding-states principle is an approximation only and can be used for substances of similar chemical constitution and molecular shape only. Therefore, one might use a reference equation for argon to predict thermodynamic data of krypton, but it would not be a good idea to predict data of decane with an equation of state for methane.

An immediate consequence of the corresponding-states principle is that the critical compression factor Z_c should be a universal constant, which evidently is not the case.

A first extension to the corresponding-states principle was proposed by Pitzer *et al.* [96, 97], who introduced the so-called acentric factor ω defined by Eq. (7.15). For spherical molecules, ω is close to zero, whereas it has positive values for nonspherical molecules. Basically, the acentric factor accounts for different curvatures of the vapor pressure curves and relates them to the sphericity of the molecules within an extended corresponding-states principle.

A significant improvement was achieved by Lee and Kesler, who proposed an extended corresponding-states scheme using two reference fluids, here denoted as “0” and “1”:

$$Z(\tilde{V}, \tilde{T}) = Z_0(\tilde{V}, \tilde{T}) + \frac{\omega - \omega_0}{\omega_1 - \omega_0} Z_1(\tilde{V}, \tilde{T}). \tag{7.71}$$

This approach performs a linear interpolation between the equations of state of the two reference fluids. The control parameter is the acentric factor ω. Usually the “0” compound is a spherical or nearly spherical molecule, e.g., argon or methane, so that $\omega_0 \approx 0$.

This extended corresponding-states scheme is useful for series of chemically similar compounds, e.g., n-alkanes. For substances differing in more than one way from argon-like behavior (e.g., nonspherical shape plus dipole moment), multireference corresponding-states schemes can be constructed. For instance, the scheme of Xiang [147] uses a two-dimensional interpolation based on the acentric factor and the “asphericity factor” (related to the deviation of Z_c from a reference value); other schemes use dipole moments or other molecular parameters related to polar behavior. The reader is referred to the original literature or to specialized textbooks, e.g., [148].

7.8 NEAR-CRITICAL BEHAVIOR

All equations of state mentioned above are so-called classical equations of state or, more accurately, analytical equations of state, because they have in common that they are analytical at the critical point. The term “analytical” is here understood in the mathematical sense; an analytical function can be differentiated an infinite number of times and can therefore be represented as an infinite Taylor series. This mathematical property inevitably leads to so-called “classical behavior” in the vicinity of the critical point.

What “classical behavior” means can be determined from a Taylor expansion at the critical point:

$$\begin{aligned} p(V_\mathrm{m},T) = {} & p_\mathrm{c} + \left(\frac{\partial p}{\partial V_\mathrm{m}}\right)(V_\mathrm{m}-V_\mathrm{mc}) + \frac{1}{2}\left(\frac{\partial^2 p}{\partial V_\mathrm{m}^2}\right)(V_\mathrm{m}-V_\mathrm{mc})^2 \\ & + \frac{1}{6}\left(\frac{\partial^3 p}{\partial V_\mathrm{m}^3}\right)(V_\mathrm{m}-V_\mathrm{mc})^3 + \cdots . \end{aligned} \tag{7.72}$$

Since the first and the second derivatives of the pressure with respect to the volume vanish at the critical point, the cubic term is the leading term of the Taylor series. Consequently, the limiting behavior of the critical isotherm at the critical point is a cubic function. This is a general result for all analytical equations of state.

The limiting behavior at the critical point can be expressed by power laws. In the case of the critical isotherm, this law is

$$p = p_\mathrm{c} + A(V_\mathrm{m}-V_\mathrm{mc})^3, \tag{7.73}$$

or, in terms of the density,

$$p = p_\mathrm{c} + A_\rho(\rho-\rho_\mathrm{c})^3. \tag{7.74}$$

In a similar way, one can derive the temperature–density power law for the coexistence curve. In this case, the quadratic term is leading because the coexistence curve has a maximum at the critical point:

$$T = T_\mathrm{c} + B(\rho-\rho_\mathrm{c})^2. \tag{7.75}$$

The proportionality factors A, A_ρ, and B are called critical amplitudes. The exponents 3 and 2 are the critical exponents; these values derived for analytic equations of state are called classical values.

Additional power laws can be defined for other properties, e.g., the surface tension, the viscosity, or the heat capacity, and their critical exponents be derived from analytic equations of state.

However, already during the very early experimental studies of van der Waals and Kamerlingh-Onnes at the beginning of the previous century, it turned out that the near-critical behavior of real fluids deviates from the classical prediction. For example, the coexistence curve is so flat in the critical region that it cannot be represented by a quadratic power law. In order to account for this behavior by means of power laws, general exponents δ and β have been defined:

$$p = p_c + A_\rho (\rho - \rho_c)^\delta \tag{7.76}$$

$$T = T_c + B(\rho - \rho_c)^{\frac{1}{\beta}}. \tag{7.77}$$

Hence the classical behavior is characterized by the critical exponents $\delta = 3$ and $\beta = 0.5$. The experimentally determined values are $\delta \approx 4.76$ and $\beta \approx 0.326$, independent of the substance.

The formulation of the power laws based on equations of state goes back to Widom [149]. The nonclassical critical exponents for two-dimensional systems were derived by Onsager [150]. Wilson [151] calculated the values of the critical exponents by renormalization group theory for three-dimensional systems.

One might wonder why the deviation of the exponents from their classical values leads to nonanalytical behavior at the critical point. In case of the critical isotherm, an exponent $\delta > 3$ does not affect the critical conditions of vanishing first and second derivatives. A problem appears, however, if the exponent δ is not an integer and has a value between 3 and 4. Then the fourth derivative, being a factor in the fourth term of the Taylor expansion, has a negative exponent. Such a term diverges on approaching the critical point, and hence, the Taylor expansion does not exist.

This discrepancy between the widely used classical equations of state and the nonclassical, near-critical behavior at present does not seem reconcilable and has generated its own area of research, namely the equations-of-state development for the near-critical behavior. Roughly one may distinguish two approaches: (1) the improvement of the near-critical behavior of classical equations of state and (2) the development of nonclassical equations of state.

The first approach is typically based on classical equations of state, which are modified to mimic the nonclassical behavior in the critical region. In the very limit of the critical point, the classical exponents are still recovered. But the distance from the critical point at which the critical exponents begin to deviate from the nonclassical values can be made very small, and some of the reference equations of state mentioned above have driven this to perfection. However, the good effective representation of noncritical behavior by analytical functions may work for the exponents δ and β but not necessarily for derived properties. This has to be verified in each case before using such equation of state for properties not involved in its development.

The second approach, the development of nonclassical equations of state, consists usually of a combination of a classical equation of state with a power law. The classical equation of state represents the background behavior determined by the interactions between the molecules, while the power law represents the universal, i.e., substance-independent, behavior in the critical region. The connection of these two contributions is accomplished by so-called crossover approach. Early attempts using a switch function (a multiplicative factor moving from 0 to 1 on approaching the near-critical region) worked well for the representation of the *pVT* behavior. However, the derived properties exhibited artifacts, because the switch function itself contributed in an unfavourable way to the derived properties in the state region where the crossover took place.

A more natural way of crossover from classical to nonclassical, near-critical behavior has been accomplished by the group of Sengers [152]. Their crossover approach combines the asymptotic near-critical behavior with a classical mean-field model, such as the van der Waals equation of state [153]. The equation of state is expanded at the classical critical point and then the deviations from the critical point such as ΔT are replaced by crossover functions. As the result of an iterative procedure, the classical mean-field critical point is modified, and in the end, a nonclassical critical point is obtained. The resulting critical compression factor moves from 0.375 (if the van der Waals equation is used) to more realistic values below 0.29. Also the quantitative behavior in the near-critical region changes, and the isochoric heat capacity diverges at the critical point – a feature that is not present in the classical case.

Recently, there have been several successful attempts to introduce nonanalytic behavior into SAFT equations of state (Section 7.5.4.5), which are very powerful and flexible classical equations [154, 155].

As a criterion whether critical fluctuations need to be taken into account, the Ginzburg number can be used. The Ginzburg number is a measure of the extent of the fluctuations in the system, which diverge at the critical point. If the reduced temperature deviation from the critical point is larger than that number, the classical behavior dominates.

The nonclassical equations of state are usually mathematically complicated; they often cannot be represented in a closed form, i.e., with a finite number of algebraic operations and elementary functions, but require iterative or recursive schemes. However, if an accurate description of the limiting behavior in the critical region is required, their application is necessary.

At sufficient distances from the critical point, appropriate classical equations of state can be used. In the context of modelling supercritical fluids, a good description of the critical region is required but not necessarily an accurate representation of the nonclassical limiting behavior. In such case, one may apply an equation with improved near-critical behavior mimicking the nonclassical behavior sufficiently close to the critical point. A common feature of many equations of state of this kind is the presence of exponential functions of the density. This feature often leads to the desired flattening of the functions in the critical region of classical equations.

7.9 WHICH EQUATION OF STATE IS BEST?

This question touches personal preferences and sometimes even politics. We shall refrain from answering it. Still, some warnings against pitfalls can and should be given.

Readers interested in a comprehensive overview over equations of state are referred to the book of Sengers *et al.* [114], which reflects the state of the art.

Many equations of state contain terms or subfunctions that are based on tabulated data. Sometimes, these data are experimental results, but sometimes intractable integrals in statistical thermodynamics are solved numerically, resulting in data tables. By fitting suitable correlation functions, often polynomials, to these data, equations of state in closed form can be obtained.

But correlation functions, especially complicated ones, often have a tendency to "wriggle" through the tabulated data. The unwanted extrema or inflection points sometimes lead to artifacts in derivatives and in phase equilibrium calculations. Users of such equations of state are advised to test them thoroughly before applying them to phase-diagram calculations.

Another problem concerns the limiting behavior of equations of state. Sometimes, equations of state have been created with a small set of compounds or a limited range of reduced temperature in mind – and are then used under completely different conditions. An example is the temperature dependence of the attractive term of the Redlich–Kwong–Soave equation of state, which must not be used for $T/T_c > 9$, a value reached by hydrogen at room temperature. It is therefore advisable to check the limiting behavior of equations of state, their behavior at high densities or high pressures.

An easily applicable test is the computation of *Brown's characteristic curves* [156]. These are curves in the pT plane along which some derivatives of the equation of state have the same values as an ideal gas. The characteristic curves of first order are the following:

(1) The Amagat curve, also known as Joule inversion curve; its mathematical condition is any of the these:

$$\left(\frac{\partial Z}{\partial T}\right)_V = 0 \quad \left(\frac{\partial Z}{\partial p}\right)_V = 0 \quad \left(\frac{\partial U}{\partial V}\right)_T = 0 \quad \left(\frac{\partial p}{\partial T}\right)_V = \frac{p}{T}. \tag{7.78}$$

This curve is related to intermolecular potentials with soft repulsion. It starts on the T axis at the temperature where the second virial coefficient has its maximum (typically 15–20 T_c), passes through a pressure maximum around $100\,p_c$, and then ends on the vapor pressure curve. Equations of state that cannot generate a maximum of the second virial coefficient, $B_2(T)$, do not have a physically meaningful Amagat curve.

(2) The Boyle curve; its mathematical condition is anyone of these:

$$\left(\frac{\partial Z}{\partial V}\right)_T = 0 \quad \left(\frac{\partial Z}{\partial p}\right)_T = 0 \quad \left(\frac{\partial p}{\partial V}\right)_T = -\frac{p}{V}. \tag{7.79}$$

This curve starts on the T axis at the Boyle temperature (where $B_2 = 0$), passes through a pressure maximum, and ends on the spinodal near to the critical point.

(3) The Charles curve, also known as Joule–Thomson inversion curve; its mathematical condition is anyone of these:

$$\left(\frac{\partial Z}{\partial T}\right)_p = 0 \quad \left(\frac{\partial Z}{\partial V}\right)_p = 0 \quad \left(\frac{\partial T}{\partial p}\right)_H = 0 \quad \left(\frac{\partial H}{\partial p}\right)_T = 0$$
$$\left(\frac{\partial V}{\partial T}\right)_p = \frac{V}{T}. \tag{7.80}$$

This curve starts on the T axis at the temperature where $\mathrm{d}B_2/\mathrm{d}T = B_2/T$. It passes through a pressure maximum and ends on the vapor pressure curve.

These three curves start and end with vertical slopes. They have one pressure maximum and no inflection points. The Boyle curve must lie within the Charles curve and the Charles curve within the Amagat curve. Fig. 7.6 shows an example computed for the “soft SPHCT” equation of state [92].

If these curves cannot be computed for an equation of state or have the wrong shape, the equation of state should not be used in the indicated pressure or temperature range. Few equations of state are able to yield physically meaningful Amagat curves.

There are, of course, more tests that can be made. The interested reader is referred to the original literature, e.g., the “IUPAC Guidelines for publication of equations of state” [157].

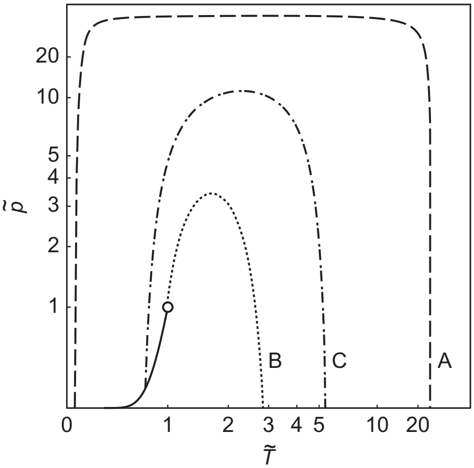

FIGURE 7.6 Brown’s characteristic curves of first order, computed for the “soft SPHCT” equation [92]. – – : Amagat curve (A), ········: Boyle curve (B), –·– : Charles curve (C), and ——: vapor pressure curve. Note that the coordinate axes are distorted in order to keep the critical region recognizable. (*Reprinted from Int. J. Thermophys. 31: O. L. Boshkova and U. K. Deiters, “Soft repulsion and the behavior of equations of state at high pressures”, pp. 227–252, ©2010, with permission from Springer*)

7.10 HOW TO OBTAIN THE PARAMETERS

So far, we have always assumed that the parameters of the equations of state or interaction potentials are known. This is usually the case for reference equations, and for several equations of technical relevance, there exist large collections of parameters. But sooner or later, most users of equations of state have to face the problem of determining parameters of new substances and/or for new equations of state.

Unfortunately, there is no perfect equation of state.[4] A given equation of state will represent some properties better than others, and the accuracy will depend on pressure and temperature. Conversely, fitting an equation of state to experimental data may result in different parameter sets, depending on the nature as well as the temperature and pressure ranges of the experimental data. It is therefore not possible to give a general recommendation on how to fit parameters. A user interested in vapor–liquid equilibrium calculations is well advised to use experimental vapor pressure data, whereas someone interested in density correlations should perhaps use pVT data.

Generally, it is a good idea to determine parameters from the critical pressure and temperature – of course, only if these properties have been measured with a reasonable accuracy. For some equations of state, the *reduced* critical properties are fixed, and then the calculation of parameters is particularly easy. An example is the Peng–Robinson equation: combining the critical properties given in Section C.4 in the following ways,

$$\begin{aligned} Z_c\xi_c &= \frac{p_c v^*}{RT_c} = 0.077796 \quad \Rightarrow \quad b = v^* = 0.077796\,\frac{RT_c}{p_c} \\ \frac{Z_c\xi_c}{\tilde{T}_c} &= \frac{p_c v^* T^*}{RT_c^2} = 0.057154 \quad \Rightarrow \quad a_c = 8RT^*v^* = 0.45724\,\frac{(RT_c)^2}{p_c}, \end{aligned} \tag{7.81}$$

immediately gives the first two parameters of this equation of state. The third parameter, ω, can be read off the vapor pressure curve.

For the van der Waals equation and the Redlich–Kwong equation (including the Soave variant), similar equations exist; only the numerical constants are different.

For equations whose reduced critical properties are not fixed, it is necessary to solve the critical conditions,

$$p(V_{mc}, T_c) = p_c \quad p_{(V)}(V_{mc}, T_c) = p_{(2V)}(V_{mc}, T_c) = 0, \tag{7.82}$$

iteratively. Computing the derivatives by numerical differentiation is a viable and often time-saving option.

---

[4] except perhaps Eq. (7.69)

Caution is advised when using the critical condition $p(V_{\mathrm{mc}}, T_{\mathrm{c}}) = p_{\mathrm{c}}$ (cf. Section 5.4): this condition can only be used for equations of state that have a variable Z_{c} in the experimentally accessible range – and these are a minority!

Another good way to determine parameters of equations of state is fitting to vapor pressures and, if available, orthobaric liquid volumes. This amounts to using Maxwell's criterion, Eq. (5.28), within the object function of a suitable parameter fitting algorithm, e.g., the Marquardt–Levenberg method (see Section A.13). A computational problem of this approach is that Maxwell's criterion can only be evaluated if the equation of state yields distinct liquid and gas volumina at the given pressure and temperature conditions; this may not be the case if the initial choices for the parameter values are not good. The problem can usually be minimized (although not completely avoided) by estimating the parameters from critical data first and using the results as initial values for the fitting to vapor–liquid equilibrium data.

In principle, many other thermodynamic properties can be and have been used for the determination of parameters, like speeds of sound or *pVT* data. Especially with the latter, one must ask to which extent they are influenced by molecular interactions. For example, a gas at 0.1 MPa will most likely have a molar volume close to the value given by the ideal-gas law, regardless of the equation of state chosen or its parameters. Conversely, it would be difficult to estimate parameters from such a molar volume. Therefore, *pVT* data used for the determination of parameters should belong to dense states – liquid or compressed gas – where the deviations from the ideal-gas behavior are large.

7.11 PROBLEMS

1. Derive an expression for the second virial coefficient of a gas whose molecules have a square-well pair potential (Eq. (7.35)). Discuss the temperature dependence of the second virial coefficient at high temperatures.

2. If an equation of state is not good enough for a given task, it is a common trick to make its parameters temperature dependent. Check whether using temperature-dependent covolumes,

a. $b = b_0 + b_1/T$

b. $b = b_0 + b_1 T$

with $b_1 < 0$ can cause isotherm crossing in connection with the van der Waals equation of state.

3. Another "trick of the trade" is turning constant exponents into substance-specific parameters. It may be tempting to improve a simple van der Waals type equation of state

$$p = p_{\mathrm{rep}} - \frac{a}{V_{\mathrm{m}}^2}$$

by turning it into

$$p = p_{\text{rep}} - \frac{a}{V_{\text{m}}^{\nu}},$$

with ν being a parameter that can be fitted to experimental data. Analyze this modification with respect to physical plausibility and its effect on the second virial coefficient.

4. Derive an expression for the isochoric heat capacity for the van der Waals equation of state.

5. Calculate the second and third virial coefficients of the Redlich–Kwong equation of state.

6. Discuss Soave's $\alpha(T)$ temperature function, which appears in some cubic equations of state (e.g., Eq. (7.13)): are there extrema? what is the limiting behavior?

7. Derive the so-called optimized SAFT equation of state (OSAFT) by repeating the derivation in Section 7.5.4.5 for a different hard-sphere equation of state, namely Eq. (7.33).

8. Derive an expression for the effective collision diameter of a gas whose molecules have a linear repulsive pair potential with a hard core:

$$u(r) = \begin{cases} \infty & r < \sigma \\ \frac{\epsilon}{\lambda - 1}\left(\lambda - \frac{r}{\sigma}\right) & \sigma \leq r < \lambda\sigma \\ 0 & r \geq \lambda\sigma \end{cases}.$$

9. Derive an expression for the effective collision diameter of a gas whose molecules have a "rectangular" repulsive pair potential with a hard core:

$$u(r) = \begin{cases} \infty & r < \sigma \\ +\epsilon & \sigma \leq r < \lambda\sigma \\ 0 & r \geq \lambda\sigma \end{cases}.$$

Chapter 8

Equations of State for Mixtures

For the calculation of thermodynamic properties, especially phase equilibria, of mixtures, it is evidently necessary to know their equations of state or their fundamental equations. The previous chapter introduced some important equations of state for pure fluids; now we will consider the generalization of these equations to mixtures. This is usually accomplished with mixing rules.

8.1 FUNDAMENTALS

Genuine equations of state for mixtures, i.e., equations designed for mixtures from the beginning, are quite rare. The common approach is to generalize an existing pure-fluid equation of state to mixtures. But accurate generalizations exist for a few model systems only; in the general case, approximations have to be used, the so-called mixing theories.

As shown before, the compression factor of a pure fluid is related to the pair potential and the radial distribution function by [cf. Eq. (7.21)]

$$Z^{(1)} = 1 - \frac{2\pi}{3}\frac{\hat{\rho}}{k_\mathrm{B}T}\int\limits_0^\infty \frac{\mathrm{d}u(r)}{\mathrm{d}r}\, r^3 g(r)\mathrm{d}r. \tag{8.1}$$

Here pairwise additivity of interaction potentials is assumed. The equation holds for spherically symmetric pair potentials; for nonspherical potentials, it would be necessary to integrate over all orientations. The following considerations, however, do not depend on the shape of the pair potential. We can therefore use the simpler equations for the spherical case without a loss of generality.

The analogous expression for an N-component mixture is given by

$$Z^{(N)} = 1 - \frac{2\pi}{3}\frac{\hat{\rho}}{k_\mathrm{B}T}\sum_{i=1}^{N}\sum_{j=1}^{N} x_i x_j \int\limits_0^\infty \frac{\mathrm{d}u_{ij}(r_{ij})}{\mathrm{d}r_{ij}}\, r_{ij}^3 g_{ij}(r_{ij})\mathrm{d}r_{ij}. \tag{8.2}$$

The summations extend overall species present in the mixture. We observe that we now have not only one pair potential, but several, because the strength

High-Pressure Fluid Phase Equilibria. DOI: 10.1016/B978-0-444-56347-7.00008-6

of the interactions between the molecules depends on their species. Similarly, there will be a set of radial distribution functions. Our task is now to somehow relate $Z^{(N)}$ to $Z^{(1)}$.

This is easy for low densities (only), for here a comparison with the virial series,

$$Z^{(N)} = 1 + \frac{B_2}{N_\mathrm{A}}\hat{\rho} + \dots, \tag{8.3}$$

shows that the terms of the double sum correspond to second virial coefficients.[1] Consequently,

$$B_2^{(N)} = \sum_{i=1}^{N}\sum_{j=1}^{N} x_i x_j\, B_{2,ij} \tag{8.4}$$

is the exact equation for mixture second virial coefficients.

In order to evaluate Eq. (8.2) for arbitrary densities, we assume that all pair potentials are conformal, i.e., that all pair potentials have the same mathematical form if expressed with reduced variables. For a pair potential having an attractive well depth ϵ and a collision diameter σ one can set

$$u_{ij}(r) = \epsilon_{ij}\tilde{u}(\tilde{r}) \quad \text{with} \quad \tilde{r} = \frac{r}{\sigma_{ij}}. \tag{8.5}$$

E.g., the Lennard-Jones potential can then be written as

$$\tilde{u}(\tilde{r}) = 4(\tilde{r}^{-12} - \tilde{r}^{-6}), \tag{8.6}$$

and this equation is applied to all interactions in a mixture.

8.2 THE RANDOM MIXING APPROXIMATION

As a first approximation, we now assume that all radial distribution functions in the mixture are the same, $g_{ij}(r) = \bar{g}(r)$. Substituting this into Eq. (8.2) and switching to reduced variables yield

$$Z^{(N)} = 1 - \frac{2\pi}{3}\frac{\hat{\rho}}{k_\mathrm{B}T}\sum_{i=1}^{N}\sum_{j=1}^{N} x_i x_j \epsilon_{ij}\int_0^\infty \frac{\mathrm{d}\tilde{u}(r)}{\mathrm{d}r}\, r^3 \bar{g}(r)\,\mathrm{d}r. \tag{8.7}$$

---

[1] A proof can be obtained by comparing Eqs (7.21) through (7.23).

The integral can be regarded as an expression for a hypothetical pure fluid, and can therefore be replaced by Eq. (8.1):

$$Z^{(N)} = 1 - \sum_{i=1}^{N}\sum_{j=1}^{N} x_i x_j \frac{\epsilon_{ij}}{\bar{\epsilon}}\left[1 - Z^{(1)}\left(\frac{k_B T}{\bar{\epsilon}}, \hat{\rho}\right)\right] \tag{8.8}$$

If the (still undefined) energy parameter of the hypothetical pure fluid is chosen as

$$\bar{\epsilon} = \sum_{i=1}^{N}\sum_{j=1}^{N} x_i x_j \epsilon_{ij} \tag{8.9}$$

the double sum cancels, and the final result is

$$Z^{(N)} = Z^{(1)}\left(\frac{k_B T}{\bar{\epsilon}}, \hat{\rho}\right), \tag{8.10}$$

i.e., the equation of state of the mixture can be expressed by the equation of state of a hypothetical pure fluid.

This (very crude) approximation is called *random mixing approximation*. It owes its name to a combinatorial interpretation: the mole fraction x_i can be regarded as the probability that a selected particle belongs to species i. Then $x_i x_j$ is the probability that a neighbor molecule of an i-molecule will be of species j, and this is therefore the statistical weight of the interaction parameter ϵ_{ij} in Eq. (8.9). However, this reasoning implies that the probabilities of finding molecules in given locations are independent of their nature, and this is a rather dubious assumption.

The random mixing approximation can be used for mixtures of molecules with very similar sizes only, because it is based on the assumption that all g_{ij} and hence also all σ_{ij} are equal.

8.3 ONE-FLUID THEORY

A significant improvement over the random mixing approximation can be achieved if it is assumed that all radial distribution functions $g_{ij}(r)$ of the mixture have a similar shape and can be made to coincide by rescaling the r-axis:

$$g_{ij}(\tilde{r}) = \bar{g}\left(\tilde{r}, \frac{k_B T}{\bar{\epsilon}}, \hat{\rho}\bar{\sigma}^3\right) \tag{8.11}$$

$\bar{g}$ denotes the common radial distribution function, which is defined in terms of reduced units and does not depend on the species.

Insertion of this approximation into Eq. (8.2) gives

$$Z^{(N)} = 1 - \frac{2\pi}{3}\frac{\hat{\rho}}{k_\mathrm{B}T}\sum_{i=1}^{N}\sum_{j=1}^{N} x_i x_j \epsilon_{ij}\sigma_{ij}^3 \int_0^\infty \frac{\mathrm{d}\tilde{u}(\tilde{r})}{\mathrm{d}\tilde{r}}\tilde{r}^3\bar{g}(\tilde{r})\,\mathrm{d}\tilde{r}. \tag{8.12}$$

Now the integral does not contain any functions that depend on the species, and therefore can be treated as a pure-fluid expression. Substitution of Eq. (8.1) gives

$$Z^{(N)} = 1 - \sum_{i=1}^{N}\sum_{j=1}^{N} x_i x_j \frac{\epsilon_{ij}\sigma_{ij}^3}{\bar{\epsilon}\bar{\sigma}^3}\left(1 - Z^{(1)}\left(\frac{k_\mathrm{B}T}{\bar{\epsilon}}, \hat{\rho}\bar{\sigma}^3\right)\right). \tag{8.13}$$

If we now set

$$\bar{\epsilon}\bar{\sigma}^3 = \sum_{i=1}^{N}\sum_{j=1}^{N} x_i x_j \epsilon_{ij}\sigma_{ij}^3, \tag{8.14}$$

the expression for $Z^{(N)}$ can be simplified to

$$Z^{(N)} = Z^{(1)}\left(\frac{k_\mathrm{B}T}{\bar{\epsilon}}, \hat{\rho}\bar{\sigma}^3\right). \tag{8.15}$$

The parameter $\bar{\sigma}$ is usually obtained from

$$\bar{\sigma}^3 = \sum_{i=1}^{N}\sum_{j=1}^{N} x_i x_j \sigma_{ij}^3, \tag{8.16}$$

but the latter equation is arbitrary and not a consequence of the considerations made above.

Equations (8.14) and (8.16) together constitute the one-fluid theory: the equation of state of the mixture can be written as the equation of state of a single hypothetical pure fluid with the potential parameters $\bar{\epsilon}$ and $\bar{\sigma}$.

Generally, any set of mixing rules like Eqs (8.14) and (8.16) that relates the properties of a mixture to those of a hypothetical pure fluid can be called a one-fluid theory. Equations (8.14) and (8.16) constitute the so-called van der Waals one-fluid theory. The name is derived from the fact that the parameters of the van der Waals equation of state are related to the pair potential parameters by

$a \propto \epsilon\sigma^3$ and $b \propto \sigma^3$. The commonly used quadratic mixing rules

$$\begin{aligned} a &= \sum_{i=1}^{N}\sum_{j=1}^{N} x_i x_j a_{ij} \\ b &= \sum_{i=1}^{N}\sum_{j=1}^{N} x_i x_j b_{ij} \end{aligned} \tag{8.17}$$

are therefore equivalent to Eqs (8.14) and (8.16).

The reverse conclusion, that every set of quadratic mixing rules constitutes a van der Waals one-fluid mixing theory, is not true. The relation between the attraction parameter a and the pair potential parameters may differ for some equations of state (if such a parameter can be defined at all), and therefore a quadratic mixing rule may not always be a van der Waals mixing rule in the strict sense, nor an optimal implementation of one-fluid theory derived above.

The hypothesis of the scalability of the radial distribution functions, Eq. (8.11) is not exactly fulfilled even for hard spheres. When molecules of different diameters are mixed, it is easier for the smaller molecules to find places in the gaps between the other molecules than for the larger ones: the accessible volume depends on the sizes of the molecules. This effect can be accounted for by giving the free volume not its Euclidean dimension of 3, but an effective, fractal dimension $\gamma \leq 3$ [82]. The corrected one-fluid mixing rule for ϵ then becomes

$$\bar{\epsilon}\bar{\sigma}^{\gamma} = \sum_{i=1}^{N}\sum_{j=1}^{N} x_i x_j \epsilon_{ij} \sigma_{ij}^{\gamma}. \tag{8.18}$$

The fractal exponent depends on the shape and range of the pair potential. For a square-well pair potential of the range 1.5σ, the exponent is approximately

$$\gamma = 3(1-\xi^2) \quad \text{with} \quad \xi = \frac{\pi}{6}\frac{N_\mathrm{A}}{V_\mathrm{m}}\sum_{i=1}^{N} x_i \sigma_{ii}^3, \tag{8.19}$$

and for Lennard-Jones particles

$$\gamma = 3\left(1 - \frac{1}{4}\xi^{1.5}\right). \tag{8.20}$$

In the limit of low density, $\xi \to 0$, the exponent becomes 3, and the van der Waals mixing rule is recovered.

Because of the density dependence of γ, the fractal mixing rule complicates the calculation of derivatives of the Helmholtz energy and the pressure. It is advisable to use numeric differentiation.

The fractal mixing theory is superior to the van der Waals theory for mixtures of small molecules at high pressures, e.g., for the calculation of gas–gas equilibria.

For nonspherical molecules, it is sometimes advisable to use special mixing theories. The extension of the fractal mixing theory to short chain molecules is

$$\bar{\epsilon}\bar{\sigma}^{\gamma} = \sum_{i=1}^{N}\sum_{j=1}^{N} x_i x_j (s_i s_j)^{\eta-1} \epsilon_{ij} \sigma_{ij}^{\gamma} . \tag{8.21}$$

Here s_i denotes the number of segments per molecule i, and ϵ_{ij} and σ_{ij} are the attraction well depth and collision diameter of a segment, respectively. The exponent η in this mixing rule accounts for the shielding of segments against contacts with other molecules by their neighbor segments; its value is about 0.8 and does not significantly depend on density or composition [158].

Whether one-fluid mixing rules lead to the correct formula for second virial coefficients depends on the equation of state used; it cannot be taken for granted.

8.4 COMBINING RULES

The question remains how to obtain the pair potential parameters ϵ_{ij} and σ_{ij}, or the parameters of the equation of state, e.g., a_{ij} and b_{ij} in the case of the van der Waals equation.

The parameters ϵ_{ii} and σ_{ii}, or a_{ii} and b_{ii}, respectively, are parameters of the pure compounds i, and can therefore be fitted to critical data, vapor pressure data, or other thermodynamic properties.

By analogy, the unlike interaction parameters ϵ_{ij} and σ_{ij}, or a_{ij} and b_{ij}, respectively, for $i \neq j$ should be fitted to appropriate mixture data. Here, however, often the problem occurs that such data are not available in the literature, because the number of possible mixtures exceeds the number of pure compounds.

It is therefore necessary to have ways to predict these parameters, or at least to estimate them. This is achieved by *combining rules*. The most famous set of such rules is called Berthelot–Lorentz rules:

$$\begin{aligned} \epsilon_{ij} &= (1-k_{ij})\sqrt{\epsilon_{ii}\epsilon_{jj}} \\ \sigma_{ij}^3 &= \frac{1-l_{ij}}{2}\left(\sigma_{ii}^3+\sigma_{jj}^3\right) \end{aligned} \tag{8.22}$$

Sometimes, however, this name is also used for rules that compute mean values of $a \propto \epsilon\sigma^3$ and σ. k_{ij} and l_{ij} are “fudge factors”, which can be adjusted to obtain a better representation of experimental data. Particularly, l_{ij} is usually close to zero and therefore often omitted. In this case, the σ^3 mixing rule Eq. (8.16) reduces to

$$\bar{\sigma}^3 = \sum_i^N x_i \sigma_{ii}^3, \tag{8.23}$$

and the covolume mixing rule in Eq. (8.17) to

$$\bar{b} = \sum_i^N x_i b_{ii}. \tag{8.24}$$

For mixtures of nonpolar molecules $|k_{ij}| < 0.2$ is usually found. Polar molecules or molecules of very different sizes may require larger corrections. Large deviations from 0 are often a sign that the equation of state or the mixing theory are not appropriate for the investigated mixture, or that the pure-fluid parameters are wrong.

The justification of the geometric mean rule for ϵ_{ij} is tenuous: London's theory of dispersion forces between two spherical molecules gives an r^{-6} distance dependence for the leading term of the multipole expansion series, and its coefficient contains the geometric mean of the electronic polarizabilities (which are related to the ϵ_{ij}) and the harmonic mean of the ionization energies. Real molecules, however, are not always spherical and can interact by other forces than merely dipolar dispersion. It is therefore not surprising that there is a large number of other combining rules that outperform the Berthelot–Lorentz rules–but usually only for "families" of chemically similar compounds.

The need to fit interaction parameters to experimental data can be avoided by using methods that predict the parameters by means of increment schemes or group contribution methods (see Section 8.8) – but only, because someone else did an extensive amount of parameter fitting during the development of the method.

Prediction of interaction parameters *ab initio* is at present possible for very simple mixtures only, e.g., mixtures of noble gases [159]. The problem is the calculation of dispersion forces, which requires high-level quantum mechanical methods. It is to be expected that future developments in quantum mechanics and computer technology will make this approach feasible. The prediction of dipole moments or parameters of hydrogen bonds is less demanding and can be done even now with a reasonable accuracy.

As it will be necessary for quite a while to determine interaction parameters by fitting to experimental data, we will briefly address some problems associated with this task:

- The task of calculating interaction parameters from a set of experimental $px_1'x_1''T$ data sets may be ambiguous. Figure 8.1 shows a case where the experimental data can be matched by the computed curves either by assuming a slightly distorted regular supercritical phase envelope (curve 1) or by an envelope typical for gas–gas equilibria (curve 2). According to Murphy's

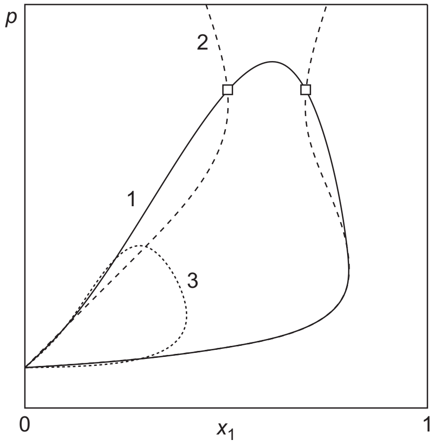

FIGURE 8.1 Schematic illustration of some problems concerning the estimation of interaction parameters. ——, – – , ··········: calculated phase equilibrium boundaries and □: experimental data. See the text for explanation.

laws, the parameter fitting algorithm would probably converge against the unwanted solution.

This problem can evidently be resolved by using more experimental data points, but this is not always an available option.

Similar ambiguities exist if there are coexisting ll and lg phase separations, so that it is not clear[2] to which phases the experimental data belong.

- If the initial guess for the interaction parameters corresponded to curve 3, the phase equilibrium calculation for the indicated data points would fail, and the object function (the function defining the deviation from the experimental values) of the parameter fitting program would not return a pressure or mole fraction deviation that could be minimized.

  In order to overcome this problem, it is usually advisable to start from initial values which correspond to large two-phase regions. But it is difficult to give a general advice in this matter.

- The object function for the parameter estimation from phase equilibrium data can be set up in various ways. If the compositions of coexisting phases are available, the object function can simply be

$$\Delta\mu_i = \mu_i\left(p_{\text{exp}}, T_{\text{exp}}, \vec{x}'_{\text{exp}}\right) = \mu_i\left(p_{\text{exp}}, T_{\text{exp}}, \vec{x}''_{\text{exp}}\right) \overset{!}{=} 0. \tag{8.25}$$

Now minimizing $\Delta\mu_i$ is equivalent to minimizing deviations of logarithms of K factors. For instance, if the experimental mole fractions are $x'_1 = 0.2$ and

---

[2] to the computer.

$x_1'' = 0.999$ (a typical case for vapor–liquid equilibria involving a heavy subcritical and a light supercritical compound), the K factors are $\ln K_1 = 1.6084$ and $\ln K_2 = -6.6846$. A mismatch of x_1' by 0.0001 changes the $\ln K_i$ to $1.6079/-6.6845$, whereas a mismatch of x_1'' gives $1.6085/-6.7900$: in the first case, the deviation is almost negligible, in the second rather massive. A parameter fitting program would therefore try to preferably match the $''$-phase. Whether this is desirable depends on the application; the user should be aware of this.

Alternatively, the object function can be defined as

$$\Delta p = p_{\text{calc}}\left(T_{\text{exp}}, \vec{x}_{\text{exp}}\right) - p_{\text{exp}} \overset{!}{=} 0, \tag{8.26}$$

where p_{calc} is the calculated equilibrium pressure for the given composition and temperature.

Care should be taken to assign weight factors to experimental data points in accordance with their uncertainties.

8.5 *n*-FLUID THEORIES

The one-fluid theory, at least in its basic form, assumes that all $g_{ij}(r)$ can be mapped onto each other by scaling the distance, i.e., that they all have the same height. This is evidently a somewhat dubious assumption.

The three-fluid theory avoids this assumption by calculating the thermodynamic functions for each pair interaction separately:

$$Z^{(N)} = \sum_{i=1}^{N}\sum_{j=1}^{N} x_i x_j Z^{(1)}\left(\frac{k_B T}{\epsilon_{ij}}, \hat{\rho}\sigma_{ij}^3\right) \tag{8.27}$$

Instead of averaging the molecular parameters, the three-fluid theory averages thermodynamic functions of the mixture. For a binary mixture of components 1 and 2, it is therefore necessary to evaluate the equation of state of pure 1, pure 2, and of a hypothetical fluid showing 1–2 interactions only; the name of the theory is derived from this peculiarity.

The assumption of this theory concerning the radial distribution functions is

$$g_{ij}(\tilde{r}) = \bar{g}\left(\frac{k_B T}{\epsilon_{ij}}, \hat{\rho}\sigma_{ij}^3\right). \tag{8.28}$$

The three-fluid theory is exact for second virial coefficients, but of little use at high densities, at least if the components of the mixture differ much in size. If, for instance, a small amount of a low-volatile compound (2) is dissolved in a large amount of a solvent having small molecules (1), it can happen that the reduced state variables of the pure fluid 2, $k_B T/\epsilon_{22}$ and $\hat{\rho}\sigma_{22}^3$, are already deep in the solid domain, and that the fluid equation of state cannot be evaluated for this component, although the solution in solvent 1 is still a fluid.

A compromise that combines the disadvantages of the one- and the three-fluid theory is the two-fluid theory. It assumes that the radial distribution function of the mixture can be represented by arithmetic means of the radial distribution functions of some hypothetic fluids:

$$
\begin{aligned}
g_{ij}(\tilde{r}) &= \frac{1}{2}\left[\bar{g}\left(\tilde{r}, \frac{k_{\mathrm{B}}T}{\epsilon_i}, \hat{\rho}\sigma_i^3\right) + \bar{g}\left(\tilde{r}, \frac{k_{\mathrm{B}}T}{\epsilon_j}, \hat{\rho}\sigma_j^3\right)\right] \\
\text{with } \sigma_i^3 &= \sum_{j=1}^{N} x_j \sigma_{ij}^3 \\
\epsilon_i \sigma_i^3 &= \sum_{j=1}^{N} x_j \epsilon_{ij} \sigma_{ij}^3
\end{aligned}
\tag{8.29}
$$

The resulting recipe for thermodynamic functions is then

$$
Z^{(N)} = \sum_{i=1}^{N} x_i Z^{(1)}\left(\frac{k_{\mathrm{B}}T}{\epsilon_i}, \hat{\rho}\sigma_i^3\right). \tag{8.30}
$$

Like the three-fluid theory, the two-fluid theory can become unreliable at high densities. It does not become exact at low densities.

In contrast to three- and two-fluid theory, one-fluid theory can always be used, and is therefore the preferred method.

8.6 THE MEAN-DENSITY APPROXIMATION

An interesting superposition of one-fluid and three-fluid theory is the *mean-density approximation*. Like one-fluid theory, it scales the radial distribution functions along the distance axis, but is does not assume that their peaks have the same heights:

$$
\begin{aligned}
g_{ij}(\tilde{r}) &= g\left(\tilde{r}, \frac{k_{\mathrm{B}}T}{\epsilon_{ij}}, \hat{\rho}\bar{\sigma}^3\right) \\
\text{with } \bar{\sigma}^3 &= \sum_{i}^{N}\sum_{j}^{N} x_i x_j \sigma_{ij}^3 \\
Z^{(N)} &= \sum_{i}^{N}\sum_{j}^{N} x_i x_j \frac{\sigma_{ij}^3}{\bar{\sigma}^3} Z^{(1)}\left(\frac{k_{\mathrm{B}}T}{T}, \hat{\rho}\bar{\sigma}^3\right).
\end{aligned}
\tag{8.31}
$$

The mean-density approximation involves averaging over parameters as well as thermodynamic functions. Like the one-fluid theory, it can always be applied. In contrast to the one-fluid theory, however, the mean-density approximation reduces to the exact mixing rule for second virial coefficients at low densities.

Some modern equations of state apply the superposition to their attraction term only. An example is the SPHCT equation, Eq. (7.43), which we write here as:

$$Z = Z^{\text{rep}} - \frac{za}{V_{\text{m}}(V_{\text{m}}+b)\left(e^{\epsilon/2k_{\text{B}}T}-1\right)} \tag{8.32}$$

with the mixing rules

$$\begin{aligned} a &= \sum_i^N \sum_j^N x_i x_j a_{ij} \\ a_{ij} &= b_{ij}\left(e^{\epsilon_{ij}/2k_{\text{B}}T}-1\right). \end{aligned} \tag{8.33}$$

This is practically a mean-density approximation.

Although the mean-density approximation avoids some theoretical shortcomings of the one-fluid theory, it is often found to be slightly inferior in practical applications. The reason for this is that the structure of fluids at high densities (in the liquid state) is mainly determined by repulsive forces. Then the one-fluid theory, which ignores the influence of the ϵ_{ij} on the peak heights of the radial distribution functions, is closer to reality than the mean-density approximation, which exaggerates the influence.

Of course, it is possible to construct (density-dependent) mixing rules, which interpolate between the mean-density approximation at low and medium densities and one-fluid theory at high densities [78].

8.7 ADVANCED THEORY

The mixing theories in the previous sections assume that the radial distributions functions for the various interactions in mixtures are similar, and that they can be transformed into each other by relatively simple mathematical operations. This assumption is plausible and even produces good results, but a closer investigation shows that it is not really true.

For a few model fluids, a statistical thermodynamic analysis proved possible. So there is an extension of the hard-sphere equation of state to mixtures by Mansoori *et al.* [160] :

$$Z = 1 + \frac{a_1\xi + (2-a_1+3a_2)\xi^2 - a_2\xi^3}{(1-\xi)^3} \tag{8.34}$$

The coefficients in the numerator are defined as

$$\begin{aligned} &a_1 = \frac{3\bar{r}^*\bar{s}^*}{\bar{v}^*}+1 \quad a_2 = \frac{(\bar{s}^*)^3}{(\bar{v}^*)^2}-1 \\ &\text{with } \bar{r}^* = \sum_{i=i}^N x_i\sigma_i \quad \bar{s}^* = \sum_{i=i}^N x_i\sigma_i^2 \quad \bar{v}^* = \sum_{i=i}^N x_i\sigma_i^3, \end{aligned} \tag{8.35}$$

and the reduced density $\xi = (\pi/6)\mathcal{N}\bar{v}^*/V$. The auxiliary properties $\bar{r}^*$, $\bar{s}^*$, and $\bar{v}^*$ can be regarded as measures of the average curvatures, surfaces, and volumes of the molecules, respectively. For spheres of equal size, this equation reduces to the Carnahan–Starling equation of state, Eq. (7.28).

For mixtures of hard convex bodies, Eq. (7.55) can still be used, but the nonsphericity parameter has to be obtained from

$$\alpha = \frac{\bar{r}^*\bar{s}^*}{\bar{v}^*}$$
$$\text{with } \bar{r}^* = \sum_{i=i}^{N} x_i r_i^* \quad \bar{s}^* = \sum_{i=i}^{N} x_i s_i^* \quad \bar{v}^* = \sum_{i=i}^{N} x_i v_i^*, \tag{8.36}$$

where r_i^*, s_i^*, and v_i^* are the mean curvature, the surface, and the volume of the species i, respectively.

Neither the equation of state for hard-sphere mixture nor the one for hard-convex-body mixtures reduce to one of the simple mixing rules.

Many advanced statistical theories of fluids, such as the perturbation theory of polar fluids or SAFT, come with their own set of mixing rules; it is usually better to use these instead of one-fluid theory.

8.8 G^E-BASED MIXING RULES

A sensitivity analysis of calculations of low-pressure vapor–liquid equilibria would show that their outcome mostly depends on the quality with which equations of state and mixing rules describe the liquid phase. The description of the gas phase, which is close to the ideal-gas state, is not influenced much by the model.

As there exists a huge amount of experimental data for low-pressure vapor–liquid equilibria, many empirical or semiempirical models for the nonideality of liquid mixtures have been developed in the past, usually formulated as equations for the excess Gibbs energy, G^E.

Huron and Vidal proposed an interesting approach that could integrate the knowledge stored in the G^E models into equations of state. First of all, they inserted a cubic equation of state into the equation of the Gibbs energy of a mixture, Eq. (4.18), and carried out the necessary integrations. Doing this for the van der Waals equation with its original mixing rules gives

$$\begin{aligned}\frac{G_\mathrm{m}}{RT} &= \sum_{i=1}^{N} x_i\left(G_{\mathrm{m},i}^{\ominus}(T) + RT\ln x_i\right) + \frac{pV_\mathrm{m}}{RT} - 1\\ &\quad - \ln\frac{V_\mathrm{m}-b}{V_\mathrm{m}^{\ominus}} - \frac{a}{V_\mathrm{m}RT}.\end{aligned} \tag{8.37}$$

Expanding with an ideal-gas term, $\pm \ln pV_{\mathrm{m}}^{\ominus}/RT$, and subtracting the pure-fluid terms as described by Eq. (4.44) leads to

$$\begin{aligned}\frac{G^{\mathrm{E}}}{RT} = &+\frac{pV_{\mathrm{m}}}{RT} - \sum_{i=1}^{N} x_i \frac{pV_{\mathrm{m},i}}{RT} \\ &\underbrace{-1+\sum_{i=1}^{N} x_i}_{=0} - \ln\frac{p(V_{\mathrm{m}}-b)}{RT} + \sum_{i=1}^{N} x_i \ln\frac{p(V_{\mathrm{m},i}-b_{ii})}{RT} \\ &-\frac{1}{RT}\left(\frac{a}{V_{\mathrm{m}}} - \sum_{i=1}^{N} x_i \frac{a_{ii}}{V_{\mathrm{m},i}}\right).\end{aligned} \tag{8.38}$$

In the limit of high pressure, the van der Waals equation gives

$$\lim_{p\to\infty} V_{\mathrm{m}} = b \qquad \lim_{p\to\infty} V_{\mathrm{m},i} = b_{ii}. \tag{8.39}$$

Furthermore,

$$\lim_{p\to\infty} \frac{p(V_{\mathrm{m}}-b)}{RT} = \lim_{p\to\infty}\left(1-\frac{a(V_{\mathrm{m}}-b)}{V_{\mathrm{m}}^2 RT}\right) = 1, \tag{8.40}$$

and hence the high-pressure limit of the excess Gibbs energy is

$$\lim_{p\to\infty} \frac{G^{\mathrm{E}}}{RT} = -\left(\frac{a}{bRT} - \sum_{i=1}^{N} x_i \frac{a_{ii}}{b_{ii}RT}\right). \tag{8.41}$$

Conversely, if a G^{E} model for the liquid phase is available (and it is assumed that liquids are sufficiently close to the highest possible density), then

$$a = b\left(\sum_{i=1}^{N} x_i \frac{a_{ii}}{b_{ii}} - G^{\mathrm{E}}(\vec{x})\right) \tag{8.42}$$

is a mixing rule for a that will give the equation of state the composition dependence of the G^{E} model.

For other cubic equations of state than the van der Waals equation the result is the same, except for one numerical constant:

$$a = b\left(\sum_{i=1}^{N} x_i \frac{a_{ii}}{b_{ii}} - \frac{1}{\lambda} G^{\mathrm{E}}(\vec{x})\right). \tag{8.43}$$

For example, for the Redlich–Kwong equation a value of $\lambda = \ln 2$ results.

The Huron–Vidal mixing rule has seen numerous modifications. Michelsen proposed shifting the reference pressure from infinity to 0, which results in an additional term [161, 162]:

$$a = b\left[\sum_{i=1}^{N} x_i \frac{a_{ii}}{b_{ii}} - \frac{1}{\lambda}\left(G^{\mathrm{E}}(\vec{x}) + RT\sum_{i=1}^{N} x_i \ln\frac{b}{b_{ii}}\right)\right] \tag{8.44}$$

Huang and Sandler pointed out that a formulation in terms of the Helmholtz energy can help to avoid inconsistencies [163]:

$$a = b\left(\sum_{i=1}^{N} x_i \frac{a_{ii}}{b_{ii}} - \frac{1}{\lambda}A^{\mathrm{E}}(\vec{x})\right) \tag{8.45}$$

Naturally, at some point in history the numerical constant λ was made composition dependent.

G^{E}-based mixing rules can "cooperate" with a large number of G^{E} models, thus providing an enormous flexibility to computation. In particular, they can be used in connection with group contribution models. These are increment schemes that write G^{E} as a sum of contributions of a relatively small number of atom groups making up the molecules; this gives the models some predictivity.

On the other hand, the basic assumption of G^{E}-based models – that it is sufficient to represent the liquid phase well – is not always true: in high-pressure fluid phase equilibria, the coexisting phase may have intermediate densities.

Also, it should be noted that for many cubic equations of state the ratio a/b is proportional to the characteristic temperature, T^*. The leading term of the G^{E}-based mixing rules therefore corresponds to a random-mixing theory, the weakest of the theory-based mixing rules. This may create problems with mixtures of molecules of different sizes, but small excess Gibbs energies.

8.9 ANYTHING GOES?

The number of existing mixing theories and their variants is large. This is due to the need to perform thermodynamic calculations for complex mixtures – mixtures of nonpolar with polar or even associating compounds, perhaps with widely differing molecular sizes – for which the "standard mixing theories" are not sufficient.

It might seem logical to deal with a phenomenon like hydrogen bonding with an association theory, but in the past it was often considered more practical to "tweak" an existing simple mixing theory by adding a few more parameters or terms than to develop a molecular mixing theory.

But the designer of a new mixing rule is not totally free: there are some restrictions to observe, e.g.:

- The equation of state of a mixture must reduce, at very low densities, to a quadratic mixing rule for the second virial coefficients of the pure components.
- The residual properties of a mixture must not change if one of its components is split into two identical subspecies. This is known as the Michelsen–Kistenmacher test.

Mixing theories not obeying these restrictions may still be useful for correlating thermodynamic data, but can be expected to give inferior results when data must be predicted. The reader is advised to consult the literature for more insight into mixing rule design [114, 164].

8.10 FUZZY COMPONENTS

Many mixtures occurring in nature or technical applications are multicomponent mixtures of a special kind:

- Their number of components is *huge*,
- but nobody cares about particular components, at least not about all of them.

An example are polymers: a batch of polyethylene with a degree of polymerization between 10,000 and 12,000 evidently contains 2001 different chemical compounds, but the amount of the polymer species with chain length 11,049 is probably not relevant. Moreover, the calculation of the solubility of this polymer batch in a solvent would constitute a phase equilibrium problem with 2002 unknowns ...

Perhaps the problem could be solved – theoretically, but in such cases even the input data, the amounts of all polymer species, are not known accurately, and the huge numerical effort would be wasted. Evidently, a simpler approach is desirable.

Another example is mixtures of compounds that can occur in many isomeric forms. Sometimes it is permissible to ignore the chemical complications.

In such cases where the mixture components can or should not be distinguished, i.e., if their definition gets fuzzy, a different approach is necessary. The proper modeling of fuzzy components is an art about which many publications have been written. Here we outline two important approaches to the problem.

8.10.1 Continuous Thermodynamics

In continuous thermodynamics, it is assumed that the thermodynamic properties of the components of a multicomponent mixture can be related to a single parameter. For polymers, this might evidently be the chain length; for other systems, the molar mass or the normal boiling point can be good choices. We name this parameter s, with $0 \le s < \infty$, and observe that it can always be made dimensionless with a suitable normalizing factor. Continuous thermodynamics then treats this parameter as a real-valued (instead of integer-valued) entity; this idea goes back to Raetzsch and Kehlen [165] and to Cotterman *et al.* [166, 167]. Then the set of mole fractions defining the composition becomes a distribution function,

$$\vec{x} \rightarrow x(s) \qquad \sum_{i=1}^{N} x_i \rightarrow \int_{0}^{\infty} x(s)\,\mathrm{d}s = 1, \tag{8.46}$$

and the parameters of the equation of state become functions,

$$a_i \rightarrow a(s) \qquad b_i \rightarrow b(s), \tag{8.47}$$

if we assume a van der Waals type equation of state.

Consequently, the one-fluid covolume mixing rule (Eq. (8.24)) must be rewritten as

$$\bar{b} = \sum_{i=1}^{N} b_i x_i \rightarrow \int_{0}^{\infty} b(s)x(s)\,\mathrm{d}s \tag{8.48}$$

and the mixing rule for the energy parameter in (Eq. (8.17)) as

$$\bar{a} = \sum_{i=1}^{N}\sum_{j=1}^{N} a_{ij}x_i x_j \rightarrow \int_{0}^{\infty}\int_{0}^{\infty} \sqrt{a(s)a(s')}x(s)x(s')\,\mathrm{d}s\,\mathrm{d}s', \tag{8.49}$$

where we have now assumed the Berthelot–Lorentz rules with $k_{ij} = 0$ for simplicity.

For many practical applications, however, this approach is too simplistic. For the case of a polymer dissolving in a (mixed) solvent, one cannot expect the solvent to be described properly with a similar, continuous $x(s)$ distribution as the polymer. Instead, here a semicontinuous approach is better, where the constituents of the solvent are treated as discrete compounds, and only the polymer as a continuous compound [168], i.e., the mole fractions are

$$\begin{gathered} x_1, x_2, \ldots, x_N \longleftrightarrow x(s) \\ \sum_{i=1}^{N} x_i = x_\mathrm{d} \longleftrightarrow \int_{s_0}^{\infty} x(s)\,\mathrm{d}s = 1 - x_\mathrm{d}, \end{gathered} \tag{8.50}$$

where N is the number of the discrete components making up the solvent, x_d the sum of their mole fractions, and s_0 the minimal s value of the continuous distribution, e.g., the minimal chain length. Then the equations for the parameters of the equation of state are

$$\begin{aligned}\bar{a}=&\sum_{i=1}^{N}\sum_{j=1}^{N}x_i x_j a_{ij}+2\sum_{i=1}^{N}x_i\sqrt{a_{ii}}\int_{s_0}^{\infty}\sqrt{a(s)}x(s)\,\mathrm{d}s\\&+\int_{s_0}^{\infty}\int_{s_0}^{\infty}\sqrt{a(s)a(s')}\,\mathrm{d}s\,\mathrm{d}s'\end{aligned}\tag{8.51}$$

and

$$\bar{b}=\sum_{i=1}^{N}x_i b_{ii}+\int_{s_0}^{\infty}b(s)x(s)\,\mathrm{d}s.\tag{8.52}$$

These equations are examples only; the expressions for the averaged parameters depend on the equation of state and the mixing rules.

A popular distribution function is the Γ distribution,

$$x(s)=\frac{(s-s_0)^{\alpha-1}}{\beta^{\alpha}\Gamma(\alpha)}\exp\left(-\frac{s-s_0}{\beta}\right),\tag{8.53}$$

where $\Gamma(\alpha)$ denotes Euler's generalized factorial function. The exponential distribution, which is also frequently used,

$$x(s)=\frac{1}{\beta}\exp\left(-\frac{s-s_0}{\beta}\right),\tag{8.54}$$

can be obtained from the Γ distribution by setting $\alpha=1$.

The mean value and the standard deviation of the Γ distribution are

$$\bar{s}=s_0+\alpha\beta\quad\sigma=\beta\sqrt{\alpha}.\tag{8.55}$$

Once the averaged parameters of the equation are known, the calculation of most thermodynamic properties can proceed as usual. For entropy-related properties the ideal-gas terms have to be modified [cf. Eq. (4.19)], too:

$$\begin{aligned}A_{\mathrm{m}}(V_{\mathrm{m}},T)=&\sum_{i=1}^{N}x_i\left(G_{\mathrm{m},i}^{\ominus}(T)+RT\ln x_i\right)\\&+\int_{s_0}^{\infty}x(s)\left(G_{\mathrm{m}}^{\ominus}(T,s)+RT\ln x(s)\right)\mathrm{d}s-RT-\int_{V_{\mathrm{m}}^{\ominus}}^{V_{\mathrm{m}}}p(V_{\mathrm{m}},T;\bar{a},\bar{b})\,\mathrm{d}V_{\mathrm{m}}\end{aligned}\tag{8.56}$$

If the shape of the $x(s)$ distribution is constant, it is thus possible to treat a phase equilibrium calculation of a semicontinuous mixture practically as a calculation for an $(N+1)$-component discrete mixture; only the parameters of the $x(s)$ distribution have to be adjusted so that the balance

$$\int_{s_0}^{\infty} x(s)\,\mathrm{d}s = 1 - x_\mathrm{d} \tag{8.57}$$

is maintained for both phases. An example is the calculation of the vapor–liquid equilibrium of a polymer dissolved in a mixed solvent: the polymer remains almost entirely in the liquid phase, and only the mole fractions of the solvent differ between the phases.

A more difficult case is a phase equilibrium, where the polymer occurs in both phases with different distribution functions. Here it would be necessary to optimize the distribution function parameters, e.g., by minimizing the overall Gibbs energy. The – admittedly rather complicated – derivation of the equilibrium conditions can be found in the original literature [165–167].

8.10.2 Pseudocomponents

The integrals appearing in the equation of (semi)continuous thermodynamics will usually have to be evaluated numerically, which means that they are replaced by weighted sums of the integrand functions, computed for some representative s values.

It is therefore only consequential to do away with the complicated formalism of continuous thermodynamics and to use discrete thermodynamics for a set of representative s values. These s values are then chosen not for optimal efficiency of the numerical integration, but with some regard for chemical information and engineering needs.

It is thus common practice to regard light natural gas as a mixture of methane, ethane, …, hexane, and "C_{7+}". The latter is a so-called pseudocomponent, a heavy alkane with a properly chosen molar mass that represents the heavy alkane content of the gas.

The customary formulation of the pseudocomponent approach makes use of the fact that, for many cubic equations of state, the reduced critical properties are fixed numbers (cf. Sections C.1 ff.). The a and b parameters of these equations can then be written as

$$a = \Omega_a \frac{T_\mathrm{c}^2}{p_\mathrm{c}} \alpha(T) \quad b = \Omega_b \frac{T_\mathrm{c}}{p_\mathrm{c}} \beta(T), \tag{8.58}$$

where Ω_a and Ω_b are numerical constants which depend on the equation of state only. Consequently, the effective critical properties of a pseudocomponent can be obtained by

$$\begin{aligned}\frac{T_{\mathrm{c,ps}}^2}{p_{\mathrm{c,ps}}} &= \sum_i \sum_j x_i x_j \frac{T_{\mathrm{c},i} T_{\mathrm{c},j}}{\sqrt{p_{\mathrm{c},i} p_{\mathrm{c},j}}} \sqrt{\alpha_i(T)\alpha_j(T)} \\ \frac{T_{\mathrm{c,ps}}}{p_{\mathrm{c,ps}}} &= \sum_i \sum_j x_i x_j \left(\frac{T_{\mathrm{c},i}}{p_{\mathrm{c},i}} \beta_i(T) + \frac{T_{\mathrm{c},j}}{p_{\mathrm{c},j}} \beta_j(T) \right).\end{aligned} \tag{8.59}$$

If desired, corrections factors k_{ij} and l_{ij} can be included. The summations run over all components that make up the pseudocomponent.

These two equations are by no means the only way to set up a pseudocomponent. More recipes – particularly rational recipes for arbitrary equations of state – can be found in the literature[3] [169].

The effective critical data of the pseudocomponent are then used to obtain the parameters of the equation of state, and then the calculation of phase equilibria can proceed as usual. The drawback, of course, is that the internal composition of the pseudocomponent is fixed, and cannot change upon evaporation or condensation anymore. Using pseudocomponents therefore introduces a systematic error.

But representing complex mixtures by pseudocomponents is sometimes the only way to achieve a moderately accurate thermodynamic description. A typical example is crude oil, which contains not only *n*-alkanes, but also isomers, unsaturated, cyclic, and aromatic compounds, as well as asphaltenes, whose chemical constitution is still discussed.

Although pseudocomponents have been introduced here (and are mostly used) as a last-resort tool to deal with otherwise intractable mixtures, they are more important than one might think at a first glance. For what is a chemical component? Even an innocent noble gas like argon is a mixture of isotopes (mostly ^{40}Ar, ^{38}Ar, and ^{36}Ar), which have slightly different thermodynamic properties. Treating argon as a single component is therefore a kind of lumping.

Other cases of inadvertent lumping are ignoring conformations and stereoisomers. For example, butane is a mixture of two conformers that are produced by the rotation of the CH_3 groups around the central C–C bond. The conformers cannot be isolated, at least not in the fluid state, hence they need not to be considered in fluid phase equilibria, but they would have to be accounted for in *ab initio* calculations. Another example is the refrigerant R124 (1-chloro-1,2,2,2-tetrafluoroethane), which is chiral and therefore comes as a mixture of two enantiomers.

---

[3] The process of combining a set of substances into a single pseudocomponent is sometimes referred to as “lumping”.

8.11 PROBLEMS

1. Splitting one of the components of a mixture into two identical subspecies should not affect the residual properties of the mixture. This is known as the Michelsen–Kistenmacher test. Prove that one-fluid theory with quadratic or linear mixing rules [Eqs (8.14) and (8.23)] passes the test.

2. One might be tempted to improve one-fluid theory by letting the k_{ij} in the Berthelot–Lorentz rules, Eq. (8.22), depend on composition, e.g., $k_{ij} = k_{ij,0} + k_{ij,1}(x_i - x_j)$. Does such a mixing theory pass the Michelsen–Kistenmacher test?

3. Does the van der Waals equation of state reduce to the physically correct mixing rule for second virial coefficients, Eq. (8.4), in the low-density limit if it is combined with
   - **a.** the density-dependent mixing rule, Eq. (8.18); for the van der Waals equation use $a \propto \epsilon\sigma^3$, $b \propto \sigma^3$, $\gamma = 3[1 - (b/(4V_\mathrm{m}))^2]$.
   - **b.** a quadratic mixing rule using volume fractions, $\varphi_i = x_i b_{ii}/(\sum_k x_k b_{kk})$.

4. It has been suggested to add more flexibility to one-fluid mixing rules by making the k_{ij} in the Berthelot–Lorentz rules, Eq. (8.22), pressure-dependent: $k_{ij} = k_{ij,0} + k_{ij,1}p$. Use this combining rule in the expression for the Helmholtz energy of the van der Waals model and discuss the feasibility of this approach.

5. The commonly used mixing rule, Eq. (8.23), implies the combining rule $\sigma_{ij}^3 = \frac{1}{2}(\sigma_{ii}^3 + \sigma_{jj}^3)$ for the hard-sphere diameter. From geometric consideration, one might conclude that $\sigma_{ij} = \frac{1}{2}(\sigma_{ii} + \sigma_{jj})$ ought to be preferred. Which combining rule is better? (Note: This problem should be solved numerically.)

Chapter 9

Global Phase Diagrams

Chapter 2 dealt with the experimentally known phase diagram classes. But as not all possible experiments have been performed, yet, the list of phase diagram classes is necessarily incomplete.
This chapter looks at ways of discovering phase diagram classes systematically, as well as their relation to the equation of state.

9.1 THE CONCEPT

In Chapter 2.2, an overview over the experimentally known phase diagram classes of binary fluid mixtures has been given. Even for the relatively simple case of two-component mixtures, the number of classes is surprisingly large. But can we be sure that we have seen all possible phase diagram classes?

We cannot! Until now, not all possible combinations of substances have been investigated, yet. Moreover, for many systems that have been studied experimentally, the experiments did not cover all relevant pressure, temperature, or concentration ranges. It is therefore possible that phase diagram classes have been overlooked – perhaps even classes which might be relevant for technical processes.

For example, Gibbs' phase rule allows the coexistence of four fluid phases for a binary mixture. None of the classes listed in Chapter 2.2 contains such a quadruple state lllg, but it cannot be ruled out. Certainly, the chemical engineer designing a liquid-extraction unit would appreciate knowing whether there are two or three liquid phases in this device.

Another fact that calls for a more systematic investigation of phase diagram classes is the observation that for *families*[1] of binary mixtures, i.e., binary systems where one component is always the same, there are often systematic trends for the phase diagram classes. For instance, the {carbon dioxide + n-alkane} family moves from class I {CO_2 + CH_4} through class I-A {CO_2 + C_2H_6} to class III {CO_2 + $C_{16}H_{34}$}. In a similar way, the {CF_4 + n-alkane} family runs

---

[1] This term was coined by G. M. Schneider, who performed systematic studies of several families.

High-Pressure Fluid Phase Equilibria. DOI: 10.1016/B978-0-444-56347-7.00009-8

from class II via III_m to III. This leads to the questions why one system of a family belongs to one class and a chemically very similar system to another and how the transition between these classes takes place.

Evidently, such a transition cannot be studied experimentally for a family of binary systems,[2] for here the phase diagram class is a fixed property, and the transition from one family member to the next one is necessarily a discontinuous one (e.g., $\{CO_2 + C_nH_{2n+2}\}$ to $\{CO_2 + C_{n+1}H_{2n+4}\}$). Only with quasibinary mixtures, one can approach the transitional phase diagrams between classes experimentally by adjusting the C_nH_{2n+2} to $C_{n+1}H_{2n+4}$ ratio.

How can we then obtain an overview over all possible phase diagram classes or, in other words, over the *global phase behavior*? It is evident that the experimental work has to be complemented by computation.

When a phase diagram of a mixture is computed, this mixture is characterized by a set of parameters for its equation of state and mixing theory. In the previous sections, we have treated these parameters as fixed properties of the mixture; in this chapter, we will treat them as variables.

Already at the begin of the 20th Century, van Laar undertook systematic studies of the phase behavior of binary mixtures, using the van der Waals equation of state as thermodynamic model [170]. Instead of calculating large sets of px or Tx diagrams – a too arduous task in the age of logarithmic tables and mechanical calculators – van Laar focused on the computation of critical curves and three-phase coexistence curves. He presented pT projections of his results, similar to the ones shown in Chapter 2.2, and discussed the changes of the topology when he varied the parameters of the equation of state. An example of his work is shown in Fig. 9.1. As each critical point in these diagrams had to be calculated by hand, the number of such diagrams in his publication was not very large.

A major step beyond the work of van Laar became possible after the advent of electronic computers in the 1960s. Scott and van Konynenburg introduced *global phase diagrams* as tools for the systematic study of fluid phase diagrams [171]. Global phase diagrams are maps in which each location corresponds to a set of molecular parameters; the indicated property is the phase diagram class resulting for this parameter set. With other words, global phase diagrams visualize the parameter combinations that lead to class I, class II, etc. behavior. Examples are given below.

Now even for the simplest of all models, the van der Waals equation of state in combination with one-fluid mixing rules, there are six model parameters. One might be tempted to generate a global phase diagram by simply trying out parameter combinations, but this would not be feasible: the approach amounts to a mapping of a six-dimensional space and would therefore require much time, especially as the recognition of phase diagram classes cannot be reliably done by a computer. Moreover, such a brute-force mapping would miss all phase

---

[2] In (polydisperse) polymers, the average molar mass provides an additional degree of freedom.

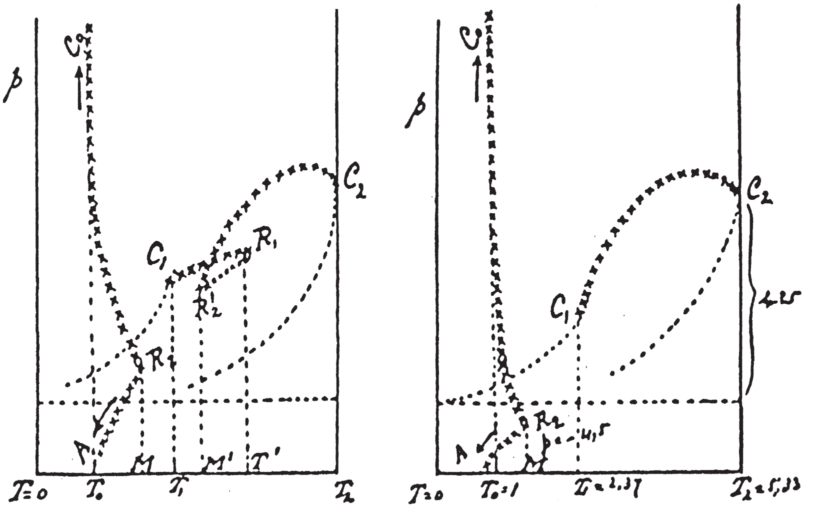

FIGURE 9.1 Phase diagrams of a binary mixtures of classes IV and II calculated by van Laar. Crosses: binary critical points (stable as well as unstable). *(Reprinted from van Laar [170] © 1905, with permission from the Royal Dutch Academy of Sciences.)*

diagram classes whose parameter ranges are smaller than the increments of the search method.

In order to make the construction of global phase diagrams feasible, two steps are required, namely a reduction of the dimensionality of the search space and a more intelligent search strategy.

9.2 THE COORDINATES OF GLOBAL PHASE DIAGRAMS

We have already mentioned in the previous section that, for the construction of global phase diagrams, we will treat the parameters of the equation of state as variables that can be chosen freely. If a simple two-parameter equation of state, e.g., the van der Waals equation, is combined with the one-fluid mixing theory, the total number of parameters of a binary mixture is six. The parameters are the attraction parameters a_{11} and a_{22} of the two pure components, their covolume parameters b_{11} and b_{22}, and furthermore the cross interaction parameters a_{12} and b_{12}.

Now the assignment of a phase diagram to a class depends on the connectivities and relative positions of critical curves and three-phase curves only, not on absolute pressure and temperature values. For the discussion of phase behavior, it is therefore not necessary to consider all the six parameters a_{ij}, b_{ij}; instead, it is sufficient to consider properly defined ratios of these parameters. This brings the number of the coordinates of the global phase diagram down to four.

In principle, the definitions of the parameter ratios are arbitrary. Here, we use a set of definitions which is suitable for all two-parameter equations of state. They include the original definitions of van Konynenburg and Scott [171].

Instead of using the attraction parameters a_{ij}, which may have different physical interpretations for different equations of state, we here use the attraction density

$$d_{ij} = T^*_{ij}\frac{b_{ij}}{b_{ii}b_{jj}}. \tag{9.1}$$

The characteristic temperature is a measure of the pair potential well depth, $T^*_{ij} = \epsilon_{ij}/k_{\mathrm{B}}$; it is related to the attraction parameter by $a_{ij} \propto b_{ij}RT^*_{ij}$ for the van der Waals equation of state (cf. Section C.1) or $a_{ij} \propto b_{ij}R(T^*_{ij})^{1.5}$ for the Redlich–Kwong equation of state (cf. Section C.2). The dimensionless parameter ratios that serve as coordinates of the global phase diagrams are as follows:

$$\zeta = \frac{d_{22}-d_{11}}{d_{22}+d_{11}} \tag{9.2}$$

$$\xi = \frac{b_{22}-b_{11}}{b_{22}+b_{11}} \tag{9.3}$$

$$\lambda = \frac{d_{11}-2d_{12}+d_{22}}{d_{11}+d_{22}} \tag{9.4}$$

$$\eta = \frac{b_{11}-2b_{12}+b_{22}}{b_{11}+b_{22}} \tag{9.5}$$

The parameters ζ and ξ represent differences of the pure-component parameters, whereas the parameters λ and η are related to the cross interaction parameters.

The global parameters ζ and ξ can have values between -1 and $+1$. λ and η must lie between $-\infty$ and $+1$; however, values below -1 are physically unrealistic and usually need not be considered.

Rearrangement of Eq. (9.5) gives

$$b_{12} = (1-\eta)\frac{b_{11}+b_{22}}{2}, \tag{9.6}$$

i.e., η describes the deviation of b_{12} from the arithmetic mean of the pure-component parameters and is therefore equivalent to the $\mathfrak{l}_{12}$ parameter in the Berthelot–Lorentz combining rules. A similar expression relates d_{12} to λ.

Of course, four dimensions are still too much to be visualized in a diagram. Therefore, only two-dimensional cross sections of the four-dimensional global phase diagram are calculated, of which the $\zeta\lambda$ cross section is perhaps the most prominent one. In this cross section, the covolume parameters are kept constant, and thus only the effect of the variation of the attraction parameters on the phase behavior is visualized. The influence of molecular sizes is then studied by calculating a series of $\zeta\lambda$ cross sections for various values of ξ.

The global parameter η is usually set to zero. Few publications have ever considered the influence of η, and then for very small deviations from zero only [172]. This is in accordance with practical experience, for correlations of experimental data with equations of state usually give b_{12} values very close to the arithmetic mean of b_{11} and b_{22}.

9.3 BOUNDARY STATES

Instead of calculating pT phase diagrams at a large number of grid points of the global parameter space (and risking to overlook phase diagram classes which happen to lie between the grid points), it is much more efficient to search directly for the boundaries between phase diagram classes.

9.3.1 Double Critical Endpoints

The comparison of the various phase diagram classes intuitively leads to the insight that they can be transformed into each other by distortions or displacements of critical curves. For example, class III$_\mathrm{m}$ ($1^C W 1^Z$) can be transformed to class IV ($2^P l$) by moving the major critical curve[3] toward the three-phase curve. The phase diagram in which the critical curve touches ("osculates") the three-phase curve represents a transition state between classes III$_\mathrm{m}$ and IV (see Fig. 9.2). If the critical curve is moved further downward so that it intersects[4] the three-phase curve, we obtain class IV behavior.

According to this view, the two three-phase curves of class IV are actually two parts of the same three-phase curve; the critical curve "interrupts" the three-phase curve, and this leads to a small miscibility region between the two critical endpoints.

The point in the transitional phase diagram in Fig. 9.2 where the critical curve and the three-phase curve touch is a *double critical endpoint* (DCEP). The reason for this names becomes clear if we approach the transition from the class IV phase diagram: here, we have a three-phase curve with a gap, which represents a region of miscibility. The two branches of the three-phase curve terminate in critical endpoints. If we vary the model parameters in a suitable way, the gap shrinks and the two critical endpoints approach each other, until they coincide in the DCEP. Beyond the transition phase diagram, the three-phase curve as well as the critical curve are continuous.

---

[3] The one originating at the critical point of the less volatile substance, 1^C.

[4] The three-phase curve in this projection in fact represents a set of three curves, one for each phase, lying on top of each other in the pT projection and spanning a three-phase plane between them.

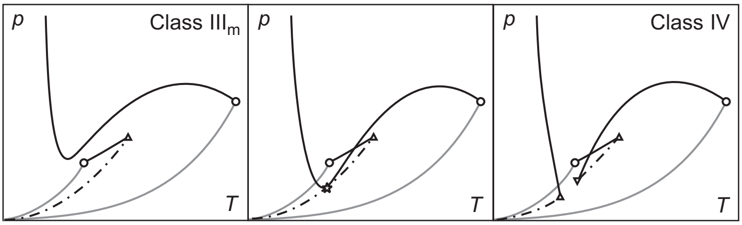

FIGURE 9.2 Hypothetical transition from class III$_\mathrm{m}$ to class IV phase behavior via a phase diagram with a double critical endpoint.

The mathematical conditions of a DCEP can be readily derived, considering the facts that, at such a point,

- there is a two-phase equilibrium between a critical phase (c) and a noncritical phase (n), so that the chemical potentials of the components in these phases have to be equal,
- the critical conditions for the former phase must be fulfilled,
- and finally the slopes of the critical curve and the three-phase curve must be equal:

$$\begin{aligned} \mu_i^\mathrm{c} &= \mu_i^\mathrm{n} \quad i = 1,2 \\ G^\mathrm{c}_{(2x)} &= G^\mathrm{c}_{(3x)} = 0 \\ \frac{S^\mathrm{c}_{(2x)}}{V^\mathrm{c}_{(2x)}} &= \frac{S^\mathrm{c}_\mathrm{m} - S^\mathrm{n}_\mathrm{m} - (x_1^\mathrm{c} - x_1^\mathrm{n}) S^\mathrm{c}_{(x)}}{V^\mathrm{c}_\mathrm{m} - V^\mathrm{n}_\mathrm{m} - (x_1^\mathrm{c} - x_1^\mathrm{n}) V^\mathrm{c}_{(x)}} \end{aligned} \tag{9.7}$$

In the last equation, the left-hand side represents the slope of the critical curve [Eq. (5.103)] and the right-hand side the slope of the three-phase curve [Eq. (5.142)].

9.3.2 Tricritical Points

Another transition can be constructed between classes I (1^P) and V (2^P). In this case, the three-phase curve of class V shrinks and eventually, at the transition state, vanishes in one point (see Fig. 9.3), the so-called *tricritical point* (TCP). Beyond this state, we have class I behavior.

This transition should not be confused with the DCEP transition discussed above: in both cases, an upper and a lower critical endpoint coincide, and two parts of a critical curve merge. But in the TCP transition, the two endpoints are connected by a three-phase curve, which shrinks to zero length, whereas in the DCEP transition, the two endpoints are on different three-phase curve branches.

The transition from class II to class IV phase behavior ($1^P l \rightarrow 2^P l$) involves a phase diagram with a tricritical point, too.

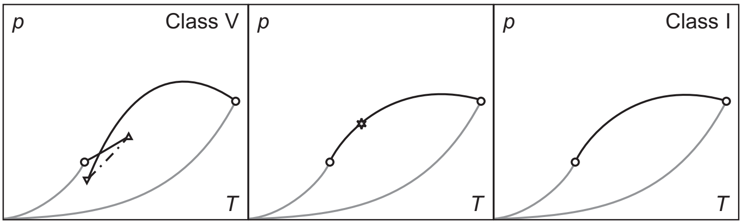

FIGURE 9.3 Hypothetical transition from class V to class I phase behavior via a phase diagram with a tricritical point.

Incidentally, the rational nomenclature of phase diagram classes helps to recognize tricritical boundary states: A tricritical point indicates a contraction of a three-phase curve within a critical-curve sequence. Hence, all phase diagram transitions of the type $(i)^X \to (i-1)^X$ involve a tricritical point, regardless of what the segment count i and the sequence target X are, or how many other critical curves are present. In contrast to this, a DCEP involves a change of the targets of critical-curve sequences, e.g., $1^C 1^Z \to 2^P$ (III → IV).

In order to derive the mathematical criteria for a tricritical point, we must remember that the general criterion for phase stability is that the Helmholtz energy density function, $\Psi(\vec{\rho})$, must be convex (using the symbology of Section 5.8). For pure fluids, this is equivalent to state that the molar Helmholtz energy, $A_\mathrm{m}(V_\mathrm{m})$, must be convex. In the Taylor series of the Helmholtz energy around a reference volume V_m,

$$\begin{aligned} A_\mathrm{m}(\delta V_\mathrm{m}) &= A_\mathrm{m}(0) + A_{(1V)}\delta V_\mathrm{m} + \frac{1}{2}A_{(2V)}(\delta V_\mathrm{m})^2 + \frac{1}{6}A_{(3V)}(\delta V_\mathrm{m})^3 \\ &\quad + \frac{1}{24}A_{(4V)}(\delta V_\mathrm{m})^4 + \dots, \end{aligned} \tag{9.8}$$

the first two terms have no relevance for the convexity. The quadratic term ensures local convexity if $A_{(2V)} = -(\partial p/\partial V_\mathrm{m}) > 0$. But if $A_{(2V)} = 0$, i.e., at a critical point, convexity can only be achieved if $A_{(3V)} = 0$, too,[5] and $A_{(4V)} > 0$. In general, convexity requires that the first non-zero derivative (disregarding the first two terms of the series) is of even order and positive.

Consequently, the criteria for a stable critical point of a pure fluid are $A_{(2V)} = A_{(3V)} = 0$, while $A_{(4V)} > 0$. A higher-order critical point with $A_{(4V)} = A_{(5V)} = 0$ is forbidden by the phase rule.

Figure 9.4 gives a graphical representation of the situation. The subcritical isotherms in the pV_m diagram show van der Waals loops, i.e., they have a minimum and a maximum with an unstable region in between. The extrema in the pV_m diagram correspond to inflection points in the $A_\mathrm{m}V_\mathrm{m}$ diagram ($A_{(2V)} = 0$).

---

[5] The cubic term of the Taylor expansion is an odd function of δV_m and thus necessarily causes concave behavior, if it dominates the series.

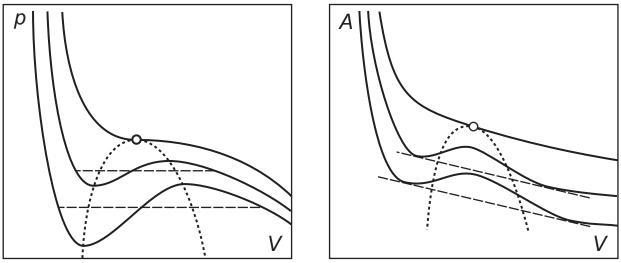

FIGURE 9.4 Schematic pressure-volume and Helmholtz energy-volume diagrams for a pure fluid. ——: isotherms, ·········: spinodals, ○: critical point.

At the critical point, these two inflection points coincide. In order to have convex behavior, $A_{(3V)}$ must be zero and $A_{(4V)}$ positive.

The situation is similar for binary mixtures. Here, the convexity criterion for $\Psi(\vec{\rho})$ translates into one for $G_\mathrm{m}(x_1)$ at constant pressure and temperature. In analogy to the pure-fluid case, local convexity requires that, if $G_{(2x)}=0$ at a binary critical point, $G_{(3x)}$ must be zero and $G_{(4x)}$ must be positive.

If, however, $G_{(4x)}$ vanishes, too, we have a critical point of higher order. Diffusion stability then requires that $G_{(5x)}$ must be zero, too, and the first non-zero derivative must be of even order and positive. In particular, the mathematical conditions for a tricritical point are

$$G_{(2x)} = G_{(3x)} = G_{(4x)} = G_{(5x)} = 0 \quad G_{(6x)} > 0. \tag{9.9}$$

The name “tricritical point” is derived from the fact that, at such a point, three phases become identical. But here it is important to pay attention to a detail in Fig. 9.3: The shrinking three-phase curve is of the type $\mathsf{l}_1\mathsf{l}_2\mathsf{g}$. Its upper critical endpoint is $\mathsf{l}_1\mathsf{l}_2{=}\mathsf{g}$, and its lower critical endpoint $\mathsf{l}_1{=}\mathsf{l}_2\mathsf{g}$. An experiment following the three-phase curve would start at low temperature with an lg two-phase state and show, upon heating, the liquid phase splitting into two phases. Then, there would be three phases in the vessel until, at higher temperatures, the gas phase and one of the liquid phases would merge. Exactly at the tricritical point, the sequence of phases would be

$$\mathsf{lg} \;\rightarrow\; \mathsf{l}_1{=}\mathsf{l}_2{=}\mathsf{g} \;\rightarrow\; \mathsf{l}_1\mathsf{l}_2,$$

i.e., the tricritical point occurs as the transition state between two different two-phase equilibria (see Fig. 9.5). Such a point is called an *asymmetric tricritical point*, and this is the usual case in binary fluid phase equilibria (as far as such points can be reached experimentally at all).

In contrast to this, a *symmetric tricritical point* corresponds to the sequence (see Fig. 9.6)

$$\mathsf{l}_1\mathsf{l}_2\mathsf{g} \;\rightarrow\; \mathsf{l}_1{=}\mathsf{l}_2{=}\mathsf{g} \;\rightarrow\; \mathsf{f},$$

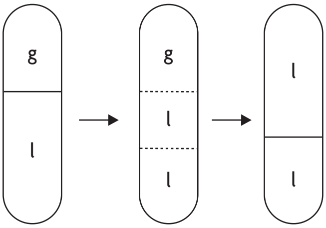

FIGURE 9.5 Schematic representation of the phases in an experiment passing through an asymmetric tricritical point.

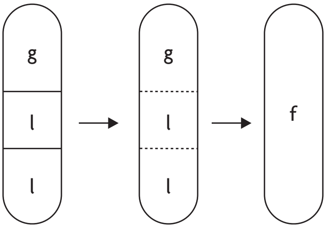

FIGURE 9.6 Schematic representation of the phases in an experiment passing through a symmetric tricritical point.

Such a point, however, requires additional mathematical conditions and will be discussed in Section 9.4 (van Laar point).

Now the question arises whether boundary states like tricritical points or double critical endpoints states are consistent with Gibbs' phase rule, Eq. (2.1). The phase rule is the result of a balance between the number of variables and the number of equations restricting the thermodynamic degrees of freedom. The form of the phase rule usually given in textbooks is a specific form for the assessment of "real" phase and chemical reaction equilibria.

As mentioned at the beginning of Chapter 2, at the critical point of a pure fluid there is one phase and one component, yet the number of degrees of freedom is zero because of the additional constraints $A_{(2V)} = A_{(3V)} = 0$, and therefore, the point is invariant. For a tricritical point or a double critical endpoint of a binary mixture, the number of additional constraints is four, and therefore, the number of the degrees of freedom is -1. Consequently, these states cannot be reached experimentally with binary mixtures. They can and have been reached, however, with ternary (particularly quasi-binary) mixtures.

If we compute a global phase diagram, we treat (at least) two parameters of the underlying thermodynamic model as free variables. This brings the number of the degrees of freedom to $+1$. We can therefore conclude that tricritical states and double critical endpoints can appear in global phase diagrams; in two-dimensional global phase diagrams, they form curves.

The evaluation of convexity criteria can be extended to higher-order critical points, e.g., tetracritical points. While such a point does not exist in real binary systems, it is theoretically necessary to explain transitions between various types of global phase diagrams, as we will see later in this chapter.

9.3.3 Border Azeotropy

As will be discussed in Section 9.4, it is possible that the mole fraction of azeotropes depends on molecular size ratios only, but not on pressure or temperature. In such a case, the transition from class I (1^P) to the azeotropic class I-A ($1^P A$) or from II ($1^P l$) to II-A ($1^P A l$) is represented by a phase diagram in which the azeotropic curve is at $x_1^{\mathrm{az}} = 0$ or $x_1^{\mathrm{az}} = 1$. The mathematical conditions for this boundary state are therefore

$$\begin{aligned} \mu_i^{\mathrm{l}} &= \mu_i^{\mathrm{g}}, \quad i = 1,2 \\ x_i^{\mathrm{l}} &= x_i^{\mathrm{g}} = x_i^{\mathrm{az}} \\ x_i^{\mathrm{az}} &\to 0 \quad \text{or} \quad x_i^{\mathrm{az}} \to 1 \end{aligned} \tag{9.10}$$

If x_1^{az} is not constant along the azeotropic curve, this criterion gives different results depending on whether one wants to have the begin or the end of the azeotropic curve on the border.

9.3.4 Critical Azeotropic Endpoints

Class III-A ($1^C 1^Z A$) can be transformed into the heteroazeotropic class III-H by letting the critical azeotrope move to the critical endpoint of the minor (1^Z) critical curve. The result is a critical azeotropic endpoint. Its mathematical conditions are a combination of those of a critical azeotrope and a critical endpoint:

$$\begin{aligned} A^{\mathrm{c}}_{(2V)} &= A^{\mathrm{c}}_{(3V)} = A^{\mathrm{c}}_{(Vx)} = 0 \\ \mu_i^{\mathrm{c}} &= \mu_i^{\mathrm{n}} \quad i = 1,2 \end{aligned} \tag{9.11}$$

9.3.5 Zero-Kelvin Endpoints

Several phase diagram classes differ from each other by the presence or absence of a liquid–liquid critical curve only, which is indicated by an l symbol in the rational class symbol, e.g., classes I and II ($1^P l$ and 1^P). In order to define the boundary between these classes, we start with a class II diagram and let the three-phase curve shrink. The miscibility improves, and the critical endpoint – and with it the ll critical curve – moves to lower temperatures. The transition to class I is achieved when the critical endpoint is at zero temperature and zero pressure; then the ll critical curve coincides with the pressure axis. Beyond this diagram, no ll critical curve exists anymore in the phase diagram.

The mathematical conditions of this so-called *zero-Kelvin endpoint* are those of a regular binary critical point, solved in the limit of absolute zero, $p, T = 0$.

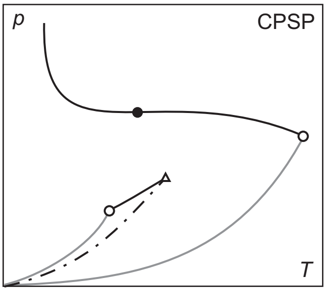

FIGURE 9.7 Phase diagram containing a critical step point, an inflection point with zero slope.

For cubic equations without temperature-dependent attraction terms, such as the original van der Waals equation, simple analytic solutions exist. For other equations, the conditions have to be solved numerically.

9.3.6 Critical Pressure Step Points

In addition to the major boundary states at which the topology, i.e. the connectivity, of critical curves is changed, there are also boundaries at which merely their shapes change. An example is a phase diagram with a critical curve having a horizontal inflection point, as shown in Fig. 9.7. Such a diagram marks the boundary between phase diagrams with no extremum and phase diagrams with two extrema, e.g., classes III and $\mathrm{III_m}$. This special critical point has been called *critical pressure step point* (CPSP) by Boshkov [173]. Its mathematical conditions are

$$\begin{aligned} G_{(2x)} = G_{(3x)} &= G_{(2xT)} = 0 \\ G_{(4x)}G_{(2x2T)} - (G_{(3xT)})^2 &= 0. \end{aligned} \tag{9.12}$$

These conditions can be obtained with the so-called *bifurcation method* developed by Boshkov [173].

Two other boundary states related to the appearing or disappearing of extrema in critical curves are the degenerated critical pressure maximum or minimum (dCPM) and the critical pressure end maximum/minimum (CPEM). At the dCPM, the extremum is located at $T \to 0$ (see Fig. 9.20), whereas at a DCEM, the extremum coincides with a critical endpoint.

There are many more boundary states related to the shapes of critical curve; their mathematical conditions can be derived by the same method.

In order to solve the mathematical conditions for the boundary states, the derivatives of the Gibbs energy and the volume must be expressed in terms of derivatives of the Helmholtz energy, which then can be directly calculated from an equation of state. This transformation can be accomplished by means of Jacobi determinants, as described in Section 4.4.

For the calculation of tricritical curves, $G_{(5x)}$ is required. It can be obtained from the expression for $G_{(4x)}$, Eq. (5.55), either numerically or analytically.

The analytical expression, however, is too long to be listed here. The reader interested in the analytical expressions for $G_{(5x)}$ and $G_{(6x)}$ is referred to the literature [174].

9.4 GLOBAL PHASE DIAGRAMS FOR SPECIFIC MODELS

9.4.1 The van der Waals Equation of State

The first global phase diagram was calculated by van Konynenburg and Scott for the van der Waals equation of state [26, 171]. In their pioneering work, they investigated two different values for the covolume size ratio only, namely $\xi = 0$ and $\xi = \frac{1}{3}$, both for $\eta = 0$.

The $\lambda\zeta$ global phase diagram for equal-sized molecules, $\xi = 0$, is shown in Fig. 9.8. As here all covolumes have the same values, the diagram has a mirror symmetry with respect to the λ axis.

For equal-sized molecules, $\xi = \eta = 0$, the van der Waals model gives constant, temperature-independent azeotropic compositions. Applying the conditions for border azeotropy for this special case leads to a very simple result, namely $a_{12} = a_{ii}, i = 1, 2$ or, expressed with global parameters, $\lambda = \pm\zeta$: the boundaries between azeotropic and non-azeotropic classes are the diagonals of the $\lambda\zeta$ global phase diagram. In Fig. 9.8, the triangular regions above and

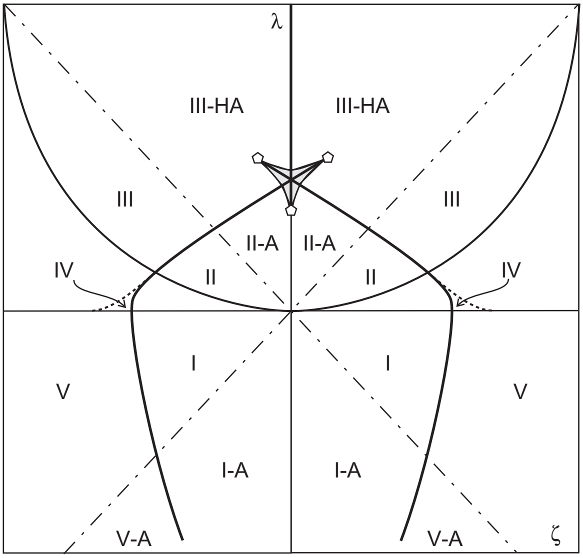

FIGURE 9.8 Global phase diagram for the van der Waals equation of state for $\xi = \eta = 0$. ——: tricritical curves, ··········: double critical endpoint curves, —·— : border azeotropy boundary, ⬠: tricritical endpoints, and shaded area: "shield region". The zero-Kelvin endpoint curve coincides with the abscissa.

below the origin are the domains of the azeotropic phase diagram classes, whereas the triangular regions to the left and the right side are the domains of the non-azeotropic classes.

It should be noted that the azeotropic systems in the lower part of the diagram ($\lambda < 0$) show negative azeotropy, i.e., for the van der Waals model, class I-A has negative azeotropy, whereas class II-A has positive azeotropy. In the global phase diagram, there is no class I with positive azeotropy. Consequently, all mixtures exhibiting positive azeotropy are bound to undergo a liquid–liquid separation at low temperatures. In reality, this phase separation is often obscured by solid–fluid equilibria.

For the van der Waals equation of state, the condition of the zero-Kelvin boundary state results in a very simple expression, namely $\lambda = 0$, i.e. the arithmetic-mean rule for a_{12}. Consequently, systems with positive λ show a liquid–liquid immiscibility, whereas for negative values of λ only vapor–liquid critical curves, but no liquid–liquid critical curves are present.[6]

Figure 9.8 contains three tricritical curves, i.e., loci of phase diagrams containing tricritical points. The first one of these curves forms an arc running from a tricritical endpoint at approximately $\zeta = -0.1$, $\lambda = 0.43$ via $\zeta = 0.56$, $\lambda = 0$ to $\zeta = 0.4$, $\lambda = -0.75$. The second tricritical curve is the mirror image of the first one. The region between these tricritical curves is the locus of phase diagram classes with continuous vapor–liquid critical curves (rational symbol 1^P), such as classes I and II. Outside that region, all phase diagram classes have interrupted vapor–liquid critical curves, e.g., class V or class III (rational symbols other than 1^P).

A third tricritical curve coincides with the ordinate. It starts at about $\lambda = +0.4$ and runs upward.

There are also three double critical endpoint curves (DCEPs), one coinciding (in this graphical representation) with the vertical tricritical curve, the other two following the tricritical curves very closely and turning away from them only when approaching $\lambda = 0$. The little triangles formed between the tricritical curves, the DCEP curves, and the abscissa are domains of class IV.

Figure 9.8 clearly shows domains of the classes I to V with some subdomains pertaining to the presence or absence of azeotropy and heteroazeotropy. It does not show domains for classes VI to VIII: These classes cannot be calculated with the van der Waals equation of state.

A detailed analysis shows that the tricritical curve and the DCEP curve intersect at the top of the class IV domain (see Fig. 9.9). This intersection point is called a *van Laar point*. It evidently combines the properties of a tricritical point and a double critical endpoint, and it represents a symmetrical tricritical point.

---

[6] In class V phase diagrams, there is an llg three-phase curve, and therefore liquid–liquid immiscibility is involved. But there is no liquid–liquid critical curve running to the jamming point (rational symbol: l).

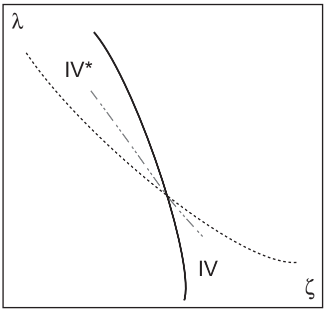

FIGURE 9.9 Global phase diagram in the vicinity of the van Laar point. ——: tricritical curve, ·········: double critical endpoint curve, and —·—: mathematical double point curve.

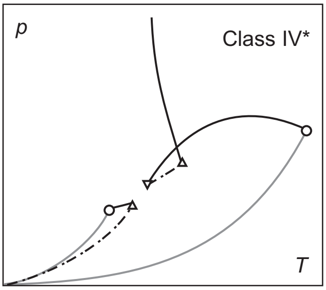

FIGURE 9.10 *pT* phase diagram of class IV*$(= 2^C 1^Z)$.

Beyond the van Laar point, there exists an extremely narrow domain of a new phase diagram class, IV* $(2^C 1^Z)$ [171, 175]. Figure 9.10 shows its *pT* phase diagram. It has not been found experimentally yet, but its existence is necessary for topological reasons. Incidentally, this is an example for the "discovery" of a new phase diagram class from an analysis of boundary curves, which could never have been accomplished by a brute-force grid search of global parameter space.

The triangular area between the three tricritical endpoints in Fig. 9.8 is called *shield region* because of its shape. It contains domains of phase diagram classes with four-phase equilibria **lllg**. Moreover, in the shield region, the azeotropic boundary curves cross these domains and give rise to a very confusing pattern of domains of rather complicated phase diagram classes; Figure 9.11 may serve as an example (class II-A*, rational symbol $1^P AlnQ$). There is not sufficient space here to list all of them. The interested reader is referred to the original literature [32, 171, 176, 177].

Figure 9.12 shows the $\lambda\zeta$ global phase diagram from the original publication of van Konynenburg and Scott [26]. It contains the positive-ζ half of the total global phase diagram only; as stated before, the negative-ζ half is symmetric to it.

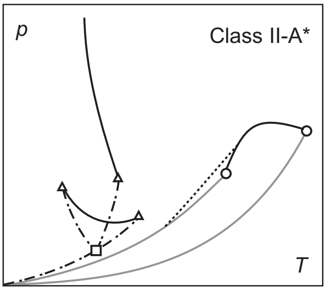

FIGURE 9.11 pT phase diagram of class II-A* ($= 1^P AlnQ$).

There are some auxiliary curves in Fig. 9.12 which deserve attention: For many mixtures of nonpolar compounds, the Berthelot–Lorentz combining rules Eq. (8.22) provide reasonable approximations for the cross interaction parameters. For the attraction parameter of the van der Waals equations, these rules yield

$$a_{12} = (1 - k_{12})\sqrt{a_{11}a_{22}}. \tag{9.13}$$

For the "ideal case" $k_{12} = 0$, the cross attraction parameter becomes the geometric mean of the pure-component parameters. Converting this to global parameters results in

$$\lambda = 1 - \sqrt{1 - \zeta^2}, \tag{9.14}$$

i.e., the geometric-mean rule corresponds to a semicircle in the $\lambda\zeta$ global phase diagram, with the center at $\zeta = 0$, $\lambda = 1$. This semicircle is shown as a dotted-dashed curve in Fig. 9.12 and labeled "g.m." We would expect the loci of real systems to lie in the vicinity of this curve.

Incidentally, an arithmetic mean instead of a geometric mean for the attraction cross parameter would result in a horizontal line at $\lambda = 0$ (labeled "a.m." in the global phase diagram). Except for a special case to be discussed later, however, the arithmetic mean represents a hypothetical condition only.

Van Konynenburg and Scott could show that, for the {methane + n-alkane} family, the global phase diagram Fig. 9.12 qualitatively agrees with experimental observations. With increasing chain length of the n-alkane, the difference in attraction between methane and the n-alkanes increases, and hence ζ increases, too. While the {methane + pentane} system belongs to class II, {methane + hexane} is class IV and {methane + heptane} is class III. This corresponds to the sequence that one can read off Fig. 9.12.

The shield region lies far away from the geometric-mean curve. This gave rise to the view that it is merely a mathematical figment without physical reality. We defer the discussion of this view to Section 9.4.7.

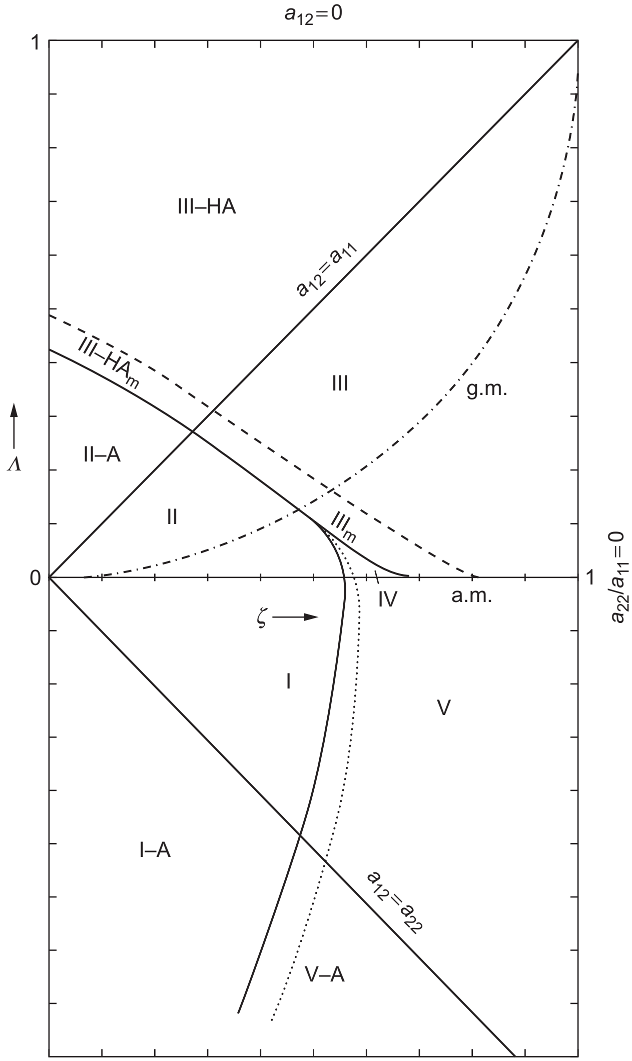

FIGURE 9.12 Global phase diagram for the van der Waals equation of state for $\xi=\eta=0$. See the text for an explanation of the curves.*(Reprinted from van Konynenburg and Scott [26, 171], © 1980, with permission from the Royal Society.)*

There are some additional curves in Fig. 9.12, such as the dashed curve running parallel to the double critical end point curve. That curve is the *critical pressure step point boundary* [173]. It separates the region of phase diagram class III$_m$ from the regions of class III and the related azeotropic subclasses.

The dotted curve taking a similar course as the tricritical curve is a so-called *mathematical double point curve* or *double critical cusp curve*. At such a point, two different critical curves swap branches. This curve runs through the van Laar point, and it is only here that a mathematical double point is stable. Therefore, the other parts of that curve cannot be observed experimentally. Nevertheless, the mathematical double point is very useful for the interpretation of global phase diagrams in general [178].

The main features of the global phase diagram obtained for the van der Waals equation of state are very much the same for other equations of state. The global phase diagrams for other equations of state differ mostly in the quantitative locations of the boundary curves. Qualitative differences, i.e., different arrangements of domains or even new domains, occur in some special regions only, which will be discussed below.

As one might expect, the global phase diagram becomes asymmetric if the mixture is asymmetric with respect to the covolumes of the components. Such diagram is shown in Fig. 9.13 for $\xi = \frac{1}{3}$, i.e., for mixtures where the covolume of component 2 is twice the covolume of component 1. Obviously the curves are distorted, but the general features of the global phase diagram are the same as for the symmetric case, $\xi = 0$.

A topological change is the splitting of the border azeotropic curves (the "diagonal" lines). For mixtures of molecules of different sizes, the azeotropic composition varies along the azeotropic curve. Consequently, there is now a low-temperature limit (border azeotropy at $T \rightarrow 0$) and a high-temperature limit.

In the rectangle formed by the four intersecting border azeotropy boundary curves, a region of double azeotropic behavior has been found [171]. This means that there are mixtures which have both a pressure maximum azeotrope and a pressure minimum azeotrope in some of their isothermal phase diagrams (cf. Figs. 2.34–2.35). Such a phase behavior has been found experimentally for the system {benzene + hexafluorobenzene} [14].

9.4.2 The Redlich–Kwong Equation of State

The second cubic equation of state that was analyzed with respect to its global phase behavior is the Redlich–Kwong (RK) equation of state [93, 175]. Its attraction term has a different density dependence than the van der Waals equation. The major difference, however, consists in the temperature dependence ($\propto T^{-0.5}$) of the attraction term. This affects the zero-Kelvin endpoint curve separating systems with and without liquid–liquid critical curves. While this curve coincides with the abscissa for the van der Waals equation, it turns to negative λ for the RK equation (see Fig. 9.14). As a consequence, the DCEP curve can cross the abscissa; it ends at a negative λ value.

A qualitative difference between the global phase diagram of the van der Waals and the RK equations of state is the appearance of a fourth tricritical curve at large negative ζ values for mixtures of molecules of different sizes. With increasing ξ, the termination point of this curve approaches the regular tricritical curve. For sufficiently large size ratios, the two tricritical curves exchange branches, as can be seen in Fig. 9.14 for $\xi = 0.3457$.

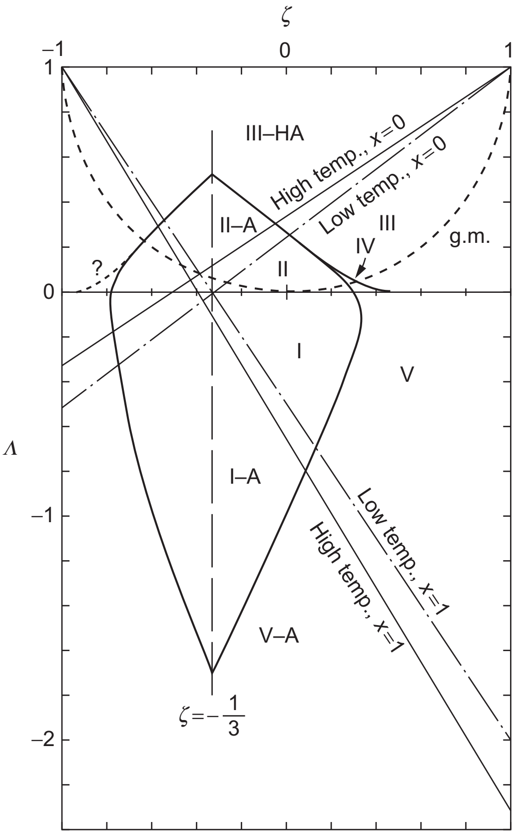

FIGURE 9.13 Global phase diagram for the van der Waals equation of state for $\xi = \frac{1}{3}$ and $\eta = 0$. *(Reprinted from van Konynenburg and Scott [171], © 1980, with permission from the Royal Society.)*

As a result of this exchange, the tricritical curves and the DCEP curves accompanying them demarcate a domain that has later been named *sword region* because of its shape. It contains domains of several new phase diagram classes which can be regarded as extensions of class IV; one of them even contains a fluid quadruple point lllg (see Fig. 9.15). An in-depth analysis of the rather complex phase behavior in this region requires the definition of several new boundary curves.

One might think that the sword region lies so far below the geometric-mean curve that it cannot be reached experimentally, but it will be shown in Section 9.4.7 that this may not be true.

Kolafa calculated global phase diagrams for the RK equation, using reduced coordinates similar to the global parameters ζ and ξ, and keeping the cross interaction parameter k_{ij} constant [179]. In this work, a large variety of azeotropic phase diagrams was found.

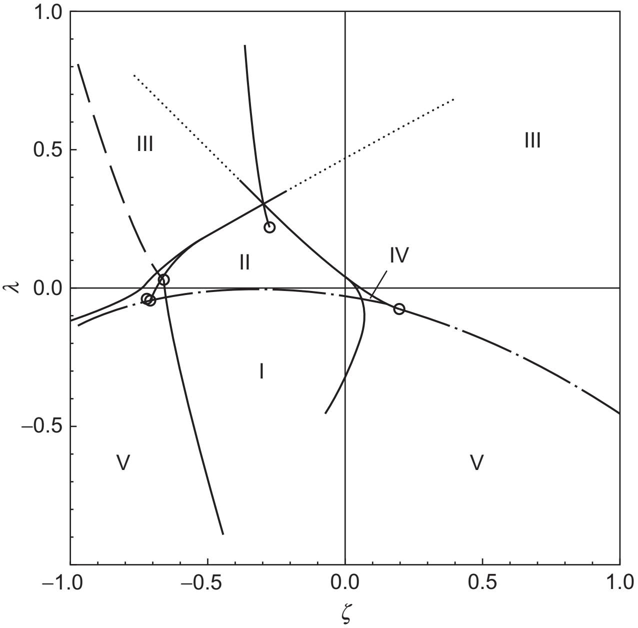

FIGURE 9.14 Global phase diagram for the Redlich–Kwong equation of state for $\xi = 0.3457$ and $\eta = 0$. —·—·— : zero-Kelvin endpoint curve, ··········: metastable parts of tricritical curves, and ○: tricritical endpoint. *(Reprinted from Deiters and Pegg [175], © 1989, with permission from the American Institute of Physics.)*

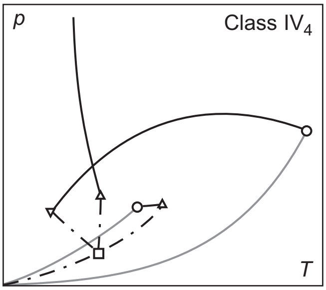

FIGURE 9.15 pT phase diagram of class IV_4 ($= 1^{Q}1^{Q}l$).

9.4.3 The Carnahan–Starling–Redlich–Kwong Equation of State

For $\xi = 0$, the global phase diagram of an equation of state consisting of the Carnahan–Starling hard-sphere repulsion and the Redlich–Kwong (RK) attraction term (CSRK) looks quite similar to that of the RK equation [180]. The region of the systems with continuous vapor–liquid critical curves, i.e., the region enclosed by the tricritical curves, is smaller, but topologically the

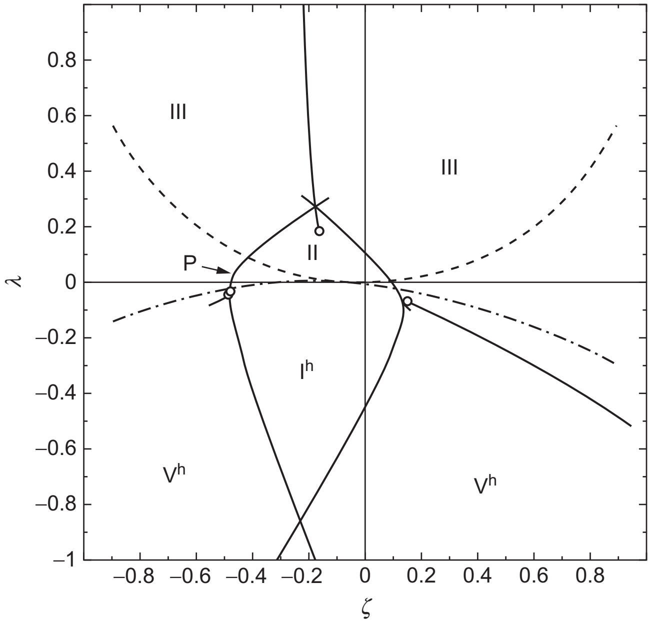

FIGURE 9.16 Global phase diagram for the CSRK equation of state for $\xi = 0.2$ and $\eta = 0$. I^{h} $(= 1^P u)$, V^{h} $(= 2^P u)$: classes with an ll immiscibility at high pressures. The short curve marked "P" is calculated with the DCEP criteria. But here the critical curve is not osculating (touching) the three-phase curve, but crossing it with an inflection point. *(Reprinted from Kraska and Deiters [180], © 1992, with permission from the American Institute of Physics.)*

diagrams are the same. Similar to the RK equation, additional tricritical curves appear when ξ deviates from 0. While for the RK equation only one new tricritical curve has been found for molecules differing very much in size, and then only on the left side of the global phase diagram, for the CSRK equation these new tricritical curves appear already at about $\xi = 0.2$ and on both sides (Fig. 9.16).

The additional tricritical curve on the right side emerges at a ξ value somewhat below 0.2 and spans almost the total range of ζ at $\xi = 0.2$. At $\xi = 0.2552$, the new tricritical curve touches the regular tricritical curve; beyond this ξ value, the connectivity of the tricritical curves changes.

The transitional phase diagram at which this exchange of tricritical curve branches takes place contains a *tetracritical point*. Such a point is similar to a van Laar point (stable mathematical double point), at which the connectivity of binary critical curves changes; here, however, the change takes place at a higher level, namely the connectivity of tricritical curves.

The three-dimensional diagram shown in Fig. 9.17 gives an overview over the evolution of the new tricritical curve on the right side of the diagram with increasing size ratio ξ.

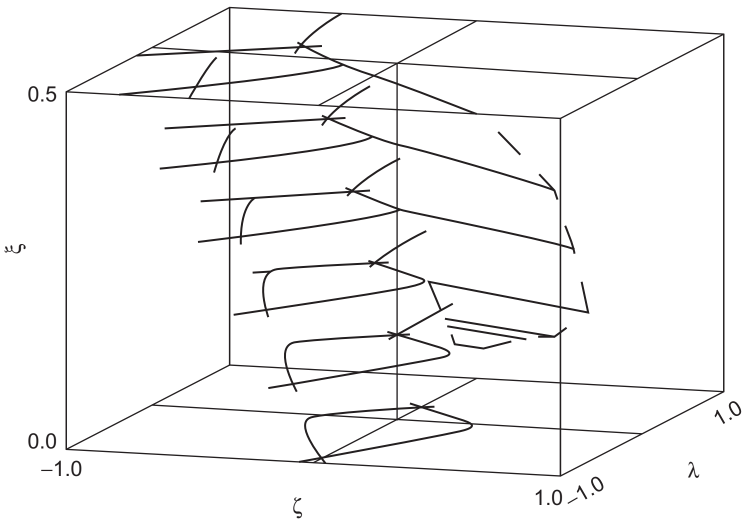

FIGURE 9.17 Three-dimensional global phase diagram for the CSRK equation of state for $\eta = 0$. Only the tricritical curves are shown [181].

The change of the connectivity at a tetracritical point gives rise to several phase diagram classes with four coexisting phases. This has implications for cases where experimental data are fitted for systems having parameters in the vicinity of a tetracritical point. From a more general perspective, a phase diagram with a tetracritical point represents a boundary between two topologically different global phase diagram sections.

9.4.4 The Carnahan–Starling–van der Waals Equation of State

In order to separately investigate the influence of the attraction and the repulsion term on the global phase behavior, it is interesting to combine the Carnahan–Starling hard-sphere repulsion term with the van der Waals attraction term [182]. This combination is called the Carnahan–Starling–van der Waals (CSvdW) equation of state. While the general topology of the global phase diagram is quite similar to that of the equations of state treated above, there is a new feature that had not been found for van der Waals type equations of state before, namely the appearance of liquid–liquid closed-loop immiscibility regions (rational nomenclature: curve types n, u, or ll).

This phenomenon, which gives rise to class VI and class VII behavior, has usually been attributed to the existence of directional forces between the molecules [183]. With increasing temperature, the liquid–liquid immiscibility region usually shrinks, because thermal fluctuations can then overcome the unfavorable interactions between the two kinds of molecules. However, with

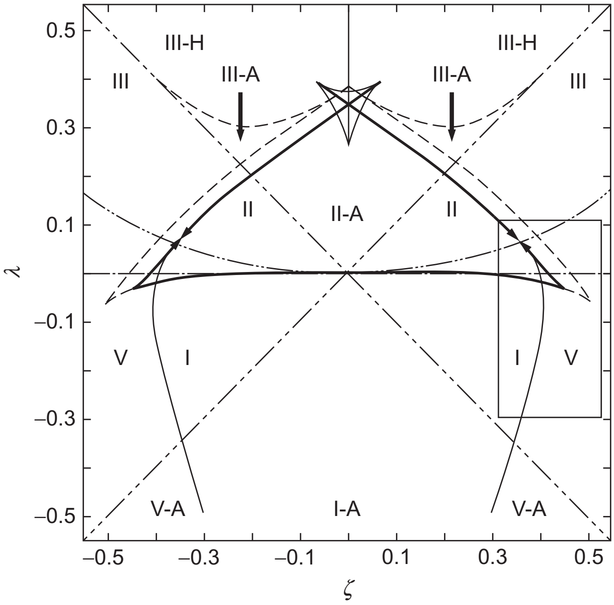

FIGURE 9.18 Global phase diagram for the CSvdW equation of state for $\xi = \eta = 0$. - - - : CPSP curves, ━━: DCEP curves, —— tricritical curves. A magnification of the indicated region is shown in Fig. 9.21. *(Reprinted from Yelash and Kraska [182], © 1998, with permission from the German Bunsen Society for Physical Chemistry.)*

decreasing temperature there is no such mechanism. The usual explanation is that, in systems with directional forces, the entropic contribution of ordering may cause an increasing miscibility with decreasing temperature.

The global phase diagram of the CSvdW equation of state shows that directional forces are not necessary for the appearance of a closed-loop liquid–liquid immiscibility. Figure 9.18 contains the global phase diagram for equal-sized molecules ($\xi = \eta = 0$) [182]. The major difference to the equations of state discussed before is an additional DCEP curve below the abscissa. Together with the critical pressure step curve (CPSP), this curve demarcates a region where closed-loop liquid–liquid immiscibility occurs. A detail view of the relevant region in the global phase diagram is shown in Fig. 9.21. The left diagram reveals the existence of domains of two closed-loop phase diagram classes VI and VII as well as its precursor class V_m. The latter contains phase diagrams with two maxima along the binary critical curve originating at the critical point of the less volatile substance (Fig. 9.19). This class was also found for the Redlich–Kwong equation of state [184], for which, however, the transformation to classes VI and VII does not take place.

The maximum at high temperature is a regular vapor–liquid critical point, whereas the other maximum must be regarded as a critical point of a liquid–

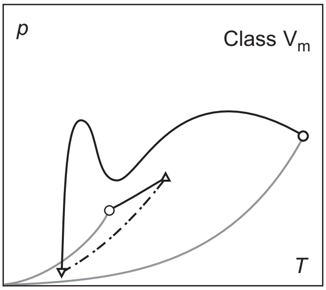

FIGURE 9.19 pT phase diagram of class $V_m(2^P M)$.

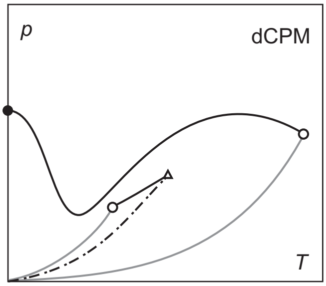

FIGURE 9.20 pT phase diagram with a degenerated critical pressure maximum (dCPM), boundary case between classes III and V.

liquid phase equilibrium. With decreasing difference in the attraction parameters of the pure substances (ζ), the minimum in the critical curve moves to lower pressure and eventually intersects the three-phase curve in a DCEP. Beyond that boundary state, class VII phase behavior exists. At even lower ζ values, there is an additional tricritical curve at which class VII turns to class VI.

Topologically, the closed-loop liquid–liquid immiscibility region appears due to a splitting of the zero-Kelvin curve present in the global phase diagram of the van der Waals equation into two other boundary states [185]. These are phase diagrams containing a CPSP and the so-called degenerated critical pressure maximum (dCPM). The latter is a pressure maximum of a critical curve at $T=0$ (Fig. 9.20).

From a molecular point of view, mixtures located in the region between these two boundary curves have a larger cross attraction parameter than the geometric-mean rule predicts. On the other hand, the cross interaction is still so small that it affects the phase behavior at low temperatures only, and hence does not lead to a phase diagram with pronounced immiscibility.

The CSvdW equation of state is one of few which have also been investigated with respect to the deviation of the cross-covolume from the arithmetic mean [172]. In Fig. 9.21, the right diagram shows a part of the global phase diagram for $\eta=0.2$, which is actually a rather large value. The effect on the

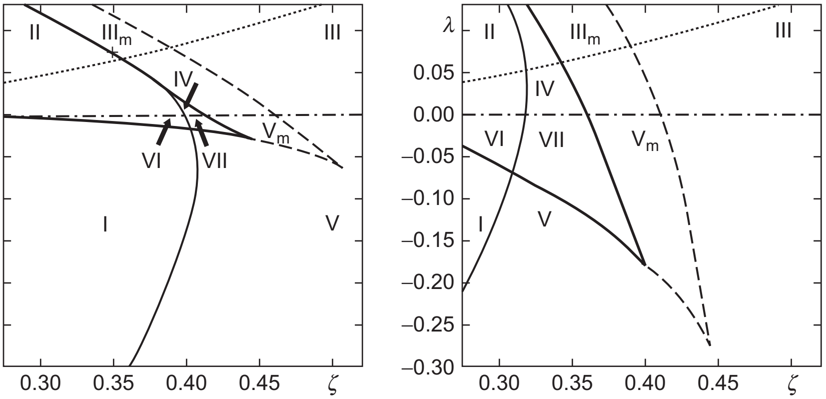

(a) $\eta = 0.0$ (b) $\eta = 0.2$

FIGURE 9.21 Global phase diagrams for the CSvdW equation of state for $\xi = 0$ and $\eta = 0$ or $\eta = 0.2$. *(Reprinted from Yelash and Kraska [172], © 1999, with permission from Oldenbourg Wissenschaftsverlag.)*

global phase diagram is a major enlargement of the class IV region and also a significant enlargement of the classes VI, VII, and V_m regions.

The unexpected existence of class VI and VII phase behavior for an equation of state model without directional forces has been confirmed by many investigations of global phase diagrams. Wang *et al.* [186] used the Guggenheim equation of state, which is similar to the Carnahan–Starling–van der Waals equation of state, but has another repulsion term, and found classes VI and VII phase behavior emerging by the same mechanisms as for the CSvdW equation of state. Scott [187] calculated the global phase diagram for the Sanchez–van Rensburg equation of state and found even larger domains of classes VI and VII.

Since the CS repulsion and also many other hard-sphere repulsion terms overestimate the close packing limit, the liquid–liquid closed-loop is found at very high packing fractions. With a so-called mapping approach, several new hard-sphere repulsion terms could be developed [185] which have their density limit at 0.75, very close to the close-packing fraction. With these repulsion terms, it was possible to obtain class VI and VII phase behavior, too, but now at a significantly lower packing fraction.

Bhimalapuram and Widom calculated the isobaric heat capacity for four models having a closed-loop liquid–liquid immiscibility and found an anomalously high positive excess heat capacity in all cases [188]. Since that effect is related to hydrophobic interaction [189], it turns out that the mechanism of the emergence of class VI behavior in attractive-hard-sphere fluids is very much the same as in systems with directional forces, namely entropy related. However, the extent of the hydrophobicity is smaller for the attractive-hard-sphere fluids than for models with directional forces.

9.4.5 Lattice Gas Models

Historically, two lattice gas models were the first models whose global phase behavior was studied after the seminal work of Scott and van Konynenburg. These models are the ternary symmetric lattice gas and the related van der Waals model.

The *ternary symmetric lattice gas model* assumes that there is a lattice of fixed size of which each site can be occupied by one molecule belonging to species 0, 1, or 2. The coordination number z, the number of nearest neighbors for each molecule, is fixed and the same for all species. Nearest neighbors interact with an energy of ϵ_{ij}; the interaction energy with more distant molecules is zero. The random mixing approximation is made: for each phase, the molecules distribute randomly over the available lattice sites. This leads to a very simple ansatz for the Helmholtz energy:

$$A_\mathrm{m} = N_\mathrm{A} z \left(\sum_{i=0}^{2} \sum_{j=0}^{2} x_i x_j \epsilon_{ij} \right) + RT \left(\sum_{i=0}^{2} x_i \ln x_i \right) \tag{9.15}$$

The simplifications – the assumption of equal sizes for all components as well as the neglecting of long-distance interactions and local ordering – render this model unsuitable for quantitative modelling. But it does capture essential points of phase equilibria. Because of its simple structure, many equilibrium and boundary conditions can be treated analytically.

Of course, the ternary lattice gas is rather a model for an alloy than for a compressible fluid mixture. An exhaustive analysis was given by Griffiths and his coworkers [190] in 1977. The global phase diagram of the ternary lattice gas consists of eight “leaves”, where for each of these leaves the interaction energies have different signs. For an alloy, positive interaction energies are physically possible, whereas for typical fluid mixtures, the interaction energies are usually negative.

There is no need to repeat the (rather extensive) results of Furman *et al.* [190] here; the interested reader is referred to the original literature. The important point, however, is that in the leaves corresponding to fluid phase equilibria, there appear three tricritical curves and that these tricritical curves intersect in a shield region. In fact, the intricacies of the shield region were discovered for this model.

The *van der Waals lattice gas model* is obtained from the ternary symmetric lattice gas by letting component 0 represent “holes”, i.e., empty space. Thus, the rigid ternary lattice model is turned into a model for compressible binary fluid mixtures. Its Helmholtz energy equation is

$$A_\mathrm{m} = N_\mathrm{A} z \left(x_1^2 \epsilon_{11}^2 + 2 x_1 x_2 \epsilon_{12} + x_2^2 \epsilon_{22} \right) + RT \left(x_1 \ln x_1 + x_2 \ln x_2 + (x_0 - 1) \ln x_0 \right). \tag{9.16}$$

The differences to the symmetric lattice gas model are due to the facts that there is no interaction energy between a molecule and a hole and that the expansion of empty space does not generate mixing entropy.

This model was analyzed by Furman and Griffiths in 1978 [177]. Its global phase diagram is equivalent to that of the van der Waals equation of state for equal-sized molecules and therefore needs not be reproduced here.

But an interesting insight can be gained from the lattice gas model by plotting the projections of critical curves in an x_1x_2 diagram, i.e., in a map of the lattice gas mole fractions. Such maps are called *Meijer diagrams*; they have a triangular shape, because the sum of the three mole fractions must be 1. The density diagrams of Section 5.8 are the equivalent maps for regular equations of state.

The critical curves can have three anchor points:

- In terms of lattice gas coordinates, the critical point of pure fluid 1 is a critical point of the binary subsystem {0 + 1}, i.e., of component 1 mixed with holes, in the absence of component 2. It is represented by a point on the abscissa.
- Likewise, the critical point of pure fluid 2 is a critical point of the binary subsystem {0 + 2} in the absence of 1; it is represented by a point on the ordinate.
- The hypothetical jamming point, the high-pressure limit of liquid–liquid critical curves, is consequently a critical point of the subsystem {1 + 2} in the absence of holes; it is represented by a point on the hypothenuse.

Figures 9.22 and 9.23 are schematic Meijer diagrams for systems belonging to class II and class III. It is evident that these two classes, even if they have rather different *pT* representations, are topologically very similar. They only differ in the connectivity of the three critical points on the borders: For class II, the critical points of {0 + 1} and {0 + 2} are connected by a critical curve, whereas the critical curve coming from the critical point of {1 + 2} runs to an endpoint. For class III, the critical points {0 + 2} and {1 + 2} are connected.

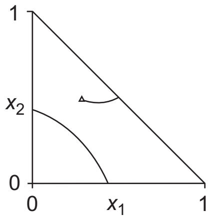

FIGURE 9.22 Schematic Meijer diagram of class II for the van der Waals lattice gas.

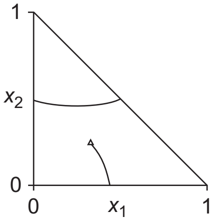

FIGURE 9.23 Schematic Meijer diagram of class III.

9.4.6 Other Equations of State

Van Pelt *et al.* computed global phase diagrams for the SPHCT equation of state, Eq. (7.43) [174, 178]. He discovered class VIII as well as several others which have not been found in experiments, yet.

Global phase diagrams have been computed not only for van der Waals-type equations of state, which incorporate a hard-sphere repulsion in a more or less accurate way, but also for equations of state for soft-sphere fluids. So Boshkov and Mazur investigated an equation of state for the Lennard-Jones fluid which was based on molecular simulation data [32, 176, 191]. In addition to the usual global phase diagram they found a triangular region of liquid–liquid closed-loop phase diagrams. The interplay of boundary curves that is responsible for its formation is different from the one of the CSvdW equation of state. Historically, Boshkov and Mazur were the first to show that closed-loop immiscibility may be possible even without directional forces, and their work, disagreeing with the traditional views, was at first received with doubts. But with so many later studies of global phase diagrams finding closed-loop immiscibility regions for simple models, the issue appears to be resolved.

Various other investigations focus on the global phase behavior of non-spherical molecules. Wang and Sadus especially investigated the appearance of phase diagram classes related to class IV [192] using an equation of state containing the hard-convex-body term of Boublík and Nezbeda, Eq. (7.55).

The next step beyond the spherical shape are chain molecules. The global phase diagram of monomer–dimer mixtures was investigated by Attwood and Hall [193] (a dimer is evidently the shortest possible chain molecule). The underlying equation of state model was a generalized Flory dimer equation of state based on a square-well attraction. The obtained global phase diagram is topologically similar to that of the van der Waals equation of state. Due to the asymmetry of the mixture, the global phase diagram is asymmetric, too. Of course, there are quantitative differences to the global phase diagram of other equations of state.

Recently, Flores *et al.* [194] analyzed the phase behavior related to a CPSP, and especially its limiting behavior in the global phase diagram. In addition to the known CPSP curves, they found an additional one in the region of strong deviation of the cross-attraction from the geometric mean, i.e., in the regions of class I and V. Their publication contains a detailed analysis of the shield region in global phase diagrams of four different equations of state for comparison.

A qualitatively rather different phase diagram has been found for the Dieterici equation of state. This equation has an unusual mathematical structure: in contrast to van der Waals type equations, which are sums of a repulsion and an attraction term, the Dieterici equation is a product of a repulsion term and an exponential function representing the intermolecular attraction. As a consequence, the Dieterici equation cannot give negative pressures. An analysis of its global phase diagram revealed the existence of more tricritical curves and a hypercritical curve as well as differences in the azeotropic phase behavior [195, 196].

9.4.7 Are Shield and Sword Regions Realistic?

The types and arrangements of the domains in the various global phase diagrams are generally similar for all equations of state investigated so far. Differences exist in the quantitative location and sizes of these domains. In some small and very sensitive regions of the global phase diagrams, however, also qualitative differences can be observed. One of these regions is the so-called *shield region* located around $\zeta = 0$ and $\lambda = 0.3 \ldots 0.4$ for the van der Waals equation (Fig. 9.12) in case of equal-sized molecules, $\xi = 0$. The other regions are the two *sword regions* located near the ζ axis. In these regions, one finds a very rich phase behavior, i.e., small changes of the interaction parameters lead to radical topological changes in the phase behavior. The shield region as well as the sword regions contain domains of phase diagram classes with four-phase equilibria lllg. Moreover, in the shield region various azeotropic boundary curves cross these domains and give rise to a very complex pattern of domains of rather complicated phase diagram classes [32, 171, 176, 177, 190, 197, 198].

The shield region and the sword regions are usually located far away from the geometric-mean curve. One might therefore conclude that these regions are fictitious and not accessible experimentally with molecules of this universe [197].

This is probably true for mixtures in which the molecules are more or less randomly distributed and where therefore cross interactions (interactions between unlike species) have large statistical weights. But fluids with microscopic structuring, e.g., micellar solutions, can have a far smaller influence of cross interactions; for them the arithmetic-mean curve is a better approximation. Indeed, coexistence of three liquid phases has been observed for mixtures of water with some non-ionic surfactants, e.g., $\{H_2O + C_{10}H_{21}\text{-}(OC_2H_4)_4\text{-}OH\}$ [199] (see Fig. 9.24). Findenegg *et al.* observed "isotropic channels" in water–surfactant phase diagrams, another phenomenon occurring in phase diagrams of the sword region [200]. The isothermal phase diagrams of these systems are rather complicated, and their pressure dependence has not been studied up to now. Still, the coexistence of three liquid phases necessitates the existence of an lllg four-phase state, and in phase diagram classes containing such a state indeed one-phase regions inmidst two-phase regions can occur. Figure 9.25 shows an isobaric cross section through a class IV_4 phase diagram (cf. Fig. 9.15) slightly above the four-phase point, so that three 3-phase lines are intersected. The experimentally observed phase diagram Fig. 9.24 is still more complicated due to the existence of lyotropic liquid-crystalline phases, but Fig. 9.25 can already explain the existence of the "anomalous" liquid phase.

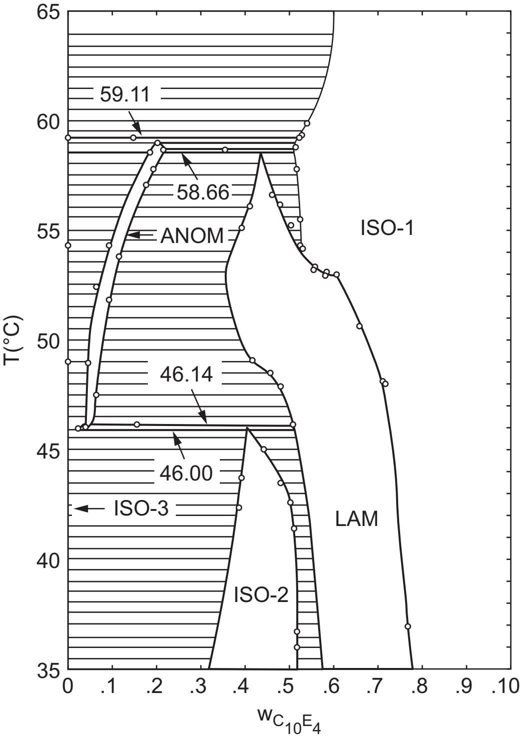

FIGURE 9.24 Isobaric phase diagram of {water + $C_{10}E_4$} at ambient pressure (the acronym stands for tetraethyleneglycol decyl ether, a nonionic surfactant), in the region of high water concentration. Note the appearance of an "anomalous" isotropic liquid phase. The phase diagram also contains liquid-crystalline domains. *(Reprinted from Lang and Morgan [199], © 1980, with permission from the American Institute of Physics.)*

While the application of equations of state to such complex mixtures is still seldomly attempted, it is already evident that only equations showing global phase diagrams with sword regions can be of any use in this context.

Another reason for large deviations from the geometric-mean curve may be strong polar interactions or hydrogen bonding. There are indeed some experimental data that make the real existence of this region likely: The phase diagrams of the {water + n-alkane} family [22] all belong to class III, but for the lower alkanes water is the less volatile component, whereas it is the alkane otherwise (see Fig. 9.26). The transition $1^C 1^Z \rightarrow 1^Z 1^C$ takes place near to the {water + $C_{26}H_{54}$} system. In all global phase diagrams shown so far, such a transition can only be made through the high-λ tricritical curve *above the shield region*. One might therefore expect that mixtures of water with slightly less hydrophobic compounds than long n-alkanes might have phase diagrams in the shield region.

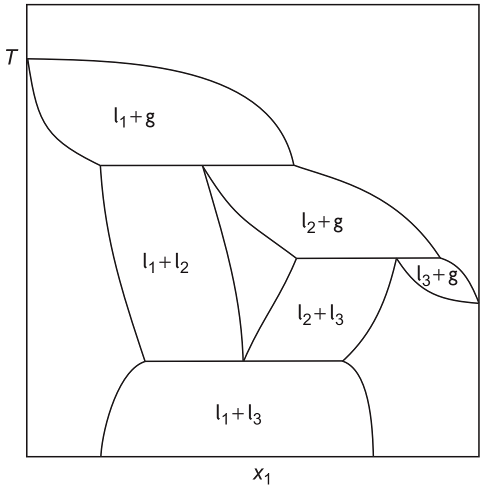

FIGURE 9.25 Possible isobaric cross section of a class IV_4 phase diagram (cf. Fig. 9.15) at a pressure slightly above that of the four-phase point (schematic), showing a one-phase region inmidst the two-phase regions. (*Reprinted from Kraska and Deiters [180], © 1992, with permission from the American Institute of Physics.*)

9.5 APPLICATIONS OF GLOBAL PHASE DIAGRAMS

Is the knowledge of such very detailed studies of global phase diagrams relevant for practical applications? The answer must be yes, for if a system is known to be in or close to one of the regions of complex phase behavior – the shield region [171, 176, 197, 198], the sword region [180, 201], or a class VI/VII region [32, 172, 182] – it may be very difficult to correlate experimental data quantitatively while reproducing the correct qualitative phase diagram class at the same time. In other words, if a system is located in such region, one should be very careful with any extrapolation of experimental data using an equation of state correlation. For example, one might fail to compute a liquid–liquid immiscibility if the parameter set fitted to the data is located on the wrong side of a tricritical curve in the global phase diagram.

Furthermore, if a system is known to be in one of the complex regions, special precautions must be taken to ensure that no phase is overlooked.

As we will see below, in applications of global phase diagrams to chemical engineering problems, it is often not necessary to calculate the complete global phase diagram. Instead, it is usually sufficient to calculate a few boundary states in the vicinity of the parameters of the system under investigation. On the other hand, if a specific system is located in the middle of large domain in the global phase diagram, one can be reasonably sure that the fitting of the equation of state parameters does not affect the phase diagram class.

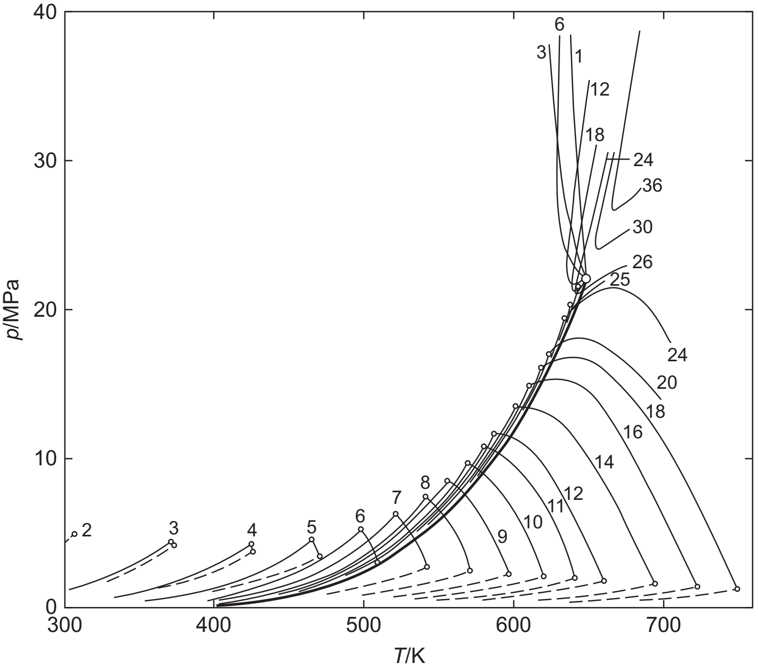

FIGURE 9.26 Critical curves and llg 3-phase curves of {water + alkane} systems, with the alkanes ranging from methane to $C_{40}H_{82}$. ——: critical or llg three-phase curves, – – : vapor pressure curves; curve parameter: carbon number of the alkane. Note that the phase diagram topology changes at C_{26}. *(Reprinted from Brunner [22], © 1990, with permission from Elsevier.)*

Since for a specific system the pure substance parameters are fixed, one can analyze the influence of the cross interaction parameters in a $\lambda\eta$ or directly in a $k_{12}l_{12}$ diagram (cf. Eq. (8.22)). Such a global phase diagram was used by Polishuk *et al.* [202] for the qualitative and quantitative analysis of the phase behavior of the system {methane + n-pentane}, which happens to be very close to a tricritical curve.

Global phase diagrams have also been used to locate specific parameter sets, representing specific binary mixtures, which are of interest for the investigation of other properties. For example, Mejía *et al.* [203] investigated interface properties of class I and class V Lennard-Jones mixtures selected from the corresponding global phase diagram calculated with the softSAFT equation of state.

Another system being close to a tricritical boundary state is {carbon dioxide + ethanol}. This technically relevant mixture is supposed to exhibit class I phase behavior. But since it is located close to tricritical curve, parameters fitted to experimental data may lead to a small liquid–liquid immiscibility. In the context of the so-called gas antisolvent crystallisation process (GAS), a third substance, a solute which is to be crystallized, influences the phase behavior of the mixture. By calculating a part of the tricritical boundary, it could be shown that solutes which influence the {ethanol + carbon dioxide} phase behavior can move the system across the tricritical boundary curve [204]. In this special case, the location of the system in the global phase diagram affects the morphology of the solid particles formed by the process: the closer a binary solvent system is to the tricritical curve, the more likely undesired big hollow-sphere particles are obtained in GAS experiments. The distance of the system to a tricritical curve in the global phase diagram has been found to be a criterion for finding solvent mixtures which give the desired very fine particles with GAS.

Global phase diagrams have also been used to analyze the development of the phase behavior within system families. An example is the family {water + n-alkane} [205], which was modelled with statistical associating fluid theory (SAFT). Here relative critical temperatures and densities were used as global coordinates. Furthermore, a rather qualitative investigation of the {methane + n-alkane} family was performed, which included the effect of co- and anti-solvents on the phase behavior [206]. Shape effects in the context of global phase behavior were studied for {carbon dioxide + C_4} mixtures, where C_4 stands for five hydrocarbons with four carbon atoms [207]. Another work focused on miscibility holes in polymer blend systems consisting of poly(dimethylsiloxane) and poly(hexylmethylsiloxane) [46]. As these holes are related to temperature minima in the liquid–liquid critical curves in these systems, a boundary state of a critical temperature minimum at zero pressure was calculated in order to follow the formation of the holes.

In (polydisperse) polymer–solvent mixtures, the average chain length or the percentage of copolymers can provide additional degrees of freedom, which can then be used to experimentally reach boundary states. For example, {acetone + polystyrene} belongs to class IV for a molar mass below 2×10^4 g/mol, but to class III above [208]. When handling polymer mixtures, it is evidently good to know what the relevant phase diagram classes are.

Investigations of the global phase behavior have inspired the further development of equations of state. For example, the insight into the appearance of the liquid–liquid closed-loop phase behavior has led to approaches to simplify the Carnahan-Starling repulsion term [112]. Also, an equation of states of chain molecules [209, 210] has been simplified in this context. Finally, global phase diagrams have been used for a general analysis of attraction terms in equations of state [211].

9.6 TERNARY SYSTEMS

Almost all investigations of global phase behavior are for binary mixtures, whereas little has been done so far for ternary systems. Sadus collected many ternary *pTx* phase equilibrium data and presented them mainly as *pT* diagrams

[212]. The mixtures in his compilation include many organic compounds, water, carbon dioxide, nitrogen, noble gases, etc.

There is also a systematic study of ternary phase behavior based on the van der Waals equation of state [213]. As a ternary system has more independent molecular parameters, the number of global parameter increases. In order to reduce the number of free parameters, the work focused on equal-sized molecules and fixed the cross-attraction parameters to the geometric mean. Hence the global phase diagram was spanned by the parameters ζ_{12} and ζ_{13} (the third parameter, ζ_{23}, then depends on the other two). This work identified some basic ternary phase diagram classes, which in turn could be related to the phase diagram classes of their binary subsystems (see Fig. 9.27).

An example is shown in Fig. 9.28. This ternary system is of the quasibinary type (cf. Fig. 2.105); it consists of two subsystems of class $\mathrm{III_m}$ {1 + 2} and {1 + 3} and one of class I {2 + 3}.

In fact, most of the systematic experimental work that has been made for ternary mixtures concerns quasibinary systems. With quasibinary systems of the type I + (II + III), it is possible, by variation of the ratio of components 2 and 3, to realize a tricritical point or a double critical endpoint. Gibbs' phase rule forbids this for binary mixtures, but for ternary mixtures it can and has been

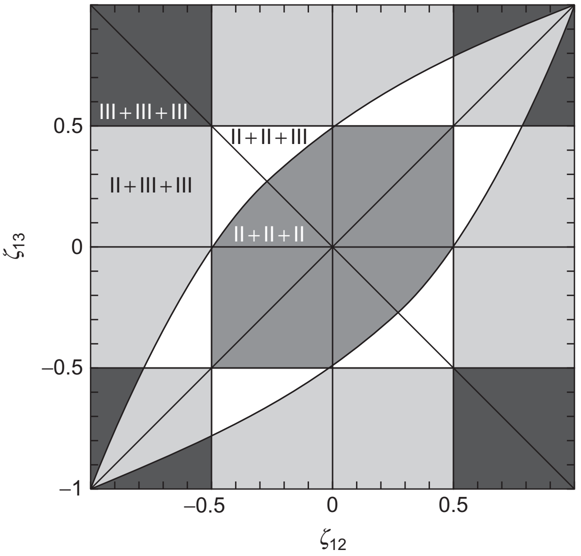

FIGURE 9.27 Ternary global phase diagram for mixtures of equal-sized molecules obeying the Berthelot–Lorentz combining rules [213]. The grey shades indicate the ternary phase diagram class: middle grey: II + II + II, white: II + II + III, light grey: II + III + III, dark grey: III + III + III. *(Reprinted from Phys. Chem. Chem. Phys. 1: M. Bluma and U. K. Deiters, "A classification of phase diagrams of ternary fluid systems", pp. 4307–4313, © 1999, with permission from the Royal Society of Chemistry.)*

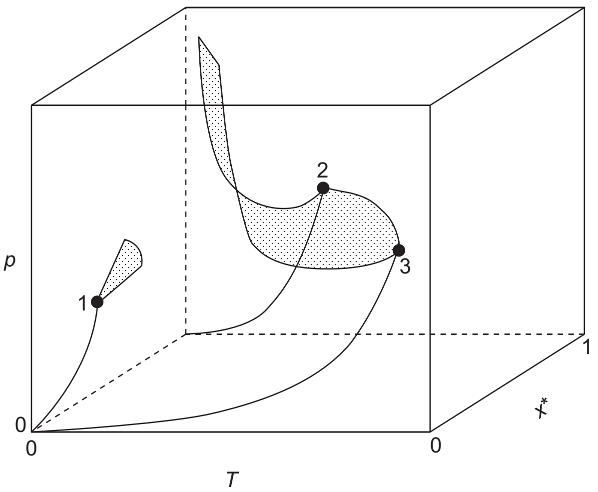

FIGURE 9.28 Example of a ternary phase diagram calculated with the van der Waals equation of state [213]. The numbers indicate the critical points of the three pure substances. The shaded planes are ternary critical planes. $x^* = x_2/(x_2 + x_3)$. *(Reprinted from Phys. Chem. Chem. Phys. 1: M. Bluma and U. K. Deiters, "A classification of phase diagrams of ternary fluid systems", pp. 4307–4313, © 1999, with permission from the Royal Society of Chemistry.)*

done, e.g., for the system {carbon dioxide + dodecane + o-nitrophenol} [214] or for mixtures of carbon dioxide with small alkanols [215].

Conversely, global phase diagrams of binary mixtures can be used to interpret phase diagrams of quasibinary mixtures. For ternary mixtures in general, however, the number of possible combinations of binary subclasses is large, and we must expect a huge variety of ternary phase diagrams. So far, only a minor portion has been explored.

9.7 PROBLEMS

1.

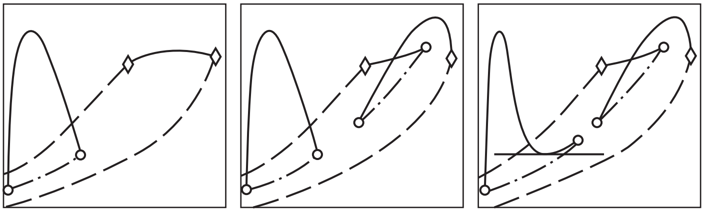

The figure shows a sequence of pT diagrams. Determine the transitional phase diagrams and suggest boundary states. *(Reprinted from Yelash and Kraska [182], © 1998, with permission from the German Bunsen Society for Physical Chemistry.)*

2.

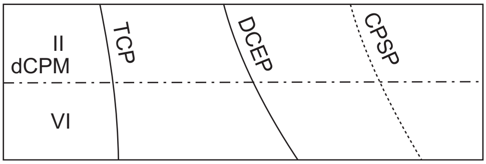

The figure shows a section of a global phase diagram. Identify the phase diagram classes of the regions between the boundary curves.

3. Derive the equation for the zero-Kelvin endpoint curve (see Section 9.3.5) in a $\lambda\zeta$ global phase diagram with $\xi = 0$ (equal-sized molecules), (a) for the van der Waals equation of state, (b) for the Redlich–Kwong equation of state.

4. Derive all functions required for the evaluation of $G_{(2x)}$ for the van der Waals equation of state [see Eq. (5.117)].

Appendix A

Algebraic and Numeric Methods

The calculation of phase equilibria frequently involves mathematical operations like differentiation or solving equations. These are standard operations; readers who want to write their own programs for phase diagram calculations are advised to look up existing subroutines or program libraries for these operations: there is no need to reinvent the wheel. On the other hand, programmers should be aware of the principles, limitations, and pitfalls of the algorithms they are using.

This book focuses on thermodynamics, not on numerical mathematics. Even so, the readers might find a section on mathematical algorithms useful, which offers background information especially related to thermodynamic problems and can help to choose the best method for a given numerical problem.

A.1 ERRORS

A.1.1 Round-off Errors

Inside a computer, real numbers are represented with a finite number of bits. The difference between this representation and the intended value is the round-off error.

Round-off errors are inherent in all numerical work on digital computers; they cannot be avoided. However, it is possible (and the programmer's duty) to ensure that round-off errors do not affect the final results. For this, it is necessary

- to assess their size,
- to choose algorithms that avoid the accumulation of errors,
- and to use a sufficient computational precision.

The internal representation of a real number is usually of the form $m \times 2^b$, where m (mantissa) and b (binary exponent) are integer numbers. Most modern programming languages offer at least two different precisions for real numbers, "single precision" and "double precision," in accordance to standard IEEE 754:

- "Single precision" (Fortran: real, real*4; C, C++: float) refers on modern computers to a representation of a real number by 32 bits (4 bytes), of which 24 are used for the mantissa and 8 for the exponent. This results in a range

High-Pressure Fluid Phase Equilibria. DOI: 10.1016/B978-0-444-56347-7.00010-4

of approximately 10^{-38} to 10^{+38} and a relative precision of 10^{-7}, which is inadequate for most scientific purposes.

- "Double precision" (Fortran: double precision, real*8; C, C++: double) refers to a representation by 64 bits (8 bytes), of which 53 are used for the mantissa and 11 for the exponent. This results in a range of approximately 10^{-308} to 10^{+308} and a relative precision of 10^{-16}.

Higher precisions have also been defined (e.g., "quad precision", Fortran: real*16; C, C++: long double) but are not required for most problems discussed in this book. Programmers using such precisions should make sure that libraries of algebraic and transcendental functions with the required precision are available on their computers.

Some programming environments offer arithmetics with arbitrary precision or interval arithmetics. Although these environments are very useful for assessing round-off errors, they significantly reduce the computational speed.

A.1.2 Termination Errors

Most of the equations describing phase equilibria of fluid mixtures cannot be solved analytically but solved only numerically by iterative methods. Generally speaking, iteration methods start from an estimate of the solution, $x^{(0)}$, and construct from it a (hopefully) better estimate $x^{(1)}$, which in turn is used to generate $x^{(2)}$, etc. *ad infinitum.*

There exist iteration schemes that require more than one initial estimate, and in the case of systems of equations with more than one unknown, the $x^{(0)}$ have to be defined as vectors, but we will ignore such complications for the moment.

The $x^{(i)}$ generated by the iteration scheme constitute an infinite sequence converging – if everything works as intended – to the desired solution $x_0 = x^{(\infty)}$. In practice, however, an iteration is terminated after a finite number of steps. Consequently, the result is not the true solution but can deviate from it by the termination error.

An important measure of the sensitivity of iteration algorithms to termination errors is the *convergence order C*, defined by

$$\lim_{i\to\infty} \frac{|x^{(i+1)} - x^{(\infty)}|}{|x^{(i)} - x^{(\infty)}|^C} = Q, \tag{A.1}$$

which compares the termination errors of two successive iteration steps; Q is a nonzero constant:

- In case of linear convergence order, $C = 1$, the termination error decreases by an approximately constant factor with each step. If this factor is close to 1, the difference between two successive steps may become small and trigger the termination of the iteration, even if the termination error (difference to the true solution) is still large.

- In case of quadratic convergence, $C=2$, the number of significant digits doubles with each iteration step. If two successive iteration results differ relatively by 10^{-6}, one can assume that the last value is good to 10^{-12} and that it is safe to terminate the iteration.

For many iterative algorithms presented in this appendix, the convergence order has been established by mathematical analysis. A practical way to determine C is measuring the slope of a $\ln|x^{(i+1)}-x^{(\infty)}|$ vs. $\ln|x^{(i)}-x^{(\infty)}|$ graph. This implies, of course, that $x^{(\infty)}$ is known and the computating precision is sufficient for the evaluation of the differences.

A.2 ROOT OF A ONE-DIMENSIONAL FUNCTION: SUBSTITUTION METHODS

To find the zeros ("roots") of an arbitrary nonlinear function $f(x)$,[1] i.e., to solve the equation $f(x)=0$, it is sometimes useful to rewrite the search criterion as

$$x=g(x), \tag{A.2}$$

where $g(x)$ is the so-called iteration step function. For example, the equation $f(x)=xe^x-a=0$ can be rewritten as $x=ae^{-x}=g(x)$. The root can then sometimes be located by calculating $g(x)$ for an estimate of x and regarding the result as an improved approximation for x:

$$x^{(i+1)}=g\left(x^{(i)}\right) \quad i=0,1,2,\ldots \tag{A.3}$$

This approach is known as *direct substitution method*. The sequence of approximations $x^{(i)}$ converges against the solution if $|\mathrm{d}g(x)/\mathrm{d}x|<1$. Our example problem can be solved this way with $x^{(0)}=a$ if $|a|\leq 1$.

However, the evaluation of the convergence criterion may be impractical if the step function is complicated. Furthermore, the iteration scheme Eq. (A.3) exhibits – if it converges at all – a linear convergence order, i.e., it is susceptible to termination errors (see A.1.2).

These disadvantages are avoided by *Steffensen's accelerated substitution scheme* [216].[2] It makes use of the linear convergence order of the direct substitution method: the deviations of successive approximations from the true solution, calculated by the direct substitution method, roughly form a geometrical series, which can of course be extrapolated toward infinity. Steffensen's

---

[1] $f(x)$ is called object function.

[2] This algorithm is also known as Aitken's method.

method can be summarized as follows:

$$\begin{aligned}
x^{(i+)} &= g\left(x^{(i)}\right)\\
x^{(i++)} &= g\left(x^{(i+)}\right)\\
x^{(i+1)} &= x^{(i)} - \frac{\left(x^{(i+)} - x^{(i)}\right)^2}{x^{(i++)} - 2x^{(i+)} + x^{(i)}}
\end{aligned} \tag{A.4}$$

The algorithm converges also for $|\mathrm{d}g(x)/\mathrm{d}x| > 1$ as long as the denominator in the extrapolation step is not zero. The convergence order is usually quadratic.

A.3 ROOT OF A ONE-DIMENSIONAL FUNCTION: REGULA FALSI

The *regula falsi*, also known as *secant method*, is one of the oldest methods for solving nonlinear equations with one unknown, $f(x) = 0$. It requires two initial estimates, $x^{(0)}$ and $x^{(1)}$, for which the values of the object function $y^{(0)} = f(x^{(0)})$ and $y^{(1)} = f(x^{(1)})$ have opposite signs, respectively. The iteration scheme can then be summarized as follows:

$$\begin{aligned}
x &= x^{(1)} - \frac{x^{(1)} - x^{(0)}}{y^{(1)} - y^{(0)}} y^{(1)}\\
y &= f(x)
\end{aligned} \tag{A.5}$$

The new estimate must then overwrite one of the old ones:

$$\begin{cases}
x^{(0)} := x^{(1)}, y^{(0)} := y^{(1)}, x^{(1)} := x, y^{(1)} := y & \text{if } \operatorname{sign}(y) = \operatorname{sign}(y^{(0)})\\
x^{(1)} := x, y^{(1)} := y, y^{(0)} := \frac{1}{2} y^{(0)} & \text{if } \operatorname{sign}(y) = \operatorname{sign}(y^{(1)})
\end{cases} \tag{A.6}$$

The idea of this scheme is to keep the location where the change of sign occurs between $x^{(0)}$ and $x^{(1)}$. The reduction of the function value by $\frac{1}{2}$ in the second case provides a significant acceleration in cases where the object function runs almost parallel to the abscissa.

This version of the *regula falsi* (sometimes denoted as *Illinois regula falsi* or *Pegasus regula falsi*) achieves sure convergence with an almost quadratic convergence order. As only one function value has to be computed for each iteration step, this is effectively one of the fastest existing iteration methods.

A.4 ROOT OF A ONE-DIMENSIONAL FUNCTION: NEWTON'S METHOD

Newton's method is one of the most popular and efficient ways for solving nonlinear equations. It assumes that the object function $f(x)$ can be written as a

Taylor series in the vicinity of the solution x_0:

$$f(x) = \underbrace{f(x_0)}_{=0} + f'(x_0)\Delta x + \frac{1}{2} f''(x_0)(\Delta x)^2 + \cdots \quad \text{with } \Delta x = x - x_0 \tag{A.7}$$

Truncation of the series after the linear term and solving for x_0 gives

$$x_0 \approx x - \Delta x \approx x - \frac{f(x)}{f'(x)} \tag{A.8}$$

This result for x_0 is then used as initial value for the next iteration step. Newton's method converges rapidly (quadratic convergence order!) if the initial value is close enough to the solution. Experience shows, however, that this method is likely to fail if the object function has extrema or inflection points between the initial value and the solution.

The correction steps Δx of Newton's method are systematically too small. Therefore, often a modified version is used,

$$x^{(i+1)} = x^{(i)} - \lambda \frac{f(x^{(i)})}{f'(x^{(i)})}, \tag{A.9}$$

where $\lambda \approx 1.10$ is an empirical correction.

For roots of higher order, where the slope or perhaps even higher derivatives of the object function vanish, the convergence order of Newton's method is merely linear, and usually convergence is rather slow. For an nth-order root, one can restore the quadratic convergence order by setting $\lambda = n$. In many applications, however, the order of the root at the solution is not known in advance. To ensure an optimal choice of λ in such cases, a second-order Newton algorithm can be used [216]:

$$x^{(i+1)} = x^{(i)} - \frac{f(x^{(i)}) f'(x^{(i)})}{f'(x^{(i)})^2 - f(x^{(i)}) f''(x^{(i)})}. \tag{A.10}$$

Newton's method can be extended to systems of equations. Then the single unknown x must be replaced by a vector $\vec{x}$, and the object function becomes a vector function $\vec{f}(\vec{x})$. The Taylor expansion Eq. (A.7) becomes

$$\vec{f}(\vec{x}) = \boldsymbol{J}(\vec{x} - \vec{x}_0) + \cdots, \tag{A.11}$$

where $\boldsymbol{J}$ is the Jacobian matrix of the problem with

$$J_{ik} = \left(\frac{\partial f_i(\vec{x})}{\partial x_k} \right)_{x_{l \neq k}}. \tag{A.12}$$

The solution (or rather, the next step of the iteration) is then obtained as

$$\vec{x}_0 = \vec{x} - \boldsymbol{J}^{-1} \vec{f}(\vec{x}). \tag{A.13}$$

The computation involves the inversion of the Jacobian matrix, which can be a costly step. For the discussion of fast matrix inversion techniques, convergence acceleration methods, stabilization against round-off errors, and alternative algorithms, the reader is referred to the literature (e.g., [217] and literature cited therein).

It is often convenient to use parameter fitting methods (see A.13) instead of Newton's multidimensional root finder.

A.5 ROOTS OF CUBIC POLYNOMIALS

A.5.1 Cardano's Method

In thermodynamic calculations, a frequently required operation is the computation of the molar volume or density of a fluid for given temperature and pressure. For the so-called cubic equations of state, this problem can transformed into the problem of finding the roots of a cubic polynomial.

The general cubic equation,

$$A_3x^3+A_2x^2+A_1x+A_0=0, \tag{A.14}$$

can be transformed with the substitution of $a_i=A_i/A_3$ (only if $A_3\neq 0$) into

$$f(x)=x^3+a_2x^2+a_1x+a_0=0. \tag{A.15}$$

With the further substitution of $y=x+a_2/3$, the quadratic term can be eliminated:

$$\begin{aligned} &y^3+py+q=0\\ &\quad\text{with } p=-\frac{1}{3}a_2^2+a_1\\ &\quad\quad q=\frac{2}{27}a_2^3-\frac{1}{3}a_1a_2+a_0 \end{aligned} \tag{A.16}$$

If the so-called discriminant D is negative,

$$D=\frac{p^3}{27}+\frac{q^2}{4}\leq 0, \tag{A.17}$$

the cubic equation has three real solutions:

$$x_k=2\left(-\frac{p}{3}\right)^{1/2}\cos\left(\frac{1}{3}\arccos\frac{-q/2}{\sqrt{-p^3/27}}+\frac{2\pi k}{3}\right)-\frac{a_2}{3} \qquad \text{with } k=0,1,2 \tag{A.18}$$

Of the three real solutions, two can coincide if $D=0$. If $p=q=0$, there is one triply degenerate solution.

If the discriminant is positive, only one real solution is possible:

$$x=\sqrt[3]{-\frac{q}{2}+\sqrt{D}}+\sqrt[3]{-\frac{q}{2}-\sqrt{D}}-\frac{a_2}{3} \tag{A.19}$$

This formula in known as Cardano's equation.

It must be noted that in both cases – positive or negative discriminant – the algebraic solution of a cubic equation is rather complicated and requires the evaluation of several algebraic or transcendental functions. The computation is likely to suffer from round-off errors. Therefore, it is advisable to follow the evaluation of Eq. (A.18) or (A.19) with one step of an iteration, for instance with Newton's method. If x is a result of Eq. (A.18) or (A.19), then the following expression,

$$\bar{x}=x-\frac{f(x)}{\frac{\mathrm{d}f(x)}{\mathrm{d}x}}=x-\frac{x^3+a_2x^2+a_1x+a_0}{3x^2+2a_2x+a_1}, \tag{A.20}$$

is a more accurate and reliable solution of the cubic equation than Eqs (A.18)–(A.19).

A.5.2 Fast Numeric Method

A faster way of determining the real roots of a cubic equation starts from the normalized form of the cubic equation, Eq. (A.15) [94, 218]. It should be noted that, by proper scaling or choosing a proper system of units, the values of the polynomial coefficients can be made to be less than 1, $|a_i|\leq 1$. It can then be shown that the interval $-r\leq x_k\leq +r$ with $r=1+\max(|a_i|)$ must contain all real roots.

The first real root can then be located by an iteration using Halley's method,

$$x^{(i+1)}=x^{(i)}-\frac{f(x^{(i)})f'(x^{(i)})}{f'(x^{(i)})^2-\frac{1}{2}f(x^{(i)})f''(x^{(i)})}, \tag{A.21}$$

starting from an initial value

$$x^{(0)}=\begin{cases}-r & \text{if } f(x_{\text{infl}})>0\\ +r & \text{if } f(x_{\text{infl}})\leq 0\end{cases}, \tag{A.22}$$

where $x_{\text{infl}}=-a_2/3$ is the location of the inflection point. This choice of the initial value ensures that no extremum lies between the initial value and the nearest root.

Once the first root, x_1, is known, it is possible to deflate $f(x)$ (i.e., divide by a linear factor), thus generating a quadratic polynomial:

$$\begin{aligned} g(x) &= x^2 + b_1 x + b_0 \\ \text{with } b_1 &= x_1 + a_2 \\ b_0 &= b_1 x_1 + a_1 \end{aligned} \tag{A.23}$$

Its roots can then be determined in the usual way.

A.6 THE ROOTS OF QUARTIC POLYNOMIALS

For the fourth order polynomial equations, there exists an analytic solution. As with cubic equations, the general quartic equation,

$$A_4 x^4 + A_3 x^3 + A_2 x^2 + A_1 x + A_0 = 0, \tag{A.24}$$

has to be written as

$$f(x) = x^4 + a_3 x^3 + a_2 x^2 + a_1 x + a_0 = 0 \quad \text{with } a_i = \frac{A_i}{A_4}. \tag{A.25}$$

We now define an auxiliary cubic equation, the cubic resolvent:

$$\begin{aligned} g(x) &= x^3 + b_2 x^2 + b_1 x + b_0 = 0 \\ \text{with } b_2 &= a_2 \\ b_1 &= a_1 a_3 - 4a_0 \\ b_0 &= a_1^2 + a_0(a_3^2 - 4a_2) \end{aligned} \tag{A.26}$$

This equation can be solved with the methods introduced in the previous sections. Let z denote its largest root and t the expression

$$t = \sqrt{\frac{z^2}{4} - a_0}, \tag{A.27}$$

which is always real. Then z and t can be used to set up a pair of quadratic equations:

$$\begin{aligned} h(x) &= x^2 + c_1 x + c_0 \\ \text{with } c_0 &= -\frac{z}{2} \pm t \\ c_1 &= \begin{cases} \pm\frac{1}{2t}(c_0 a_3 - a_1) & \text{if } t > 0 \\ \frac{a_3}{2} \pm \sqrt{\frac{1}{4}a_3^2 - z - a_2} & \text{if } t = 0 \end{cases} \end{aligned} \tag{A.28}$$

Each of these equations has a pair of roots,

$$x_{\pm} = -\frac{c_1}{2} \pm \sqrt{\frac{c_1^2}{4} - c_0}, \tag{A.29}$$

if its discriminant $c_1^2/4 - c_0$ is not negative. Therefore, a quartic polynomial can have 4, 2, or no real roots.

Note: This algorithm can be *very* sensitive to round-off errors. It is advisable to have polynomial coefficients of comparable orders of magnitude. This can be achieved by proper scaling, i.e., by replacing Eq. (A.25) by

$$\begin{gathered} y^4 + b_3 y^3 + b_2 y^2 + b_1 y + b_0 \\ \text{with } y = sx,\, b_i = a_i s^{4-i}, \end{gathered} \tag{A.30}$$

where s is a scaling factor approximately given by $s \approx \max(|a_i|^{1/i})$. Usually, the rather time consuming computations of the fractional powers can be avoided by working with the exponents of the binary representations of the coefficients.[3]

As with cubic polynomials, it is advisable to follow-up the analytical solution procedure with a single Newton iteration step to reduce round-off errors.

A.7 THE ROOTS OF QUINTIC POLYNOMIALS

Except for some special cases, no analytic solution exists for fifth-order polynomial equations. But even so, an efficient solving strategy can be devised.

The polynomial has to be normalized, i.e., converted from its general form,

$$\sum_{i=0}^{4} A_i x^i = 0, \tag{A.31}$$

into

$$f(x) = x^5 + a_4 x^4 + a_3 x^3 + a_2 x^2 + a_1 x + a_0 = 0 \quad \text{with } a_i = \frac{A_i}{A_5}. \tag{A.32}$$

It can be then shown that the interval $-r \le x_k \le +r$ with $r = 1 + \max(|a_i|)$ must contain all real roots. Furthermore, as we are dealing with a polynomial of odd order, there must be at least one real root. Consequently, a regula falsi search (see Section A.3) between $-r$ and $+r$ must find a first root, x_1.

---

[3] C, C++: use `frexp()` to extract the exponent part of a double-precision number, and `ldexp()` to multiply with powers of 2.

With this root, the quintic polynomial can be "deflated," i.e., divided by $(x-x_1)$. The result is a quartic polynomial equation,

$$\begin{gathered} g(x)=b_4x^4+b_3x^3+b_2x^2+b_1x+b_0 \\ \text{with } b_4=1 \text{ and } b_i=a_{i+1}+x_1b_{i+1},\, i=3,\ldots 0 \end{gathered} \tag{A.33}$$

This can then be solved as described in the previous section.

A.8 NUMERICAL DIFFERENTIATION

The numerical differentiation of functions, i.e., the estimation of derivatives from finite differences of function values, is often considered as a crude, "quick and dirty" approach, whereas the symbolic differentiation ("calculus") is considered as the proper way.

In numerical computations involving floating-point arithmetics, however, all calculations are imprecise, and the choice is not between an exact calculation and an approximation but rather between computing efficiently and inefficiently or between choosing numerically stable and unstable methods.

With regard to differentiation, one should realise that, with the exception of polynomials, derivatives tend to be more complicated and longer than the original functions. It is then necessary to weigh the known uncertainty of numerical differentiation against the often hard to assess cumulative round-off error of the "exact" calculation.

A.8.1 Symmetric Differentiation Methods

Numerical differentiation methods are usually based on the Taylor expansion of a function. Thus, the function value at $x+h$ is

$$\begin{aligned} f(x+h) &= f(x)+f'(x)h+\frac{1}{2}f''(x)h^2+\frac{1}{6}f'''(x)h^3+\cdots \\ &= \sum_{i=0}^{\infty}\frac{1}{i!}f^{(i)}(x)h^i \end{aligned} \tag{A.34}$$

Likewise, the function value at $x-h$ can be written as

$$f(x-h)=f(x)-f'(x)h+\frac{1}{2}f''(x)h^2-\frac{1}{6}f'''(x)h^3+\cdots. \tag{A.35}$$

On subtracting these two equations from each other, the even-order terms cancel:

$$f(x+h)-f(x-h)=2f'(x)h+\frac{1}{3}f'''(x)h^3+\cdots \tag{A.36}$$

Rearrangement then gives the first-order derivative:

$$f'(x)=\frac{1}{2h}(f(x+h)-f(x-h))+O(h^2) \tag{A.37}$$

The error caused by the truncation of the Taylor series decreases with the square of the differentiation increment. There is no point in making h too small, because otherwise too much precision is lost in the difference in the numerator. If the overall relative precision is 10^{-10}, which is a reasonable assumption in double-precision arithmetics, a choice of $h \approx 10^{-5} x_0$ usually gives a sufficiently good estimate of the derivative.

On no account the approximation

$$f'(x) = \frac{1}{h}(f(x+h) - f(x)) + O(h) \tag{A.38}$$

should be used. This equation seems to be suggested by the mathematical definition of the first-order derivative, but its truncation error is $O(h)$ instead of $O(h^2)$.

Adding instead of subtracting the two Taylor series makes the odd-order terms cancel and leads to a simple estimation formula for second-order derivatives:

$$f''(x) = \frac{1}{h^2}(f(x+h) - 2f(x) + f(x-h)) + O(h) \tag{A.39}$$

By combining the Taylor expansions at the nodes $x \pm h$, $x \pm \lambda h$, $x \pm \lambda^2 h$, ..., $x \pm \lambda^k h$ (λ being a constant expansion factor usually chosen between 1.4 and 2), it is possible to generate approximation formulas for derivatives of all orders with any desired order of the truncation error. Rombergs's differentiation scheme uses the following basic differentiation formulas for differentiation orders 1–4 [216],

$$\begin{aligned}
f_k^{(1)}(x) &= \frac{1}{2\lambda^k h}(f(x+\lambda^k h) - f(x-\lambda^k h)) \\
f_k^{(2)}(x) &= \frac{1}{(2\lambda^k h)^2}(f(x+2\lambda^k h) - 2f(x) + f(x-2\lambda^k h)) \\
f_k^{(3)}(x) &= \frac{1}{(2\lambda^k h)^3}(f(x+3\lambda^k h) - 3f(x+\lambda^k h) + 3f(x-\lambda^k h) \\
&\quad - f(x-3\lambda^k h)) \\
f_k^{(4)}(x) &= \frac{1}{(2\lambda^k h)^4}(f(x+4\lambda^k h) - 4f(x+2\lambda^k h) + 6f(x) \\
&\quad - 4f(x-2\lambda^k h) + f(x-4\lambda^k h)),
\end{aligned} \tag{A.40}$$

and combines them as follows:

$$\begin{array}{lll}
L_{00} = f_0^{(n)}(x) & & \\
L_{10} = f_1^{(n)}(x) & L_{11} = \frac{L_{00} - L_{10}\lambda^{-2}}{1-\lambda^{-2}} & \\
L_{20} = f_2^{(n)}(x) & L_{21} = \frac{L_{10} - L_{20}\lambda^{-2}}{1-\lambda^{-2}} & L_{22} = \frac{L_{11} - L_{21}\lambda^{-4}}{1-\lambda^{-4}} \\
\vdots & \vdots & \vdots
\end{array} \tag{A.41}$$

The L_{kk} rapidly converge against the desired derivative; with each row of the scheme, the order of the truncation error increases by 2. In most cases, the L_{11} or L_{22} approximations are already sufficient. To minimize round-off errors, a larger value for the increment h should be chosen, e.g., $h \approx 10^{-3}x$ for double-precision arithmetics.

Ridder's method is similar to Romberg's method but includes a self-checking feature that terminates the calculation when no further reduction of the numerical uncertainty is possible [219].

A.8.2 Asymmetric Differentiation Methods

The differentiation methods explained above invoke the function symmetrically at $x \pm h$. This can be a problem if the function argument has got a restricted range; e.g., a numerical differentiation with respect to a mole fraction with a differentiation increment $h = 10^{-3}$ at $x = 0.9995$ would require a function evaluation at a mole fraction of 1.0005; this might lead to unpredictable results or even a program crash. If the function argument is close to the boundary of the permissible range, x_b, it is better to construct an interpolation polynomial through $f(x_\mathrm{b})$ and a few more function values and then to differentiate that analytically. According to Lagrange, such an interpolation polynomial of order n through $n+1$ function values $y_k = f(x_k), k = 0, \ldots n$ can be constructed as

$$\begin{aligned} \sum_{0}^{n} a_i x^i &= \sum_{k=0}^{n} L_k(x) y_k \\ \text{with } L_k(x) &= \frac{\prod_{j \neq k}^{n} (x - x_i)}{\prod_{j \neq k}^{n} (x_k - x_i)}. \end{aligned} \tag{A.42}$$

The coefficients a_i of the interpolation polynomial can be obtained as

$$\begin{aligned} a_i &= \sum_{k=0}^{n} \frac{y_k q_{i,k}}{p_k}, \quad i = 0, \ldots n \\ \text{with } p_k &= \prod_{j \neq k}^{n} (x_k - x_j); \end{aligned} \tag{A.43}$$

the $q_{i,k}$ are sums of all $x_{j \neq k}$ and all their possible doublet, triplet, etc., products:

$$q_{0,k} = (-1)^n x_0 x_1 \ldots x_n = \prod_{j \neq k} (-x_j)$$

$$
\begin{aligned}
q_{1,k} &= (-1)^{n-1}(x_1x_2\ldots x_n + x_0x_2\ldots x_n + \cdots + x_0x_1\ldots x_{n-1}) \\
&= \sum_{l\neq k}\prod_{j\neq k,l}(-x_j) \\
q_{2,k} &= (-1)^{n-2}x_2x_3\ldots x_n + x_0x_3\ldots x_n + \cdots + x_0x_1\ldots x_{n-2} \\
&= \sum_{l\neq k}\sum_{m<l}\prod_{j\neq k,l,m}(-x_j) \qquad \text{(A.44)} \\
&\vdots \\
q_{n-1,k} &= (-1)^1(x_0 + x_1 + x_2 + \cdots + x_n) = \sum_{l\neq k}(-x_j) \\
q_{n,k} &= (-1)^0 = 1
\end{aligned}
$$

This looks complicated at a first glance, but the sums and products can be programmed very efficiently (see Algorithm 11). Moreover, the p_k and $q_{i,k}$ do not depend on the function values but on the x_k only. For a given differentiation problem, e.g., of molar densities ρ_i near to 0, the p_k and $q_{i,k}$ need to be determined only once and can be reused.

An example is the calculation of a first-order derivative of a function with respect to a mole fraction near $x=0$. For this, we choose a second-order polynomial and use equidistant x_k, i.e., $x_0=0$, $x_1=h$, and $x_2=2h$. Then the

---

Algorithm 11: Lagrange Interpolation Polynomial.

```
Data: n data pairs $(x_i, y_i), i=0\ldots n-1$
Result: coefficients of interpolation polynomial, $a_i, i=0\ldots n-1$

forall $a_i$ do $a_i := 0$;
for $k := 0\ldots n-1$ do
    $q_{0,k} := 1$, all other $q_{i,k} := 0$;
    $p_k := 1$;
    for $j := s := 0\ldots n-1$ do
        if $j \neq k$ then
            $s := s+1$;
            for $i := s\ldots 1$ do $q_{i,k} := -q_{i,k}x_j + q_{i-1,k}$;
            $q_{0,k} := -q_{0,k}x_j$;
            $p_k := p_k(x_k - x_j)$;
        end
    end
    forall $a_i$ do $a_i := a_i + y_k q_{i,k}/p_k$
end
```

interpolation coefficients are

$$\vec{p}=\begin{pmatrix} 2h^2 & -h^2 & 2h^2 \end{pmatrix}$$
$$\boldsymbol{q}=\begin{pmatrix} 2h^2 & 0 & 0 \\ -3h & -2h & -h \\ 1 & 1 & 1 \end{pmatrix}, \tag{A.45}$$

and so the coefficients of the interpolation polynomial are

$$\begin{aligned} a_0 &= y_0 \\ a_1 &= h^{-1}\left(-\frac{3}{2}y_0+2y_1-\frac{1}{2}y_2\right) \\ a_2 &= h^{-2}\left(\frac{1}{2}y_0-y_1+\frac{1}{2}y_2\right). \end{aligned} \tag{A.46}$$

The desired derivative is then obtained as a_1+2a_2x. Its truncation error is of the order $O(h^2)$, which is the same as that of the "symmetric" formula Eq. (A.37). But the "asymmetric" formula requires the evaluation of three function values instead of merely two and is therefore less efficient.

Finally, a word of caution is in order: numerical differentiation should only be used where the derivatives are known to exist! This may seem a trivial advice, but a dangerous pitfall exists in connection with thermodynamic functions that contain logarithms of mole fractions, such as the Gibbs energy of a mixture:

$$G_\mathrm{m}=\sum\left(x_iG_{\mathrm{m},i}(p,T)+RTx_i\ln x_i\right)+G^\mathrm{E}(p,T,\vec{x}) \tag{A.47}$$

The slope, curvature, and all higher derivatives of $\ln x_i$ diverge for $x_i \to 0$. Applying numerical differentiation to G_m at high dilution of a component is bound to be unreliable. In such a case, it is advisable to differentiate the logarithmic terms analytically and to apply numerical differentiation to the excess part only, which is usually well behaved.

A.9 NUMERICAL INTEGRATION

Some equations of state have a functional form that makes analytic integration (to obtain the Helmholtz energy) difficult or impossible. Equations of state for mixtures containing density-dependent mixing rules or contributions of chemical equilibria often belong to this class. In such cases, numerical integration can be used.

An overview of all existing methods would fill a book. The interested reader is referred to textbooks of numerical mathematics. For convenience, however, we will mention a few methods that have proven useful in connection with thermodynamic calculations.

A measure of the quality of a numerical integration methods often used in mathematical textbooks is its polynomial order: an integration method of order n will give an exact result for polynomials of nth order. Analytical functions that are not polynomials still can be approximated by them to any desired degree of accuracy, for instance in the form of Taylor series. Therefore, a higher polynomial order of an integration method means an exact representation of more terms of the series, and this usually leads to a better accuracy of the integration.

For the practical selection of integration methods, however, the polynomial order is of secondary importance only. The most important question is how the integrand is supplied. Here is a short (and very incomplete!) list of integration methods:

1. *The integrand is supplied as a table*
   - **i.** *With equidistant nodes (abscissa values):*
     Consider Simpson's/Newton's rule.
   - **ii.** *With irregularly spaced nodes:*
     Construct a cubic spline function through the data points and integrate analytically. If the data contain noise, use a smoothing spline function [220].
2. *The integrand is supplied as a function, i.e., can be evaluated for any desired abscissa value.*
   - **i.** *The polynomial order required to achieve the desired accuracy is already known; speed is essential:*
     Use Gauss' integration scheme of the appropriate order.
   - **ii.** *Same as before, but the integrand can be evaluated with a limited accuracy only:*
     Use Chebyshev's integration scheme or divide the integration range into a number of panels and apply a lower-order Gauss method to each of them.
   - **iii.** *The required polynomial order is not known in advance:*
     Use Romberg's method.

A.9.1 Simpson's/Newton's Method

This is a simple, yet powerful method of third order, i.e., it will integrate cubic polynomials exactly. The underlying principle is the construction of quadratic interpolation polynomials.

If the integrand is supplied as a table of (x_i, y_i) pairs $(y_i = f(x_i))$ with equidistant x_i, $i = 0, \ldots N$, Simpson's rule for the integral is

$$\begin{aligned}\int_{x_0}^{x_N} f(x)\,\mathrm{d}x &\approx I_{\text{Simpson}}(0, N)\\ &= \left(y_0 + 4 \sum_{i=1,3,\ldots}^{N-1} y_i + 2 \sum_{i=2,4,\ldots}^{N-2} y_i + y_N \right) \frac{h}{3},\end{aligned} \tag{A.48}$$

where $h = x_{i+1} - x_i$ is the spacing of the abscissa values.

Note that this scheme only works if N is an even number, i.e., if there is an odd number of data points! Otherwise (N odd, even number of data points), Simpson's rule should only be used for the data points $0, \ldots N-3$, and the remaining part be treated with "Newton's $\frac{3}{8}$ rule":

$$\int_{x_0}^{x_N} f(x)\,\mathrm{d}x \approx I_{\text{Simpson}}(0, N-3) + (y_{N-3} + 3y_{N-2} + 3y_{N-1} + y_N)\,\frac{3h}{8} \tag{A.49}$$

Simpson's and Newton's $\frac{3}{8}$ rules are the first elements of a series of integration methods known as Newton–Cotes formulas.

For the sake of completeness, we also mention the trapezoidal formula,

$$\int_{x_0}^{x_N} f(x)\,\mathrm{d}x \approx \left(y_0 + 2\sum_{i=1}^{N-1} y_i + y_N\right)\frac{h}{2}. \tag{A.50}$$

It should never be used, for it is merely of first order; Eq. (A.49) gives a far more accurate result with the same amount of data.

A.9.2 Gauss′ and Chebyshev's Methods

For a given number of data points, Gauss' integration method gives the highest possible polynomial order, namely $2N+1$ for an Nth-order Gauss formula (which needs $N+1$ function values). The method divides the integration range into two strips of width $h = (b-a)/2$ and calculates a weighted average of the function values at selected locations:

$$\int_{a}^{b} f(x)\,\mathrm{d}x \approx h \sum_{i=-N,-N+2,\ldots}^{N} w_{N,i} f\left(\frac{a+b}{2} + h\,d_{N,i}\right) \tag{A.51}$$

The $w_{N,i}$ and $d_{N,i}$ are fixed weight factors and relative abscissa values, respectively. Some coefficient sets are given in Table A.1. Incidentally, the $d_{N,i}$ are the roots of the Nth-order Legendre polynomial.

It should be noted that, with increasing N, the weight factors for each Gauss coefficient set differ more and more. This can cause problems if the function values can be calculated with a limited precision only.

For the integration of "noisy" functions, Chebyshev's method should be preferred. It is also described by Eq. (A.51), but now the $w_{N,i}$ are all 1, and the $d_{N,i}$ are roots of Chebyshev polynomials instead of Legendre polynomials.

A.9.3 Romberg's Method

Like Romberg's differentiation method, his integration algorithm achieves a cancellation of higher-order residuals by means of a clever superposition of

TABLE A.1 Relative Abscissae $d_{N,i}$ and Weight Factors $w_{N,i}$ for Gauss' Numerical Integration Formulas of *N*th order

N	i	$d_{N,i}$	$w_{N,i}$
0	0	0.000000000000000	2.000000000000000
1	1	0.577350269189626	1.000000000000000
2	0	0.000000000000000	0.888888888888889
	2	0.774596669241483	0.555555555555556
3	1	0.339981043584856	0.652145154862546
	3	0.861136311594053	0.347854845137454
4	0	0.000000000000000	0.568888888888889
	2	0.538469310105683	0.478628670499366
	4	0.906179845938664	0.236926885056189
5	1	0.238619186083197	0.467913934572691
	3	0.661209386466265	0.360761573048139
	5	0.932469514203152	0.171324492379170
6	0	0.000000000000000	0.417959183673469
	2	0.405845151377397	0.381830050505119
	4	0.741531185599394	0.279705391489277
	6	0.949107912342759	0.129484966168870
7	1	0.183434642495650	0.362683783378362
	3	0.525532409916329	0.313706645877887
	5	0.796666477413627	0.222381034453374
	7	0.960289856497536	0.101228536290376
8	0	0.000000000000000	0.330239355001261
	2	0.324253423403809	0.312347077040002
	4	0.613371432700590	0.260610696402936
	6	0.836031107326636	0.180648160694857
	8	0.968160239507626	0.081274388361574
9	1	0.148874338981631	0.295524224714753
	3	0.433395394129247	0.269266719309996
	5	0.679409568299024	0.219086362515982
	7	0.865063366688985	0.149451349150581
	9	0.973906528517172	0.066671344308688

Note that $d_{N,-i} = -d_{N,i}$ *and* $w_{N,-i} = w_{N,i}$.

simpler approximations. We assume that the integrand can be represented by a Taylor series:

$$f(x)=f(a)+f'(a)(x-a)+\frac{1}{2}f''(a)(x-a)^2+\cdots \tag{A.52}$$

Then integration by means of the trapezoidal rule Eq. (A.50), using only one panel of the width $h=b-a$, treats the constant and linear terms accurately but not the higher-order terms:

$$\begin{gathered}\int_a^b f(x)\,\mathrm{d}x=I_{0,0}+\frac{1}{6}f''(a)h^3+O(h^4)\\ \text{with } I_{0,0}=\frac{h}{2}(f(a)+f(a+h))\end{gathered} \tag{A.53}$$

Integration with the trapezoidal rule using *two* panels of the width $h/2$ gives

$$\begin{gathered}\int_a^b f(x)\,\mathrm{d}x=I_{1,0}+2\times\frac{1}{6}f''(a)\frac{h^3}{8}+O(h^4)\\ \text{with } I_{1,0}=\frac{h}{4}\left(f(a)+2f\left(a+\frac{h}{2}\right)+f(a+h)\right).\end{gathered} \tag{A.54}$$

Evidently, by adding Eqs (A.53) and (A.54) with the weights -1 and 4, respectively, the cubic (f'') term can be eliminated:

$$\begin{gathered}\int_a^b f(x)\,\mathrm{d}x=I_{1,1}+O(h^4)\\ \text{with } I_{1,1}=\frac{1}{3}(4I_{1,0}-I_{0,0})\end{gathered} \tag{A.55}$$

In an analogous way, one can make the $O(h^4)$ term disappear by including the result of a trapezoidal integration with panel width $h/4$. This is the idea behind Romberg's algorithm, which can be summarized as follows:

Let $I_{k,0}$ denote the result of an integration with the trapezoidal rule, using 2^k panels,

$$I_{k,0}=\frac{h}{2^k}\left(f(a)+2\sum_{i=1}^{2^k-1}f\left(a+i\frac{h}{2^k}\right)+f(b)\right), \tag{A.56}$$

i.e., the $I_{k,0}$ are a series of approximations where each one uses twice as many function values as the previous one. Then, for each $k>0$, construct the interpolations

$$I_{k,i} = \frac{2^{2i} I_{k,i-1} - I_{k-1,i-1}}{2^{2i}-1}, i = 1, \ldots k. \tag{A.57}$$

The $I_{k,k}$ converge quadratically against the value of the integral. As soon as two successive $I_{k,k}$ differ by less than the desired threshold, the calculation can be safely terminated.

Romberg's method can give wrong results if the function "slips through the tabulation grid." For instance, if a function is integrated over the interval [0, 1], but has nonzero values between 0.59 and 0.60 only, the algorithm would find $L_{0,0} = L_{1,1} = L_{2,2} = 0$ and then terminate prematurely. Evidently, the algorithm is not a substitute for the programmer's insight.

A.9.4 Improper Integrals

Improper integrals are integrals where either the integrand becomes infinite in some location or where the integration limits are infinite. We will address the latter case here, because several integrals in this book are of this kind, e.g., the statistical thermodynamics expressions for the equation of state or the virial coefficient, Eqs (7.21) and (7.23).

In principle, such integrals can be broken up into a series of definite integrals, e.g.,

$$\int_0^\infty f(x)\,\mathrm{d}x = \int_0^a f(x)\,\mathrm{d}x + \int_a^{2a} f(x)\,\mathrm{d}x + \int_{2a}^{3a} f(x)\,\mathrm{d}x + \cdots. \tag{A.58}$$

These can then be evaluated with one of the methods described before; the computation is terminated when the contribution of these "chunks" becomes negligible.

Unless the structure of the integrand function suggests this approach, it must be considered inefficient and unreliable. For even if the chunks beyond a certain distance have negligible values, there are many of them (infinity is far away by definition!), and their total sum may be significant. Therefore, this approach should be used only if its convergence order has been established.

It is usually better to evaluate improper integrals by means of an appropriate coordinate transformation, e.g.,

$$\int_0^\infty f(x)\,\mathrm{d}x = \int_0^a f(x)\,\mathrm{d}x + \int_a^\infty f(x)\,\mathrm{d}x = \int_0^a f(x)\,\mathrm{d}x + \int_0^{a^{-1}} s^{-2} f(s^{-1})\,\mathrm{d}s \tag{A.59}$$

with $s = \frac{1}{x}$, where a is a conveniently chosen abscissa value.

All numerical integration methods discussed in this section assume that the integrand function is continuous. Integration of discontinuous functions, e.g., the heat capacity $C_p(T)$ over a temperature interval in which the system has a phase transition, can lead to unpredictable results.

A.10 ORDINARY DIFFERENTIAL EQUATIONS: RUNGE–KUTTA METHOD

As the conditions of phase equilibrium and criticality can be written as differential equations, we want to mention at least one algorithm that can be used to solve such equations. The reader should be advised, however, that there exists an impressive number of of variants of the algorithm presented here, as well as other methods.

For the Runge–Kutta algorithm, it is assumed that the differential equation can be written as

$$\frac{\mathrm{d}y(x)}{\mathrm{d}x} = f(x, y), \tag{A.60}$$

i.e., that the slope of the unknown function $y(x)$ can be calculated from the function argument and value.

Starting at some initial state (x_0, y_0), the method constructs several intermediate approximations for the change of $y(x)$:

$$\begin{aligned} v_0 &= f(x_0, y_0)h \\ v_1 &= f\left(x_0 + \frac{h}{2}, y_0 + \frac{v_0}{2}\right)h \\ v_2 &= f\left(x_0 + \frac{h}{2}, y_0 + \frac{v_1}{2}\right)h \\ v_3 &= f\left(x_0 + h, y_0 + v_2\right)h \end{aligned} \tag{A.61}$$

Here, h denotes the increment of the argument x. In the beginning, it can be set to $h = x_{\text{final}} - x_0$, i.e., to the size of the x range for which $y(x)$ to be computed. With the intermediate approximations, the Lifshitz criterion is evaluated:

$$L = 2\left|\frac{v_1 - v_2}{v_0 - v_1}\right| \tag{A.62}$$

If $L > 0.2$, the increment was too large. It must be divided by 2, and then the calculation of the v_i and the evaluation of L are repeated, until the condition is met. Likewise, if $L < 0.005$, h must be increased until L becomes acceptable (but not beyond $h = x_{\text{final}} - x_0$!). If L is in the permissible range, the step is accepted, and

$$\begin{aligned} x_1 &= x_0 + h \\ y_1 &= \frac{1}{6}(v_0 + 2v_1 + 2v_2 + v_3) \end{aligned} \tag{A.63}$$

is the next point on the curve $y(x)$. The procedure is repeated from here until x_{final} has been reached.

A.11 LINEAR ALGEBRA

Let a system of linear equations be defined by

$$\begin{aligned} a_{11}x_1 + a_{12}x_2 + \cdots a_{1N}x_N &= b_1 \\ a_{21}x_1 + a_{22}x_2 + \cdots a_{2N}x_N &= b_2 \\ &\vdots \\ a_{n1}x_1 + a_{n2}x_2 + \cdots a_{1N}x_N &= b_N \end{aligned} \tag{A.64}$$

With the definition of the vectors

$$\vec{x} = \begin{pmatrix} x_1 \\ x_2 \\ \vdots \\ x_N \end{pmatrix} \quad \text{and} \quad \vec{b} = \begin{pmatrix} b_1 \\ b_2 \\ \vdots \\ b_N \end{pmatrix} \tag{A.65}$$

and the system matrix

$$\boldsymbol{A} = \begin{pmatrix} a_{11} & a_{12} & \dots & a_{1N} \\ a_{21} & a_{22} & \dots & a_{2N} \\ \vdots & \vdots & \ddots & \vdots \\ a_{N1} & a_{N2} & \dots & a_{NN} \end{pmatrix}, \tag{A.66}$$

the system of equations can be expressed in a compact way as

$$\boldsymbol{A}\vec{x} = \vec{b}. \tag{A.67}$$

This equation can be formally solved by multiplying it from the left side with the inverse of $\boldsymbol{A}$

$$\vec{x} = \boldsymbol{A}^{-1}\vec{b}, \tag{A.68}$$

provided that $\boldsymbol{A}$ it not singular, i.e., that its determinant does not vanish,

$$\det \boldsymbol{A} \neq 0. \tag{A.69}$$

Except for special cases, however, solving systems of linear equation by matrix inversion cannot be recommended, because other methods, e.g., Gauss elimination or Cholesky decomposition, are much faster. The CPU time of all these direct methods of solving linear equations scales approximately with N^3; for large numbers of unknowns, iterative schemes like the Gauss–Seidel method are to be preferred, which scales with N^2 only.

A special case where matrix inversion is easy is *unitary matrices*: here, the transposed matrix is the inverse, $\boldsymbol{A}^{\mathrm{T}} = \boldsymbol{A}^{-1}$. Examples are rotation matrices.

An equation of the form

$$\boldsymbol{A}\vec{x} = \lambda\vec{x}, \tag{A.70}$$

where λ is a scalar, is called an eigenvalue equation. If $\vec{x}$ is interpreted as a vector in N-dimensional space and $\boldsymbol{A}$ as a geometrical transformation matrix, the eigenvalue equation describes the problem of finding a vector that is not affected by the transformation except for a change of size. Such a vector is called an eigenvector of the matrix, and the size scaling factor λ is the associated eigenvalue. For example, if $\boldsymbol{A}$ represents a reflection in a plane, then the eigenvectors are vectors that are either parallel or perpendicular to the mirror axis. The former have the eigenvalue 1 (no change in size) and the latter have the eigenvalue -1 (change of direction).

The eigenvalue problem can also be stated as

$$\boldsymbol{B}\vec{x} = (\boldsymbol{A} - \lambda\boldsymbol{I})\vec{x} = 0, \tag{A.71}$$

where $\boldsymbol{I}$ denotes the unity matrix. This equation evidently has a trivial solution, $\vec{x} = 0$. But if $\det \boldsymbol{B} = 0$, nontrivial solutions $\vec{x} \neq 0$ are possible.

These nontrivial solutions can, in principle, be found by evaluating the determinant; this leads to a polynomial equation of Nth order in λ, the so-called secular equation. There are some interesting facts to observe:

- In principle, the polynomial has N roots. Hence, there are N eigenvalues λ_i, and each one is associated with an eigenvector $\vec{x}_i$.
- The lengths of the eigenvectors are not fixed: the product of an eigenvector and an arbitrary scalar is also a solution of the eigenvalue equation.
- If the matrix $\boldsymbol{A}$ is symmetric, all eigenvalues λ are real; otherwise, complex eigenvalues can occur.
- An “unitary transformation,” i.e., a transformation with an unitary matrix $\boldsymbol{U}$ of the form $\boldsymbol{C} = \boldsymbol{U}^{\mathrm{T}}\boldsymbol{A}\boldsymbol{U}$ does not change the eigenvalues. This can easily be shown by substituting $\boldsymbol{C}$ into Eq. (A.71):

$$(\boldsymbol{C} - \lambda\boldsymbol{I})\vec{x} = (\boldsymbol{U}^{\mathrm{T}}\boldsymbol{A}\boldsymbol{U} - \lambda\boldsymbol{U}^{\mathrm{T}}\boldsymbol{U})\vec{x} = \boldsymbol{U}^{\mathrm{T}}(\boldsymbol{A} - \lambda\boldsymbol{I})\boldsymbol{U}\vec{x} = 0. \tag{A.72}$$

Evidently, an eigenvector/eigenvalue combination that fulfills $(\boldsymbol{A} - \lambda\boldsymbol{I})\vec{x} = 0$ must also fulfill $(\boldsymbol{C} - \lambda\boldsymbol{I})\vec{x} = 0$.

This invariance of the eigenvalues under unitary transformations can be used to determine them, as will be shown in the next section.

A particularly interesting subclass of the symmetric matrices is the *positive definite matrices*. For these, the “quadratic form” $\vec{v}^{\mathrm{T}}\boldsymbol{A}\vec{v}$ is positive for arbitrary nonzero vectors $\vec{v}$.

Let $\boldsymbol{A}$ be a positive definite matrix, and $\boldsymbol{U}$ a unitary matrix that diagonalizes it:

$$\boldsymbol{U}^{\mathrm{T}}\boldsymbol{A}\boldsymbol{U} = \mathrm{diag}(\lambda_1, \lambda_2, \ldots, \lambda_N) \tag{A.73}$$

Now a matrix multiplication as the one shown above involves the multiplication of a column vector of $\boldsymbol{U}$ with matrix $\boldsymbol{A}$ and then a multiplication of the result with a row vector of $\boldsymbol{U}^{\mathrm{T}}$:

$$c_{ij} = \vec{u}_j^{\mathrm{T}}\boldsymbol{A}\vec{u}_i = \begin{cases} \lambda_i & \text{if } i = j \\ 0 & \text{if } i \neq j \end{cases} \tag{A.74}$$

The matrix-vector product in this equation represents a quadratic form, which has to be positive. Therefore, we conclude that a positive definite matrix has only positive eigenvalues.

In the context of the calculation of critical states of mixtures, we observe that the term second-order fluctuation in the expansion of the Helmholtz energy, Eq. (5.124), represents a quadratic form:

$$\sum_{i=1}^{N}\sum_{j=1}^{N}\left(\frac{\partial^2 A}{\partial n_i \partial n_j}\right)\Delta n_i \Delta n_j = \Delta\vec{n}^{\mathrm{T}}\boldsymbol{Q}\cdot\Delta\vec{n}. \tag{A.75}$$

If $\boldsymbol{Q}$ is positive definite, this product is positive for arbitrary fluctuations $\Delta\vec{n}$, and the system is stable (each possible fluctuation increases the Helmholtz energy). All eigenvalues are positive.

If the system moves toward a critical point, one of the eigenvalues decreases. It becomes zero at the critical point, and then its eigenvalue equation becomes

$$\boldsymbol{Q}\Delta\vec{n} = 0, \tag{A.76}$$

which is one of the central equations of the Heidemann–Khalil algorithm for the calculation of critical points.

A.12 EIGENVALUES OF A SYMMETRIC MATRIX

As explained in the previous section, the eigenvalues of a symmetric matrix having only real elements must all be real. Fortunately, the matrices encountered in phase equilibrium calculations are of this kind.

As eigenvalue problems play a central role in engineering as well as quantum mechanics, many methods for solving them have been developed in the past. Some of these methods find all eigenvalues and the associated eigenvectors, and others find only the eigenvalue with largest (or smallest) absolute value. As a thermodynamic stability analysis at least requires the lowermost eigenvalue, regardless of its absolute size, the latter methods are not useful in this context.

As mentioned above, a possible way to find the eigenvalues of a symmetric matrix is constructing and then solving the secular equation. This means the expansion of the determinant of the matrix $\boldsymbol{B}$ in Eq. (A.71) and then the calculation of the roots of the resulting polynomial with an appropriate root finder. This is a very fast approach for small matrices but becomes inefficient when the root finder requires iterations.

A generally viable alternative is the rotation method of Jacobi. Here, the original matrix is multiplied with a series of rotation matrices, the prescription for the mth multiplication being

$$\begin{aligned}
&\boldsymbol{A}^{(m+1)} = \boldsymbol{R}_m^{\mathrm{T}} \boldsymbol{A}^{(m)} \boldsymbol{R}_m \\
&\text{with } \boldsymbol{R}_m = \begin{pmatrix} 1 \ldots & 0 & \ldots & 0 & \ldots 0 \\ \vdots \ddots & \vdots & & \vdots & \vdots \\ 0 \ldots & \cos(\phi) & \ldots & \sin(\phi) & \ldots 0 \\ \vdots & \vdots & \ddots & \vdots & \vdots \\ 0 \ldots & -\sin(\phi) & \ldots & \cos(\phi) & \ldots 0 \\ \vdots & \vdots & & \vdots & \vdots \\ 0 \ldots & 0 & \ldots & 0 & \ddots 1 \end{pmatrix}
\end{aligned} \tag{A.77}$$

The (double) matrix multiplication is a unitary transformation. Therefore, it does not change the eigenvalues, as shown in the previous section. If the angle-dependent terms in the rotation matrix are in the rows and columns k and l, the transformation affects the matrix elements a_{kk}, a_{kl}, a_{lk}, and a_{ll} in the following way:

$$\begin{aligned}
a_{kk}^{(m+1)} &= a_{kk}^{(m)} \cos^2\phi - 2a_{kl}^{(m)} \cos\phi \, \sin\phi + a_{ll}^{(m)} \sin^2\phi \\
a_{kl}^{(m+1)} = a_{lk}^{(m+1)} &= \left(a_{kk}^{(m)} - a_{ll}^{(m)}\right) \cos\phi \, \sin\phi + a_{kl}^{(m)} \left(\cos^2\phi - \sin^2\phi\right) \\
&= \left(a_{kk}^{(m)} - a_{ll}^{(m)}\right) \frac{1}{2} \sin 2\phi + a_{kl}^{(m)} \cos 2\phi \\
a_{ll}^{(m+1)} &= a_{kk}^{(m)} \sin^2\phi + 2a_{kl}^{(m)} \cos\phi \, \sin\phi + a_{ll}^{(m)} \cos^2\phi
\end{aligned} \tag{A.78}$$

With the choice

$$\begin{aligned}
&\cos\phi = \frac{1}{\sqrt{1+\tan^2\phi}} \qquad \sin\phi = \tan\phi \, \cos\phi \\
&\tan\phi = \begin{cases} \frac{1}{\omega + \sqrt{1+\omega^2}} & \omega > 0 \\ 1 & \omega = 0 \\ \frac{1}{\omega - \sqrt{1+\omega^2}} & \omega < 0 \end{cases} \qquad \omega = \frac{a_{ll}^{(m)} - a_{kk}^{(m)}}{2a_{kl}^{(m)}},
\end{aligned} \tag{A.79}$$

the matrix elements a_{kl} and a_{lk} become zero.

Of course, the transformation also affects the other matrix elements in the rows and columns k and l.

Such rotations must then be applied to all off-diagonal elements of the matrix. After several "sweeps," the off-diagonal elements approach zero, and the diagonal elements converge against the eigenvalues. This is why the calculation of eigenvalues of a matrix is often called "matrix diagonalization."

Applying the same sequence of Jacobi rotations to an identity matrix produces a matrix composed of the eigenvectors.

A.13 PARAMETER FITTING AND SYSTEMS OF NONLINEAR EQUATIONS

The problem of "parameter fitting" can be stated as follows: there is a set of experimental data (t_i, Y_i), which is supposed to be described by a model function $f(t;\vec{x})$; the function has the argument t and a set of parameters $\vec{x}$. The goal is now to determine $\vec{x}$ in such a way that the deviations of the function from the experimental data y_i (the so-called residuals) become minimal:

$$y_i = f(t_i;\vec{x}) - Y_i \quad \text{with } i = 1, \ldots n \tag{A.80}$$

This consideration can easily be extended to functions with more than one argument, but this is not relevant for the discussion of the optimization methods.

The parameter fitting problem can be solved only if the number of experimental data, n, is at least as large as the number of the adjustable parameters, m.

We will now turn the goal of having "minimal deviations" into a quantitative criterion by postulating

$$\sum_{i=1}^{n} y_i^2 \overset{!}{=} \text{min.} \tag{A.81}$$

This is by no means the only way of setting up such a criterion, but the most common. Moreover, many other ways can be related to this one. By using vector notation, the criterion can be written as

$$\vec{y}^2 = \vec{y}^{\mathrm{T}} \cdot \vec{y} \overset{!}{=} \text{min.} \tag{A.82}$$

To find this minimum, we calculate the gradient with respect to the adjustable parameters:

$$\nabla(\vec{y}^{\mathrm{T}} \cdot \vec{y}) = 0 \tag{A.83}$$

This can be rearranged to give

$$(\nabla \vec{y}^{\mathrm{T}})\vec{y} = 0. \tag{A.84}$$

Now the first term represents the Jacobian matrix of the problem, a matrix containing derivatives of all y_i with respect to all x_k:

$$\boldsymbol{J} = \nabla \vec{y}^{\mathrm{T}} = \begin{pmatrix} \frac{\partial y_1}{\partial x_1} & \frac{\partial y_2}{\partial x_1} & \cdots & \frac{\partial y_n}{\partial x_1} \\ \frac{\partial y_1}{\partial x_2} & \frac{\partial y_2}{\partial x_2} & \cdots & \frac{\partial y_n}{\partial x_2} \\ \vdots & \vdots & \ddots & \vdots \\ \frac{\partial y_1}{\partial x_m} & \frac{\partial y_2}{\partial x_m} & \cdots & \frac{\partial y_n}{\partial x_m} \end{pmatrix} \tag{A.85}$$

Therefore, the minimization criterion can be written as

$$\boldsymbol{J}\,\vec{y} = 0. \tag{A.86}$$

We now assume that the y_i can be expanded into Taylor series at the location of the minimum:

$$\begin{aligned} y_i = y_{i0} + \left(\frac{\partial y_i}{\partial x_1}\right)\Delta x_1 + \left(\frac{\partial y_i}{\partial x_2}\right)\Delta x_2 + \ldots \left(\frac{\partial y_i}{\partial x_m}\right)\Delta x_m \\ + O((\Delta x_k)^2), \quad i = 1, \ldots n \end{aligned} \tag{A.87}$$

y_{i0} is the value of y_i at the minimum. This Taylor series is truncated after the linear term. In vector notation, it can be written as

$$\vec{y} = \vec{y}_0 + \boldsymbol{J}^{\mathrm{T}} \Delta\vec{x}. \tag{A.88}$$

This equation contains the transposed Jacobian matrix of the problem, i.e., matrix $\boldsymbol{J}$ with rows and columns exchanged.

Multiplying this equation from the left side with $\boldsymbol{J}$ gives

$$\boldsymbol{J}\,\vec{y} = \boldsymbol{J}\vec{y}_0 + \boldsymbol{J}\boldsymbol{J}^{\mathrm{T}} \Delta\vec{x}. \tag{A.89}$$

$\boldsymbol{J}\vec{y}_0$ is zero, because this is the minimization criterion. $\boldsymbol{B} = \boldsymbol{J}\boldsymbol{J}^{\mathrm{T}}$ is a quadratic $m \times m$ matrix. Therefore, the equation can be written as

$$\boldsymbol{J}\,\vec{y} = \boldsymbol{B}\Delta\vec{x}. \tag{A.90}$$

From this, the correction vector can be obtained,

$$\Delta\vec{x} = \boldsymbol{B}^{-1}(\boldsymbol{J}\,\vec{y}), \tag{A.91}$$

and then $\vec{x} - \Delta\vec{x}$ is a parameter vector that is (perhaps) nearer to the minimum.

This is the *Gauss–Newton method* for parameter optimization. It locates the minimum in one step if the model function is a linear combination of some basis functions, $f(t;\vec{x}) = \sum_i x_i g_i(t)$; otherwise iteration is necessary. The Gauss–Newton method converges with quadratic convergence order – if it converges at all. If the model function does not locally behave like a linear combination, it diverges rapidly. In practical applications, the radius of convergence is often found to be rather small.

The Gauss–Newton method requires the solution of a linear system of equations. There are other ways of doing this than matrix inversion, but in this case, the matrix changes slowly and can often be kept for several iteration steps. Even so, matrix inversion becomes inefficient above $m \approx 20$. The Jacobian matrix can be obtained by numerical differentiation; Eq. (A.37) is sufficient. Small errors of the Jacobian matrix can be tolerated, because they are corrected at the next iteration step.

An alternative to the Gauss-Newton method is the *gradient method*, also called "method of steepest descent." It starts from the same initial equation as the Gauss–Newton method, Eq. (A.82), but takes a different point of view: $\vec{y}^2$ is a function of $\vec{x}$ and can be represented graphically as a curved hypersurface ("landscape") in an $(m+1)$-dimensional space. The optimization problem is then equivalent to locating the deepest valley in the landscape. The gradient method amounts to choosing a trial solution and then to move "downhill." The mathematical formulation is

$$\Delta\vec{x} = -\lambda^{-1}\nabla(\vec{y}^{\mathrm{T}}\vec{y}) = -\lambda^{-1}\boldsymbol{J}\,\vec{y}. \tag{A.92}$$

λ is a positive factor that sets the step size. There are several strategies for choosing λ (see for instance [216]). The important aspects here are that a properly controlled gradient method surely converges to a minimum, if one exists (Whether it is the deepest one or only a local minimum is another question.), but that the convergence is slow (first-order only). Premature termination of the iteration is a common source of error with this method. It is not necessary to solve any linear equations within the gradient method.

The *Marquardt–Levenberg method* tries to combine the advantages of the Gauss–Newton and the gradient methods [217, 221]. Both methods derive their correction steps from the gradient of $\vec{y}^2$; the Marquardt–Levenberg method superimposes their results:

$$\boldsymbol{J}\,\vec{y} = \boldsymbol{B}\Delta\vec{x} - \lambda\Delta\vec{x} = (\boldsymbol{B} - \lambda\boldsymbol{I})\,\Delta\vec{x} \tag{A.93}$$

Here, $\boldsymbol{I}$ denotes the unity matrix. The correction step is then obtained as

$$\Delta\vec{x} = (\boldsymbol{B} - \lambda\boldsymbol{I})^{-1}\cdot(\boldsymbol{J}\,\vec{y}). \tag{A.94}$$

λ is now a control parameter: $\lambda = 0$ gives the correction step of the Gauss–Newton method, whereas a large value makes the Marquardt–Levenberg method behave like the gradient method. The iteration is usually started with a large $\lambda \approx 1$. If an iteration step achieves a decrease of $\vec{y}^2$, λ is decreased by a factor of 2–10; if a step makes $\vec{y}^2$ increase or causes an error of the object function, it is canceled and then repeated with a larger λ. Thus, the Marquardt–Levenberg method has a large radius of convergence like the gradient method but converges rapidly when it comes into the vicinity of the solution.

It is good technique to set $\lambda = 0$ when it falls below a certain threshold, e.g., 10^{-4}, and to start at this threshold when it has to be increased. If λ gets large, one can switch over to a pure gradient method and thus save the CPU time required for the matrix inversion.

However, the tricks of the trade – the determination of λ thresholds, the stabilization against round-off errors (if the adjustable parameters have very different sizes), and the definition of termination criteria, etc. – would probably fill a book. The reader is advised to consult textbooks on this matter or to look up the original literature.

The Marquardt–Levenberg method can of course also be used if $m = n$, and then it is an excellent method for solving systems of nonlinear equations.

An interesting alternative to the Marquardt–Levenberg method is the gradient search method of Powell [219, 222]. It works by doing sequential one-dimensional minimizations along different directions by local parabola fitting. This methods avoids the computation of derivatives and inverse matrices.

The so-called simplex algorithm by Nelder and Mead [223] constructs a “simplex,” i.e., an $(n+1)$-dimensional object in the n-dimensional space spanned by an n-parameter problem. So a problem with two adjustable parameters requires three initial guesses, which constitute a triangle in the two-dimensional parameter space. The algorithm moves the simplex systematically about and makes it contract about the solution. The simplex algorithm is known to converge when most other methods fail. But its convergence order is linear only, and so the algorithm is prone to have large termination errors. It should be used as a last resort only and then – if it found a solution – be followed by a parameter fitting method with a better convergence order.

Appendix B

Proofs

B.1 LEGENDRE TRANSFORMATION

In thermodynamics, some variables appear to be associated, e.g., pressure p and volume V or entropy S and temperature T. Other examples would be voltage and electric charge or surface tension and area: in these pairs of variables, one variable is always a density-style variable and the other one a field-style variable. Which of the two is better suited as independent variable of thermodynamic functions depends very much on the application.

A Legendre transformation is, somewhat loosely expressed, a method for swapping associated variables.

Consider a differentiable function f of the variable x and let $y = \mathrm{d}f(x)/\mathrm{d}x$ denote its derivative; i.e., the differential of f is $\mathrm{d}f = y\,\mathrm{d}x$. Then

$$g = f - x\frac{\mathrm{d}f}{\mathrm{d}x} = f - xy \tag{B.1}$$

is a function of y only, as can be seen from the differential of this equation:

$$\mathrm{d}g = \mathrm{d}(f - xy) = y\,\mathrm{d}x - x\,\mathrm{d}y - y\,\mathrm{d}x = x\,\mathrm{d}y. \tag{B.2}$$

Eq. (B.1) is called a Legendre transformation.

A geometric interpretation is attempted in Fig. B.1: The function $f(x)$ can evidently be given as a set of data pairs $(x, f(x))$ or it can be represented by a set of tangents. Each of these tangents is characterized by its slope y and its ordinate intercept $g(y)$. Therefore, we can write for the tangent in the point $(x_0, f(x_0))$:

$$t_{x_0}(x) = \underbrace{\frac{\mathrm{d}f(x_0)}{\mathrm{d}x}}_{=y}\, x + \underbrace{f(x_0) - \frac{\mathrm{d}f(x_0)}{\mathrm{d}x}x_0}_{=g(y)}\,. \tag{B.3}$$

The function $y \to g(y)$ is then the Legendre transform of $x \to f(x)$ (Fig. B.2). Both representations, $(x, f(x))$ and $(y, g(y))$, contain the same information.

Integration of y by parts gives

$$f = \int y(x)\,\mathrm{d}x = xy - \int x(y)\,\mathrm{d}y = xy - g\,, \tag{B.4}$$

High-Pressure Fluid Phase Equilibria. DOI: 10.1016/B978-0-444-56347-7.00011-6

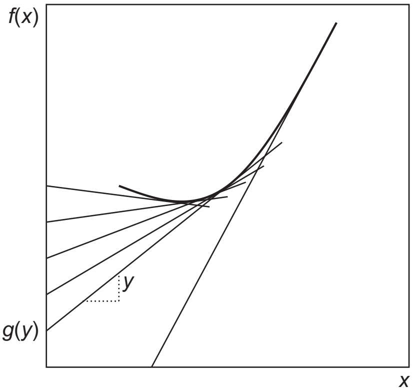

FIGURE B.1 Representation of a function $f(x)$ by a set of tangents with slopes $y = \mathrm{d}f(x)/\mathrm{d}x$ and intercepts $g(y)$.

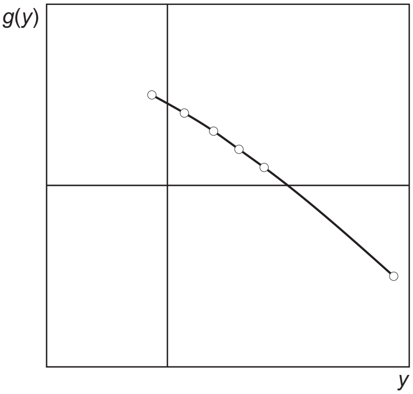

FIGURE B.2 Legendre transform of the function in Fig. B.1, a plot of the intercepts versus the slopes. ○: representation of the tangents in Fig. B.1.

or, using definite integrals,

$$\int_{x_0}^{x_1} y(x)\,\mathrm{d}x = (x_1 y_1 - x_0 y_0) - \int_{y_0}^{y_1} x(y)\,\mathrm{d}y. \tag{B.5}$$

This is illustrated in Fig. B.3: The area ABCD $(=f(x))$ is equal to the difference of the rectangle areas OBDF and OACE minus the area ECDF $(=g(y))$. Evidently, $f(x)$ and $g(y)$ describe the same object, but from different points of view.

These considerations can easily be generalized to functions of more than one variable. A more detailed derivation of Legendre transformations can be found in [141].

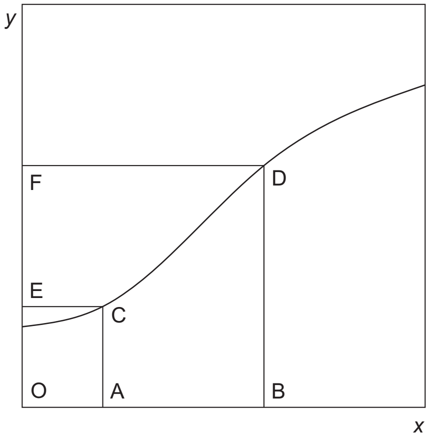

FIGURE B.3 Illustration of the integration by parts of a function.

B.2 THE SLOPES OF ISOCHORES

A widely used experimental method for determining phase equilibria is the study of isochores: a sample is introduced into a pressure vessel with a fixed volume. Then the temperature is increased and the pressure recorded. Transitions between one-phase and two-phase states cause a change of the slope of the isochore.

Griffiths [224, 225] proved that this change of the slope does not always occur. The mathematical proof makes use of the following theorem:

Let $\xi(\psi, \omega)$ denote a continuous function of the variables ψ and ω. It is then assumed that there is a curve in the (ψ, ω) plain that divides it into two domains (designated $'$ and $''$). Along this curve, the derivatives of ξ are discontinuous.

Because of the continuity of ξ, its total differential along this curve is given by

$$\mathrm{d}\xi = \left(\frac{\partial \xi}{\partial \psi}\right)'_{\omega} \mathrm{d}\psi + \left(\frac{\partial \xi}{\partial \omega}\right)'_{\psi} \mathrm{d}\omega = \left(\frac{\partial \xi}{\partial \psi}\right)''_{\omega} \mathrm{d}\psi + \left(\frac{\partial \xi}{\partial \omega}\right)''_{\psi} \mathrm{d}\omega\,. \tag{B.6}$$

Rearrangement of the terms then leads to:

$$\left[\left(\frac{\partial \xi}{\partial \psi}\right)'_{\omega} - \left(\frac{\partial \xi}{\partial \psi}\right)''_{\omega}\right] \mathrm{d}\psi = -\left[\left(\frac{\partial \xi}{\partial \omega}\right)'_{\psi} - \left(\frac{\partial \xi}{\partial \omega}\right)''_{\psi}\right] \mathrm{d}\omega \tag{B.7}$$

$$\Delta \left(\frac{\partial \xi}{\partial \psi}\right)_{\omega} = -\frac{\mathrm{d}\omega}{\mathrm{d}\psi} \Delta \left(\frac{\partial \xi}{\partial \omega}\right)_{\psi}\,. \tag{B.8}$$

It is now assumed that the two domains are a one-phase and two-phase region of a phase diagram, and the dividing curve is a phase boundary. We set

$\xi = p$, $\psi = \rho$, and $\omega = T$ and apply the theorem Eq. (B.8):

$$\Delta\left(\frac{\partial p}{\partial \rho}\right)_T = -\frac{\mathrm{d}T}{\mathrm{d}\rho}\,\Delta\left(\frac{\partial p}{\partial T}\right)_\rho . \tag{B.9}$$

$\Delta(\partial p/\partial T)_\rho$ is the desired change of the slope of an isochore at a phase boundary (here: an isopleth). The derivative $\mathrm{d}T/\mathrm{d}\rho$ is taken along the phase boundary. For low densities below the maxcondentherm (MT) point ($\rho < \rho_{\mathrm{MT}}$), this derivative is positive; for densities above the maxcondentherm point, the derivative is negative.

In order to prove that $\Delta(\partial p/\partial \rho)_T$ cannot be negative, we invoke the theorem Eq. (B.8) with $\xi = \rho$, $\psi = p$, and $\omega = x_1$:

$$\Delta\left(\frac{\partial \rho}{\partial p}\right)_{x_1,T} = -\frac{\mathrm{d}x_1}{\mathrm{d}p}\,\Delta\left(\frac{\partial \rho}{\partial x_1}\right)_{p,T} . \tag{B.10}$$

The last term of this equation can be expressed with a Maxwell relation:

$$\left(\frac{\partial \rho}{\partial x_1}\right)_{p,T} = -\rho^2\left(\frac{\partial^2 G_{\mathrm{m}}}{\partial x_1 \partial p}\right)_T = -\rho^2\left(\frac{\partial G_{(x)}}{\partial p}\right)_{x_1,T} . \tag{B.11}$$

Eq. (B.10), therefore, becomes

$$\Delta\left(\frac{\partial \rho}{\partial p}\right)_{x_1,T} = +\frac{\mathrm{d}x_1}{\mathrm{d}p}\rho^2\,\Delta\left(\frac{\partial G_{(x)}}{\partial p}\right)_{x_1,T} . \tag{B.12}$$

The last term in this equation can be resolved by invoking theorem Eq. (B.8) with $\xi = G_{(x)}$, $\psi = p$, and $\omega = x_1$:

$$\Delta\left(\frac{\partial G_{(x)}}{\partial p}\right)_T = -\frac{\mathrm{d}x_1}{\mathrm{d}p}\,\Delta\left(\frac{\partial G_{(x)}}{\partial x_1}\right)_{p,T} = -\frac{\mathrm{d}x_1}{\mathrm{d}p}G_{(2x)} . \tag{B.13}$$

Substitution of this expression into Eq. (B.12) gives

$$\Delta\left(\frac{\partial \rho}{\partial p}\right)_{x_1,T} = -\rho^2\left(\frac{\mathrm{d}x_1}{\mathrm{d}p}\right)^2 \Delta G_{(2x)} . \tag{B.14}$$

The two quadratic factors cannot become negative. $\Delta G_{(2x)} = G'_{(2x)} - G''_{(2x)}$ cannot become negative, too: because of the requirement of diffusion stability in the one-phase region, $G'_{(2x)} > 0$ must hold; in the two-phase region, the Gibbs energy is a linear function of composition, hence $G''_{(2x)} = 0$, and

$$\Delta\left(\frac{\partial \rho}{\partial p}\right)_{x_1,T} = \left(\frac{\partial \rho}{\partial p}\right)'_{x_1,T} - \left(\frac{\partial \rho}{\partial p}\right)''_{x_1,T} \leq 0. \tag{B.15}$$

Now for each phase

$$\left(\frac{\partial \rho}{\partial p}\right)_{x_1,T} > 0 \tag{B.16}$$

must be true because of the requirement of mechanical stability. Therefore, one can conclude from the last two inequalities that

$$\Delta\left(\frac{\partial p}{\partial \rho}\right)_{x_1,T} \geq 0. \tag{B.17}$$

Application of this result to Eq. (B.12) then leads to the insight that $-\mathrm{d}x_1/\mathrm{d}p$ and $\Delta(\partial\rho/\partial x_1)_{p,T}$ must have the same sign. As $-\mathrm{d}x_1/\mathrm{d}p$ changes its sign and becomes zero at $\rho = \rho_{\mathrm{MT}}$, so must $\Delta(\partial\rho/\partial x_1)_{p,T}$. Consequently, the change of the isochore slope is zero at the maxcondentherm point.

One must conclude that experiments determining phase equilibria from the slopes of isochores have a "blind spot" at the maxcondentherm point.

An analogous study of the behavior of isentropes shows that these do not show a discontinuity of the slope in the vicinity of a maxcondenbar point.

B.3 THE EXPANSION THEOREM OF JACOBIAN DETERMINANTS

The expansion theorem of Jacobian determinants can be stated as follows:

$$\frac{\partial(x,y)}{\partial(u,v)} = \frac{\partial(x,y)}{\partial(z,w)}\,\frac{\partial(z,w)}{\partial(u,v)}. \tag{B.18}$$

For a proof, we consider the multiplication of the two determinants on the right-hand side. Applying the multiplication rules for determinants then gives

$$\frac{\partial(x,y)}{\partial(z,w)}\,\frac{\partial(z,w)}{\partial(u,v)} = \begin{vmatrix} x_z z_u + x_w w_u & x_z z_v + x_w w_v \\ y_z z_u + y_w w_u & y_z z_v + y_w w_v \end{vmatrix}. \tag{B.19}$$

The first element of the resulting determinant can be rewritten assuming $v =$ constant as

$$\left(\frac{\partial x}{\partial z}\right)_w \left(\frac{\partial z}{\partial u}\right)_v + \left(\frac{\partial x}{\partial w}\right)_z \left(\frac{\partial w}{\partial u}\right)_v = \left.\frac{(\partial x/\partial z)_w \mathrm{d}z + (\partial x/\partial w)_z \mathrm{d}w}{\mathrm{d}u}\right|_v. \tag{B.20}$$

Evidently, the numerator of the fraction is a total differential, and hence it is possible to write

$$\left(\frac{\partial x}{\partial z}\right)_w \left(\frac{\partial z}{\partial u}\right)_v + \left(\frac{\partial x}{\partial w}\right)_z \left(\frac{\partial w}{\partial u}\right)_v = \left.\frac{\mathrm{d}x}{\mathrm{d}u}\right|_v = \left(\frac{\partial x}{\partial u}\right)_v. \tag{B.21}$$

The other three elements of the determinant can be transformed in a similar manner; combining the results for all elements gives

$$\frac{\partial(x,y)}{\partial(z,w)}\frac{\partial(z,w)}{\partial(u,v)} = \begin{vmatrix} \left(\frac{\partial x}{\partial u}\right)_v & \left(\frac{\partial x}{\partial v}\right)_u \\ \left(\frac{\partial y}{\partial u}\right)_v & \left(\frac{\partial y}{\partial v}\right)_u \end{vmatrix}. \tag{B.22}$$

The result of this equation, however, is the definition equation of the Jacobian determinant $\partial(x,y)/\partial(u,v)$, which completes the proof.

Appendix C

Equations of State: Auxiliary Equations for Programming

For some popular equations of state, we present auxiliary information to facilitate programming.

Conventions:

- All equations of state for real gases have at least two parameters, a characteristic volume (size parameter, covolume, molecular size), v^*, and a characteristic temperature, $T^* = \epsilon / k_\mathrm{B}$, where ϵ denotes a pair potential well depth or similar (energetic) measure of the attraction between pairs of molecules.
- We write all equations in terms of reduced (dimensionless) densities, $\xi = v^*/V_\mathrm{m}$, and reduced temperatures, $\tilde{T} = T/T^*$.

C.1 THE van der WAALS EQUATION OF STATE

The original van der Waals attraction parameter is identified with $a_\mathrm{vdW} = 2\pi v^* R T^*$.

$$Z = \frac{1}{1-\xi} - \frac{2\pi}{\tilde{T}}\xi \tag{C.1}$$

$$\frac{A_\mathrm{m}^\mathrm{r}}{RT} = -\ln(1-\xi) - \frac{2\pi}{\tilde{T}}\xi \tag{C.2}$$

Cubic polynomial needed for inversion:

$$2\pi\xi^3 - 2\pi\xi^2 + (\tilde{p} + \tilde{T})\xi - \tilde{p} = 0 \qquad \text{with } \tilde{p} = \frac{pv^*}{RT^*} \tag{C.3}$$

Critical point: $\tilde{T}_\mathrm{c} = 1.861685$, $\xi_\mathrm{c} = 0.333333$, $Z_\mathrm{c} = 0.375$.

High-Pressure Fluid Phase Equilibria. DOI: 10.1016/B978-0-444-56347-7.00012-8

C.2 THE REDLICH–KWONG EQUATION OF STATE

The original attraction parameter is identified with $a_{\mathrm{RK}} = 8v^*R(T^*)^{3/2}$. The factor 8 is arbitrary; this choice ensures that $k_\mathrm{B}T^*$ is approximately equal to the Lennard-Jones energy parameter.

$$Z = \frac{1}{1-\xi} - \frac{8\xi}{1+\xi}\tilde{T}^{-3/2} \tag{C.4}$$

$$\frac{A_\mathrm{m}^\mathrm{r}}{RT} = -\ln(1-\xi) - 8\ln(1+\xi)\tilde{T}^{-3/2} \tag{C.5}$$

Cubic polynomial needed for inversion:

$$8\tilde{T}^{-1/2}\xi^3 + (\tilde{T}+\tilde{p}-8\tilde{T}^{-1/2})\xi^2 + \tilde{T}\xi - \tilde{p} = 0 \qquad \text{with } \tilde{p} = \frac{pv^*}{RT^*} \tag{C.6}$$

Critical point: $\tilde{T}_\mathrm{c} = 1.380160$, $\xi_\mathrm{c} = 0.259921$, $Z_\mathrm{c} = 0.333333$.

C.3 THE REDLICH–KWONG–SOAVE EQUATION OF STATE

The original attraction parameter is identified with $a_\mathrm{c} = 8v^*RT^*$; again, the constant 8 is arbitrary.

$$Z = \frac{1}{1-\xi} - \frac{8\xi}{1+\xi}\frac{\alpha(\tilde{T})}{\tilde{T}} \tag{C.7}$$

$$\frac{A_\mathrm{m}^\mathrm{r}}{RT} = -\ln(1-\xi) - 8\ln(1+\xi)\,\frac{\alpha(\tilde{T})}{\tilde{T}} \tag{C.8}$$

Cubic polynomial needed for inversion:

$$8\xi^3 + (\tau+\tilde{p}-8)\xi^2 + \tau\xi - \tilde{p} = 0 \qquad \text{with } \tilde{p} = \frac{pv^*}{RT^*\alpha(\tilde{T})},\ \tau = \frac{\tilde{T}}{\alpha(\tilde{T})} \tag{C.9}$$

Critical point: $\tilde{T}_\mathrm{c} = 1.380160$, $\xi_\mathrm{c} = 0.259921$, $Z_\mathrm{c} = 0.333333$.

C.4 THE PENG–ROBINSON EQUATION OF STATE

The original attraction parameter is identified with $a_\mathrm{c} = 8v^*RT^*$; the factor 8 is arbitrary.

$$Z = \frac{1}{1-\xi} - \frac{8\xi}{1+2\xi-\xi^2}\frac{\alpha(\tilde{T})}{\tilde{T}} \tag{C.10}$$

$$\frac{A_\mathrm{m}^\mathrm{r}}{RT} = -\ln(1-\xi) - 2\sqrt{2}\ln\frac{1+\xi(\sqrt{2}+1)}{1-\xi(\sqrt{2}-1)}\,\frac{\alpha(\tilde{T})}{\tilde{T}} \tag{C.11}$$

Cubic polynomial needed for inversion:

$$(8-\tau-\tilde{p})\xi^3 + (2\tau+3\tilde{p}-8)\xi^2 + (\tau-\tilde{p})\xi - \tilde{p} = 0$$
$$\text{with } \tilde{p} = \frac{pv^*}{RT^*\alpha(\tilde{T})},\ \tau = \frac{\tilde{T}}{\alpha(\tilde{T})} \tag{C.12}$$

Critical point: $\tilde{T}_\mathrm{c} = 1.361155$, $\xi_\mathrm{c} = 0.253077$, $Z_\mathrm{c} = 0.307401$.

C.5 THE CARNAHAN–STARLING–van der WAALS EQUATION OF STATE

The van der Waals attraction parameter is identified with $a_\mathrm{vdW} = 8v^*RT^*$, where f is an arbitrary numerical constant.

$$Z = 1 + \frac{4\xi - 2\xi^2}{(1-\xi)^3} - \frac{8}{\tilde{T}}\xi \tag{C.13}$$

$$\frac{A_\mathrm{m}^\mathrm{r}}{RT} = -\frac{4\xi - 3\xi^2}{(1-\xi)^2} - \frac{8}{\tilde{T}}\xi \tag{C.14}$$

Fifth-order polynomial needed for inversion:

$$-8\xi^5 + (\tilde{T}+24)\xi^4 - (\tilde{T}+\tilde{p}+24)\xi^3 + (3\tilde{p}-\tilde{T}+8)\xi^2 - (3\tilde{p}+\tilde{T})\xi + \tilde{p} = 0$$
$$\text{with } \tilde{p} = \frac{pv^*}{RT^*} \tag{C.15}$$

Critical point: $\tilde{T}_\mathrm{c} = 0.754630$, $\xi_\mathrm{c} = 0.130444$, $Z_\mathrm{c} = 0.358956$.

C.6 THE SIMPLIFIED PERTURBED–HARD–CHAIN EQUATION OF STATE

$$Z = 1 + c\frac{4\xi - 2\xi^2}{(1-\xi)^3} - \frac{18c\xi f}{1+\xi f}$$
$$\text{with } f = \frac{1}{\tau}\left(\exp\left(\frac{1}{2\tilde{T}}\right) - 1\right), \quad \tau = \frac{\pi}{6}\sqrt{2} \tag{C.16}$$

$$\frac{A_\mathrm{m}^\mathrm{r}}{RT} = c\frac{4\xi - 3\xi^2}{(1-\xi)^2} - 18c\ln(1+\xi f) \tag{C.17}$$

Fifth-order polynomial needed for inversion:

$$\begin{aligned}(18c-1)\tilde{T}f\xi^5 &+ \big(\tilde{T}(3f-56cf-1)+\tilde{p}f\big)\xi^4 + \big(\tilde{T}(-3f+58cf-2c+3)\\ &+\tilde{p}(1-3f)\big)\xi^3 + \big(\tilde{T}(4c-3+f-18cf)+3\tilde{p}(f-1)\big)\xi^2\\ &+\big(\tilde{T}+\tilde{p}(3-f)\big)\xi-\tilde{p}=0\end{aligned} \tag{C.18}$$

The roots of this equation can then be calculated with a suitable polynomial root finder. But the application of a general nonlinear equation solver to Eq. (C.16) might be more efficient.

The location of the critical point depends on the parameter c in a complicated way. The following expressions are merely approximations: $\tilde{T}_\mathrm{c} \approx 1.253540 - 0.4642899(c-1)$, $\xi_\mathrm{c} \approx 0.157179 - 0.033608(c-1)$, $Z_\mathrm{c} \approx 0.348018 - 0.001302(c-1)$.

Appendix D

Solutions of the Problems

CHAPTER 2 – PHENOMENOLOGY OF PHASE DIAGRAMS

Problem 1

There are three components, HCl, NH_3, and NH_4Cl, in two phases, namely gas (HCl, NH_3) and solid (NH_4Cl). There is a chemical reaction equilibrium

$$NH_3 + HCl \rightleftharpoons NH_4Cl,$$

which must be counted as one thermodynamic constraint. The number of the degrees of freedom is therefore

$$F = N - P + 2 - C = 2,$$

if the system is made from arbitrary amounts of the compounds. The two degrees of freedom might be the temperature and the NH_3/HCl ratio, for instance.

If the system is made by heating NH_4Cl, the gas phase can contain equal amounts of HCl and NH_3 only. This is another thermodynamic constraint, and in this case the number of the degrees of freedom is 1, i.e., NH_4Cl has an apparent sublimation pressure curve like an ordinary sublimating compound.

If the chlorine isotopes are taken into account, the number of components is $N = 5$. But if there is no process or manipulation that can change the isotopic ratios, the $H^{37}Cl/H^{35}Cl$ and $NH_4{}^{37}Cl/NH_4{}^{35}Cl$ ratios are constrained, so that in the end F remains the same.

Problem 2

The mixture under consideration contains N components and consists of k coexisting phases. Let n_i^α denote the amount of component i in the phase α. The total amount of component i in the system can be expressed with the overall

High-Pressure Fluid Phase Equilibria. DOI: 10.1016/B978-0-444-56347-7.00013-X

composition,

$$n_i = x_i n = x_i \sum_\alpha n^\alpha, \tag{D.1}$$

or with the phase compositions,

$$n_i = \sum_\alpha x_i^\alpha n^\alpha. \tag{D.2}$$

Equating these two expressions yields

$$x_i \sum_\alpha n^\alpha = \sum_\alpha x_i^\alpha n^\alpha, \tag{D.3}$$

which can be rearranged to

$$\sum_\alpha n^\alpha (x_i^\alpha - x_i) = 0, \quad i = 1, \ldots N. \tag{D.4}$$

This is the general lever rule for a multicomponent system. Eq. (D.4) must be fulfilled for all components i, i.e., it represents a set of N linear equations for the n^α.

Of this set, only $N-1$ equations are independent (The summation of all N equations gives a trivial expression, $0=0$). Furthermore, the right side of this set of equations is zero, so that $n^\alpha = 0$ is a trivial solution. This problem can be resolved by assigning a positive, nonzero value either to one of the n^α or to n, the total amount of substance. Thus there are $N-1$ independent linear equations for $k-1$ unknown variables.

Now several cases must be distinguished:

1. $k = N$, e.g., two-phase equilibrium of a binary mixture, or three-phase equilibrium of a ternary mixture: we have to solve a set of $N-1$ independent linear equations for $N-1$ variables: the n^α can be computed.
2. $k < N$, e.g., two-phase equilibrium in a ternary mixture: now there are fewer unknown variables, but at the same time more equations become linearly dependent. In our example, the lever arms are parts of the same connode, and thus collinear: the n^α can be computed.
3. $N < k \leq N+2$, e.g., three-phase equilibrium of a binary mixture, like the three-phase line in Figs 2.37 and 2.38: now there are fewer equations than unknown phase amounts. This case has no unique solution: the phase amounts depend on how the equilibrium state was reached.

Problem 3

The azeotropic curve ends on the critical curve in a critical azeotropic point, and here the two curves must have the same slope. Placing the critical azeotropic point on the temperature minimum of the critical curve implies an infinite slope for the azeotropic curve. This is not possible: because of Eq. (5.98), an infinite slope means $\Delta_{\text{vap}} V_\text{m} = 0$, whereas $\Delta_{\text{vap}} S_\text{m} \neq 0$. But if two phases have the same composition (azeotrope!) and the same molar volume, they must be identical and cannot have different entropies.

Problem 4

The *px* cross sections will look qualitatively the same: a *vertical* path through the *pT* diagram intersects the vapor pressure curve of component 2 and then either the vapor pressure curve of component 1 or the critical curve.

If the critical pressure of component 1 is higher, a *horizontal* path through the *pT* diagram at a pressure between the critical pressures of the pure components will intersect the vapor pressure curve of component 1 and then the critical curve. Consequently, the phase envelopes will originate at the $x = 1$ ordinate. If component 2 has the higher critical pressure, they will originate at the $x = 0$ ordinate as in Fig. 2.19.

Problem 5

The isopleths look similar to the one shown in Fig. 2.18, except for one detail: the liquid and gas branches of the isopleths cross.

Problem 6

It is possible. In contrast to the usual class II, however, *px* cross sections like curve B of Fig. 2.49 appear. In contrast to class III, the ll two-phase region contracts and the lg two-phase region persists when the temperature is increased.

Problem 7

The *px* cross sections are the same as in Fig. 2.27; at low temperatures, there are cross sections like curves A and B of Fig. 2.38.

The *Tx* cross sections can be obtained by complementing the curves in Fig. 2.24 with low-temperature ll demixing regions as in Fig. 2.37.

CHAPTER 3 – EXPERIMENTAL TECHNIQUES

Problem 1

Given properties: the total amounts of substance in experiment A, $n_{1,\text{A}}$ and $n_{2,\text{A}}$, the observed phase volumes, V'_A and V''_A, as well as the analogous properties for experiment B.

Auxiliary properties: total mole fractions $x_{1,\text{A}} = n_{1,\text{A}} / (n_{1,\text{A}} + n_{2,\text{A}})$; amounts of substance per phase, $n'_\text{A} + n''_\text{A} = n_\text{A} = n_{1,\text{A}} + n_{2,\text{A}}$.

Equations: the lever rule,

$$(x_{1,\mathrm{A}} - x_1')n_\mathrm{A}' = (x_1'' - x_{1,\mathrm{A}})n_\mathrm{A}'', \tag{D.5}$$

two volume relations,

$$V_\mathrm{A}' = n_\mathrm{A}' V_\mathrm{m}' \qquad V_\mathrm{A}'' = n_\mathrm{A}'' V_\mathrm{m}'', \tag{D.6}$$

and the analogous equations for experiment B. This gives a total of six equations for six unknown properties.

The ratios of the volume relations, Eq. (D.6), for experiments A and B are

$$\frac{V_\mathrm{A}'}{V_\mathrm{B}'} = \frac{n_\mathrm{A}'}{n_\mathrm{B}'} \qquad \frac{V_\mathrm{A}''}{V_\mathrm{B}''} = \frac{n_\mathrm{A}''}{n_\mathrm{B}''}. \tag{D.7}$$

Now the lever rule can be written with $n_\mathrm{A}'' = n_\mathrm{A} - n_\mathrm{A}'$ as

$$(x_{1,\mathrm{A}} - x_1')n_\mathrm{A}' = (x_1'' - x_{1,\mathrm{A}})(n_\mathrm{A} - n_\mathrm{A}') \tag{D.8}$$

or

$$(x_1'' - x_1')n_\mathrm{A}' = (x_1'' - x_{1,\mathrm{A}})n_\mathrm{A} \tag{D.9}$$

An analogous expression can be derived for experiment B. The ratio of these two expressions is

$$\frac{n_\mathrm{A}'}{n_\mathrm{B}'} = \frac{V_\mathrm{A}'}{V_\mathrm{B}'} = \frac{x_1'' - x_{1,\mathrm{A}}}{x_1'' - x_{1,\mathrm{B}}}, \tag{D.10}$$

which, after some rearrangements, gives the desired phase composition:

$$x_1'' = \frac{x_{1,\mathrm{A}} - x_{1,\mathrm{B}} \frac{V_\mathrm{A}'}{V_\mathrm{B}'}}{1 - \frac{V_\mathrm{A}'}{V_\mathrm{B}'}}. \tag{D.11}$$

Switching the phase indicators gives

$$x_1' = \frac{x_{1,\mathrm{A}} - x_{1,\mathrm{B}} \frac{V_\mathrm{A}''}{V_\mathrm{B}''}}{1 - \frac{V_\mathrm{A}''}{V_\mathrm{B}''}}. \tag{D.12}$$

Once the mole fractions of the equilibrium phases are known, the amounts of substance per phase can be obtained from the lever rule Eq. (D.9), e.g.,

$$n_\mathrm{A}' = \frac{x_1'' - x_{1,\mathrm{A}}}{x_1'' - x_1'} n_\mathrm{A}, \tag{D.13}$$

and then $V_\mathrm{m}' = V_\mathrm{A}'/n_\mathrm{A}'$ gives the desired molar volume of the first phase; a similar expression holds for the second phase.

Problem 2

Given properties: total mole fraction, x_1, phase boundaries $x_1'(T), x_1''(T)$.

When the sample passes through the two-phase region, the amounts of the phases can be obtained from the lever rule, which we write here as

$$n' = nf' = n\frac{x_1'' - x_1}{x_1'' - x_1'}, \tag{D.14}$$

with a similar expression for n''.

The enthalpy of the sample is [cf. Eq. (5.181)]

$$H = \begin{cases} nH_\mathrm{m}' & \text{below the two-phase region} \\ n'H_\mathrm{m}' + n''H_\mathrm{m}'' & \text{in the two-phase region} \\ nH_\mathrm{m}'' & \text{above the two-phase region.} \end{cases} \tag{D.15}$$

Substitution of Eq. (D.14) into the expression for the two-phase region gives

$$H = n(H_\mathrm{m}'f' + H_\mathrm{m}''f'') \tag{D.16}$$

The heat flow of the instrument is

$$\dot{q} = \left(\frac{\partial H}{\partial t}\right)_p = \frac{\mathrm{d}T(t)}{\mathrm{d}t}\left(\frac{\partial H}{\partial T}\right), \tag{D.17}$$

where $\dot{T} = \mathrm{d}T(x)/\mathrm{d}t$ is the (usually constant) heating or cooling rate. Carrying out the differentiations yields

$$\dot{q} = n\dot{T}\begin{cases} C_{p\mathrm{m}}' & \text{below} \\ \left(C_{p\mathrm{m}}'f' + C_{p\mathrm{m}}''f''\right) + f_H & \text{in the 2-phase region} \\ C_{p\mathrm{m}}'' & \text{above} \end{cases} \tag{D.18}$$
$$\text{with } f_H = \sum_{\alpha = ','' } \left(\left(\frac{\partial H_\mathrm{m}^\alpha}{\partial x_1}\right)_{p,T} - \frac{H_\mathrm{m}'' - H_\mathrm{m}'}{x_1'' - x_1'}\right)\frac{\mathrm{d}x_1^\alpha}{\mathrm{d}T}f^\alpha.$$

When the two-phase region is entered, we have $x_1'(T) = x_1$, when it is left, $x_1''(T) = x_1$. Consequently, the entry value of the $C_{p\mathrm{m}}$ term for the two-phase region is $C_{p\mathrm{m}}'$ and the exit value $C_{p\mathrm{m}}''$. The $C_{p\mathrm{m}}$ term in the two-phase region is therefore a smooth interpolation between the baselines of the one-phase regions.

The entry and exit values of f_H are

$$\begin{aligned} f_{H,\mathrm{in}} &= \left(H_{(x)}' - \frac{\Delta H_\mathrm{m}}{\Delta x_1}\right)\frac{\mathrm{d}x_1'}{\mathrm{d}T} \\ f_{H,\mathrm{out}} &= \left(H_{(x)}'' - \frac{\Delta H_\mathrm{m}}{\Delta x_1}\right)\frac{\mathrm{d}x_1''}{\mathrm{d}T}. \end{aligned} \tag{D.19}$$

Therefore, the enthalpy term is abruptly turned on or off when the phase boundary is crossed, and this causes a discontinuity. It can be shown that f_H is always positive, i.e., that it increases the apparent heat capacity (cf. Section 5.9). f_H can also be written as

$$f_H = \sum_{\alpha={}',{}''} H^{\alpha}_{(x)} f^{\alpha} \frac{\mathrm{d}x_1^{\alpha}}{\mathrm{d}T} - \frac{\Delta H_\mathrm{m}}{\Delta x_1} \left(\frac{\mathrm{d}x_1'}{\mathrm{d}T} + \frac{\mathrm{d}(x_1'' - x_1')}{\mathrm{d}T} f'' \right). \tag{D.20}$$

If $x_1'(T)$ and $x_1''(T)$ always have the same slopes, f_H is approximately constant, and the resulting DSC trace has a rectangular or trapezoidal shape. In Fig. 3.5, however, the difference of the slopes changes from negative to positive, as $x_1 - x_1'$ moves from 0 to $x_1'' - x_1'$. Consequently, the second term between the parentheses has a minimum, and this gives rise to the double spike.

CHAPTER 4 – THERMODYNAMIC VARIABLES AND FUNCTIONS

Problem 1

We can make use of Eq. (4.55):

$$\mu_1^\mathrm{E} = G^\mathrm{E} + x_2 \left(\frac{\partial G^\mathrm{E}}{\partial x_1} \right)_{p,T}. \tag{D.21}$$

Substitution of the Redlich–Kister function

$$G^\mathrm{E} = x_1 x_2 \left(A_0 + A_1 (x_1 - x_2) \right) \tag{D.22}$$

gives

$$\mu_1^\mathrm{E} = A_0 x_2^2 + A_1 (3 x_1 x_2^2 - x_2^3) = (A_0 + 3A_1) x_2^2 - 4 A_1 x_2^3. \tag{D.23}$$

The expression for μ_2^E can be obtained from this equation by switching the subscripts.

At high dilution of component 2, only the first term is significant:

$$\mu_1^\mathrm{E} \simeq (A_0 + 3A_1) x_2^2. \tag{D.24}$$

Evidently, the excess chemical potential of the majority component is proportional to x_2^2. This is a general feature of analytic excess functions.

Problem 2

There is nothing wrong with an excess Helmholtz energy defined as a difference of real- and ideal-mixture Helmholtz energy at fixed pressure:

$$A^{\mathrm{E}}(p,T,\vec{x}) = A_{\mathrm{m}}(p,T,\vec{x}) - \sum_{i=1}^{N} x_i (A_{\mathrm{m},i}(p,T) + RT\ln x_i). \tag{D.25}$$

We can assemble A^{E} from the primary excess functions:

$$A^{\mathrm{E}} = H^{\mathrm{E}} - pV^{\mathrm{E}} - TS^{\mathrm{E}}. \tag{D.26}$$

Therefore an ideal mixture (H^{E}, V^{E}, $S^{\mathrm{E}} = 0$) has a zero excess Helmholtz energy.

For an excess property defined for isochoric mixing we would start from the pure components at the molar volume of the mixture, which might imply a compression to a huge pressure. We would then expand to the ideal-gas state, mix, and recompress to the given molar volume. According to Eq. (4.19), the questionable "isochoric excess Helmholtz energy" A^{e} would then be

$$A^{\mathrm{e}} = -\int_{V_{\mathrm{m}}^{\ominus}}^{V_{\mathrm{m}}} p(V_{\mathrm{m}},T,\vec{x})\,\mathrm{d}V_{\mathrm{m}} + \sum_{i=1}^{N} x_i \int_{V_{\mathrm{m}}^{\ominus}}^{V_{\mathrm{m}}} p(V_{\mathrm{m}},T;i)\,\mathrm{d}V_{\mathrm{m}}. \tag{D.27}$$

It should be noted that we must use the mole fractions x_i as statistical weights, because otherwise the intrinsic terms of Eq. (4.19) would not cancel out.

Evidently, each component of a mixture can have a different equation of state (or at least different parameters for the same equation of state): the $p(V_{\mathrm{m}},T;i)$ differ, and so do the integrals. There is no reason why an ideal mixture should have a zero *isochoric* excess Helmholtz energy.

The only exception is the case where all pure components obey the same equation of state, for instance the ideal-gas law. Then, and only then, the definition of an isochoric excess Helmholtz energy might be meaningful.

Problem 3

Excess properties are differences between properties of real fluids and ideal mixtures. So what is the compressibility of an ideal mixture? This property can be derived from the molar volume of an ideal mixture (see Eq. 4.42),

$$V_{\mathrm{m}}^{\mathrm{idmix}} = \sum_{i=1}^{N} x_i V_{\mathrm{m},i}, \tag{D.28}$$

by taking the derivative with respect to pressure:

$$\left(\frac{\partial V_\mathrm{m}^\mathrm{idmix}}{\partial p}\right)_T = \sum_{i=1}^{N}\left(\frac{\partial V_{\mathrm{m},i}}{\partial p}\right)_T. \tag{D.29}$$

Inserting these two equations into the definition of the isothermal compressibility gives

$$\begin{aligned}\kappa_T^\mathrm{idmix} &= -\frac{1}{V_\mathrm{m}^\mathrm{idmix}}\left(\frac{\partial V_\mathrm{m}^\mathrm{idmix}}{\partial p}\right)_T = -\frac{\sum x_i\left(\frac{\partial V_{\mathrm{m},i}}{\partial p}\right)}{\sum x_i V_{\mathrm{m},i}}\\ &= \frac{\sum x_i V_{\mathrm{m},i}\kappa_{T,i}}{\sum x_i V_{\mathrm{m},i}}.\end{aligned} \tag{D.30}$$

Now $\varphi_i = x_i V_{\mathrm{m},i}/\sum_k x_k v_{\mathrm{m},k}$ is the volume fraction of the mixture. We can therefore write

$$\kappa_T^\mathrm{idmix} = \sum_{i=1}^{N}\varphi_i\kappa_{T,i}, \tag{D.31}$$

and thus the definition of the excess isothermal compressibility is

$$\kappa_T^\mathrm{E} = \kappa_T - \kappa_T^\mathrm{idmix} = \kappa_T^\mathrm{E} = \kappa_T - \sum_{i=1}^{N}\varphi_i\kappa_{T,i}. \tag{D.32}$$

Problem 4

$$p = \frac{RT}{V_\mathrm{m}} + \frac{RTB_2}{V_\mathrm{m}^2} \tag{D.33}$$

$$A_\mathrm{m} - A_\mathrm{m}^\ominus = -\int_{V_\mathrm{m}^\ominus}^{V_\mathrm{m}} p\,\mathrm{d}V_\mathrm{m} = -RT\ln\frac{V_\mathrm{m}}{V_\mathrm{m}^\ominus} + RTB_2\left(\frac{1}{V_\mathrm{m}} - \frac{1}{V_\mathrm{m}^\ominus}\right). \tag{D.34}$$

The term $B_2/V_\mathrm{m}^\ominus$ can be neglected, because $V_\mathrm{m}^\ominus$ is supposed to be very large. The residual Helmholtz energy is therefore

$$A_\mathrm{m}^\mathrm{r} = RT\frac{B_2}{V_\mathrm{m}}. \tag{D.35}$$

The isothermal compressibility is best obtained as

$$\kappa_T = -\frac{1}{V_\mathrm{m}}\left(\frac{\partial V_\mathrm{m}}{\partial p}\right)_T = -\frac{1}{V_\mathrm{m}\left(\frac{\partial p}{\partial V_\mathrm{m}}\right)}. \tag{D.36}$$

With

$$\left(\frac{\partial p}{\partial V_\mathrm{m}}\right)_T = -\frac{RT}{V_\mathrm{m}^2} - \frac{2RTB_2}{V_\mathrm{m}^3}, \tag{D.37}$$

the result is

$$\kappa_T = \frac{V_\mathrm{m}}{RT(1+2B_2/V_\mathrm{m})}. \tag{D.38}$$

Evidently, the virial equation can lead to negative compressibilities if $B_2 < 0$ and the molar volume is small.

Problem 5

From the definitions of the thermodynamic functions we have

$$C_p - C_V = \left(\frac{\partial H}{\partial T}\right)_p - \left(\frac{\partial U}{\partial T}\right)_V = \left(\frac{\partial U}{\partial T}\right)_p + p\left(\frac{\partial V}{\partial T}\right)_p - \left(\frac{\partial U}{\partial T}\right)_V. \tag{D.39}$$

For the isobaric U derivative we invoke Eq. (4.62) with $x = U$, $r = u = T$, $y = p$, and $s = V$. The result is

$$\begin{aligned}\left(\frac{\partial U}{\partial T}\right)_p &= \frac{\left(\frac{\partial U}{\partial T}\right)_V \left(\frac{\partial p}{\partial V}\right)_T - \left(\frac{\partial p}{\partial T}\right)_V \left(\frac{\partial U}{\partial V}\right)_T}{\left(\frac{\partial p}{\partial V}\right)_T} \\ &= C_V - \left(\frac{\partial V}{\partial p}\right)_T \left(\frac{\partial p}{\partial T}\right)_V (T\beta_V - p) \\ &= C_V + \left(\frac{\partial V}{\partial T}\right)_p (T\beta_V - p).\end{aligned} \tag{D.40}$$

Insertion into the previous equation then gives the desired result,

$$C_p - C_V = V\alpha_p T\beta_V = \frac{VT\alpha_p^2}{\kappa_T}. \tag{D.41}$$

Problem 6

We first derive $(\partial p/\partial V)_S$. This can be done with Eq. (4.62) by setting $x = p$, $r = u = V$, $y = S$ and $r = T$. The result is

$$\left(\frac{\partial p}{\partial V}\right)_S = \frac{\left(\frac{\partial p}{\partial V}\right)_T \left(\frac{\partial S}{\partial T}\right)_V - \left(\frac{\partial S}{\partial V}\right)_T \left(\frac{\partial p}{\partial T}\right)_V}{\left(\frac{\partial V}{\partial V}\right)_T \left(\frac{\partial S}{\partial T}\right)_V - \left(\frac{\partial S}{\partial V}\right)_T \left(\frac{\partial V}{\partial T}\right)_V} \tag{D.42}$$

Now $(\partial V/\partial V)_T = 1$, $(\partial V/\partial T)_V = 0$, and $(\partial S/\partial T)_V = C_V/T$, hence

$$\left(\frac{\partial p}{\partial V}\right)_S = \left(\frac{\partial p}{\partial V}\right)_T - \frac{T}{C_V}\left[\left(\frac{\partial p}{\partial T}\right)_V\right]^2. \tag{D.43}$$

We note that the factors in the second term are all positive. Therefore, the adiabatic pressure derivative is smaller than the isothermal derivative.

The adiabatic compressibility is then

$$\kappa_S = -\frac{1}{V}\left(\frac{\partial V}{\partial p}\right)_S = -\left(V\left(\left(\frac{\partial p}{\partial V}\right)_T - \frac{T}{C_V}\left[\left(\frac{\partial p}{\partial T}\right)_V\right]^2\right)\right)^{-1} \tag{D.44}$$

or, using the definition of the isothermal compressibility,

$$\kappa_S = \frac{\kappa_T}{1 + \frac{VT}{C_V}\beta_V^2 \kappa_T}. \tag{D.45}$$

With the definition of the isobaric expansivity and the result of the previous problem, this equation can be further simplified:

$$\kappa_S = \frac{\kappa_T}{1 + \frac{VT\alpha_p^2}{C_V \kappa_T}} = \frac{\kappa_T}{1 + \frac{C_p - C_V}{C_V}} = \frac{\kappa_T C_V}{C_p}. \tag{D.46}$$

Problem 7

For the Redlich–Kwong equation,

$$p = \frac{RT}{V_\mathrm{m} - b} - \frac{a}{\sqrt{T} V_\mathrm{m}(V_\mathrm{m} + b)}, \tag{D.47}$$

the required derivatives are

$$\begin{aligned} \beta_V &= \left(\frac{\partial p}{\partial T}\right)_V = \frac{R}{V_\mathrm{m} - b} + \frac{a}{V_\mathrm{m}(V_\mathrm{m} + b)}\frac{1}{2}T^{-3/2} \\ \pi_T &= \frac{3a}{2\sqrt{T} V_\mathrm{m}(V_\mathrm{m} + b)} \propto p_\mathrm{att}. \end{aligned} \tag{D.48}$$

This proportionality is found for all equations of state with $p_\mathrm{rep} \propto T$ and $p_\mathrm{att} \propto T^c$, with c denoting a constant.

CHAPTER 6 – SOLID–FLUID EQUILIBRIA

Problem 1

We have to solve Eq. (6.13), which for an incompressible solid can be written as

$$G_\mathrm{m}^\mathrm{f}(p_2^\mathrm{sf}, T, x_2^\mathrm{f} = 1) + (p - p^\mathrm{sf}) V_\mathrm{m}^\mathrm{s} = \mu_2^\mathrm{f}(p, T, x_2^\mathrm{f}). \tag{D.49}$$

This equation can be simplified by assuming $p \gg p_2^\mathrm{sf}$.

For an ideal gas, Eq. (4.18) gives

$$G_\mathrm{m}(p, T, x_2) = \sum_i x_i (G_{\mathrm{m},i}^\ominus + RT \ln x_i) + RT \ln \frac{p}{p^\ominus} \tag{D.50}$$

and, after differentiation with respect to the amount of component 2,

$$\mu_2(p,T,x_2) = G^{\ominus}_{\mathrm{m},2} + RT\ln x_2 + RT\ln\frac{p}{p^{\ominus}}. \tag{D.51}$$

Insertion into the equilibrium condition, Eq. (D.49), then yields

$$G^{\ominus}_{\mathrm{m},2} + RT\ln\frac{p^{\mathsf{sf}}}{p^{\ominus}} + pV^{\mathsf{s}}_{\mathrm{m}} = G^{\ominus}_{\mathrm{m},2} + RT\ln x^{\mathsf{f}}_2 + RT\ln\frac{p}{p^{\ominus}} \tag{D.52}$$

or, after some rearrangements,

$$\ln x^{\mathsf{f}}_2 = \ln\frac{p^{\mathsf{sf}}}{p} + \frac{pV^{\mathsf{s}}_{\mathrm{m}}}{RT}. \tag{D.53}$$

p^{sf}/p is the mole fraction of component 2 (by Dalton's law) that one would expect if component 1 would merely dilute component 2. But there is evidently a deviation: we have the somewhat paradoxical effect that even a gas that has no interactions with component 2 can increase its sublimation pressure.

Problem 2

The standard Gibbs energy of the decomposition reaction is

$$\begin{aligned}\Delta_{\mathrm{r}}G^{\ominus} &= G^{\ominus}_{\mathrm{m}}(\mathrm{CaSO_4\cdot 2H_2O}) - G^{\ominus}_{\mathrm{m}}(\mathrm{CaSO_4\cdot 0.5H_2O}) - \frac{3}{2}G^{\ominus}_{\mathrm{m}}(\mathrm{H_2O}) \\ &= -4.865\,\mathrm{kJ/mol}\end{aligned} \tag{D.54}$$

for liquid water; for vapor, a contribution $1.5RT\ln(p^{\sigma}/p^{\circ})$ has to be added. The total Gibbs energy of the reaction must be zero, but only the water in the vapor phase gives a pressure-dependent contribution:

$$\Delta_{\mathrm{r}}G = \Delta_{\mathrm{r}}G^{\ominus} - \frac{3}{2}RT\ln\frac{p}{p^{\sigma}} = 0. \tag{D.55}$$

The resulting equilibrium pressure of water is 0.857 kPa.

Problem 3

It is assumed that the components do not mix in the solid state. Hence the solids s_1 and s_2 are pure, and their representations in the px cross sections coincide with the vertical axes. The figures below show the px diagrams at a temperature slightly below the quadruple point Q_1 as well as slightly above. In the latter case, three three-phase lines are crossed when the pressure is increased. In both cases, the high-pressure state is $\mathsf{s}_1\mathsf{s}_2$, i.e., two coexisting pure solid phases. In experiments, this usually is a solid which is not a mixture, but a conglomerate of small pure crystals.

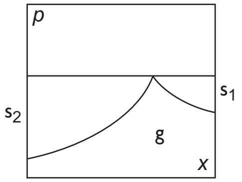

px cross section for the binary system with phase diagram Fig. 6.10 at a temperature below quadruple point Q_1.

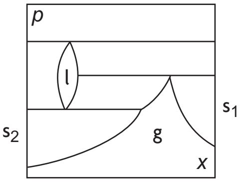

… and slightly above.

CHAPTER 7 – EQUATIONS OF STATE

Problem 1

We make use of Eq. (7.23) and note that the Boltzmann factor is

$$\exp\left(-\frac{u(r)}{k_\mathrm{B}T}\right)=\begin{cases}0 & r<\sigma\\ \exp\left(+\frac{\epsilon}{k_\mathrm{B}T}\right) & \sigma\le r<\lambda\sigma\,.\\ 1 & r\ge\lambda\sigma\end{cases} \tag{D.56}$$

Consequently, Eq. (7.23) can be written as a sum of three integrals, one for each range:

$$\begin{aligned}B_2(T)&=-2\pi N_\mathrm{A}\left[\int_0^\sigma(-r^2)\,\mathrm{d}r+\int_\sigma^{\lambda\sigma}\left(\exp\left(\frac{\epsilon}{k_\mathrm{B}T}\right)-1\right)r^2\,\mathrm{d}r+\int_{\lambda\sigma}^{\infty}0\,\mathrm{d}r\right]\\ &=2\pi N_\mathrm{A}\left[\frac{\sigma^3}{3}-\left(\exp\left(\frac{\epsilon}{k_\mathrm{B}T}\right)-1\right)\left(\frac{\lambda^3\sigma^3}{3}-\frac{\sigma^3}{3}\right)\right].\end{aligned} \tag{D.57}$$

With the substitutions $T^*=\epsilon/k_\mathrm{B}$ (characteristic temperature) and $b=(2\pi/3)N_\mathrm{A}\sigma^3$ (van der Waals covolume), Eq. (7.35) is immediately obtained.

At high temperatures, the Boltzmann factor can be approximated by a truncated Taylor series ($e^x=1+x+\cdots$); the result is

$$B_2(T)\approx b\left(1-(\lambda^3-1)\frac{\epsilon}{k_\mathrm{B}T}\right). \tag{D.58}$$

The virial coefficient exhibits a T^{-1} temperature dependence and converges asymptotically against the hard-sphere value. This is the behavior of the second virial coefficient of the van der Waals equation.

Problem 2

In order to have isotherm crossing, i.e., the same pressure for two fluid states α, β at the same volume, but different temperatures, the following equation has to be solved:

$$p_\alpha = \frac{RT_\alpha}{V_\mathrm{m} - (b_0 + \frac{b_1}{T_\alpha})} - \frac{a}{V_\mathrm{m}^2} = \frac{RT_\beta}{V_\mathrm{m} - (b_0 + \frac{b_1}{T_\beta})} - \frac{a}{V_\mathrm{m}^2} = p_\beta. \tag{D.59}$$

Multiplying with the denominators and collecting the linear terms gives

$$R(V_\mathrm{m} - b_0)(T_\alpha - T_\beta) = Rb_1 \left(\frac{T_\alpha}{T_\beta} - \frac{T_\beta}{T_\alpha} \right). \tag{D.60}$$

Division by $R(T_\alpha - T_\beta)$ then yields

$$V_\mathrm{m} - b_0 = b_1 \frac{T_\alpha + T_\beta}{T_\alpha T_\beta}. \tag{D.61}$$

If we consider T_α as a given property, our result constitutes a linear equation for T_β, for which always a solution exists. But as temperatures should be positive and $b_1 < 0$, an acceptable solution exists for $V_\mathrm{m} < b_0$ only.

Consequently, using a covolume with a T^{-1} temperature dependence necessarily causes isotherm crossing with the van der Waals equation, although at high densities only ($b_0 + b_1/T < V_\mathrm{m} < b_0$).

For the case of a linear temperature dependence of the covolume, the criterion for isotherm crossing is

$$p_\alpha = \frac{RT_\alpha}{V_\mathrm{m} - (b_0 + b_1 T_\alpha)} - \frac{a}{V_\mathrm{m}^2} = \frac{RT_\beta}{V_\mathrm{m} - (b_0 + b_1 T_\beta)} - \frac{a}{V_\mathrm{m}^2} = p_\beta. \tag{D.62}$$

Multiplication with the denominators and rearranging gives $T_\alpha = T_\beta$, i.e., isotherm crossing is not possible. But now the covolume can turn negative at high temperatures, which is undesirable.

That the linear temperature dependence of the covolume with $b_1 < 1$ *does not cause isotherm crossing is a peculiarity of the van der Waals equation of state. For practically all other equations of state, such a temperature dependence ensures isotherm crossing at high densities.*

Problem 3

First of all, there is a formal problem: The mathematical operation "raising to a real power" is meaningful for dimensionless properties only. In the "improved" equation of state, the term a/V_m^ν implies that the parameter a has dimensions $\mathrm{Pa\,m}^{3\nu}\,\mathrm{mol}^{-\nu}$, which may be different for each substance. Writing a one-fluid theory mixing rule,

$$a = \sum_{i=1}^{N} \sum_{j=1}^{N} x_i x_j a_{ij}, \tag{D.63}$$

then clearly results in nonsense.

This problem can be overcome by using reduced properties only:

$$p = p_{\mathrm{rep}} - a \left(\frac{b}{V_{\mathrm{m}}} \right)^{\nu}. \tag{D.64}$$

Here b denotes a covolume parameter or perhaps the critical volume.

The second problem of the "improved" equation of state becomes evident when the Taylor series of the compression factor is calculated:

$$\begin{aligned} Z &= Z_{\mathrm{rep}} - \frac{a}{RT} \rho^{\nu-1} \\ &= Z_{\mathrm{rep}} - \left(\frac{a}{RT} (\nu - 1) \rho^{\nu-2} |_{\rho=0} \right) \rho + \cdots \end{aligned} \tag{D.65}$$

For $\nu < 2$, $\rho^{\nu-2}|_{\rho=0}$ is infinite, and the Taylor series undefined; for $\nu > 0$, $\rho^{\nu-2}|_{\rho=0}$ is zero. Consequently, the second virial coefficient would have no contribution from attraction term of the equation of state. This is possible only for molecules without attractive interactions, or in the limit of infinite temperature.

Conclusion: the introduction of the variable exponent ν is not a very good idea.[1]

Problem 4

It is best to start with the Helmholtz energy expression given in Section C.1. Differentiation with respect to temperature gives

$$\begin{aligned} \left(\frac{\partial A^{\mathrm{r}}_{\mathrm{m}}/RT}{\partial T} \right) &= +2\pi T^* \xi T^{-2} \\ \left(\frac{\partial^2 A^{\mathrm{r}}_{\mathrm{m}}}{\partial T^2} \right) &= -4\pi T^* \xi T^{-3}. \end{aligned} \tag{D.66}$$

Inserting these results into Eq. (4.31) yields

$$\frac{C^{\mathrm{r}}_{V\mathrm{m}}}{R} = 0. \tag{D.67}$$

---

[1] The attentive reader might remember that there are equations of state containing a multitude of substance-specific exponents, e.g., Eq. (7.69). This equation, however, is formulated entirely in terms of reduced (dimensionless) variables, and it contains integer-valued exponents for the density, so that the computation of virial coefficients is possible.

This is one of the few properties for which the van der Waals equation gives a qualitatively wrong answer.

For the total isochoric heat capacity it is necessary to add the ideal-gas contribution, which is $\frac{3}{2}R$ for single atoms, $\frac{5}{2}R$ for linear molecules, and $3R$ for nonlinear ones. The latter two values are only correct if the molecular vibrations are not excited; otherwise, $C_{V\mathrm{m}}^{\mathrm{id}}$ becomes temperature-dependent.

Problem 5

We first use Eq. (7.12) to derive the compression factor and then substitute $V = 1/\rho$:

$$Z = \frac{pV_\mathrm{m}}{RT} = \frac{1}{1-b\rho} - \frac{\alpha\rho}{1+b\rho} \quad \text{with } \alpha = \frac{a}{RT^{3/2}}. \tag{D.68}$$

Then we calculate some derivatives and their values at $\rho = 0$:

$$\begin{aligned} & & Z(0) &= 1 \\ \left(\frac{\partial Z}{\partial \rho}\right) &= \frac{b}{(1-b\rho)^2} - \frac{\alpha}{(1+b\rho)^2} & \left.\left(\frac{\partial Z}{\partial \rho}\right)\right|_{\rho=0} &= b - \alpha \\ \left(\frac{\partial^2 Z}{\partial \rho^2}\right) &= \frac{2b^2}{(1-b\rho)^2} + \frac{2\alpha b}{(1+b\rho)^2} & \left.\left(\frac{\partial^2 Z}{\partial \rho^2}\right)\right|_{\rho=0} &= 2b^2 + 2\alpha b. \end{aligned} \tag{D.69}$$

The Taylor series of Eq. (D.68) is therefore

$$Z = 1 + (b-\alpha)\rho + \frac{1}{2}(2b^2 + 2\alpha b)\rho^2 + \cdots \tag{D.70}$$

Comparison with the virial series, Eq. (7.9), then gives

$$B_2 = b - \alpha \qquad B_3 = b^2 + \alpha b. \tag{D.71}$$

The contribution of the attraction term to B_3 is always positive, which is not what one would expect for simple nonpolar molecules.

Problem 6

In order to locate extrema in $\alpha(T)$, we calculate the first derivative:

$$\frac{\mathrm{d}\alpha}{\mathrm{d}T} = -\frac{m}{\sqrt{TT_\mathrm{c}}}\left[1 + m\left(1 - \sqrt{\frac{T}{T_\mathrm{c}}}\right)\right]. \tag{D.72}$$

Setting this to zero and solving for T gives

$$T_\mathrm{min} = T_\mathrm{c}\left(\frac{m+1}{m}\right)^2. \tag{D.73}$$

$\alpha(T)$ has a local minimum at this temperature. Substitution into the definition of $\alpha(T)$ shows $\alpha(T_{\text{min}}) = 0$.

With typical values for m, the minimum is located above $8T_{\text{c}}$. This is far above the physically accessible temperature range for most substances — but not for all. Moreover, the zero of $\alpha(T)$ causes a too small influence of the attraction term of the equation of state, and the increase after the minimum is physically unreasonable.

Problem 7

The procedure is described by Eqs. (7.57) through (7.61), with the only change that the other hard-sphere equation is used. The solution can be found in the literature (Eq. (9) of [209], there with an attraction term which has been omitted here for clarity):

$$p = \frac{RT}{V_{\text{m}}}\left(1 + m\frac{2\xi(6+\xi)}{4(1-\xi)(3-4\xi)} + (m-1)\frac{37\xi^2 - 30\xi}{4(1-\xi)(3-4\xi)}\right). \tag{D.74}$$

Problem 8

We invoke Eq. (7.54), noting that

- the integrand is 1 in the range $0 \leq \tilde{r} < 1$. The integral over this range is therefore 1.
- the integrand is zero for $\tilde{r} \geq \lambda$; this range does not contribute to σ_{eff}.

We can therefore write, using reduced variables,

$$\frac{\sigma_{\text{eff}}}{\sigma} = 1 + \int_1^{\lambda} \left[1 - \exp\left(-\frac{\lambda - \tilde{r}}{\tilde{T}(\lambda-1)}\right)\right] \mathrm{d}\tilde{r} \qquad \text{with } \tilde{r} = \frac{r}{\sigma} \quad \tilde{T} = \frac{k_{\text{B}}T}{\epsilon}. \tag{D.75}$$

The contribution of the intermediate range [the integral in Eq. (D.75)] is

$$\begin{aligned} &\lambda - 1 - \int_1^{\lambda} \exp\left(-\frac{\lambda - \tilde{r}}{\tilde{T}(\lambda-1)}\right)\mathrm{d}\tilde{r} \\ &= \lambda - 1 - \exp\left(-\frac{\lambda}{\tilde{T}(\lambda-1)}\right)\int_1^{\lambda} \exp\left(+\frac{\tilde{r}}{\tilde{T}(\lambda-1)}\right)\mathrm{d}\tilde{r} \\ &= \lambda - 1 - \tilde{T}(\lambda-1)\left[1 - \exp\left(-\frac{1}{\tilde{T}}\right)\right]. \end{aligned} \tag{D.76}$$

Together with the contribution of the hard core, the result is

$$\frac{\sigma_{\text{eff}}}{\sigma} = \lambda - \tilde{T}(\lambda - 1)\left[1 - \exp\left(-\frac{1}{\tilde{T}}\right)\right]. \tag{D.77}$$

For high temperatures, the exponential can be approximated by a truncated Taylor series, $\exp(-\tilde{T}^{-1}) \approx 1 - \tilde{T}^{-1}$, and the resulting effective collision diameter is $\sigma_{\text{eff}} = \sigma$. For low temperatures, the exponential term vanishes, so that the effective collision diameter becomes $\lambda\sigma$.

Problem 9

This problem can be solved in a similar way as the previous one. The contributions of the core region and the "rectangular barrier" are

$$\begin{gathered} \frac{\sigma_{\text{eff}}}{\sigma} = 1 + \int_1^\lambda \left[1 - \exp\left(-\frac{1}{\tilde{T}}\right)\right] \mathrm{d}\tilde{r} \\ \text{with } \tilde{r} = \frac{r}{\sigma} \quad \tilde{T} = \frac{k_{\mathrm{B}}T}{\epsilon}. \end{gathered} \tag{D.78}$$

Here the integrand is constant. The result is therefore

$$\frac{\sigma_{\text{eff}}}{\sigma} = 1 + (\lambda - 1)\left[1 - \exp\left(-\frac{1}{\tilde{T}}\right)\right]. \tag{D.79}$$

Taking the high-temperature limit and making use of the expansion of the exponential as in the previous problem yields an effective collision diameter of σ. For low temperatures $\lambda\sigma$ is obtained.

The temperature dependence of the effective collision diameter should be compared with the one from the previous problem. It is interesting to observe how a minor change of the interaction potential can effect this property.

CHAPTER 8 – EQUATIONS OF STATE FOR MIXTURES

Problem 1

In one-fluid theory, all residual thermodynamic functions are pure-fluid functions. The composition dependence enters through the mixing rules only. It is therefore sufficient to apply the Michelsen–Kistenmacher test to the mixing rules.

Linear case, binary mixture:

$$b = x_1 b_1 + x_2 b_2. \tag{D.80}$$

Split component 1 into identical subcomponents, $x_1 \to x_{11} + x_{12}$:

$$b = x_{11} b_1 + x_{12} b_1 + x_2 b_2 = (x_{11} + x_{12}) b_1 + x_2 b_2. \tag{D.81}$$

Evidently, the original mixing rule is recovered: test passed.

Quadratic mixing rule:

$$a = x_1^2 a_{11} + 2x_1x_2a_{12} + x_2^2 a_{22}. \tag{D.82}$$

Splitting component 1:

$$\begin{aligned} a &= x_{11}^2 a_{11} + x_{12}^2 a_{11} + x_2^2 a_{22} + 2x_{11}x_{12}a_{11} + 2x_{11}x_2a_{12} + 2x_{12}x_2a_{12} \\ &= (x_{11}^2 + 2x_{11}x_{12} + x_{12}^2)a_{11} + (2x_{11}x_2 + 2x_{12}x_2)a_{12} + x_2^2 a_{22} \\ &= (x_{11} + x_{12})^2 a_{11} + 2(x_{11} + x_{12})x_2a_{12} + x_2^2 a_{22}. \end{aligned} \tag{D.83}$$

This is the original mixing rule again: test passed.

Problem 2

The "improved" mixing rule for a binary mixture is

$$a = x_1^2 a_{11} + 2x_1x_2[1 - k_{12,0} - k_{12,1}(x_1 - x_2)]a_{12} + x_2^2 a_{22}. \tag{D.84}$$

Splitting component 1 into subcomponents, $x_1 \to x_{11} + x_{12}$ gives

$$\begin{aligned} a &= x_{11}^2 a_{11} + x_{12}^2 a_{11} + x_2^2 a_{22} + 2x_{11}x_{12}a_{11} \\ &\quad + 2x_{11}x_2[1 - k_{12,0} - k_{12,1}(x_{11} - x_2)]a_{12} \\ &\quad + 2x_{12}x_2[1 - k_{12,0} - k_{12,1}(x_{12} - x_2)]a_{12} \\ &= (x_{11} + x_{12})^2 a_{11} + x_2^2 a_{22} + 2[(x_{11} + x_{12})(1 - k_{12,0} + x_2k_{12,1}) \\ &\quad - (x_{11}^2 + x_{12}^2)k_{12,1}]x_2a_{12}. \end{aligned} \tag{D.85}$$

Setting $x_1 = x_{11} + x_{12}$ does not reduce this to Eq. (D.84): test failed!

Problem 3

Case (a): the resulting mixing rule for the a parameter is

$$a = \frac{\sum\sum x_ix_ja_{ij}b_{ij}^{\frac{\gamma-3}{3}}}{\sum\sum x_ix_jb_{ij}^{\frac{\gamma-3}{3}}}, \tag{D.86}$$

which is evidently not quadratic anymore. But in the limit of low density ($V_\mathrm{m} \to \infty$, $\gamma \to 3$) a quadratic mixing rule is recovered.

The second virial coefficent of the van der Waals equation is

$$B_2 = b - \frac{a}{RT}. \tag{D.87}$$

Substituting the mixing rules and rearranging gives

$$\begin{aligned} B_2 &= \sum_{i=1}^{N}\sum_{j=0}^{N} x_i x_j \left(b_{ij} - \frac{a_{ij}}{T}\right) \\ &= \sum_{i=0}^{N}\sum_{j=0}^{N} x_i x_j B_{ij}, \end{aligned} \tag{D.88}$$

which is the correct limiting behavior.

Case (b): the result for the virial coefficient is

$$\begin{aligned} B_2 &= \sum_{i=1}^{N}\sum_{j=1}^{N} \varphi_i \varphi_j \left(b_{ij} - \frac{a_{ij}}{T}\right) \\ &= \sum_{i=1}^{N}\sum_{j=1}^{N} \varphi_i \varphi_j B_{ij}, \end{aligned} \tag{D.89}$$

which is not the correct formula.

Problem 4

Collecting the pressure-dependent terms in the combining rule for a gives

$$\begin{aligned} a &= \sum_{i=1}^{N}\sum_{j=1}^{N} x_i x_j (1 - k_{ij,0}) \sqrt{a_{ii} a_{jj}} - p k_{ij,1} \sum_{i=1}^{N}\sum_{j=1}^{N} x_i x_j \sqrt{a_{ii} a_{jj}} \\ &\equiv a_0 - p a_1, \end{aligned} \tag{D.90}$$

and then the Helmholtz energy equation becomes

$$A_{\mathrm{m}}^{\mathrm{r}} = -RT \ln\left(1 - \frac{b}{V_{\mathrm{m}}}\right) - \frac{a_0 - p a_1}{V_{\mathrm{m}}}. \tag{D.91}$$

The pressure is then obtained by differentiation:

$$p = \frac{RT}{V_{\mathrm{m}}} - \left(\frac{\partial A_{\mathrm{m}}^{\mathrm{r}}}{\partial V_{\mathrm{m}}}\right) = \frac{RT}{V_{\mathrm{m}} - b} - \frac{a_0}{V_{\mathrm{m}}^2} + \frac{a_1 V_{\mathrm{m}} p_{(V)} - p a_1}{V_{\mathrm{m}}^2}. \tag{D.92}$$

This is a differential equation for the pressure. An analytic solution does not seem to exist. In the course of a phase equilibrium calculation it would be necessary to solve this equation for the molar volume. This can possibly be done numerically with an iterative equation solver, but the computational effort makes this model unattractive.

Problem 5

Figure D.1 shows the compression factor of hard-sphere mixtures with a diameter ratio of 2 for three different mole fractions. The calculations were

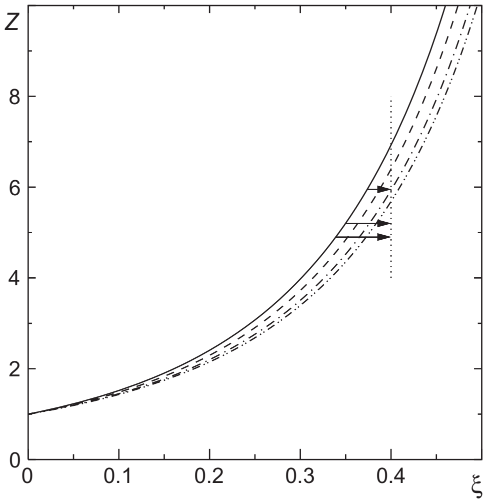

FIGURE D.1 Compression factor as a function of reduced density for hard-sphere mixtures with a diameter ratio of $\sigma_{22}/\sigma_{11} = 2$. – – : $x_1 = 0.25$; —·— : $x_1 = 0.5$; —··— : $x_1 = 0.75$; and ——: pure-fluids equation of state; the linear combining rule for σ_{12} leads to a lower reduced density.

made with the equation of state of Mansoori et al. for hard-sphere mixtures, Eq. (8.34), and with the Carnahan–Starling equation, Eq. (7.28) for pure hard spheres.

We compare the compression factors for a fixed number of molecules in a fixed volume. The cubic combining rule always gives a too large result. The linear combining rule yields a smaller $\bar{\sigma}^3$ and hence a smaller reduced density; it predicts too low compression factors. Closer inspection of the results shows that the linear combining rule gives slightly smaller deviations. But it is evident that, for mixtures with such a large diameter ratio, none of the combining rules gives satisfactory results.

CHAPTER 9 – GLOBAL PHASE DIAGRAMS

Problem 1

The left diagram is of class VI and the middle diagram of class VII. The transitional *pT* diagram is one where the class VII "swallow tail" in the $\mathsf{l} = \mathsf{g}$ critical curves contracts to a tricritical point.

The middle and the right phase diagram differ by the appearing of a pressure minimum in the low-temperature critical curve. The boundary state needed for the transition between them is a critical pressure end minimum (CPEM).

Problem 2

The solution is shown in the figure below.

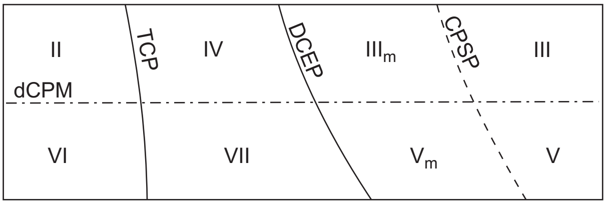

Problem 3

We have to evaluate $G_{(2x)} = 0$ for $p, T \to 0$. At absolute zero, A_m and G_m become identical. Furthermore, the repulsion term can be neglected, because it is proportional to temperature. Therefore, we have only to consider the curvature of $-a/V_m$.

At absolute zero, the molar volume will converge against the covolume, $V_m \to b$. The first critical condition therefore becomes

$$G_{(2x)} \to \frac{d^2}{dx_1^2}\frac{a}{b} = 0. \tag{D.93}$$

We furthermore note that, for equal-sized molecules ($\xi, \eta = 0$), b is a constant. The critical condition therefore reduces to $d^2a/dx_1^2 = 0$.

If van der Waals one-fluid theory is used, we have

$$\begin{aligned} a &= a_{11}x_1^2 + 2a_{12}x_1x_2 + a_{22}x_2^2 \\ \frac{da}{dx_1} &= 2x_1a_{11} + 2(x_2 - x_1)a_{12} - 2x_2a_{22} \\ \frac{d^2a}{dx_1^2} &= 2a_{11} - 4a_{12} + 2a_{22}. \end{aligned} \tag{D.94}$$

Because of the definitions of λ and the d_{ij}, we have for equal-sized molecules

$$\lambda = \frac{T_{11}^* - 2T_{12}^* + T_{22}^*}{T_{11}^* + T_{22}^*} = \frac{a_{11} - 2a_{12} + a_{22}}{a_{11} + a_{22}} = 0. \tag{D.95}$$

In other words: the zero-Kelvin endpoint curve coincides with the abscissa of the global phase diagram.

Applying these considerations to the Redlich–Kwong equation leads to the same intermediate result,

$$\frac{d^2a}{dx_1^2} = 2a_{11} - 4a_{12} + 2a_{22} = 0. \tag{D.96}$$

But for this equation of state, the relation between the characteristic temperature and the attraction parameter is $a \propto T^{*3/2}$. In order to obtain the $\lambda(\zeta)$ relation of the zero-Kelvin endpoint curve, we must express T_{22}^* and T_{12}^* in terms of ζ and λ:

$$\begin{aligned} T_{22}^* &= T_{11}^* \frac{1+\zeta}{1-\zeta} \\ T_{12}^* &= \frac{1}{2}(1-\lambda)(T_{11}^* + T_{22}^*). \end{aligned} \tag{D.97}$$

Insertion into the critical condition, ${T_{11}^*}^{3/2} - 2{T_{12}^*}^{3/2} + {T_{22}^*}^{3/2} = 0$, gives, after some algebraic manipulations,

$$\lambda = 1 - (1-\zeta)\left\{\frac{1}{2}\left[1 + \left(\frac{1+\zeta}{1-\zeta}\right)^{3/2}\right]\right\}^{2/3}. \tag{D.98}$$

Problem 4

Using Jacobi transformations, we can write

$$G_{(2x)} = A_{(2x)} - \frac{A_{(Vx)}^2}{A_{(2V)}}. \tag{D.99}$$

Integration of the van der Waals equation gives (cf. Section C.1)

$$A_\mathrm{m} = A_\mathrm{m}^\ominus - RT \ln\left(\frac{V_\mathrm{m} - b}{V_\mathrm{m}^\ominus}\right) - \frac{a}{V_\mathrm{m}}. \tag{D.100}$$

Differentiation then yields

$$\begin{aligned} A_{(2V)} &= \frac{RT}{(V_\mathrm{m}-b)^2} - \frac{2a}{V_\mathrm{m}^3} \\ A_{(Vx)} &= -\frac{RTb'}{(V_\mathrm{m}-b)^2} + \frac{a'}{V_\mathrm{m}^2} \\ A_{(2x)} &= \frac{RTb''}{V_\mathrm{m}-b} + \frac{RTb'^2}{(V_\mathrm{m}-b)^2} - \frac{a''}{V_\mathrm{m}}. \end{aligned} \tag{D.101}$$

Here, the primes indicate differentiations with respect to the mole fraction x_1. For a one-fluid mixing theory, Eq. (8.17), the attraction parameter of the equation of state and its derivatives are

$$\begin{aligned} a &= x_1^2 a_{11} + 2x_1(1-x_1)a_{12} + (1-x_1)^2 a_{22} \\ a' &= 2x_1 a_{11} + 2(1-2x_1)a_{12} - 2(1-x_1)a_{22} \\ a'' &= 2a_{11} - 4a_{12} + 2a_{22}; \end{aligned} \tag{D.102}$$

analogous equations are obtained for b and its derivatives.

References

[1] J.M.H. Levelt Sengers, How Fluids Unmix: Discoveries by the School of van der Waals and Kamerlingh Onnes, Edita KNAW, Amsterdam, 2003.

[2] A.Y. Kipnis, B.E. Yavelov, J.S. Rowlinson, Van der Waals and Molecular Sciences, Oxford University Press, Oxford, 1996, 2001.

[3] J.R.R. Tolkien, The Lord of the Rings. II. The Two Towers, Book 3, George Allen & Unwin, London, 1954.

[4] S. Raeissi, C.J. Peters, Simulation of double retrograde vaporization using the Peng–Robinson equation of state, J. Chem. Thermodyn. 35 (2003) 573–581.

[5] U.K. Deiters, Some comments on the double retrograde vaporization, J. Chem. Thermodyn. 35 (2003) 583–589.

[6] S.E. Quiñones Cisneros, Barotropic phenomena in complex phase behaviour, Phys. Chem. Chem. Phys. 6 (2004) 2307–2313.

[7] J.A. Schouten, A. Deerenberg, N.J. Trappeniers, Vapor–liquid and gas–gas equilibria in simple systems. 4. The system argon–krypton, Physica A81 (1975) 151–160.

[8] J.R. Wagner, D.S. McCaffrey, J.P. Kohn, Partial miscibility phenomena in ternary system ethane–n-hexadecane–n-eicosane, J. Chem. Eng. Data 13 (1968) 22–24.

[9] A. Bolz, U.K. Deiters, C.J. Peters, T.W. de Loos, Nomenclature for phase diagrams with particular reference to vapour–liquid and liquid–liquid equilibria, Pure Appl. Chem. 70 (1998) 2233–2257.

[10] H. Kalra, D.B. Robinson, T.R. Krishnan, Equilibrium phase properties of ethane–hydrogen sulfide system at subambient temperatures, J. Chem. Eng. Data 22 (1977) 85–88.

[11] K. Ohgaki, T. Katayama, Isothermal vapor–liquid equilibrium data for ethane–carbon dioxide system at high pressures, Fluid Phase Equilib. 1 (1977) 27–32.

[12] J.P. Kuenen, Versuche über die Kondensation und die kritischen Erscheinungen von Gemischen zweier Stoffe, Z. Phys. Chem. 24 (1897) 667–696.

[13] N. Quint, Isothermen für Mischungen von Chlorwasserstoff und Äthan, Z. Phys. Chem. 39 (1901) 14–26.

[14] W.J. Gaw, F.L. Swinton, Occurrence of a double azeotrope in the binary system hexafluorobenzene+benzene, Nature 212 (1966) 283–284.

[15] R. Paas, G.M. Schneider, Phase equilibria of CH_4 + CF_4 and of CH_4 + CHF_3 in the temperature range 90 K to 140 K and at pressures up to 190 MPa, J. Chem. Thermodyn. 11 (1979) 267–276.

[16] G.M. Schneider, High-pressure phase equilibria and spectroscopic investigations up to 200 MPa on fluid mixtures containing fluorinated compounds: a review, Fluid Phase Equilib. 199 (2002) 307–317.

[17] P. Jeschke, G.M. Schneider, Phase equilibria in binary mixtures containing fluorocarbons at high pressures and low temperatures. V. Liquid–liquid and gas–gas equilibria for tetrafluoromethane + propane and + butane up to 200 MPa, J. Chem. Thermodyn. 14 (1982) 547–554.

[18] G. Schneider, Druckeinfluß auf die Entmischung flüssiger Systeme. IV. Entmischung flüssiger n-Alkan–CO_2-Systeme bis –60 °C und 1500 bar. Messungen zum Problem der sog. "Entmischung in der Gasphase", Ber. Bunsenges. Phys. Chem. 70 (1966) 10–16.

[19] D. Oeder, G.M. Schneider, Phasengleichgewichte und kritische Erscheinungen in binären Methan–Kohlenwasserstoffsystemen von – 150 bis 20 °C und bis 3000 bar, Ber. Bunsenges. Phys. Chem. 73 (1970) 229–237.

[20] J. de Swaan Arons, G.A.M. Diepen, Gas–gas equilibria, J. Chem. Phys. 44 (1966) 2322–2330.

[21] N.J. Trappeniers, J.A. Schouten, Vapour–liquid gas–gas equilibria in simple systems. III. The system neon–krypton, Physica 73 (1974) 546–555.

[22] E. Brunner, Fluid mixtures at high pressures. IX Phase separation and critical phenomena in 23 (n-alkane + water) mixtures, J. Chem. Thermodyn. 22 (1990) 335–353.

[23] Y.-N. Lin, R.J.J. Chen, P.S. Chappelear, R. Kobayashi, Vapor–liquid equilibrium of methane–n-hexane system at low temperature, J. Chem. Eng. Data 22 (1977) 402–408.

[24] D.S. Simmons, I.C. Sanchez, Pressure effects on polymer coil–globule transitions near an LCST, Macromolecules 43 (2010) 1571–1574.

[25] A.J. Davenport, J.S. Rowlinson, The solubility of hydrocarbons in liquid methane, Trans. Faraday Soc. 59 (1963) 78–84.

[26] R.L. Scott, P.H. van Konynenburg, Static properties of solutions. Van der Waals and related models for hydrocarbon mixtures. Discuss. Faraday Soc. 49 (1970) 87–97.

[27] C.S. Hudson, Die gegenseitige Löslichkeit von Nikotin in Wasser, Z. Phys. Chem. 47 (1904) 113–115.

[28] G.M. Schneider, Druckeinfluß auf die Entmischung flüssiger Systeme. I. Geschlossene Mischungslücken bis 5000 bar, Z. Phys. Chem. Neue Folge 37 (1963) 333–352.

[29] G.M. Schneider, Druckeinfluß auf die Entmischung flüssiger Systeme. II. Löslichkeit von H_2O und D_2O in Methylpyridinen und Methylpiperidinen, Z. Phys. Chem. Neue Folge 39 (1963) 187–197.

[30] Z.P. Visak, L.P.N. Rebelo, J. Szydlowski, The "hidden" phase diagram of water + 3-methylpyridine at large absolute negative pressures, J. Phys. Chem. B 107 (2003) 9837–9846.

[31] G.M. Schneider, Aqueous solutions at pressures up to 2 GPa: gas–gas equilibria, closed loops, high-pressure immiscibility, salt effects and related phenomena, Phys. Chem. Chem. Phys. 4 (2002) 845–852.

[32] L.Z. Boshkov, Description of phase diagrams of binary mixtures with closed immiscibility domains with a 1-fluid model of an equation of state (in Russian), Dokl. Akad. Nauk SSSR 294 (1987) 901–905.

[33] J. Lachwa, J. Szydlowski, V. Najdanovic-Visak, L.P. Rebelo, K.R. Seddon, M. Nunes da Ponte, et al., Evidence for lower critical solution behavior in ionic liquid solutions, J. Am. Chem. Soc. 127 (2005) 6542–6543.

[34] M.A. Urusova, V.M. Valyashko, Phase equilibria in water–borate systems at elevated temperatures, Inorg. mater. 28 (1992) 955–959.

[35] A.W. Francis, Ternary systems of liquid carbon dioxide, J. Phys. Chem. 58 (1954) 1099–1114.

[36] A.W. Francis, Liquid–Liquid Equilibriums, Interscience Publishers, New York, 1963.

[37] V.M. Valyashko, Derivation of complete phase diagrams for ternary systems with immiscibility phenomena, Pure Appl. Chem. 74 (2002) 1871–1884.

[38] J. D'Ans, D. Jänchen, E. Kaufmann, C. Kux, Landolt-Börnstein Zahlenwerte und Funktionen, vol. II/2c (Lösungsgleichgewichte II), Springer-Verlag, Berlin, 1964.

[39] A.L. Scheidgen, G.M. Schneider, Complex phase equilibrium phenomena in fluid ternary mixtures up to 100 MPa: cosolvency, holes, windows, and islands—review and new results, Fluid Phase Equilib. 194–197 (2002) 1009–1028.

[40] G.M. Schneider, Phase equilibrium investigations of fluid systems at high pressures, Pure Appl. Chem. 65 (1993) 173–182.

[41] B. Widom, Phase separation in polymer solutions, Physica A 194 (1993) 532–541.

[42] A.R. Imre, Y.C. Bae, B.H. Chang, T. Kraska, A semi-empirical method for the prediction of the Θ-lower solution boundary temperature in polymer solutions, Ind. Eng. Chem. Res. 43 (2004) 237–242.

[43] A.R. Imre, W.A. Van Hook, Continuity of solvent quality in polymer solutions. Poor solvent to Θ-solvent continuity in some polystyrene solutions, J. Polym. Sci. B: Polym. Phys. 35 (1997) 1251–1259.

[44] R. Koningsveld, Partial miscibility of multicomponent polymer solutions, Adv. Colloid Polym. Sci. 2 (1968) 151–215.

[45] L.P.N. Rebelo, H.C. de Sousa, W.A. Van Hook, Hypercritically enhanced distortion of a phase diagram: the (polystyrene + acetaldehyde) system, J. Polym. Sci. B: Polym. Phys. 35 (1997) 631–637.

[46] A.R. Imre, T. Kraska, L.V. Yelash, The effect of pressure on the liquid–liquid phase equilibrium of two polydisperse polyalkylsiloxane blends, Phys. Chem. Chem. Phys. 4 (2002) 992–1001.

[47] R. Dohrn, S. Peper, J.M. Fonseca, High-pressure fluid-phase equilibria: experimental methods and systems investigated (2000–2004), Fluid Phase Equilib. 288 (2010) 1–54.

[48] A. Goodwin, K.N. Marsh, W.L. Wakeham (Eds.), Measurement of the Thermodynamic Properties of Single Phases, vol. VI of IUPAC Monograph Series on Experimental Thermodynamics, Elsevier, Amsterdam, 2003.

[49] R.L. Weir, T.W. de Loos (Eds.), Measurement of the Thermodynamic Properties of Multiple Phases, vol. VII of IUPAC Monograph Series on Experimental Thermodynamics, Elsevier, Amsterdam, 2005.

[50] D. Richon, Experimental techniques for the determination of thermophysical properties to enhance chemical processes, Pure Appl. Chem. 81 (2009) 1769–1782.

[51] J. Specovius, M.A. Leiva, R.L. Scott, C.M. Knobler, Tricritical phenomena in "quasi-binary" mixtures of hydrocarbons: 2. binary ethane systems, J. Phys. Chem. 85 (1981) 2313–2316.

[52] F. Fontalba, D. Richon, H. Renon, Simultaneous determination of vapor–liquid equilibria and saturated densities up to 45 MPa and 433 K, Rev. Sci. Instrum. 55 (1984) 944–951.

[53] Le ROLSI™ évolution IV, Homepage on precision sampling valves. http://www.rolsi.com/ (accessed 30.11.11).

[54] D. Richon, New equipment and new technique for measuring activity coefficients and Henry's constants at infinite dilution, Rev. Sci. Instrum. 82 (2011) 025108.

[55] S.L. Randzio, Scanning transitiometry, Chem. Soc. Rev. 25 (1996) 383–392.

[56] S.L. Randzio, J.-P.E. Grolier, Supercritical transitiometry of polymers, Anal. Chem. 70 (1998) 2327–2330.

[57] U.K. Deiters, S.L. Randzio, A combined determination of phase diagrams of asymmetric binary mixtures by equations of state and transitiometry, Fluid Phase Equilib. 260 (2007) 87–97.

[58] R.A. Alberty, Use of Legendre transforms in chemical thermodynamics, J. Chem. Thermodyn. 34 (2002) 1787–1823.

[59] E.A. Coulson, E.F.G. Herington, Fractional distillation. I. The selection of test mixtures for estimating the efficiency of fractionating columns, Trans. Faraday Soc. 44 (1948) 629–636.

[60] W.B. Brown, The statistical thermodynamics of mixtures of Lennard-Jones molecules. I. Random mixtures, Phil. Trans. A 250 (1957) 157–220.

[61] J.S. Rowlinson, F.L. Swinton, Liquids and Liquid Mixtures, third ed., Butterworths, London, 1982.

[62] R.H. Baughman, S. Schafström, C. Cui, S.O. Santas, Materials with negative compressibilities in one or more dimensions, Science 279 (1998) 1522–1524.

[63] D. Kondepudi, I. Prigogine, Modern Thermodynamics, second ed., John Wiley & Sons, Chichester, 1999.

[64] U. Setzmann, W. Wagner, A new equation of state and tables of thermodynamic properties for methane covering the range from the melting line to 625 K at pressures up to 1000 MPa, J. Phys. Chem. Ref. Data 20 (1991) 1061–1155.

[65] C. Antoine, Tensions des vapeurs: nouvelle rélation entre les tensions et les températures, Comptes Rend. 107 (1888) 681–684; 836–837.

[66] J. Thomson, Considerations on the abrupt change at boiling or condensing in reference to the continuity of the fluid state of matter, Proc. R. Soc. Lond. 20 (1871) 1–8.

[67] D. Konowalow, Über die Dampfspannungen der Flüssigkeitsgemische, Ann. Physik Chemie 250 (1881) 34–52; 219–226.

[68] R. Haase, Thermodynamik der Mischphasen, Springer, Berlin, 1956.

[69] M.L. Michelsen, The isothermal flash problem. Part I. Stability, Fluid Phase Equilib. 9 (1982) 1–19.

[70] M.L. Michelsen, The isothermal flash problem. Part II. Phase-split calculation, Fluid Phase Equilib. 9 (1982) 21–40.

[71] U. Deiters, G.M. Schneider, Fluid mixtures at high pressures. Computer calculations of the phase equilibria and the critical phenomena in fluid binary mixtures from the Redlich–Kwong equation of state, Ber. Bunsenges. Phys. Chem. 80 (1976) 1316–1321.

[72] R.A. Heidemann, A.M. Khalil, The calculation of critical points, AIChE J. 26 (1980) 769–779.

[73] A.R. Imre, G. Melnichenko, W.A. Van Hook, Liquid–liquid equilibria in polystyrene solutions: the general pressure dependence, Phys. Chem. Chem. Phys. 1 (1999) 4287–4292.

[74] A.R. Imre, W.A. Van Hook, Liquid–liquid equilibria in polymer solutions at negative pressure, Chem. Soc. Rev. 27 (1998) 117–123.

[75] J.V. Sengers, J.M.H. Levelt Sengers, Critical phenomena in classical fluids, in: C.A. Croxton (Ed.), Progress in Liquid Physics, Wiley, Chichester, 1978, (Chapter 4).

[76] S.E. Quiñones Cisneros, Critical Behavior in Fluid Mixtures, Ph.D. thesis, University of Minnesota, 1992.

[77] V.K. Filippov, G.G. Chernik, Heat capacity of heterogeneous systems and thermal analysis, Thermochim. Acta. 101 (1986) 65–75.

[78] U.K. Deiters, Correlation and prediction of high-pressure phase equilibria and related thermodynamic properties of simple fluid mixtures, in: G. Brunner (Ed.), Supercritical Fluids as Solvents and Reaction Media, Elsevier, Amsterdam, 2004 (Chapter 1.8), pp. 185–209.

[79] J.M. Prausnitz, R.N. Lichtenthaler, E. Gomes de Azevedo, Molecular Thermodynamics of Fluid-Phase Equilibria, third ed., Prentice Hall PTR, Upper Saddle River, NJ, 1999.

[80] U.K. Deiters, A new semiempirical equation of state for fluids. I. Derivation, Chem. Eng. Sci. 36 (1981) 1139–1146.

[81] U.K. Deiters, A new semiempirical equation of state for fluids. II. Application to pure substances, Chem. Eng. Sci. 36 (1981) 1146–1151.

[82] U.K. Deiters, Density-dependent mixing rules for the calculation of fluid phase equilibria at high pressures, Fluid Phase Equilib. 33 (1987) 267–293.

[83] S.-D. Yeo, E. Kiran, Formation of polymer particles with supercritical fluids: a review, J. Supercrit. Fluids 34 (2005) 287–308.

[84] M. Türk, D. Bolten, Formation of submicron poorly water-soluble drugs by rapid expansion of supercritical solution (RESS): results for naproxen, J. Supercrit. Fluids 55 (2010) 778–785.

[85] A. van Pelt, PHASEGRAPH—Klassifikatie van vaste stof–vloeistof-evenwichten, internal report, Laboratory of Applied Thermodynamic & Phase Equilibria, Delft University of Technology, 1988.

[86] J.D. van der Waals, J.C. Platteeuw, Clathrate solutions, Adv. Chem. Phys. 2 (1959) 1–57.

[87] R. Span, W. Wagner, A new equation of state for carbon dioxide covering the fluid region from the triple-point temperature to 1100 K at pressures up to 800 MPa, J. Phys. Chem. Ref. Data 25 (1996) 1509–1596.

[88] M. Thiesen, Untersuchungen über die Zustandsgleichung, Ann. Physik 24 (1885) 467–492.

[89] J.D. van der Waals, Over de continuiteit van den gas- en vloeistoftoestand, Ph.D. thesis, Universiteit Leiden, The Netherlands, 1873.

[90] J.D. van der Waals, On the Continuity of the Gaseous and Liquid States (with an introduction by J. S. Rowlinson), vol. XIV of Studies in Statistical Mechanics, North-Holland, Amsterdam, 1988.

[91] M.A. Trebble, P.R. Bishnoi, Accuracy and consistency comparisons of ten cubic equations of state for polar and non-polar compounds, Fluid Phase Equilib. 29 (1986) 465–474.

[92] O.L. Boshkova, U.K. Deiters, Soft repulsion and the behavior of equations of state at high pressures, Int. J. Thermophys. 31 (2010) 227–252.

[93] O. Redlich, J.N.S. Kwong, On the thermodynamics of solutions. V. An equation of state—fugacities of gaseous solutions, Chem. Rev. 44 (1949) 233–244.

[94] U.K. Deiters, The calculation of densities from cubic equations of state, AIChE J. 48 (2002) 882–886.

[95] G. Soave, Equilibrium constants from a modified Redlich–Kwong equation of state, Chem. Eng. Sci. 27 (1972) 1197–1203.

[96] K.S. Pitzer, The volumetric and thermodynamic properties of fluids. I. Theoretical basis and virial coefficients, J. Am. Chem. Soc. 77 (1955) 3427–3433.

[97] K.S. Pitzer, D.Z. Lippmann, R.F. Curl Jr., C.M. Huggins, D.E. Petersen, The volumetric and thermodynamic properties of fluids. II. Compressibility factor, vapor pressure and entropy of vaporization, J. Am. Chem. Soc. 77 (1955) 3434–3440.

[98] B.E. Poling, J.M. Prausnitz, J.O. O'Connell, The Properties of Gases and Liquids, McGraw-Hill, New York, 2001.

[99] D.Y. Peng, D.B. Robinson, A new two-constant equation of state, Ind. Eng. Chem. Fundam. 15 (1976) 59–64.

[100] J. Martin, Cubic equations of state — which?, Ind. Eng. Chem. Fundam. 18 (1979) 81–97.

[101] A. Péneloux, E. Rauzy, R. Fréze, A consistent correction for Redlich–Kwong–Soave volumes, Fluid Phase Equilib. 8 (1982) 7–23.

[102] P.H. Salim, M.A. Trebble, A modified Trebble–Bishnoi equation of state: thermodynamic consistency revisited, Fluid Phase Equilib. 65 (1991) 59–71.

[103] L.V. Yelash, T. Kraska, Volume translated equations of state: empirical approach and physical relevance, AIChE J. 49 (2003) 1569–1579.

[104] J. Ahlers, J. Gmehling, Development of an universal group contribution equation of state. I: Prediction of liquid densities for pure compounds with a volume translated Peng–Robinson equation of state, Fluid Phase Equilib. 191 (2001) 177–188.

[105] B.M. Axilrod, E. Teller, Interaction of the van der Waals type between three atoms, J. Chem. Phys. 11 (1943) 299–300.

[106] D.A. McQuarrie, Statistical Mechanics, Harper & Row, New York, 1976.

[107] F.H. Ree, W.G. Hoover, Fifth and sixth virial coefficients for hard spheres and hard disks, J. Phys. Chem. 40 (1964) 939–950.

[108] F.H. Ree, W.G. Hoover, Seventh virial coefficients for hard spheres and hard disks, J. Phys. Chem. 46 (1967) 4181–4197.

[109] N.F. Carnahan, K.E. Starling, Equation of state for nonattracting rigid spheres, J. Chem. Phys. 51 (1969) 635–636.

[110] G.A. Iglesias Silva, K.R. Hall, Accurate hard-body expressions for use as Z_{ref}, Fluid Phase Equilib. 98 (1994) 49–54.

[111] L.V. Yelash, T. Kraska, U.K. Deiters, Closed-loop critical curves in simple van der Waals fluid models consistent with the packing fraction limit, J. Chem. Phys. 110 (1999) 3079–3084.

[112] L.V. Yelash, T. Kraska, A generic equation of state for the hard-sphere fluid incorporating the high density limit, Phys. Chem. Chem. Phys. 3 (2001) 3114–3118.

[113] C.-H. Kim, P. Vimalchand, M.D. Donohue, S.I. Sandler, Simplified perturbed hard chain equation of state, AIChE J. 32 (1986) 1726–1734.

[114] J.V. Sengers, R.F. Kayser, C.J. Peters, B.H. White (Eds.), Equations of State for Fluids and Fluid Mixtures, vol. V of IUPAC Monograph Series on Experimental Thermodynamics, Elsevier, Amsterdam, 2000.

[115] C.G. Gray, K.E. Gubbins, Theory of Molecular Fluids Fundamentals, vol. 9 of International Series of Monographs on Chemistry, Oxford University Press, New York, 1984.

[116] J.A. Pople, The statistical mechanics of assemblies of axially symmetric molecules. I. General theory, Proc. Royal Soc. London Ser. A 221 (1954) 498–507.

[117] J.A. Pople, The statistical mechanics of assemblies of axially symmetric molecules. II. Second virial coefficients, Proc. Royal Soc. London Ser. A 221 (1954) 508–516.

[118] G. Stell, J.C. Rasaiah, H. Narang, Thermodynamic perturbation theory for simple polar fluids. II., Mol. Phys. 27 (1974) 1393–1414.

[119] B. Larsen, J.C. Rasaiah, G. Stell, Thermodynamic perturbation theory for multipolar and ionic liquids, Mol. Phys. 33 (1977) 987–1027.

[120] C.G. Gray, K.E. Gubbins, C.H. Twu, Perturbation theory for molecular fluids: third-order term in the Pople expansion, J. Chem. Phys. 69 (1978) 182–193.

[121] H. Reiss, H.L. Frisch, J.L. Lebowitz, Statistical mechanics of rigid spheres, J. Chem. Phys. 31 (1959) 369–380.

[122] R.M. Gibbons, The scaled particle theory for particles of arbitrary shape, Mol. Phys. 17 (1969) 81–86.

[123] T. Kihara, Virial coefficients and models of molecules in gases, Rev. Mod. Phys. 25 (1953) 831–843.

[124] T. Boublík, Hard convex body equation of state, J. Chem. Phys. 63 (1975) 4084.

[125] J.A. Barker, D. Henderson, Perturbation theory and equation of state for fluids, J. Chem. Phys. 47 (1967) 4714–1721.

[126] H.C. Andersen, J.D. Weeks, D. Chandler, Relationship between the hard-sphere fluid and fluids with realistic repulsion forces, Phys. Rev. A 4 (1971) 1597–1607.

[127] T. Boublík, Equation of state for hard convex body fluids, Mol. Phys. 42 (1981) 209–216.

[128] M.S. Wertheim, Fluids with highly directional attractive forces. 1. Statistical thermodynamics, J. Stat. Phys. 35 (1984) 19–34.

[129] M.S. Wertheim, Fluids with highly directional attractive forces. 1. Thermodynamic perturbation theory and integral-equations, J. Stat. Phys. 35 (1984) 35–47.

[130] G. Jackson, W.G. Chapman, K.E. Gubbins, Phase equilibria of associating fluids. Spherical molecules with multiple bonding sites, Mol. Phys. 65 (1988) 1–31.

[131] M. Banaszak, C.K. Chen, M. Radosz, Copolymer SAFT equation of state. Thermodynamic perturbation theory extended to heterobonded chains, Macromolecules 29 (1996) 6481–6486.

[132] N. Mac Dowell, F.E. Pereira, F. Llovell, F.J. Bias, C.S. Adjiman, G. Jackson, A. Galindo, Transferable SAFT-VR models for the calculation of the fluid phase equilibria in reactive mixtures of carbon dioxide, water, and n-alkylamines in the context of carbon capture, J. Phys. Chem. B 115 (2011) 8155–8168.

[133] S. Jain, A. Dominik, W.G. Chapman, Modified interfacial statistical associating fluid theory: a perturbation density functional theory for inhomogeneous complex fluids, J. Chem. Phys. 127 (2007) 244904.

[134] C.H. Twu, K.E. Gubbins, Thermodynamics of polyatomic fluid mixtures. II. Polar, quadrupolar and octopolar molecules, Chem. Eng. Sci. 33 (1978) 879–887.

[135] C. Kriebel, A. Müller, J. Winkelmann, J. Fischer, A hybrid equation of state for Stockmayer pure fluids and mixtures, Fluid Phase Equilib. 119 (1996) 67–80.

[136] C. Kriebel, M. Mecke, J. Winkelmann, J. Vrabec, J. Fischer, An equation of state for dipolar Lennard-Jones molecules and its application to refrigerants, Fluid Phase Equilib. 142 (1998) 15–32.

[137] R.A. Heidemann, J.M. Prausnitz, A van der Waals-type equation of state for fluids with associating molecules, Proc. Natl. Acad. Sci. USA 73 (1976) 1773–1776.

[138] U.K. Deiters, Application of an EOS chain association theory to the calculation of thermodynamic properties of (alkane + 1-alkanol) mixtures, Fluid Phase Equilib. 89 (1993) 229–242.

[139] A. Heintz, A new theoretical approach for predicting excess properties of alkanol/alkane mixtures, Ber. Bunsenges. Phys. Chem. 89 (1985) 172–181.

[140] I.G. Economou, M.D. Donohue, Chemical, quasi-chemical and perturbation theories for associating fluids, AIChE J. 37 (1991) 1875–1894.

[141] S. Malanowski, A. Anderko, Modelling Phase Equilibria, John Wiley & Sons, New York, 1992.

[142] J.P. Wolbach, S.I. Sandler, The thermodynamic properties of hydrogen-bonding fluids from *ab initio* molecular orbital calculations. 1. Water, AIChE J. 43 (1997) 1589–1596.

[143] A. Heintz, D. Wandschneider, U. Lüning, W. Marczak, Experimental and statistical mechanical studies of heats of dilution of alkanols in pyridine derivatives based on ab initio calculations of hydrogen bonding energies, Fluid Phase Equilib. 248 (2006) 123–133.

[144] T. Kraska, S.E. Quiñones Cisneros, R. Rozas, U.K. Deiters, Modelling of surface tension for the Lennard-Jones fluid based on friction theory, in: Thermodynamics 2007 Conference Proceedings, Institut Français du Pétrole, Rueil-Malmaison, France, 2007.

[145] W. Wagner, A. Pruß, The IAPWS formulation 1995 for the thermodynamic properties of ordinary water substance for general and scientific use, J. Phys. Chem. Ref. Data 31 (2002) 387–535.

[146] K. Davitt, E. Rolley, F. Caupin, A. Arvengas, S. Balibar, Equation of state of water under negative pressure, J. Chem. Phys. 133 (2010) 174507, 1–8.

[147] H.-W. Xiang, U.K. Deiters, A new generalized corresponding-states equation of state for the extension of the Lee–Kesler equation to fluids consisting of polar and larger nonpolar molecules, Chem. Eng. Sci. 63 (2007) 1490–1496.

[148] H.-W. Xiang, The Corresponding-States Principle and its Practice: Thermodynamic, Transport and Surface Properties of Fluids, Elsevier, Amsterdam, 2005.

[149] B. Widom, Equation of state in the neighbourhood of the critical point, J. Chem. Phys. 46 (1965) 3898–3905.

[150] L. Onsager, A two-dimensional model with an order-disorder transition, Phys. Rev. 65 (1944) 117–149.

[151] K.G. Wilson, Renormalization group and critical phenomena. I. Renormalization group and the Kadanoff scaling picture, Phys. Rev. B 4 (1971) 3174–3183.

[152] Z.Y. Chen, P.C. Albright, J.V. Sengers, Crossover from singular critical to regular classical thermodynamic behavior of fluids, Phys. Rev. A 41 (1990) 3161–3177.

[153] A. Kostrowicka Wyczalkowska, M.A. Anisimov, J.V. Sengers, Global crossover equation of state of a van der Waals fluid, Fluid Phase Equilib. 158–160 (1999) 523–535.

[154] C. McCabe, S.B. Kiselev, A crossover SAFT-VR equation of state for pure fluids: preliminary results for light hydrocarbons, Fluid Phase Equilib. 219 (2004) 3–9.

[155] E. Forte, F. Llovell, L.F. Vega, J.P.M. Trusler, A. Galindo, Application of a renormalization-group treatment to the statistical associating fluid theory for potentials of variable range (SAFT-VR), J. Chem. Phys. 134 (2011) 154102.

[156] E.H. Brown, On the thermodynamic properties of fluids, Bull. Intnl. Inst. Refrig., Paris, Annexe 1960-1961 (1960) 169–178.

[157] U.K. Deiters, K.M. de Reuck, Guidelines for publication of equations of state. I. Pure fluids, Pure Appl. Chem. 69 (1997) 1237–1249.

[158] U.K. Deiters, Extended 1-fluid theory for mixtures containing non-spherical molecules, Fluid Phase Equilib. 48 (1989) 185–196.

[159] A.E. Nasrabad, R. Laghaei, U.K. Deiters, Prediction of the thermophysical properties of pure neon, pure argon, and the binary mixtures neon–argon and argon–krypton by Monte Carlo simulation using ab initio potentials, J. Chem. Phys. 121 (2004) 6423–6434.

[160] G.A. Mansoori, N.F. Carnahan, K.E. Starling, T.W. Leland, Equilibrium properties of the mixture of hard spheres, J. Chem. Phys. 54 (1971) 1523–1525.

[161] M.L. Michelsen, A method for incorporating excess Gibbs energy models in equations of state, Fluid Phase Equilib. 60 (1990) 47–58.

[162] M.L. Michelsen, A modified Huron–Vidal mixing rule for cubic EOS, Fluid Phase Equilib. 60 (1990) 213–219.

[163] H. Huang, S. Sandler, Prediction of VLE at high pressures using activity coefficient parameters obtained from low-pressure data. A comparison of two equations of state mixing rules, Ind. Eng. Chem. Res. 32 (1993) 1498–1503.

[164] J. Schwarzentruber, H. Renon, Equations of state: how to reconcile flexible mixing rules, the virial coefficient constraint and the "Michelsen–Kistenmacher syndrome" for multicomponent systems, Fluid Phase Equilib. 67 (1991) 99–110.

[165] M.T. Raetzsch, H. Kehlen, Continuous thermodynamics of complex mixtures, Fluid Phase Equilib. 14 (1983) 225–234.

[166] R.L. Cotterman, R. Bender, J.M. Prausnitz, Phase equilibria for mixture containing very many components. Development and application of continuous thermodynamics for chemical process design, Ind. Eng. Chem. Process Design 24 (1985) 194–203.

[167] R.L. Cotterman, J.M. Prausnitz, Flash calculations for continuous or semicontinuous mixtures using an equation of state, Ind. Eng. Chem. Process. Des. 24 (1985) 434–443.

[168] D. Geană, V. Feroiu, Ecuaţii de stare, Editura Tehnică, Bucarest, 2000.

[169] C.F. Leibovici, A consistent procedure for the estimation of properties associated to lumped systems, Fluid Phase Equilib. 87 (1993) 189–197.

[170] J. J. van Laar, On the shape of the plaitpoint curves for mixtures of normal substances (2nd communication), Proc. K. Ned. Akad. Wet. 8 (1905) 33–48.

[171] P.H. van Konynenburg, R.L. Scott, Critical lines and phase equilibria in binary van der Waals mixtures, Phil. Trans. R. Soc. Lond. A 298 (1980) 495–540.

[172] L.V. Yelash, T. Kraska, Covolume effects on the closed loops of liquid–liquid immiscibility in binary fluid mixtures, Z. Phys. Chem. 211 (1999) 159–179.

[173] L.Z. Boshkov, Bifurcations—a possibility to generalize the thermodynamic description of phase diagrams of two-component fluids, Ber. Bunsenges. Phys. Chem. 96 (1992) 940–943.

[174] A. van Pelt, Critical Phenomena in Binary Fluid Mixtures: Classification of Phase Equilibria with the Simplified-Perturbed-Hard-Chain Theory, Ph.D. thesis, Technical University Delft, 1992.

[175] U.K. Deiters, I.L. Pegg, Systematic investigation of the phase behaviour in binary fluid mixtures. I. Calculations based on the Redlich–Kwong equation of state, J. Chem. Phys. 90 (1989) 6632–6641.

[176] L.Z. Boshkov, V.A. Mazur, Phase equilibria and critical lines of binary mixtures of Lennard-Jones molecules (in Russian), Zh. Fiz. Khim. 60 (1986) 29–33.

[177] D. Furman, R.B. Griffiths, Global phase diagram for a van der Waals model of a binary mixture, Phys. Rev. A 17 (1978) 1139–1148.

[178] A. van Pelt, U.K. Deiters, C.J. Peters, J. de Swaan Arons, Global phase behaviour based on the simplified-perturbed-hard-chain equation of state, J. Chem. Phys. 102 (1995) 3361–3375.

[179] J. Kolafa, Azeotropic phenomena in the global phase diagram of the Redlich–Kwong equation of state, Phys. Chem. Chem. Phys. 1 (1999) 5665–5670.

[180] T. Kraska, U.K. Deiters, Systematic investigation of the phase behavior in binary fluid mixtures. II. Calculations based on the Carnahan–Starling–Redlich–Kwong equation of state, J. Chem. Phys. 96 (1992) 539–547.

[181] T. Kraska, Systematische Untersuchung des globalen Phasenverhaltens binärer fluider Mischungen ausgehend von der Carnahan–Starling–Redlich–Kwong-Zustandsgleichung, diploma thesis, Ruhr-Universität Bochum, 1989.

[182] L.V. Yelash, T. Kraska, Closed loops of liquid-liquid immiscibility in binary mixtures of equal sized molecules with a simple theoretical equation of state, Ber. Bunsenges. Phys. Chem. 102 (1998) 213–223.

[183] G. Jackson, Theory of closed-loop liquid–liquid immiscibility in mixtures of molecules with directional attractive forces, Mol. Phys. 72 (1991) 1365–1385.

[184] L.Z. Boshkov, L.V. Yelash, Closed loops of liquid–liquid immiscibility in binary mixtures predicted from the Redlich–Kwong equation of state, Fluid Phase Equilib. 141 (1998) 105–112.

[185] L.V. Yelash, T. Kraska, On closed-loop liquid–liquid immiscibility, Phys. Chem. Chem. Phys. 1 (1999) 307–311.

[186] J.-L. Wang, G.-W. Wu, R.J. Sadus, Closed-loop liquid–liquid equilibria and the global phase behaviour of binary mixtures involving hard-sphere + van der Waals interactions, Mol. Phys. 98 (2000) 715–723.

[187] R.L. Scott, Van der Waals-like global phase diagrams, Phys. Chem. Chem. Phys. 1 (1999) 4225–4232.

[188] P. Bhimalapuram, B. Widom, The hydrophobic heat-capacity anomaly, Physica A 298 (2001) 229–236.

[189] H. Weingärtner, D. Klante, G.M. Schneider, High-pressure liquid–liquid immiscibility in aqueous solutions of tetra-n-butylammonium bromide studied by a diamond anvil cell technique, J. Sol. Chem. 28 (1999) 435–446.

[190] D. Furman, S. Dattagupta, R.B. Griffiths, Global phase diagram for a three-component model, Phys. Rev. B 15 (1977) 441–464.

[191] V.A. Mazur, L.Z. Boshkov, V.B. Fedorov, Phase equilibria in two-component Lennard-Jones systems (in Russian), Dokl. Akad. Nauk SSSR 282 (1985) 137–140.

[192] J.-L. Wang, R.J. Sadus, Global phase diagram for anisotropic binary fluid mixtures: reverse type IV behaviour, Mol. Phys. 101 (2003) 2211–2217.

[193] B.C. Attwood, C.K. Hall, Global phase diagram for monomer/dimer mixtures, Fluid Phase Equilib. 204 (2003) 85–106.

[194] M. Flores, H. Segura, M.J. Tardón, J. Wisniak, I. Polishuk, Limiting conditions for the critical pressure step point behavior in the global phase diagram of binary mixtures composed by spherical molecules of equal sizes, J. Supercrit. Fluids 48 (2009) 108–119.

[195] J. Bumba, J. Kolafa, Global phase diagrams of the van der Waals–Dieterici and the BMCSL–Dieterici equations of state, Phys. Chem. Chem. Phys. 6 (2004) 2301–2306.

[196] I. Polishuk, J.H. Vera, H. Segura, Azeotropic behavior of Dieterici binary fluids, Fluid Phase Equilib. 257 (2007) 18–26.

[197] I.-C. Wei, R.L. Scott, In search of the Griffiths shield region, J. Stat. Phys. 52 (1988) 1315–1324.

[198] A. Mejía, H. Segura, On the interfacial behaviour about the shield region, Int. J. Thermophys. 26 (2005) 13–29.

[199] J.C. Lang, R.D. Morgan, Nonionic surfactant mixtures. I. Phase equilibria in $C_{10}E_4$–H_2O and closed-loop coexistence, J. Chem. Phys. 73 (1980) 5849–5861.

[200] G.H. Findenegg, A. Hirtz, R. Rasch, F. Sowa, Novel phase behavior in three-component oil–water–surfactant systems. A truncated isotropic channel in the oil-rich regime, J. Phys. Chem. 93 (1989) 4580–4587.

[201] U.K. Deiters, L.Z. Boshkov, L.V. Yelash, V.A. Mazur, A new mechanism of the formation of four-phase separation in two-component fluids (in Russian), Doklady Russ. Akad. Nauk 359 (1998) 343–347.

[202] I. Polishuk, J. Wisniak, H. Segura, L.V. Yelash, T. Kraska, Prediction of the critical locus on binary mixtures using equation of state: II. Investigation of van der Waals-type and Carnahan–Starling-type equations of state, Fluid Phase Equilib. 172 (2000) 1–26.

[203] A. Mejía, J.C. Pamies, D. Duque, H. Segura, L. F. Vega, Phase and interface behaviors in type-I and type-V Lennard-Jones mixtures: theory and simulations, J. Chem. Phys. 132 (2005) 034505.

[204] A. Weber, L.V. Yelash, T. Kraska, Effect of the phase behaviour of the solvent-antisolvent systems on the gas antisolvent crystallisation of paracetamol, J. Supercrit. Fluids 33 (2005) 107–113.

[205] A. Galindo, P.J. Whitehead, J. Jackson, A.N. Burgess, Predicting the high-pressure phase equilibria of water + n-alkanes using a simplified SAFT theory with transferable intermolecular interaction parameters, J. Phys. Chem. 100 (1996) 6781–6792.

[206] L.V. Yelash, T. Kraska, The global phase behaviour of binary mixtures of chain molecules: theory and application, Phys. Chem. Chem. Phys. 1 (1999) 4315–4322.

[207] M. Bardas, N. Dahmen, T. Kraska, K.-D. Wagner, L.V. Yelash, Isothermal vapor–liquid equilibria of binary systems of carbon dioxide and 1-butyne, compared to other binary CO_2 + C_4H_n systems in terms of global parameters, Phys. Chem. Chem. Phys. 4 (2002) 987–991.

[208] A.R. Imre, W.A. Van Hook, Liquid–liquid demixing from solutions of polystyrene. 1. A review. 2. Improved correlation with solvent properties, J. Phys. Chem. Ref. Data 25 (1996) 637–661.

[209] L.V. Yelash, T. Kraska, Statistical associating fluid theory for chains of attractive hard-spheres: optimized equation of state, Phys. Chem. Chem. Phys. 1 (1999) 2449–2455.

[210] L.V. Yelash, T. Kraska, E.A. Müller, N.F. Carnahan, Simplified equation of state for non-spherical hard particles: an optimized shape factor approach, Phys. Chem. Chem. Phys. 1 (1999) 4919–4925.

[211] L.V. Yelash, T. Kraska, Investigation of a generalized attraction term of an equation of state and its influence on the phase behaviour, Fluid Phase Equilib. 162 (1999) 115–130.

[212] R.J. Sadus, High Pressure Behaviour of Multicomponent Fluid Mixtures, Elsevier, Amsterdam, 1992.

[213] M. Bluma, U.K. Deiters, A classification of phase diagrams of ternary fluid systems, Phys. Chem. Chem. Phys. 1 (1999) 4307–4313.

[214] K. Gauter, L.J. Florusse, C.J. Peters, J. de Swaan Arons, Classification of and transformations between types of fluid phase behavior in selected ternary systems, Fluid Phase Equilib. 116 (1996) 445–453.

[215] S. Raeissi, K. Gauter, C.J. Peters, Fluid multiphase behavior in quasi-binary mixtures of carbon dioxide and certain 1-alkanols, Fluid Phase Equilib. 147 (1998) 239–249.

[216] G. Jordan-Engeln, F. Reutter, Numerische Mathematik für Ingenieure, Bibliographisches Institut, Mannheim, 1985.

[217] W.C. Rheinboldt, Methods for Solving Systems of Nonlinear Equations, CBMS-NSF Regional Conference Series in Applied Mathematics, Society for Industrial Applied Mathematics (SIAM), Philadelphia, Pennsylvania, USA, 1974.

[218] U.K. Deiters, Reply to a Letter to the Editor by H. Salim, AIChE J. 51 (2005) 3310.

[219] W.H. Press, S.A. Teukolsky, W.T. Vetterling, B.P. Flannery, Numerical Recipes in C, Cambridge University Press, Cambridge, 2002.

[220] P. Craven, G. Wahba, Smoothing noisy data with spline functions, Numer. Math. 31 (1979) 377–403.

[221] D. Marquardt, An algorithm for least squares estimation of nonlinear parameters, SIAM J. Appl. Math. 11 (1964) 431–441.

[222] M. Powell, A method for minimizing a sum of squares of nonlinear functions without calculating derivatives, Comput. J. 7 (1965) 303–307.

[223] J.A. Nelder, R. Mead, A simplex method for function minimization, Comput. J. 7 (1965) 308–313.

[224] T. Doiron, R.P. Behringer, H. Meyer, Equation of state of a He-3–He-4 mixture near its liquid–vapor critical point, J. Low Temp. Phys. 24 (1976) 345–363, R. B. Griffiths' proof is contained in the appendix.

[225] J.S. Rowlinson, G.J. Esper, J.C. Holste, K.R. Hall, M.A. Barrufet, P.T. Eubank, The collinearity of isochores at single- and two-phase boundaries for fluid mixtures, in: K.C. Chao, J. Robinson, R.L. (Eds.), Equations of State – Theories and Applications, Vol. 300 of ACS Symposium Series, American Chemical Society, Washington, 1986, pp. 42–59.

Index